

VOLUME 81

OCTOBER 20, 1977

NUMBER 21

JPCA_x

THE JOURNAL OF

PHYSICAL

CHEMISTRY



PUBLISHED BIWEEKLY BY THE AMERICAN CHEMICAL SOCIETY

THE JOURNAL OF PHYSICAL CHEMISTRY

BRYCE CRAWFORD, Jr., Editor
STEPHEN PRAGER, Associate Editor
ROBERT W. CARR, Jr., **C. ALDEN MEAD**, Assistant Editors

EDITORIAL BOARD: C. A. ANGELL (1973-1977), F. C. ANSON (1974-1978), V. A. BLOOMFIELD (1974-1978), J. R. BOLTON (1976-1980), L. M. DORFMAN (1974-1978), W. E. FALCONER (1977-1978), H. L. FRIEDMAN (1975-1979), H. L. FRISCH (1976-1980), W. A. GODDARD (1976-1980), E. J. HART (1975-1979), W. J. KAUFMANN (1974-1978), R. L. KAY (1977-1981), D. W. McCLURE (1974-1978), K. MYSELS (1977-1981), R. M. NOYES (1973-1977), R. G. PARR (1977-1979), W. B. PERSON (1976-1980), J. C. POLANYI (1976-1980), S. A. RICE (1976-1980), F. S. ROWLAND (1973-1977), R. L. SCOTT (1973-1977), W. A. STEELE (1976-1980), J. B. STOTHERS (1974-1978), F. A. VAN-CATLEDGE (1977-1981), B. WEINSTOCK (1977)

Published by the
AMERICAN CHEMICAL SOCIETY
BOOKS AND JOURNALS DIVISION

D. H. Michael Bowen, Director
Marjorie Laffin, Assistant to the Director

Editorial Department: Charles R. Bertsch,
Head; Marianne C. Brogan, Associate
Head; Celia B. McFarland, Joseph E.
Yurvati, Assistant Editors

Magazine and Production Department:
Bacil Guiley, Head

Research and Development Department:
Seldon W. Terrant, Head

Advertising Office: Centcom, Ltd., 25 Sylvan
Road South, Westport, Conn. 06880.

© Copyright, 1977, by the American
Chemical Society. No part of this publication
may be reproduced in any form without
permission in writing from the American
Chemical Society.

Published biweekly by the American
Chemical Society at 20th and Northampton
Sts., Easton, Pennsylvania 18042. Second
class postage paid at Washington, D.C. and
at additional mailing offices.

Editorial Information

Instructions for authors are printed in
the first issue of each volume. Please conform
to these instructions when submitting man-
uscripts.

Manuscripts for publication should be
submitted to *The Journal of Physical
Chemistry*, Department of Chemistry, Uni-
versity of Minnesota, Minneapolis, Minn.
55455. Correspondence regarding **accepted
papers and proofs** should be directed to the

Editorial Department at the address below.

Page charges of \$60.00 per page may be
paid for papers published in this journal.
Payment does not affect acceptance or
scheduling of papers.

Bulk reprints or photocopies of indi-
vidual articles are available. For information
write to Business Operations, Books and
Journals Division at the ACS Washington
address.

Requests for **permission to reprint**
should be directed to Permissions, Books and
Journals Division at the ACS Washington
address. The American Chemical Society and
its Editors assume no responsibility for the
statements and opinions advanced by con-
tributors.

Subscription and Business Information

1977 Subscription rates—including surface
postage

	U.S.	PUAS	Canada, Foreign
Member	\$24.00	\$33.00	\$34.00
Nonmember	96.00	105.00	106.00
Supplementary material	15.00	19.00	20.00

Air mail and air freight rates are avail-
able from Membership & Subscription Ser-
vices, at the address below.

New and renewal subscriptions should
be sent with payment to the Office of the
Controller at the ACS Washington address.

Changes of address must include both old
and new addresses with ZIP code and a recent
mailing label. Send all address changes to
Membership & Subscription Services. Please
allow six weeks for change to become effec-
tive. **Claims for missing numbers** will not
be allowed if loss was due to failure of notice
of change of address to be received in the time

specified: if claim is dated (a) North Amer-
ica—more than 90 days beyond issue date, (b)
all other foreign—more than 1 year beyond
issue date; or if the reason given is "missing
from files". Hard copy claims are handled by
Membership & Subscription Services.

Microfiche subscriptions are available
at the same rates but are **mailed** first class to
U.S. subscribers, air mail to the rest of the
world. Direct all inquiries to Special Issues
Sales, at the ACS Washington address or call
(202) 872-4554. **Single issues** in hard copy
and/or microfiche are available from Special
Issues Sales at the ACS Washington address.
Current year \$4.75. Back issue rates available
from Special Issues Sales. **Back volumes** are
available in hard copy and/or microform.
Write to Special Issues Sales at the ACS
Washington address for further information.
Microfilm editions of ACS periodical pub-
lications are available from volume 1 to the
present. For further information, contact
Special Issues Sales at the ACS Washington
address. **Supplementary material** men-
tioned in the journal appears in the microfilm
edition. Single copies may be ordered directly
from Business Operations, Books and Jour-
nals Division, at the ACS Washington ad-
dress.

	U.S.	PUAS, Canada	Other Foreign
Microfiche	\$2.50	\$3.00	\$3.50
Photocopy			
1-7 pages	4.00	5.50	7.00
8-20 pages	5.00	6.50	8.00

Orders over 20 pages are available only on
microfiche, 4 × 6 in., 24X, negative, silver
halide. Orders must state photocopy or mi-
crofiche if both are available. Full biblio-
graphic citation including names of all au-
thors and prepayment are required. Prices
are subject to change.

American Chemical Society
1155 16th Street, N.W.
Washington, D.C. 20036
(202) 872-4600

Editorial Department
American Chemical Society
P.O. Box 3330
Columbus, Ohio 43210
(614) 421-6940 ext 3171

Membership & Subscription Services
American Chemical Society
P.O. Box 3337
Columbus, Ohio 43210
(614) 421-7230

THE JOURNAL OF
PHYSICAL CHEMISTRY

Volume 81, Number 21 October 20, 1977

JPCHAx 81(21) 1967-2044 (1977)

ISSN 0022-3654

- Photochemistry of Some Azoalkanes at High Pressures **S. Chervinsky and I. Oref*** 1967
- Yield and Decay of the OH Radical from 200 ps to 3 ns
. **Charles D. Jonah* and John R. Miller** 1974
- Vapor-Phase Charge-Transfer Complexes. 10. Iodine Complexes of Methanol, Ethanol,
and Diethyl Ether **Hing-Cheung Tse and Milton Tamres*** 1977
- Pressure Dependence of the Rate Constant of the Reaction $H + CH_3 \rightarrow CH_4$
. **Jung-Tsang Cheng and Chuin-tih Yeh*** 1982
- Redox Mechanisms in an Ionic Matrix. 5. A Kinetic Study on the Direct and Autocatalytic Process
 $H_2 + NO_3^- = H_2O + NO_2^-$ in Molten Alkali Nitrates
. **E. Desimoni, F. Paniccia,* and P. G. Zamboni** 1985
- Model Calculations Describing Bistability for the Stirred Flow Oxidation of Cerous Ion by Bromate
. **K. Bar-Eli and Richard M. Noyes*** 1988
- The Influence of Solvent upon Linear Enthalpy-Entropy Relationships. Proton Ionization of
Substituted Piperidines in Water-Ethanol Mixtures
. **Guy Berthon,* Marie-Jose Blais, and Octavian Enea** 1991
- The Ionization of 4-Nitrophenylacetonitrile in Water-Dimethyl Sulfoxide Mixtures
. **Edward A. Walters** 1995
- Binding of Hydrogen Ions to Anionic Micelles
. **Clifford A. Bunton,* Klaus Ohmenzetter, and Luis Sepulveda*** 2000
- The Interaction of CO with Very Small Copper Clusters **M. Moskovits* and J. E. Hulse** 2004
- Excimer-Monomer Emission Ratio in Electrochemiluminescence **Csaba P. Keszthelyi*** 2009
- Calculation of the Energies of Activation for Some Gas-Phase Reactions
. **Thomas N. Bell and Peter G. Perkins*** 2012
- The Generalized Conductance Equation **Mou-Shan Chen* and Lars Onsager** 2017
- Compatibility of Conductance Equations with Onsager's Reciprocal Relation **Mou-Shan Chen** 2022
- Electric Transport in Polyelectrolyte Solutions **Marie Kowblansky and Paul Ander*** 2024
- Activation Parameters for the Diffusion and Viscosity of Ca^{2+} and Ce^{3+} and Their Chelates with
EDTA and DCTA in Aqueous Solution
. **P. L. Mateo,* G. G. Hurtado, and J. B. Vidal-Abarca** 2032
- External Heavy-Atom Effect on the Room-Temperature Luminescence of Adsorbed Dyes
. **Wayne White and Paul G. Seybold*** 2035
- The 123.6-nm Photolysis of 1,2-Fluorochloroethane and 1,1,1-Difluorochloroethane
. **T. Ichimura, A. W. Kirk, and E. Tschuikow-Roux*** 2040

There is no supplementary material for this issue.

* In papers with more than one author, the asterisk indicates the name of the author to whom inquiries about the paper should be addressed.

มหาวิทยาลัยเกษตรศาสตร์
ห้องสมุด

21. ต.ค. 2520

AUTHOR INDEX

- Ander, P., 2024
Bar-Eli, K., 1988
Bell, T. N., 2012
Berthon, G., 1991
Blais, M.-J., 1991
Bunton, C. A., 2000
Chen, M.-S., 2017, 2022
Cheng, J.-T., 1982
Chervinsky, S., 1967
Desimoni, E., 1985
Enea, O., 1991
Hulse, J. E., 2004
Hurtado, G. G., 2032
Ichimura, T., 2040
Jonah, C. D., 1974
Keszthelyi, C. P., 2009
Kirk, A. W., 2040
Kowblansky, M., 2024
Mateo, P. L., 2032
Miller, J. R., 1974
Moskovits, M., 2004
Noyes, R. M., 1988
Ohmenzetter, K., 2000
Onsager, L., 2017
Oref, I., 1967
Paniccia, F., 1985
Perkins, P. G., 2012
Sepulveda, L., 2000
Seybold, P. G., 2035
Tamres, M., 1977
Tschuikow-Roux, E., 2040
Tse, H.-C., 1977
Vidal-Abarca, J. B., 2032
Walters, E. A., 1995
White, W., 2035
Yeh, C., 1982
Zambonin, P. G., 1985

THE JOURNAL OF PHYSICAL CHEMISTRY

Registered in U.S. Patent Office © Copyright, 1977, by the American Chemical Society

VOLUME 81, NUMBER 21 OCTOBER 20, 1977

Photochemistry of Some Azoalkanes at High Pressures

S. Chervinsky and I. Oref*

Department of Chemistry, Technion, Israel Institute of Technology, Haifa, Israel (Received April 18, 1977)

The photochemical decomposition of *trans*-azomethane, *trans*-azoethane, *trans*-azo-*n*-propane, and *trans*-azoisopropane was investigated at high helium and CO₂ pressures. It was found that the experimental results can be explained by assuming decomposition from fast and slow channels. Models which identify these channels are discussed. The slow channel rate coefficients for decomposition were found to be $k_R > 4.0 \times 10^{10}$, 6×10^9 , 4×10^7 , and $5 \times 10^8 \text{ s}^{-1}$, respectively; values for the fast channel rate coefficients, k_N , and the intramolecular rate coefficient, λ , are reported for various models of the fast channel. Sensitized photolysis is compared with direct photolysis in the gas phase, and thermalized excited electronic states are discussed and ruled out on the basis of the available experimental data.

Introduction

Existing statistical theories account very well for the observed behavior in a variety of unimolecular decomposition systems,¹ both thermal as well as non-Boltzmann systems such as photochemical, chemical activation, and molecular beam.^{1,2} The underlying principle is that the excitation energy has ample time to be statistically distributed among the normal modes of the reacting molecule. This intramolecular process is fast but under proper experimental conditions, such as high pressure, can be intercepted. Under such conditions less prominent contributions to decomposition emanating, for example, from a nonrandom channel^{3,4} may be uncovered. This contribution may be small, to be sure, but whenever detectable, provides a convenient method for calculating the intramolecular energy transfer rate within the excited molecule.

In the present work, the unimolecular decomposition of a photoexcited homologous series of *trans*-azoalkanes was investigated. The energy is introduced into the chromophore located at the center of the molecule, from whence the energy flows into the rest of the normal modes of the molecule. The longer the alkyl chain, the larger the number of modes and smaller the average energy per mode and rate coefficient for decomposition. On the other hand, any nonstatistical behavior involves only those parts of the molecule which include the absorbing and decomposing bonds and, therefore, is not necessarily a function of the

number of normal modes of the molecule but depends on the particular structural relation involved. For the azoalkanes, R-N=N-R, the absorbing and decomposing bonds are in close proximity and, therefore, the nonrandom behavior does not involve all the normal modes of the molecule.

Azoalkanes have a broad absorption band with a maximum around 360 nm, which is due to the $n\pi^*$ transition.⁵ The acyclic compounds do not phosphoresce or fluoresce,^{5,6} and in the gas phase decompose, in the primary step, to give N₂ and alkyl radicals,⁶⁻⁸ R-N=N-R + $h\nu \rightarrow 2R + N_2$. In the liquid phase, however, the primary process is *trans*-*cis* isomerization^{6,8} with only 1% of R₂ elimination.⁹ The basic low pressure mechanism for the decomposition of the azoalkanes is given by the following steps (where the asterisk denotes vibrational excitation):



A Stern-Volmer plot of ϕ^{-1} vs. [M], where ϕ is the quantum yield, should give a straight line from which slope k_a can be found. At high pressure, however, the line is not straight which indicates that other processes are taking place as well. The nature of the excited species at low and

high pressures and the reasons for the curvature in the Stern–Volmer plot will be discussed after the experimental results are presented.

Experimental Section

The experimental system consists of four main parts: (a) a low pressure gas handling glass system; (b) a stainless steel high pressure system and cell with 2.5-cm quartz windows; (c) a light source which is a 500-W high pressure mercury lamp and filters; (d) an on line gas chromatograph to detect the reaction products, mainly N_2 . The light absorbed during the reaction was detected by a digital integrator into which the differential current of a pair of RCA IP39 photodiodes was fed. The reading on the integrator was directly proportional to the number of photons absorbed by the system.

Azomethane was synthesized by the methods of Renaud and Leitch.¹⁰ The rest of the azoalkanes were obtained from Merck Sharp and Dohme of Canada. Each substance was purified by fractional distillation and no impurities were detected by chromatographic analysis on 20% dioctylphthalate on Chromosorb W. When not in use, the samples were kept at liquid air temperature. The He bath gas was obtained from Air Precision and was 99.995% pure. 99.99% CO_2 was obtained from Matheson.

Experimental Results

The quantum yield for azomethane in the pressure range up to 100 atm of He ($\omega = 1.34 \times 10^{12} \text{ s}^{-1}$) was 1.0 ± 0.05 . For CO_2 as bath gas, the quantum yield for decomposition up to a pressure of 45 atm ($\omega = 5.4 \times 10^{11} \text{ s}^{-1}$) was 0.96 ± 0.07 . This agrees well with low pressure work on the photolysis of azomethane.¹¹ The experimental results of the photolysis of azoethane, azo-*n*-propane, and azoisopropane in the presence of an inert bath gas are given in Figures 1–4. The reactant pressure never exceeded 5 cmHg and the percent conversion was kept below 5%. The Stern–Volmer plots are curved in contrast to the behavior expected from the simplistic mechanism proposed in eq I–III.

The Photochemical Mechanism for Decomposition

Curved Stern–Volmer plots for azoalkanes have been detected previously,^{7,8,11,12} but the experiments were never carried to very high pressures. The extended pressure range helps delineate the complex mechanism which is taking place during decomposition. We adopt the procedure used previously⁴ and list the possible reactions which might take place. Then by matching theory, the solid line in Figures 1–4, with experiment, the relative contribution of each channel is systematically investigated.

The general mechanism for the photolysis of azoalkane can be summed up by the following set of equations:

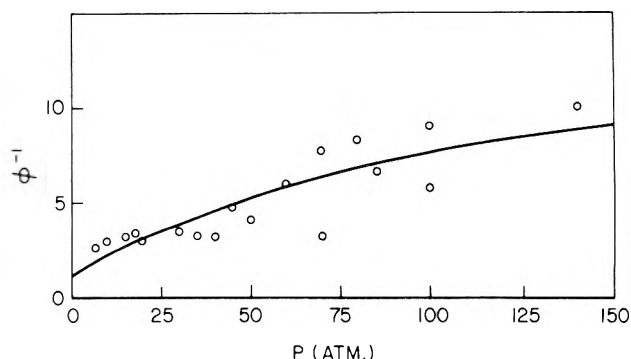
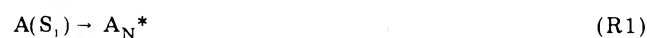


Figure 1. Reciprocal quantum yield of azoethane decomposition vs. He pressure: points, experimental results; full line, least-squares fit to eq 2; $\lambda = 366 \text{ nm}$; $T = 298 \text{ K}$.

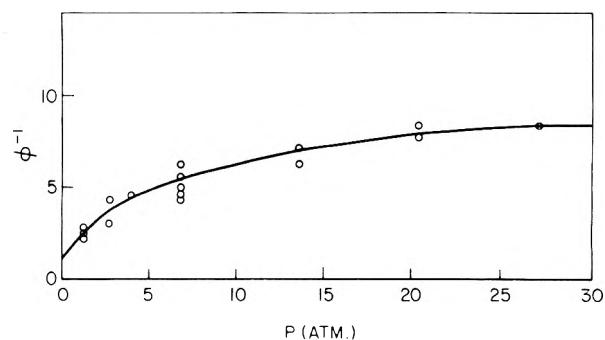


Figure 2. Reciprocal quantum yield of azoethane decomposition vs. CO_2 pressure: points, experimental results; full line, least-squares fit to eq 2; $\lambda = 366 \text{ nm}$, $T = 298 \text{ K}$.

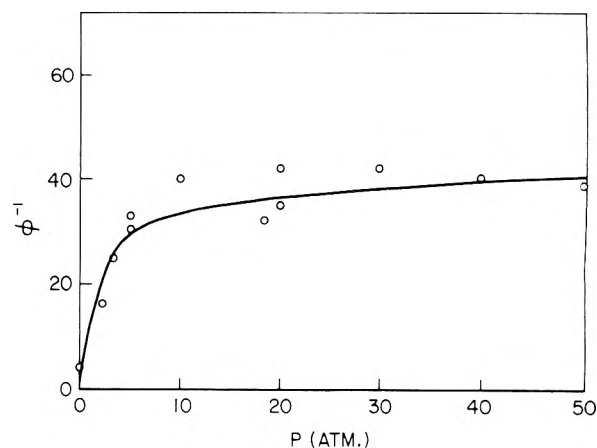


Figure 3. Reciprocal quantum yield of azo-*n*-propane decomposition vs. He pressure: point, experimental results; full line, least-squares fit to eq 2; $\lambda = 366 \text{ nm}$, $T = 298 \text{ K}$.

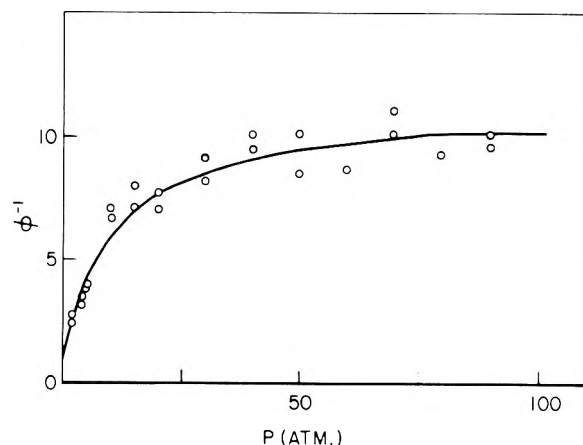


Figure 4. Reciprocal quantum yield of azoisopropane decomposition vs. He pressure: points, experimental results; full line, least-squares fit to eq 2; $\lambda = 366 \text{ nm}$, $T = 298 \text{ K}$.

TABLE I: Experimental Parameter Obtained by a Least-Squares Fit of Eq 2 to the Data Represented in Figures 1-4

	Azo-meth-ane	Azo-ethane	Azo-n-propane	Azo-isopro-pane
$\sigma, \text{\AA}$	6.5	7.5	8.5	8
$A(\text{He}), \text{atm}^{-1}$	0	0.08	14	1.1
$A(\text{CO}_2), \text{atm}^{-1}$	0	1.25		
$B(\text{He})$		0.02	0.02	0.09
$B(\text{CO}_2)$		0.09		
$\langle E_{\text{thermal}} \rangle, \text{kcal mol}^{-1}$	1.2	3.0	4.2	4.2

^a Values were calculated from the equation²⁷ $\sigma(\text{\AA}) = 7 + (n - 5)/2$. n is the number of atoms in the molecule. Values of azoethane used elsewhere are 7 \AA (ref 11), 7.7 \AA (ref 7). $\sigma = 7$ \AA was used for azoisopropane in ref 8. This value is a little smaller when compared with the value of σ (azoethane).

The subscripts N and R denote nonrandom and random, respectively. The asterisk denotes a vibrationally excited species.

The essence of the mechanism is as follows. The molecule is excited electronically (R0) by an n, π^* transition. It then undergoes (R1) intersystem crossing into a state A_N^* , later identified as a particular configuration of S_1 or T_1 , in such a manner that all available excess vibrational energy concentrates in part of the molecule. The excited moiety, in whose modes excess vibrational energy is statistically distributed, can decompose (R2) or lose energy by redistribution of energy in all available molecular modes via intramolecular processes (R3) or perturbing collisions (R4). It can as well be deactivated by collisions (R5). The energy randomized excited molecule decomposes (R6) or is deactivated (R7). Application of the steady state assumption and comparison of the

model with experimental results by a least-squares technique indicates that a good match is possible only when intramolecular energy transfer by elastic collisions (R4) and the nonrandom moiety deactivation (R5) play an insignificant role and can be ignored.

The expression for the quantum yield based on the above mechanism is

$$\phi^{-1} = \frac{1 + AP}{1 + ABP} \quad (1)$$

$$A = \beta k_{-RR} / k_R \quad B = k_N / (k_N + \lambda) \quad (2)$$

where β is the collisional efficiency. At high enough pressure (P), ϕ^{-1} approaches a constant value different than unity. A is the usual Stern-Volmer coefficient which is obtained from eq I-III, while B is the contribution of the nonrandom channel which is important only at high pressures due to deactivation of the random channel which makes the contribution to decomposition from the latter negligible.

The values of A and B are given in Table I. The experimental values of k_R were calculated from eq 2 and are given in Table II. $\beta = 0.02$ for He was found previously⁷ in the case of azoethane and was kept at this value for the rest of the homologous series. $\beta = 0.3$ was used⁸ for the collisional efficiency of CO_2 and azoethane. $\sigma_{\text{He}} = 2.6$ \AA and $\sigma_{\text{CO}_2} = 3.2$ \AA. The procedure for the calculations of k_{-RR} is given in the Appendix and in ref 7.

Calculation of the Individual Rate Coefficients

For the mechanism proposed above to be true, the following must hold: (a) The random rate coefficient, k_R , obtained from A should agree with low pressure data (ours and others). (b) The nonrandom rate coefficient, k_N , should have some physical meaning. (c) The intramolecular energy transfer coefficient, λ , should have the same

TABLE II: Summary of Experimental and Calculated Parameters for the Azoalkane Series

	Azomethane	Azoethane	Azo-n-propane	Azoisopropane
Experimental Results				
$k_R(\text{expt, He}), \text{s}^{-1}$	$> 4 \times 10^{10}$	6×10^9	4×10^7	4×10^8
$K_R(\text{expt, CO}_2), \text{s}^{-1}$		2.5×10^9		
$k_R(\text{expt}), \text{s}^{-1}$		3.8×10^9		1.1×10^8
Decomposition from T_1				
$E_T(\text{RRKM}), \text{kcal mol}^{-1}$	54.3	54.3	55.5	56.5
$E_T, \text{kcal mol}^{-1}$	55.0 ± 1.5	55.0 ± 1.5	55.5 ± 1.5	56.5 ± 1.5
$E_0(T_1), \text{kcal mol}^{-1}$	12.3	12.3	12.3	12.3
$E^*(T_1), \text{kcal mol}^{-1}$	24	26	27	27
$k_R(\text{calcd, } T_1), \text{s}^{-1}$	2.0×10^{10}	3.0×10^9	2×10^8	3×10^8
$k_N(\text{calcd, } T_1), \text{s}^{-1}$		4.8×10^{10}	5.9×10^{10}	7.4×10^{10}
λ, s^{-1}		2.4×10^{12}	2.9×10^{12}	7.5×10^{11}
		(CO_2 4.8×10^{11})		
Decomposition from S_1				
$E_S(\text{RRKM}), \text{kcal mol}^{-1}$	67	67	67	67
$E_S, \text{kcal mol}^{-1}$	66.7 ^d			$< 68^e$
$E_0(S_1), \text{kcal mol}^{-1}$	7.1	7.1	7.1	7.1
$E^*(S_1), \text{kcal mol}^{-1}$	12	14	15	15
$k_R(\text{calcd, } S_1), \text{s}^{-1}$	1.8×10^{10}	5.2×10^9	1.4×10^9	1.9×10^9
$k_N(\text{calcd, } S_1), \text{s}^{-1}$		5.9×10^{10}	8.4×10^{10}	7.0×10^{10}
λ, s^{-1}		2.9×10^{12}	4.1×10^{12}	7×10^{11}
		(CO_2 6×10^{11})		
Decomposition from S_0				
$E_a(\text{thermal}), \text{kcal mol}^{-1}$	52.5 ^f	49.7 ^g	47.7 ^h	47.9 ^g
$A(\text{thermal}), \text{s}^{-1}$	1.6×10^{16f}	2.5×10^{16g}	2.5×10^{15h}	4×10^{16g}
$E^*(\text{thermal}), \text{kcal mol}^{-1}$	79	81	82	82
$k_R(\text{calcd, } S_0), \text{s}^{-1}$	1.0×10^{10}	1.8×10^8	1.3×10^6	3×10^7

^a This work. ^b For azoethane ref 11 and 25; for azoisopropane, ref 8, 12, and 26. ^c Reference 16. ^d Reference 39. ^e Reference 6. ^f Reference 21 gives $E_a = 55.5$ kcal mol⁻¹ and $A = 17.3$ s⁻¹. ^g Reference 7. ^h The calculated value using ref 20, which agrees exactly with ref 19, is 50 kcal mol⁻¹. The experimental value of ref 18 is for the high temperature range, which is the most appropriate here. E^* is the internal vibrational energy of the excited molecule.

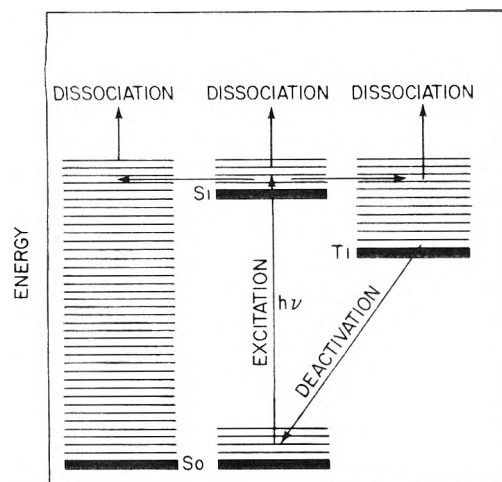


Figure 5. Energy level diagram of azoalkanes. Arrows indicate various possible channels for energy disposition.

magnitude reported for other similar processes.^{3,4,13,14} (d) The detailed parameters used in RRKM calculations of k_R and k_N should be self-consistent throughout the homologous series. The major problem in the calculation of k_R and k_N is to identify and define the physical structure of A_R and A_N and the physical parameters associated with them. There are two possibilities for the unimolecular decomposition of A . One is from an excited electronic state S_1 and/or T_1 ^{7,11,12,15} and the other from a ground state.⁸ The energetics are summarized in Figure 5. Next we calculate k_R and k_N for the molecule in S_1 or T_1 or S_0 states and compare calculations with experiment.

Decomposition from T_1 . When decomposition from the T_1 state is considered, it is found that the rate coefficient k_R can be calculated and made to agree in a consistent way with the experimental results without arbitrarily changing any of the values used in the calculation. Once E_0 was determined, it was kept constant for the whole series. It is found that agreement with experimental results require the RRKM calculated k_R to have an electronic level at 55 kcal mol⁻¹ consistent with the T_1 state of azoalkanes.¹⁶

Next, the configuration of the nonrandom channel is considered. It was found in the present experiments that the quantum yield of azomethane is unity at pressures of up to 100 atm of He and 45 atm of CO₂. This indicates a very fast channel with high values of k . Therefore, the azomethylene group in the T_1 state, which is located around the chromophore, can be identified with the fast nonrandom channel.^{3,4} RRKM calculations of k with N in this configuration agree with experimental results. These data are given in Table II.

Decomposition from S_1 . The S_1 state is^{6,16} ~67 kcal mol⁻¹ above S_0 . It is found that k_R for azomethane can be calculated and made to agree with the experimental value if E_0 is taken to be 7.1 kcal mol⁻¹. However, when this value of E_0 is applied to other members of the homologous series, no agreement is obtained. The discrepancy, as can be seen from Table II, is more than an order of magnitude for the azopropanes. It is tempting to identify, however, the fast channel with decomposition from S_1 . In such a case, λ can be interpreted as the intersystem crossing rate constant which is calculated from eq 2 to be $\sim 2.6 \times 10^{11}$, 6.9×10^{10} , and 1.8×10^{10} s⁻¹ for azoethane, azo-*n*-propane, and azoisopropane, respectively. These values of λ are 3 and 4 orders of magnitude larger for azopropane and azoethane, respectively, than the values for the $S_1 \rightarrow T_1$ intersystem crossing in aliphatic ketones.^{13b} If $S_1 \rightarrow T_1$ in azoalkanes is, unlike that in ketones, very fast and is represented by the values of λ reported above, then S_1 can

be identified as the physical entity of N .

Another possibility to consider is the assumption that the energy is not randomized on the time scale of the intersystem crossing process. N in this case is identified with the azomethylene group in the S_1 state. The values of k_N and λ agree for the homologous series and the values of λ reported before.^{3,4,13,14}

Decomposition from S_0 . RRKM calculation on a model where the azo compound decomposes from the ground state does not agree with the experimental results as can be seen from Table II. The results are, on the average, a factor of 20 below the experimental ones. The values of the A factor ($e(kT/h)e^{-\Delta S^\ddagger/R}$) are⁸ $1.6 - 4 \times 10^{16}$ s⁻¹ and the activation energy is in the range 52–48 kcal mol⁻¹ except for azo-*n*-propane where the reported values¹⁸ are smaller. For azomethane there is one value of A which is larger²¹ and two which are smaller.¹¹ We use values which are consistent with the rest of the homologous series.

There is the possibility, suggested by Fogel and Steel,⁸ that some azoisopropane decomposes from the *cis* configuration of the ground state molecule. The values for A and E_0 as reported by them are 3.1×10^{17} s⁻¹ and 40.7 kcal mol⁻¹, respectively. The combined increase of order of magnitude in the value of the A factor and decrease of 13%, relative to *trans*, of the value of E_0 gives an RRKM value of $k_R = 4 \times 10^9$ s⁻¹. This can be identified as a "fast" channel as compared with the *trans* decomposition which is the "slow" channel. The superposition of the two channels can give a curved ϕ^{-1} vs. P line. The *cis* channel model cannot be verified for lower members of the homologous series since it cannot be isolated and the thermal A factor and E_0 are not known. In addition, the agreement between the calculated and experimental results is only semiquantitative since the slope of the experimental and theoretical k vs. E do not agree.⁸

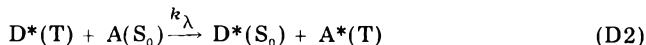
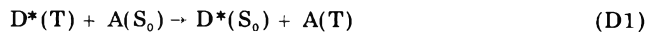
Possible Decomposition Channels. The values of k_R and k_N calculated by RRKM method and found experimentally are summarized in Table II. Details of the calculations are given in the Appendix. The results are consistent with the low pressure data as well as with independent spectroscopic measurements of the singlet and triplet levels.¹⁶ The value $E_0 = 12.3$ kcal mol⁻¹ above T_1 used in the calculation of k_R and k_N is in agreement with previous work.^{7,15} Based on the discussion above, it can be concluded that the main decomposition channel, R , is from the vibrationally excited T_1 . The fast channel is either from random S_1 or nonrandom S_1 or T_1 state, all of which require a large value for the intersystem rate constant. The concept of a fast channel, in which all available energy is confined to a fraction of phase space, is realistic since both absorbing and decomposing parts belong to the same energy-rich part of phase space. The calculated results are corroborative in nature and cannot be taken as a proof of the proposed mechanism since the vibrational frequencies and geometry of the electronically excited molecules are not known in detail.

Triplet Sensitized Decomposition of Azoalkanes

It is known that azoalkane decomposes following triplet energy transfer from a variety of triplet donors. This effect can be taken as a direct proof that azoalkanes decompose via the T_1 state.²² However, the quantum yield for this decomposition is smaller than unity and smaller than the case of direct irradiation. This was taken by Fogel and Steel⁸ as a support for the argument that there are two different mechanisms for photolysis and triplet sensitization. We consider next the triplet transfer efficiencies and show that, for a polyatomic donor with triplet level of the same value as the energy of the photon in direct

photolysis, the quantum yield of the former is only a fraction of the latter. We give only a summary of the treatment; the full development is given elsewhere.²³

Triplet energy transfer occurs via a tight complex which is formed between donor and acceptor molecules. The excess energy above the zero level of the acceptor triplet is statistically distributed among all the normal modes of the complex. The transfer reactions are written as follows



Reaction D1 describes a case in which the acceptor molecule A is left with vibrational energy below the threshold energy for decomposition E_0 . (D2) describes a case where A has energy above E_0 and hence can decompose. The asterisk denotes vibrational excitation above the zero triplet level; D denotes donor molecule; T and S are triplet and singlet, respectively; k_λ is the probability of the event which is a function of the irradiation wavelength, λ .

The probability of finding energy E_A in the acceptor molecule when there is total available energy E_T^+ in the complex is²³

$$P(E_T^+, E_A) = N^+(E_A) \sum_{E^*=0}^{E_D} P_D(E^+) / \sum_{E^*=0}^{E_T^+ - \epsilon_0} P_C(E^+) \quad (4)$$

$$E_D = E_T - E_A - \epsilon_0$$

$$E_T^+ = E_T - \epsilon_0$$

$$E_T = W_D + W_A + \lambda_D - T_A$$

W_D and W_A are the thermal energy of donor and acceptor, respectively. λ_D is the irradiation energy and T_A the triplet level of the acceptor. ϵ_0 is the minimum energy for the dissociation of the complex. $N^+(E_A)$ is the density of states of the acceptor after the triplet energy was transferred from D to A. E_D is the energy available for distribution in the donor molecule including the transition modes. $\sum P_D(E^+)$ is the sum of states of all modes not including the acceptor's and reaction coordinate and $\sum P_C(E^+)$ is the sum of the states of the complex excluding the reaction coordinate.

The quantity of interest is the fraction of molecules with energy above E_0 . This is obtained by integrating (4) over the appropriate limits.

$$P(E_T^+, E_0) = \frac{\int_{E_0}^{E_T^+} P(E_T^+, E_A) dE_A}{\int_0^{E_T^+} P(E_T^+, E_A) dE_A} \quad (5)$$

$P(E_T^+, E_0)$ is the probability that on a collision between $D^*(T)$ and $A(S_0)$ enough energy will be transferred to A to enable it to further decompose into products. If λ_D is large enough so that the distribution is almost a δ function at some energy above E_0 , then $P(E_T^+, E_0)$ is a good approximation to k_λ . However, if λ_D is $\sim T_A$ and E_T is below E_0 , it is necessary to convolute (5):

$$k_\lambda = \frac{\int_{E_0 - \Delta E_T}^{\infty} \sum_j B(W_A) B(W_D) dW \int_{E_0}^{E_T^+} P(E_T^+, E_A) dE_A}{\int_{E_0}^{E_T^+} P(E_T^+, E_A) dE_A} \quad (6)$$

$$\Delta E_T = \lambda_D - T_A$$

W is the thermal internal energy and

$$B(W_i) = \frac{N(W_i) e^{-W_i/RT}}{\int_0^{\infty} N(W_i) e^{-W_i/RT} dW_i} \quad (7)$$

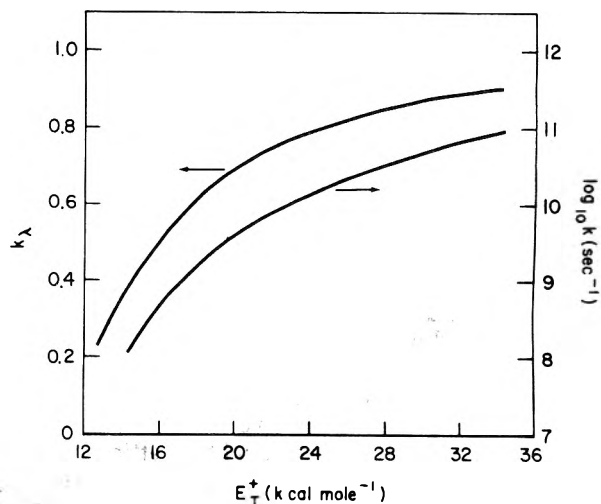


Figure 6. Left coordinate: Triplet transfer efficiency for acetone-*d*₆-azomethane vs. total available energy of the triplet transfer complex. Right coordinate: log of unimolecular rate coefficient of azomethane (T_1) calculated by RRRKM.

The index j is over all combination of W_A and W_D such that a given W is obtained. The total quantum yield is given by

$$\phi = \int_{E_0}^{E_T} \frac{k_R k_\lambda g(E)}{k_R + \omega} dE \quad (8)$$

where $g(E)$ is the normalized energy profile function,⁷ and ω the collisional frequency.

We have calculated the value of ϕ for the pair azomethane-acetone-*d*₆. This is an interesting case since the internal energy of the pair plus the thermal energy is equal to that of the direct photolysis of azomethane by a 360-nm photon which has a quantum yield of unity up to very high pressures.⁷ k_λ as a function of E_T^+ was calculated from eq 5 and is given in Figure 6. The value of k_R was calculated by RRRKM and is given as well in Figure 6. It is found that for $E_T^+ = 25$ kcal mol⁻¹ and $E_0 = 12.3$ kcal mol⁻¹, $k_\lambda = 0.8$ and $k_T = 2 \times 10^{10}$ s⁻¹. Substituting these values into eq 8 and letting $g(E) = 1$ (a delta function excitation) we obtain for pressures of 13 and 154 Torr the values of 0.78 and 0.66, respectively; that is to say, ϕ is smaller than unity, and at the lower pressure limit, $\phi_0 = k_\lambda = 0.8$. It is worthwhile to point out that the details of the complex are not known and E_0 can vary as well. However, consistency is required with k_R (expt) and therefore these values cannot be too far off. 50% changes in the value of ϕ can no doubt be expected. The experimental values reported for this pair is 0.52 and 0.31 for 13 and 154 Torr, respectively.²⁸ Similar calculations for the benzene-azoisopropane pair gave $\phi = 0.45$, again larger than the experimental value⁸ of ~ 0.1 but smaller than the value expected from direct photolysis.

Calculations on biacetyl-azomethane and -azoethane pairs indicate that ϕ is very small in all cases at 300 K since the biacetyl triplet is about the same as the azo triplet¹⁶ and therefore the latter is hardly excited vibrationally. The only contribution to decomposition is from the high energy tail of the Boltzmann distribution. At elevated temperature the sensitizers, including biacetyl, are expected to be more efficient since the average internal energy of the system is higher and therefore the fraction of acceptor molecules with energy above E_0 is higher.

It seems clear that there is no direct correspondence between direct photolysis and triplet transfer decomposition and care should be taken when such comparison is

made. In addition to donor-acceptor distribution of energy, discussed above, which tends to put an upper limit on ϕ , there are other factors which influence ϕ . The interatomic potential is no doubt not spherical symmetric and some orientations are not favorable to the formation of the donor-acceptor complex. This produces a macrosteric factor which will reduce ϕ further.

It is evident that there is a distinction, not only between direct photolysis and triplet sensitization but, also, between triplet quenching and quantum yield. A donor can be efficiently quenched, but the energy thus transferred to the acceptor will not cause it to decompose if its internal energy is below E_0 .

The above case exists in solutions where ϕ values for decomposition are known to be very small but quenching is still efficient.⁸ The reason might be efficient energy transfer to the solvent which reduces the internal energy of the acceptor below E_0 . It was shown⁸ that the quantum yield for cis-trans isomerization of azoisopropane in solution is larger for cis going to trans than the reverse case, the ratio of the two being ~ 15 . For direct photolysis, this ratio is ~ 1 . This was taken as a proof that the latter mechanism is different than the former. This need not be the only explanation. The ease of forming the donor-acceptor complex, the steric factor, has to be taken in consideration. The donor-cis acceptor is easier to form than the donor-trans acceptor, and if inversion or rotation is the preferred isomerization route, one can postulate a reaction coordinate along which the ground state donor is leaving and the acceptor inverting at the same time, a situation much preferable for the cis form.

Decomposition from Thermally Equilibrated Electronically Excited State

Pritchard, Servedio, and Marchant,¹² PSM, have proposed a modification of the triplet decomposition model based on work by Porter and Connelly who used classical RRRK expression.²⁹ PSM's proposition is that some molecules in S_1 and T_1 states achieve a thermal equilibrium and further decompose when a "thermal" barrier in the excited states is overcome. Curvature in ϕ^{-1} vs. P plots is expected since there is simultaneous decomposition from S_1 and T_1 . Another option¹² is simultaneous decomposition from initially "hot" and "thermally equilibrated" T_1 . The increase in ϕ with temperature was attributed to the higher probability of overcoming a thermal barrier in the triplet state.

This model is unnecessarily complicated. It is well known from chemical activation²⁷ as well as photochemical studies^{7,15} that the effect of raising the temperature is to increase the average energy of the molecule. Since k is a function of the energy, Figure 6, it will increase as E increases.

It was found by Cerfontain and Kutschke²⁵ that the photochemical decomposition of azoethane at several temperatures yields an "activation energy" ~ 2 kcal mol⁻¹ compared with $E_0 = 12.3$ kcal mol⁻¹ found earlier from RRRKM calculations^{7,15} as well as in the present work. There is no discrepancy if it is realized that the first number is an indication of the increase in the energy content of the electronic ground state molecule and the second number a true E_0 for decomposition.

In the model for thermal equilibration of the S_1 state, it was assumed that dissociation from this state is slow and thus lives long enough to be thermally equilibrated. This is not applicable to the present system where intersystem crossing is fast as discussed before. This case is equivalent to the high energy case of ref 29 where the same points are made.

The lifetime of T_1 is not known, but it must be short since no phosphorescence is detected. Since the T_1 surface crosses the S_0 surface for diimide,³⁰ H_2N_2 , it is possibly that this process is a fast one. In addition, it provides the needed route to explain the common precursor for cis-trans isomerization as suggested by Baird and Swenson.³⁰

If S_1 is assumed not be a significant contributor to reaction, a mechanism based on thermal triplet decomposition can be postulated:



(T1) is deactivation or "thermalization". (T2) is decomposition. (T3) is activation from unexcited T_1 . (T4) and (T5) are conversion to ground singlet state.

The expression for the quantum yield is

$$\phi^{-1} = \left[1 + \frac{k_T^*}{k_a} + \left(\frac{k_{-1}}{k_a} + \frac{k_{-1}}{k_a} \frac{k_T^*}{k_T} + \frac{k_{-1}}{k_T} \right) P \right] / \left(1 + \frac{k_{-1}}{k_T} P \right) \quad (9)$$

For a plot of ϕ^{-1} vs. P for azoethane to be linear up to 1 atm requires that $k_{-1}P/k_T \ll 1$. $k_{-1} = 2 \times 10^{10}$ atm⁻¹ s⁻¹ and with azoethane being a strong collider, this requires k_T to be $> 10^{11}$ s⁻¹ at 1 atm, a very unlikely value. Further, since $k_T^* \geq k_T$, the intercept is bound to be very large, $k_T^*/k_a > 50$. All this in contrast to the experimental results reported elsewhere^{7,12,25} and found here. It is unlikely then that there is a contribution of a thermal T_1 (reaction T3). When reaction T3 is omitted, the usual linear Stern-Volmer plot is obtained.

Conclusion

The quantum yield for decomposition of azoethane, azoisopropane, and azo-*n*-propane as a function of pressure is reported up to 140, 90, and 50 atm, respectively. It is found that the Stern-Volmer plots are curved and a mechanism consistent with the behavior of the homologous series which involves fast and slow channels is proposed. The latter is identified with T_1 and the former with S_1 or a nonrandom moiety. It is shown that this yields a limiting value of ϕ at high pressures, as is also found in solution photolysis.

Internal conversion and decomposition from the S_0^* of the cis and trans isomers is tentatively ruled out but not totally excluded since no information is available about the cis form of azomethane, azoethane, and azo-*n*-propane or indications of its existence which precludes a consistent model for the homologous series. It is shown that triplet sensitized decomposition differs from direct photolysis and differences in the quantum yield of the two can be explained without postulating different mechanisms.

Decomposition from a thermalized triplet is ruled out and shown to be in disagreement with experimental results. The nature of the temperature dependence of the rate coefficient is discussed and the difference between the "activation energy" of the excited state and the threshold energy for decomposition E_0 is explained.

Acknowledgment. One of us (I.O) thanks Professor B. S. Rabinovitch and the Department of Chemistry, University of Washington for their kind hospitality while writing part of this work, and the U.S.-Israel Binational Science Foundation for their support.

Appendix

I. Molecular and Complex Frequencies. k_N and k_R were calculated by the usual RRKM expression.⁷ For the calculations of k_N , $k_R(S_1)$, and $k_R(T_1)$ the A factor is not known; therefore, the available structural and calculational information was used in the following way. The T_1 state was assumed to be 90° out of plane.^{30,31} The ground state frequencies were used except the C-N and N=N stretches. These were estimated from bond energy bond order (BEBO) method. In the excited molecule, the first one was decreased by 20% and second increased by 10% so that the bond order was preserved. Free internal rotations were assumed around the C-N bond. In the complex, C-N stretch was reduced 10% and N=N stretch increased 50%. This takes care of tightening the N=N and loosening the C-N bonds. In addition, the bendings around the C-N bonds were reduced ~30%. The S_1 state was assumed to have a similar configuration to S_0 . Since the calculations are not sensitive to the details of the frequencies, which are not known exactly, it was felt that the above considerations were adequate as long as the same considerations applied to the whole homologous series and once decided upon were kept constant to the whole series.

E_0 was kept constant and I^*/I was unity throughout the series. Any increase in the value of the ratio will generally improve the agreement between experimental and calculated results but it was felt that this change is uncalled for at the present state of the overall knowledge of the molecular parameters of the excited state. The reaction coordinate was taken as C-N stretch. Ground state frequencies were estimated by a systematic replacement of two H atoms in azomethane by the appropriate alkyl groups. The frequencies which were thus found are in general agreement with those reported for azomethane,^{21,31,22} azoethane,^{7,15,17} and azoisopropane.^{8,17} To save space, the ground state frequencies will not be given. They can be found by changing C-N and N=N stretches of the excited molecule as described above.

Azomethane, excited molecule (cm⁻¹): 2900(6), 1400(6), 1300, 1200(2), 1000(4), 600, 350, 300. **Complex (cm⁻¹):** 2900(6), 1400(6), 1800, 1000(4), 900, 300, 200(2), 100(2). **Azoethane, excited molecule (cm⁻¹):** 2900(10), 1450(8), 1300, 1200(2), 1000(12), 600, 350, 300(4), 250. **Complex (cm⁻¹):** 2900(10), 1450(8), 1800, 1000(12), 900, 350, 300, 250, 200(2), 150(2), 100(2). **Azoisopropane, excited molecule (cm⁻¹):** 2900(14), 1450(12), 1300, 1200(2), 1000(18), 600, 350(2), 300(6), 250(2). **Complex (cm⁻¹):** 2900(14), 1450(12), 1800, 1000(18), 900, 350(2), 300(3), 250(2), 200(2), 150(2), 100(2). **Azo-n-propane, excited molecule (cm⁻¹):** 2900(14), 1450(10), 1300, 1200(2), 1000(18), 600, 450(2), 350(2), 300(6), 250(2). **Complex (cm⁻¹):** 2900(14), 1950(10), 1800, 1000(18), 900, 450(2), 350(2), 300(3), 250(2), 200(2), 150(2), 100(2).

Calculation of k_N . The nonrandom moiety was taken as the azomethylene group with the appropriate groups attached to it. k_N was calculated by RRKM with the same consideration of the C-N and N=N stretches as before.

Azomethylene, excited molecule (cm⁻¹): 2900(4), 1450(2), 1300, 1200(2), 1000(4), 600, 350, 300 (two internal rotations). **Complex (cm⁻¹):** 2900(4), 1450(2), 1800, 900, 1000(4), 300, 200(2), 100(2). For the azomethene (the moiety of isopropane) two 2900 and two 1450 frequencies were removed and two C-C stretches and two C-C-C

bends added with the same changes as before for the complex.

Calculation of k_A . The donor frequencies are given for acetone- d_6 in ref 33, benzene in ref 34, and biacetyl in ref 35. Two values for the transition modes were used, 50 and 30 cm⁻¹ for stretch and bend in agreement with Nagvi and Steel's values for the exchange interaction.³⁶ Lin and Rabinovitch³⁷ used similar values for transition modes of the collision complex of an inert atom and methyl isocyanide. Since exchange interaction is expected to be stronger than the weak long-range attractive forces of the inert-cyanide pair, the values of the transition modes were raised to 100 cm⁻¹. No significant effect was found as expected from this model since any change in the sum of the state of the donor is balanced by a similar change in the sum of states of the collision complex.

Calculation of the Pressure and Collision Frequency. The same method was used here as in the Appendix of ref 7. The Beattie-Bridgeman³⁸ equation was used to calculate the ideal pressure. The coefficients of the equations are as follows: (He) $A_0 = 0.216 \text{ atm L}^2 \text{ mol}^{-2}$, $A = 0.0598 \text{ M}^{-1}$; $B_0 = 0.0140 \text{ M}^{-1}$, $B = 0.0 \text{ M}^{-1}$, $C = 40 \text{ K}^3 \text{ L mol}^{-1}$; (CO₂) $A_0 = 5.01 \text{ atm L}^2 \text{ mol}^{-2}$, $A = 0.0713 \text{ M}^{-1}$, $B_0 = 0.105 \text{ M}^{-1}$, $B = 0.0723 \text{ M}^{-1}$, $C = 6.6 \times 10^5 \text{ K}^3 \text{ L mol}^{-1}$. The collision cross section was calculated by a Lennard-Jones correction to the hard sphere cross section;³⁸ corrections for multiple collisions were made by using the Enskog equation.^{7,38}

References and Notes

- For a comprehensive treatment of the subject, see Robinson and Holbrook "Unimolecular Reactions", Wiley-Interscience, London, 1972.
- S. S. Riley and D. R. Herschbach, *J. Chem. Phys.*, **58**, 27 (1973).
- (a) J. D. Rynbrant and B. S. Rabinovitch, *J. Phys. Chem.*, **75**, 2164 (1971); (b) J. F. Meagher, K. J. Chao, J. R. Barker, and B. S. Rabinovitch, *ibid.*, **78**, 2535 (1974); (c) A. N. Ko and B. S. Rabinovitch, *J. Chem. Phys.*, **66**, 3174 (1977).
- I. Oref, *J. Chem. Phys.*, **63**, 3168 (1975); **64**, 2756 (1976).
- (a) J. Calvert and J. N. Pitts, "Photochemistry", Wiley, New York, N.Y., 1968; (b) N. J. Turro, "Molecular Photochemistry", W. A. Benjamin, New York, N.Y., 1967.
- P. S. Engel and C. Steel, *Acc. Chem. Res.*, **6**, 275 (1973).
- S. Chervinsky and I. Oref, *J. Phys. Chem.*, **79**, 1050 (1975), and references cited therein.
- L. D. Fogel and Colin Steel, *J. Am. Chem. Soc.*, **98**, 4859 (1976).
- R. E. Rebbert and P. Ausloos, *J. Phys. Chem.*, **66**, 2253 (1962).
- R. Renaud and L. C. Leitch, *Can. J. Chem.*, **32**, 545 (1954).
- W. C. Worsham and O. K. Rice, *J. Chem. Phys.*, **46**, 2021 (1967).
- (a) G. O. Pritchard and F. M. Servedio, *Int. J. Chem. Kinet.*, **7**, 99 (1975); (b) G. O. Pritchard, F. M. Servedio, and P. E. Marchant, *ibid.*, **8**, 958 (1976).
- (a) K. F. Freed, *Chem. Phys. Lett.*, **42**, 600 (1976); (b) G. D. Gillispie and E. C. Lim, *ibid.*, **34**, 513 (1975).
- K. Spanner, A. Lanbureau, and W. Kaiser, *Chem. Phys. Lett.*, **44**, 88 (1976).
- P. G. Bowers, *J. Chem. Phys.*, **74**, 952 (1970).
- J. Metalfe, S. Chervinsky, and I. Oref, *Chem. Phys. Lett.*, **42**, 190 (1976), and references cited therein.
- M. J. Perona, P. C. Beadle, and D. M. Golden, *Int. J. Chem. Kinet.*, **5**, 495 (1973).
- G. Geiseler and J. Hoffmann, *Z. Phys. Chem.*, **57**, 318 (1968).
- P. S. Engel, J. L. Wood, J. A. Sweet, and J. L. Margrave, *J. Am. Chem. Soc.*, **96**, 2381 (1974).
- S. W. Benson and H. E. O'Neal, *Natl. Stand. Ref. Data Ser., Natl. Bur. Stand.*, **No. 21** (1970).
- W. Forst, *J. Chem. Phys.*, **49**, 2349 (1966).
- S. S. Collier, D. H. Slater, and J. G. Calvert, *Photochem. Photobiol.*, **7**, 737 (1968).
- I. Oref, *Int. J. Chem. Kinet.*, in press.
- P. S. Engle and D. J. Bishop, *J. Am. Chem. Soc.*, **97**, 6754 (1975).
- H. Cerfontain and K. O. Kutschke, *Can. J. Chem.*, **36**, 344 (1958).
- R. H. Riem and K. O. Kutschke, *Can. J. Chem.*, **38**, 2332 (1960).
- E. A. Hardwidge, B. S. Rabinovitch, and R. C. Ireton, *J. Chem. Phys.*, **58**, 340 (1973).
- R. E. Rebbert and P. Ausloos, *J. Am. Chem. Soc.*, **87**, 1847 (1965).
- G. B. Porter and B. T. Connelly, *J. Chem. Phys.*, **33**, 81 (1960).
- N. C. Baird and J. R. Swenson, *Can. J. Chem.*, **51**, 3097 (1973).
- J. R. Diring, C. B. Pate, and W. C. Harris, *J. Chem. Phys.*, **56**, 5652 (1972).

- (32) T. Shimanouchi, *J. Phys. Chem. Ref. Data*, **3**, 269 (1974).
 (33) T. Shimanouchi, *Natl. Stand. Ref. Data Ser., Natl. Bur. Stand., No. 17* (1968).
 (34) N. Herzfeld, C. K. Ingold, and H. G. Poole, *J. Chem. Soc.*, 316 (1946).
 (35) J. R. During, S. E. Hannum, and S. C. Brown, *J. Phys. Chem.*, **75**, 1950 (1971).
 (36) K. R. Naqvi and C. Steel, *Chem. Phys. Lett.*, **6**, 29 (1970).
 (37) Y. N. Lin and B. S. Rabinovitch, *J. Phys. Chem.*, **74**, 3157 (1970).
 (38) J. O. Hirschfelder, C. F. Curtis, and R. B. Bird, "Molecular Theory of Gases and Liquids", Wiley, New York, N.Y., 1954.
 (39) O. A. Mosher, M. S. Foster, W. M. Flicker, J. C. Beauchamp, and A. Kuppermann, *J. Chem. Phys.*, **62**, 3424 (1975).

Yield and Decay of the OH Radical from 200 ps to 3 ns[†]

Charles D. Jonah* and John R. Miller

Chemistry Division, Argonne National Laboratory, Argonne, Illinois 60439 (Received June 23, 1977)

Publication costs assisted by the Chemistry Division, Argonne National Laboratory

The yield of OH at 200 ps and the decay of OH from 200 ps to 3 ns have been measured. The yield of OH was 5.9 ± 0.2 mol/100 eV (error is statistical, systematic error could be larger). The OH radical decays to 0.73 ± 0.05 of its initial value from 200 ps to 3 ns. The implications of these results are compared with theoretical calculations.

Introduction

In the radiolysis of water we can divide the time scale into several regions. From 10^{-15} to 10^{-12} s ions and excited states form and decay to leave primarily H^+ , e_{aq}^- , OH, H, and possibly excited water.¹ The deposition of energy is inhomogeneous.²⁻⁴ Along the path of a high energy electron the energy is deposited, on the average, 1000–5000 Å apart in 20–100-eV packets. The radicals formed in an energy deposition event form a high concentration of reactive radicals. This localized volume of high concentration is called a spur. From 10^{-11} to 10^{-8} s these radicals will react with one another.²⁻⁷ From the rate of the reaction we can get an idea of the concentration of radicals in the spur. The concentration is dependent on the number of radicals in the spur and the radius of the spur; neither parameter is known. For moderate doses (less than 10 krd) the probability of reaction with a radical from another spur is small for times less than 10^{-8} s. We can determine the reaction within the spur by measuring the decay of the radicals.

Experimental studies have decreased the time from deposition of energy to first measurement to times on the order of 10^{-11} s.⁸ All of the previous work has been concentrated on the hydrated electron. On irradiation with high energy electrons it is the radical formed with the second largest yield, has a high absorption coefficient, and the maximum of its absorption is in an easily measured region of the spectrum. The yield of the electron and its decay from 100 ps to the time where homogeneous kinetics describes the decay has been measured.⁵

Little similar work has been done with OH. Measurements of the interaction between OH and e_{aq}^- in the spur have been done by measuring the yield of the hydrated electron as a function of OH scavenger and vice versa.⁹ The yield of OH at homogeneity has also been measured.¹ The importance of OH in biological systems and its high yield and high reactivity make the study of the decay of OH in the spur and its initial yield important.

We have measured the yield of OH at 200 ps. We have also measured the decay of OH in the spur. In a similar experiment with e_{aq}^- we measured the decay of e_{aq}^- in the presence and absence of OH and H^+ scavengers.⁵ Because of the smaller absorption (factor of 60) a more difficult region of the spectrum and the possible interfering species we have not attempted to do the similar experiment for OH.

Experimental Section

The experimental apparatus has been described previously.¹⁰ We shall only give a short description of the apparatus. The Argonne Linac generates pulses of 20–22 MeV electrons at 60 Hz. Each pulse consists of a main pulse with a width (fwhm) of 30 ps¹¹ containing greater than 90% of the charge and a satellite pulse separated from the main pulse by 770 ps. The satellite pulse may either precede or follow the main pulse. Normally the machine is tuned so that the satellite pulse precedes the main pulse. Approximately 30% of the electron beam is intercepted by a cell containing 1 atm of xenon. The Cerenkov light generated by the cell has the same time dependence as the electron beam which generates it. The remainder of the electron beam (70%) is used for irradiation of the sample. This beam will deposit 15 gy (1.5 krd, 10^{17} eV/g) in the irradiated volume of the cell. Both the electron beam and the light beam are delayed. The delay of the light beam can be varied so that the light pulse reaches the sample before, during, or after the electron irradiation pulse. The measurement of the light intensity transmitted by the cell as a function of the delay of the light beam enables one to measure the transmission of the light. An RCA C7253G photomultiplier was used for measuring light intensities. A discussion of linearity tests and criteria may be found in ref 5. While the peak of the OH absorption is around 240 nm we observed at 280 nm for two reasons: (1) there are fewer interfering absorptions at 280 nm and (2) we can get more light through our analyzing system at 280 nm.

To determine the decay of OH due to spur processes we used an interference filter centered at 280 nm instead of a monochromator. Since we are in the shot noise limit, an

[†] Work performed under the auspices of the Division of Physical Research of the U.S. Energy Research and Development Administration.

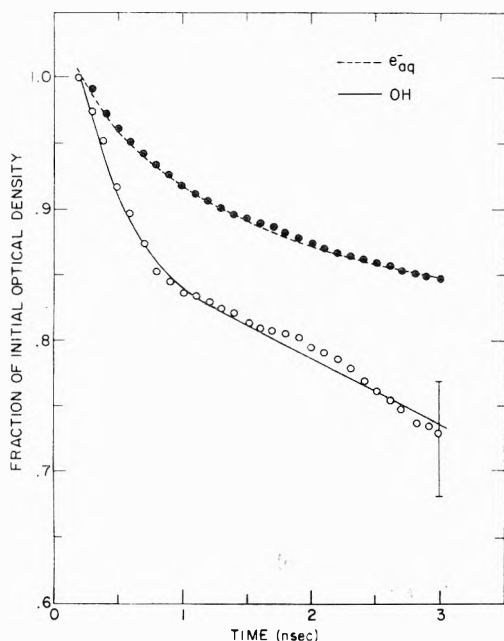


Figure 1. The decay of OH and e_{aq}^- as measured using the picosecond pulse radiolysis system. The error bar on the OH gives the difference depending on the mode of calculation (see text). The lines are just a smoothed line through the points. The e_{aq}^- decay is from ref. 5.

increase in light brings an increase in signal-to-noise ratio. Due to the wide wavelength bandpass of the filter (200 Å) it could not be used for measuring electron yields.

The G value of OH was measured through its absorption at 280 nm. An experiment would consist of measuring four kinetic curves, the absorption of pure water at 600 nm, the absorption of water, 4 M perchloric acid, and the empty cell at 280 nm. The empty cell gave a small absorption due to transient species formed in the Suprasil windows. The four curves were measured 3 or 4 times in a day to average out drifts in the intensity of the linac beam. The difference between water and perchloric acid both measured at 280 nm and the absorption of water at 600 nm were used as two independent dosimeters. Extinction coefficients used were $\epsilon_{280}(e_{aq}^-) = 715$,¹² $\epsilon_{600}(e_{aq}^-) = 12500$,¹³ and $\epsilon_{OH}(280) = 245$.¹⁴ The $G(e_{aq}^-)$ used was 4.5 mol/100 eV.⁵ There was less than a 5% difference between the measurement of dose at 600 and 280 nm.

The decay of the OH was determined from the data using two different techniques. First, we take the decay curve measured in the presence of 4 M perchloric acid and subtract the decay of the empty cell. Second, we subtract the decay of the electron in water, measured at 600 nm, from the decay curve measured in pure water at 280 nm. Thus, we shall have the decay of the OH radical in the presence of H atoms or electrons. Since the reactivity of OH with H or e_{aq}^- is comparable ($3 \times 10^{10} \text{ M}^{-1} \text{ s}^{-1}$ for e_{aq}^- and $2 \times 10^{10} \text{ M}^{-1} \text{ s}^{-1}$ for H)¹⁴ we would expect quite similar decays. In Figure 1 we plot the average of the two curves as well as the decay of the electron. The error bar at time $t = 3$ ns shows the maximum difference between the curves. The largest difference occurred at 3 ns where the 4 M perchloric acid was higher than the line shown and neutral water was lower than the line shown. The noise added by using the decay of e_{aq}^- is negligible; the decay of e_{aq}^- was evaluated at 600 nm and the signal-to-noise ratio at 600 nm is more than an order of magnitude better than at 280 nm. The maximum deviation at 280 nm is around 14% of the absorption; however, since each point is independent and there are a large number of points, we can determine decays much more accurately than that. Time was started at 200 ps so that one could avoid the

decay of the electron in the 4 M perchloric acid system. No adjustment was made in any parameters for these curves. A smooth line was drawn through the data and the points were read from the smooth curve. The points as calculated are seen in the figure.

Results and Discussion

The yield of OH determined with $5.9 \text{ mol}/100 \pm 0.2 \text{ eV}$ (standard deviation of seven separate measurements over 6 months). The systematic error, which is almost entirely due to the uncertainty in extinction coefficient, could be much larger. This yield appears to be higher than theoretical calculations predict. For instance, Schwarz⁶ calculates a G_{OH} of 5.7 relative to an electron yield of 4.78. These two values are closer together than our measured data. This could imply a larger yield of H or H_2 than was calculated by Schwarz. The yield of OH predicted from the calculations of Kuppermann¹⁵ is smaller than that predicted by Schwarz. The calculations of Kuppermann are not comparable to those of Schwarz, since Kuppermann assumed a yield of O atoms as well as OH radicals. The yield of H atoms is also lower for Kuppermann's calculations. The end result of the Kuppermann calculation is that the yield of OH is very similar to that of the electron, in contrast to our results. Even if one sums O and OH, the yield would be too small to match our data.

It appears as if our yield measurements are the same as the calculations of Schwarz, at least within our experimental uncertainty. The agreement with the calculation of Kuppermann is less satisfactory.

The reactions which remove OH radicals can be compared to the reactions which remove electrons:



In the traditional models the distribution of the electron is much larger than the other radicals. Both the calculations of Schwarz and Kuppermann found a ratio of the radius of the electron distribution to the OH distribution to be between 2 and 3.^{6,7,15} If we compare eq 1–3, we expect OH to decay faster. Reactions 2a and 2b are, of course, the same. OH should decay faster through pathway 1b than e_{aq}^- does through pathway 1a. This is because the OH distribution is much tighter and the concentration of OH is much higher (between a factor of 8 and 27 for the theoretical calculations). This reaction will not occur for a one radical pair spur because there is only one OH (or e_{aq}^-) so no reaction can take place. The relative rates of reactions 3a and 3b are not clear. There is less H than H^+ which tends to make reaction 3a faster; however, poor spatial overlap of e_{aq}^- and H^+ , so that some e_{aq}^- will have a very low probability of reaction will tend to slow reaction 3a relative to reaction 3b.

To compare the actual time dependence of the decay of OH, as shown in Figure 1, to the theoretical data previously calculated^{6,15} the same problem occurs as did for electrons, the time scale seems to be off by a multiplicative factor. Kuppermann has pointed out that the time scale of the calculations may be changed by a straightforward manipulation of the parameters.⁷ Using the decay of the electron calculated by Kuppermann⁷ and comparing our decay to his, we can find appropriate scaling factor (see below) to obtain the experimental and theoretical decay on the same time scale. The experimental time of 3 ns is

approximately equivalent to 300 ps on the theoretical decays shown in ref 7. If we apply the same time scale correction to the OH decay we find 0.72 of the OH remaining after 3 ns, which is in good agreement with 0.73 ± 0.05 , the experimentally determined value. We have calculated the decay of the OH radical using the parameters given by Schwarz. For these data we obtain 0.63 ± 0.03 (depending on spur size) for the fraction of OH remaining after 3 ns, defining the time scale using the decay of the electron as Kuppermann did. This is lower than the 0.74 ± 0.05 which we measured.

The manipulations that were used to change the time scale are quite simple. For an all-spur reaction (no homogeneously distributed reactants), if we multiply all distances by n and the number of radicals by n , then the time scale is n^2 longer. Thus, what we have done is change the radius of the spur and the number of radicals in the spur by about 3. These distances become similar to the distances proposed by Platzmann (50–60-Å radius for the electron spur).¹⁶ However, the number of radicals in a spur are much higher than that predicted by the calculations to Mozumder and Magee¹⁷ (around 6 radical pairs per spur as opposed to 1–2 as calculated by Mozumder and Magee). The numbers of Mozumder and Magee at least have relevance to gas phase water, where similar distributions were measured by Wilson from cloud chamber measurements.¹⁸

Conclusions

The OH experimental data are consistent with the previously measured electron data. The decay observed is about the same magnitude as has been predicted by theory but the time required is about an order of magnitude longer than what calculations would predict. The yield of OH is in quite reasonable agreement with the value proposed by Schwarz; however, it is considerably larger than that predicted by Kuppermann.

Spur diffusion calculations have been very useful in explaining and understanding processes occurring at longer times. The data on e_{aq}^- and OH at early times show the trends predicted by the calculations but the details are different. The ad hoc adjustments used to bring experimental and theoretical time-dependent calculations into agreement need to be justified or some other modification needs to be made. An important question revolves around the calculations of Mozumder and Magee. If those calculations are correct, the modifications of Kuppermann are not reasonable.

The spur theory has given a basic understanding to radiation chemistry. Now revisions are in order to bring

the theory into agreement with the new experimental data. An approach which shows promise has been formulated by Fanning et al.¹⁹ Their formulation has not been checked with the large body of data that Kuppermann or Schwarz have used; however their decay of the electron is in good agreement with what has been published.

It is not clear whether calculations based solely on the spur will be sufficient. The fraction of energy (around 10–20%) which is deposited in blobs may have a large effect on the measurement. New theoretical work is needed to explain these data.

We hope that future linac improvements where the dose is doubled will make it possible to make more accurate measurements of OH decay. The yield data are limited by the absolute accuracy of the extinction coefficients.

Acknowledgment. We thank the linac operators, Donald Ficht, Lee Rawson, and Joe Becker, for their patience in listening to our requests for more and more beam. Without their skilled efforts none of these measurements would be possible. We also thank Robert M. Clarke for his assistance in running these experiments. Conversations with Klaus H. Schmidt and Max S. Matheson are gratefully acknowledged.

References and Notes

- (1) I. G. Draganic and Z. D. Draganic, "The Radiation Chemistry of Water", Academic Press, New York, N.Y., 1971.
- (2) G. A. Kenney and D. C. Walker, *J. Chem. Phys.*, **50**, 4074 (1969).
- (3) G. V. Buxton, *Proc. R. Soc. London, Ser. A*, **328**, 9 (1972).
- (4) J. K. Thomas and R. V. Bensasson, *J. Chem. Phys.*, **46**, 4147 (1967).
- (5) C. D. Jonah, M. S. Matheson, J. R. Miller, and E. J. Hart, *J. Phys. Chem.*, **80**, 1267 (1976).
- (6) H. A. Schwarz, *J. Phys. Chem.*, **73**, 1928 (1969).
- (7) "Diffusion Kinetics in Radiation Biology: An Assessment", A. Kuppermann in "Physical Mechanisms in Radiation Biology", R. D. Cooper and R. W. Wood, Ed., Technical Information Center, Office of Information Services, U.S. Atomic Energy Commission, 1974.
- (8) M. J. Bronskill, R. K. Wolff, and J. W. Hunt, *J. Chem. Phys.*, **53**, 4201 (1970); R. K. Wolff, M. J. Bronskill, J. E. Aldrich, and J. W. Hunt, *J. Phys. Chem.*, **77**, 1350 (1973).
- (9) Z. D. Draganic and I. G. Draganic, *J. Phys. Chem.*, **77**, 765 (1973).
- (10) C. D. Jonah, *Rev. Sci. Instrum.*, **46**, 62 (1975).
- (11) G. S. Mavrogenes, C. Jonah, K. H. Schmidt, S. Gordon, G. R. Tripp, and L. W. Coleman, *Rev. Sci. Instrum.*, **47**, 187 (1976).
- (12) K. H. Schmidt private communication.
- (13) M. Fielden and E. J. Hart, *Trans. Faraday Soc.*, **63**, 2975 (1967).
- (14) L. M. Dorfman and G. E. Adams, *Natl. Stand. Ref. Data Ser., Natl. Bur. Stand.*, **No. 46** (1973).
- (15) A. Kuppermann in "Radiation Research", G. Siliini, Ed., North Holland Publishing Co., Amsterdam, 1972, p 212.
- (16) R. L. Platzman in "Physical and Chemical Aspects of Basic Mechanisms in Radiobiology", J. L. Magee, Ed., U.S. National Academy of Science, Publication No. 305:24, 1953.
- (17) A. Mozumder and J. L. Magee, *J. Chem. Phys.*, **45**, 3332 (1966).
- (18) C. T. R. Wilson, *Proc. R. Soc. London, Ser. A*, **104**, 192 (1923).
- (19) J. E. Fanning, C. N. Trumbore, P. Glenn Barkley, D. R. Short, and J. H. Olson, *J. Phys. Chem.*, **81**, 1026 (1977).

Vapor-Phase Charge-Transfer Complexes. 10. Iodine Complexes of Methanol, Ethanol, and Diethyl Ether

Hing-Cheung Tse and Milton Tamres*

Chemistry Department, University of Michigan, Ann Arbor, Michigan 48109 (Received July 25, 1977)

Publication costs assisted by the National Science Foundation

Spectral and thermodynamic characteristics of ethanol-iodine, methanol-iodine, and diethyl ether-iodine complexes in the vapor phase were determined either by the constant activity method or a modified Benesi-Hildebrand-Scott method. The maxima of the blue-shifted complexed visible iodine bands were obtained by extrapolation of the absorbance data in the continuum region of the spectrum of molecular iodine assuming a Gaussian band shape. It was found that the band maximum of the methanol-iodine complex is at a longer wavelength than that of the diethyl ether-iodine complex. Contrary to a report in the literature, no charge-transfer band maximum for alcohol-iodine was detected at 235 nm. In fact, no maximum was observed to below 216 nm. The internal energy of complexation was determined to be -4.3 ± 0.3 kcal/mol for diethyl ether-iodine, -4.3 ± 0.2 kcal/mol for ethanol-iodine, and -3.8 ± 0.3 kcal/mol for methanol-iodine. These values are larger than those obtained for the same complexes in *n*-heptane solution. Although the equilibrium constants cannot be determined precisely, an estimate of their values was made which shows that they also are larger than those reported in *n*-heptane solution.

Introduction

Recently, we reported a detailed study of the spectral and thermodynamic properties of the iodine complexes with methanol and with ethanol in *n*-heptane solution.^{1,2} The results clarified some of the puzzling features reported for these complexes in the earlier literature, notably with respect to the magnitude of the blue-shifted (BS) iodine visible band. The present paper reports on the study of these same complexes in the vapor phase. Vapor-phase studies are of special importance in that they not only give a quantitative measure of solvent effects when compared with solution data, but they are more pertinent in allowing a direct test of theory.

There are several reasons for focussing on the alcohol-iodine system. It had been shown for the iodine complexes with only three donors (diethyl sulfide, dimethyl sulfide, and diethyl ether) that the band maximum of the BS iodine visible band in the vapor phase was further blue shifted in *n*-heptane solution, the solvent shift being greater the weaker the complex.^{3,4} Since the data are so limited, it was thought important to determine if the still weaker alcohol-iodine complexes would continue this trend.

The enthalpy of complexation (ΔH_c°) of iodine with several donors has been reported in both the vapor phase and solution.⁵ There is a difference in the two phases which shows a systematic trend with increasing strength of interaction. Such comparison requires precise determination of ΔH_c° , and these data are quite scarce for the vapor phase. Therefore, the determination of ΔH_c° for the alcohol-iodine complexes was undertaken using both the more convenient constant activity method³ and a modified Benesi-Hildebrand-Scott procedure.⁶ As a check, the former method was applied also to the diethyl ether-iodine complex whose ΔH_c° previously was studied by the latter procedure.

Further, only one previous brief report of an alcohol-iodine system in the vapor phase has appeared, in which it is stated the CT band of ethanol-iodine has a maximum at 235 nm.⁷ The same band in *n*-heptane solution was found to be at ~ 230 nm in a study by Julien et al.⁸ and at ~ 225 nm in our recent study.¹ These data would indicate a blue shift of the charge-transfer (CT) band in

going from the vapor phase to solution. Such a shift is opposite to the trend shown by most of the iodine complexes with weak donors such as aromatic hydrocarbons⁹ and diethyl ether,⁶ and even the stronger alkyl sulfides.¹⁰

Experimental Section

Material. Ethanol, methanol, and diethyl ether were purified and handled using methods described previously.^{1,6} The tetramethylammonium enneaiodide (TMAI₉) was prepared and recrystallized according to the literature¹¹ (mp 109 °C; lit. mp 110 °C). Analytical grade iodine (Baker) was mixed with potassium iodide and sublimed twice as described in the literature.¹²

Procedure. The methods for sealing samples in the breakseal tubes, introducing the samples into the cells, measuring the length and volume of the cells, and weighing out the donor and acceptor were described in earlier papers.^{3,6}

In the constant activity method, the spectrum of the complex was measured with the donor plus the constant activity source of iodine in the sample cell and only the constant activity source of iodine in the reference cell. Cells of 100.0 cm were used for the study of alcohol-iodine, and 50.0 cm for diethyl ether-iodine. Solid TMAI₉ generally was used to control the activity of the iodine vapor. In one study to locate the BS iodine band of the methanol-iodine complex, an excess of pure iodine crystals was used as the constant activity source of iodine. In this case, 10.0-cm cells were used because of the higher vapor pressure of pure iodine. Base line corrections were determined at each temperature to ensure precise cancellation of the free iodine absorbance in both the sample and reference cells.³

The internal energy change of complexation (ΔE_c°) of the alcohol-iodine complexes was determined by a simplified Benesi-Hildebrand-Scott method. It has been shown⁵ for the condition $[D]_0 \gg [I_2]_0$ in the vapor phase

$$\frac{d \log K_c \epsilon}{d(1/T)} + \frac{d \log ([I_2]_0 - [C])}{d(1/T)} = \frac{d \log A}{d(1/T)} \quad (1)$$

where $[D]_0$ and $[I_2]_0$ are the initial concentration of the donor and iodine, respectively, K_c is the equilibrium constant of complexation, ϵ is the molar absorptivity of the

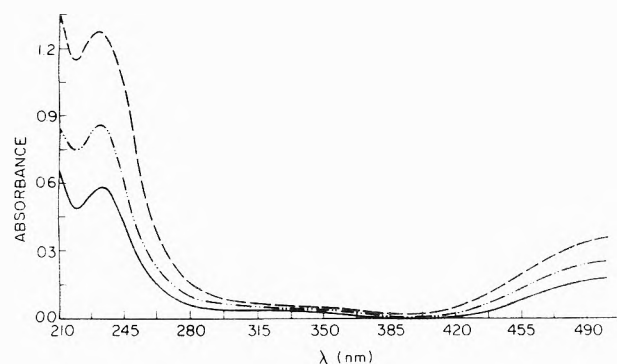


Figure 1. Spectra of diethyl ether-iodine in the vapor phase studied by the constant activity method (TMAI₉/TMAI₅): cell path = 50.0 cm. $[D]_0 = 0.0474$ M; (—) 59.9 °C, $[I_2]_0 = 3.29 \times 10^{-5}$ M; (-·-·-) 70.0 °C, $[I_2]_0 = 6.04 \times 10^{-5}$ M; (- - -) 80.4 °C, $[I_2]_0 = 1.09 \times 10^{-4}$ M.

complex at a particular wavelength, A is the absorbance of the complex at that particular wavelength, and $[C]$ is the equilibrium concentration of the complex. For a weak complex, where K_c is small, $[C]$ is only a small fraction of $[I_2]_0$ and, over a small range of temperature, the variation of $[I_2]_0 - [C]$ with temperature is very small. Thus, the second term on the left-hand side of eq 1 can be neglected. If the temperature dependence of ϵ is also negligible, eq 1 shows that plotting $\log A$ of a single mixture of donor and acceptor vs. $1/T$ is the same as plotting $\log K_c$ vs. $1/T$ to obtain ΔE_c° . In the present study, the temperature dependence of the absorbance of a single mixture of alcohol and iodine, entirely in the vapor phase, was measured in a 75.0-cm cell against an empty reference cell. The total absorbance at each temperature was corrected for the contribution of the initial concentrations of total donor and total acceptor as determined by separate experiment. It is assumed that, because the complex is weak, corrections based on initial concentrations would be within experimental error of those based on equilibrium concentrations.

Results

The continuum region of the iodine visible spectrum in the vapor phase appears below 498.5 nm.¹³ A distinct BS iodine band maximum is observed in this region for iodine complexed with the moderately strong dimethyl and diethyl sulfides as donors. For the weaker diethyl ether-iodine complex, the BS iodine band maximum is at a longer wavelength than 498.5 nm and has been estimated by extrapolation using a graphical method assuming a parabolic shape around the band maximum.³ As expected from the similarity in donor abilities of ethers and alcohols, the BS iodine band maximum for alcohol-iodine also was found to be at a longer wavelength than 498.5 nm. In the present study the extrapolation was carried out by a least-squares fitting computer program assuming a Gaussian band shape.

As a test of the procedure, a sample of 0.0474 M diethyl ether was studied at different temperatures by the constant activity method using TMAI₉ as the iodine source. The spectra are shown in Figure 1. Initially, the absorbance data over the large region from 400 to 498 nm were analyzed by the computer program. The spectral characteristics obtained are shown in Table Ia. The variation in both the band maximum and half-intensity bandwidth with temperature seems somewhat erratic. This situation is improved by neglecting the long tail of the band, i.e., the region from 400 to 440 nm. The absorbance data in this region are low anyway, and are subject to larger experimental error. Analysis utilizing the data only from 440 to 498 nm gives the spectral results shown in Table Ib. Here, there is better agreement in the band position and

TABLE I: Characteristics of the Blue-Shifted Iodine Visible Band of Diethyl Ether-Iodine in the Vapor Phase

Temp, °C	Band max, nm	Half-intensity bandwidth, cm ⁻¹	Absorbance at band max
(a) Using Absorbance Data from 400.0 to 498.0 nm			
59.9	508 ± 2	4364 ± 91	0.170 ± 0.002
65.1	517 ± 2	5049 ± 149	0.209 ± 0.005
70.0	515 ± 2	4936 ± 98	0.260 ± 0.003
74.8	521 ± 3	5249 ± 148	0.333 ± 0.007
(b) Using Absorbance Data from 440.0 to 498.0 nm			
59.9	506 ± 2	4230 ± 159	0.169 ± 0.002
65.1	509 ± 3	4588 ± 176	0.206 ± 0.003
70.0	512 ± 3	4773 ± 180	0.262 ± 0.004
74.8	512 ± 3	4720 ± 180	0.344 ± 0.004
Av	510 ± 3	4578 ± 174	

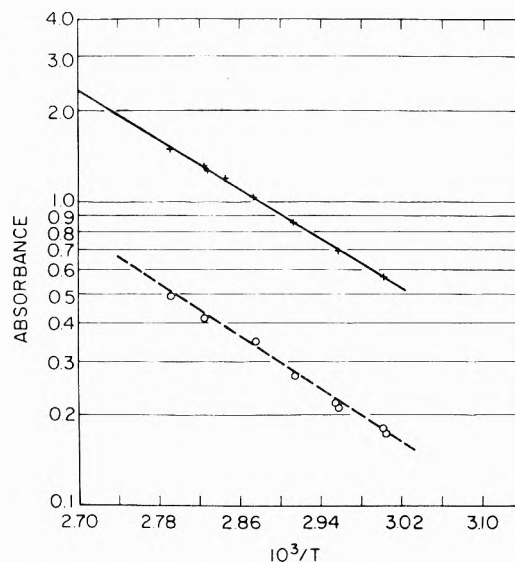


Figure 2. $\log A$ vs. $1/T$ plot for diethyl ether-iodine complex in the vapor phase studied by the constant activity method (TMAI₉/TMAI₅): (+) absorbance at 234 nm; (O) absorbance at 510 nm.

half-intensity bandwidth over the temperature range, and the band maximum also agrees with that reported previously (509 nm)³ based on a different extrapolation procedure.

The van't Hoff plots of $\log A$ vs. $1/T$, where A is the absorbance and T is the absolute temperature, are shown in Figure 2 for the data of the CT band and also of the BS iodine band. The total internal energy change (ΔE_t), obtained from the slope of the line, is -9.4 ± 0.3 kcal/mol from the data of the CT band and -9.9 ± 0.8 kcal/mol from the data of the BS iodine band. ΔE_t includes the internal energy changes of complexation (ΔE_c°) and of saturation for the TMAI₉/TMAI₅ system (ΔE_{sat}). The latter has been determined independently to be 13.7 kcal/mol.³ Thus, ΔE_c° is -4.3 ± 0.3 kcal/mol from the data of the CT band and -3.8 ± 0.8 kcal/mol from the data of the BS iodine band. The latter value is somewhat less reliable because the determination is based on absorbance data obtained by extrapolation.

A typical spectrum of the ethanol-iodine complex in the vapor phase at 82.1 °C obtained by the constant activity method is shown in Figure 3A for both the UV and visible regions. The concentration of ethanol is 0.0274 M and the known (uncomplexed) iodine concentration at this temperature from the constant activity source is 1.19×10^{-4} M. At wavelengths longer than 470 nm the absorbance increased drastically. This was expected to occur at ~ 498 nm because it is known that the vibrational structure of the iodine band at longer wavelengths is smeared out in

TABLE II: Solvent Effects on the Blue-Shifted Iodine Band of Some Complexes

Donor	Phase	$-\Delta H_c^\circ$, kcal/mol	λ^{BS} , nm	$\nu^{BS}(\text{soln}) - \nu^{BS}(\text{vap})$, cm^{-1}	Ref
Diethyl sulfide	Vapor	9.0	452		3, 5
	<i>n</i> -C ₇ H ₁₆	8.3	437	760	21
Dimethyl sulfide	Vapor	7.8	457		3, 5
	<i>n</i> -C ₆ H ₁₄		437	1000	22
Diethyl ether	Vapor	5.2	510 ± 3		3, 6
	<i>n</i> -C ₇ H ₁₆	4.2	470	1630	12, 20
Methanol	Vapor	4.4	533 ± 6		This work
	<i>n</i> -C ₇ H ₁₆	3.0	475 ± 5	2291	This work
Ethanol	Vapor	4.9	<i>a</i>		This work
	<i>n</i> -C ₇ H ₁₆	3.2	475 ± 5		This work

^a The extrapolated result (see text) of 800 ± 300 nm is not considered meaningful, and therefore is not included in the table.

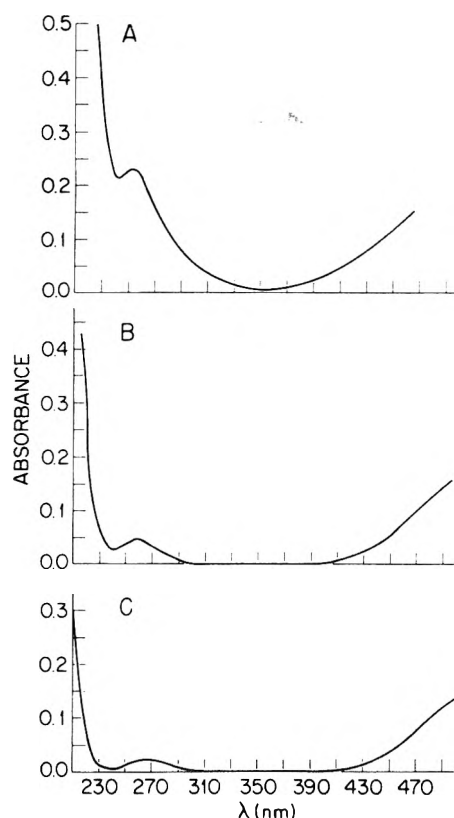


Figure 3. Alcohol-iodine complexes in the vapor phase: (A) Ethanol-iodine studied by the constant activity method (TMAI₉/TMAI₅): $t = 82.1^\circ\text{C}$, cell path = 100.0 cm, $[I_2]_0 = 1.19 \times 10^{-4}\text{ M}$, $[D]_0 = 0.0274\text{ M}$. (B) Methanol-iodine studied by the constant activity method (TMAI₉/TMAI₅): $t = 60.2^\circ\text{C}$, cell path = 100.0 cm, $[I_2]_0 = 3.35 \times 10^{-5}\text{ M}$, $[D]_0 = 0.0278\text{ M}$. (C) Methanol-iodine complex in the vapor phase studied by the constant activity method (iodine crystals): $t = 60.2^\circ\text{C}$, cell path = 10.0 cm, $[I_2]_0 = 2.29 \times 10^{-4}\text{ M}$, $[D]_0 = 0.0222\text{ M}$.

the presence of other gases.⁶ The increase at shorter wavelengths in the present case was found to be due to a spurious effect arising from a too high overall absorption. (At the temperatures studied, using 100.0-cm cells, A is >3 in the region above 470 nm.) The temperature of 82.1°C was a compromise between sufficient volatility to form the complex in the vapor phase and the high absorbance, thereby limiting the characterization of the blue-shifted iodine band to the narrow region from 440 to 470 nm. An attempt was made to estimate the band maximum from these data by the least-squares fitting computer program assuming a Gaussian band shape, but the result was not meaningful (see Table II) and merely reflects the fact that an insufficient segment of the BS iodine band was available for analysis. Nonetheless, it seems clear that the band maximum is at a wavelength that extends into the vi-

brational region of the iodine band.

It is significant that no peak at 235 nm for the CT band is observed, such as had been reported by Rao et al.⁷ The small peak observed at 260 nm is due presumably to an irreversible reaction. Its intensity increased markedly when the temperature was raised to 85°C and the increase continued with time. After 24 h, the cells were recooled to 82°C , but the initial spectrum was not reproduced either in the UV or in the visible region. The reaction most likely is the formation of ethyl iodide, which is known to have an absorption peak at 258.2 nm.¹⁴ The presence of the polyiodide crystals probably catalyzed the reaction. Therefore, quantitative study using the constant activity method was not possible.

A sample of 0.0278 M methanol also was studied by the constant activity method. The spectrum at 60.2°C is shown in Figure 3B. At this low temperature the spectrum could be measured to a wavelength of 495 nm. When the temperature was raised to 75°C , no reliable data were obtained for wavelengths longer than 480 nm, again because A is >3 as in the ethanol-iodine case. At 80°C this occurred at 475 nm. No irreversible reaction with time was detected for the duration of the experiment even at 80°C .

To locate the BS iodine band maximum, the data at 60.2°C in the region of 440 to 495 nm were extrapolated by the computer program based on a Gaussian band shape. The result of $536 \pm 5\text{ nm}$, while still not as precise as desired because of the long extrapolation of a broad band, is a marked improvement over the ethanol-iodine case, due of course to the availability of a longer segment of the band.

A further attempt was made to determine the position of the BS iodine band of the methanol-iodine complex, this time using pure iodine as the constant activity source. Since at 60.2°C the vapor pressure of pure iodine is about 6.3 times as large as that of TMAI₉, 10.0-cm cells were used instead of 100.0-cm cells. The spectrum of the complex at 60.2°C is shown in Figure 3C. The position of the BS iodine band maximum obtained from the least-squares program is at $529 \pm 7\text{ nm}$. Similar analysis of the spectrum at 64.6°C gave a band maximum at $534 \pm 4\text{ nm}$. These results lie within the experimental limits of the data obtained using TMAI₉ as the constant activity source. However, it should be pointed out that the technique of using pure iodine to control the activity may be less precise than using the polyiodides. This is because the iodine crystals in the cells tend to migrate and deposit on the coldest parts of the cell, and this might occur on the cell windows.

For methanol-iodine, as for ethanol-iodine, no CT band maximum is observed. The small band at 260 nm, whose intensity did not increase with time, likely is due to the presence of a small amount of methyl iodide (formed perhaps while the system passes from the condensed phase

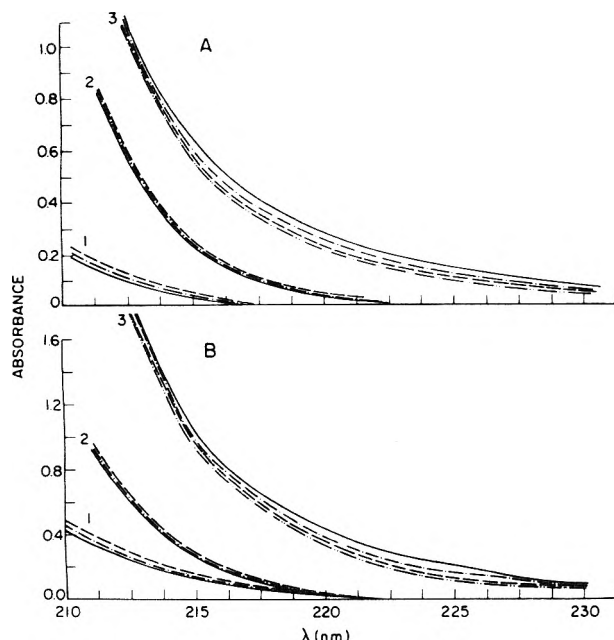


Figure 4. Alcohol-iodine complexes in the vapor phase studied by the Benesi-Hildebrand-Scott method, cell path = 75.0 cm. (A) 1, iodine vapor alone (5.03×10^{-5}); 2, ethanol vapor alone (0.0238 M); 3, ethanol + iodine mixture: (—) 81.4 °C, (---) 90.6 °C, (----) 99.9 °C, (-·-·-) 110.4 °C. (B) 1, iodine vapor alone (8.73×10^{-5} M); 2, methanol vapor alone (0.0353 M); 3, methanol + iodine mixture: (—) 80.5 °C, (---) 90.5 °C, (----) 101.0 °C, (-·-·-) 111.0 °C.

to the vapor phase), which is reported to have an absorption at 257.6 nm.¹⁴

Location of the CT band of the alcohol-iodine complexes also was sought by a study of the complexes completely in the vapor phase. Figures 4A and 4B show the spectra of the two systems at different temperatures. No band maximum was detected at the wavelength region around 235 nm.

Discussion

For the diethyl ether-iodine study, the spectral and thermodynamic results matched well those reported using other techniques, namely, λ_{\max} for the blue-shifted iodine band is 510 ± 3 nm (lit. 509 nm),³ λ_{\max} for the CT band is 234 nm (lit. 234 nm),^{3,5,6,15} and ΔE_c° is -4.3 ± 0.3 kcal/mol (lit. -4.5 ± 0.2 kcal/mol).⁶ Further, the ratio of the molar absorptivity at the CT band maximum (ϵ^{CT}) to that at the BS iodine band maximum (ϵ^{BS}) at different temperatures (given in parentheses) is as follows: 3.37 (59.9 °C); 3.37 (65.1 °C); 3.25 (70.0 °C); 3.01 (74.8 °C); 3.10 (80.4 °C). The value at 59.9 °C matches the result reported previously.³ Considering the error inherent in the extrapolated value of the absorbance at the BS iodine band maximum, the ratio of $\epsilon^{\text{CT}}/\epsilon^{\text{BS}}$ seems to be constant for these few temperatures.

Some of the more reliable data⁵ on the solvent effect on the BS iodine band are given in Table II. There appears to be a consistent relation between increasing strength of complexation and decreasing solvent shift from the vapor phase to solution. Tamres^{3,4} has pointed out that, when a weak complex in the vapor phase is dissolved in a solvent, a cavity must be created in the liquid. Since this requires energy, the size of the cavity will be a minimum. This would lead to a compression of the complex by the solvent cage and a shorter intermolecular distance between the donor and acceptor. This results in a greater exchange repulsion when the complexed iodine molecule is excited, and the λ^{BS} in solution is shifted to a shorter wavelength compared to the vapor phase. The compression is larger

the weaker the complex because of the shallower minimum in the potential energy curve of the ground state. Therefore, the magnitude of the blue shift due to the solvent is greater for a weak complex.

No CT band maximum was found in the UV region for either the ethanol- or methanol-iodine complex in the vapor phase. This was true for both the constant activity method and the conventional Benesi-Hildebrand-Scott method. In the latter study, the absorbance at around 216 nm was noticeably enhanced upon mixing the iodine and alcohol vapors. The absorbance decreased with increasing temperature, an effect which cannot be attributable either to temperature broadening or to contacts, and must be due to a CT complex. The maximum of the CT band must be at a wavelength shorter than 216 nm, with much of the band being buried under that of the alcohol absorption. Such a low wavelength for the CT band would be anticipated from a comparison of the data for alcohol-iodine and diethyl ether-iodine. The energy for electron transfer is given by^{16a}

$$h\nu^{\text{CT}} = I_D^{\text{V}} - E_A^{\text{V}} + \Delta \quad (2)$$

where I_D^{V} and E_A^{V} are the vertical ionization potential of the donor and vertical electron affinity of the acceptor, respectively, and Δ contains Coulombic, van der Waals, and resonance terms. Assuming Δ is comparable for diethyl ether-iodine and ethanol-iodine, and since E_A^{V} is the same for these systems, the position of the CT band for ethanol-iodine relative to that for diethyl ether-iodine (λ_{\max} 234 nm)^{3,5,6,15} can be estimated from the difference in ionization potential of ethanol (10.48 ± 0.05 eV)¹⁷ and diethyl ether (9.53 ± 0.03 eV).¹⁷ The calculated value for the CT band maximum is ~ 198 nm.

The present study establishes that the previously reported result of 235 nm⁷ for λ^{CT} for ethanol-iodine is erroneous. Further, since it was established that λ^{CT} for ethanol-iodine in *n*-heptane is at ~ 225 nm,¹ this means that λ^{CT} is red shifted in going from the vapor phase to solution, which is in accord with the trend observed for other weak iodine complexes.

This red shift has been rationalized in several ways. For a weak complex the CT state is ionic and will be stabilized to a greater extent through solute-solvent interaction than will the ground state which is essentially nonpolar. Therefore, the excitation energy in solution, $h\nu^{\text{CT}}(\text{soln})$, is reduced relative to that in the vapor phase, $h\nu^{\text{CT}}(\text{vap})$.⁵ In addition, the solvent cage compression of the intermolecular distance between donor and acceptor will lead to a red shift of λ^{CT} .¹⁰ Also, since the dielectric constant and refractive index for the solution phase are both larger than those for the vapor phase, the dispersion and polarization effects will result in a lowering in the energy for charge transfer in solution.¹

For the alcohol-iodine complexes, ΔE_c° could not be determined by the constant activity method due to reaction over this temperature range, most likely catalyzed by the constant activity source, with the probable formation of alkyl iodide. Therefore, the data for ΔE_c° were obtained instead from a study based on the simplified Benesi-Hildebrand-Scott method. Figure 5 shows the plot corresponding to eq 1. The absorbance data at 216 nm are used for ethanol-iodine and those at 217 nm are used for methanol-iodine. From this plot the ΔE_c° for the former is -4.3 ± 0.2 kcal/mol and for the latter, it is -3.8 ± 0.3 kcal/mol. The absorbance data at 220 nm also were used in a similar plot for comparison purposes. For both complexes, they give practically the same ΔE_c° values as those from Figure 5. The experiment was repeated using different concentrations for the two complexes, and the

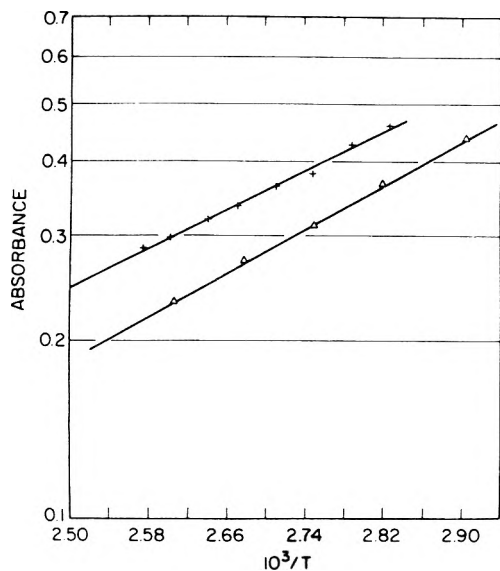


Figure 5. $\log A$ vs. $1/T$ for alcohol-iodine complexes in the vapor phase: (Δ) ethanol-iodine at 216 nm; (+) methanol-iodine at 217 nm.

results for ΔE_c° were found to be consistent. Absorbance data below 216 nm were not used for the analysis because of the very steep rise in absorbance due to the overlap of spectral bands.

The ΔH_c° values in the vapor phase for both complexes are larger than those in solution,² as has been found for other weak complexes. As pointed out, weak van der Waals attraction between donor and acceptor in the vapor phase must result in a decrease in internal energy.^{4,16b} However, in solution, this is largely cancelled by solvent effects because the forces between donor and acceptor are not much different from those between donor and solvent, acceptor and solvent, and solvent and solvent.

There have been several studies reporting on the correlation for iodine complexes of ΔH_c° with the magnitude of the blue shift of the complexed visible iodine band. This shift is given by Mulliken and Person^{16c} as $\Delta W_{\text{vis}} = h\nu^{\text{BS}} - h\nu^{520}$ where ν^{BS} is the frequency of the blue-shifted iodine band maximum and ν^{520} is the frequency corresponding to the wavelength of 520 nm where the visible iodine band maximum is observed in "inert" solvents such as *n*-heptane. The correlation obtained is $\Delta W_{\text{vis}} = -1.57\Delta H_c^\circ$ (± 1.5) in units of kcal/mol. (There is appreciable scatter in some of the data points from this line, as indicated by the error limits.) This line, shown in Figure 6, represents the correlation for data *in solution* (where $\Delta H_c^\circ \approx \Delta E_c^\circ$). In the *vapor phase*, because ΔE_c° is larger while λ^{BS} is at longer wavelengths for weak complexes, the correlation between ΔW_{vis} and ΔE_c° must have a different slope. The four data points so far available for the vapor phase are shown in Figure 6. These data are too few to establish a quantitative relation, although it is clear that the slope is larger for the vapor phase. It must be noted from the work of Paetzold et al.¹⁸ that a good linear correlation between ΔW_{vis} and ΔE_c° in solution holds best for iodine complexes with a homologous series of donors.

It has been pointed out for weak complexes, particularly in the vapor phase where pressure limitations necessitate using low concentrations, that meaningful separation of K_c and ϵ from the $K_c\epsilon$ product cannot be achieved.⁶ However, the $K_c\epsilon$ product itself can be determined precisely. In the constant activity method for a weak complex under the condition $[D]_0 \gg [I_2]_0$

$$K_c\epsilon = A/b[D]_0[I_2]_0 \quad (3)$$

where b is the cell path. From the $K_c\epsilon$ product, the K_c

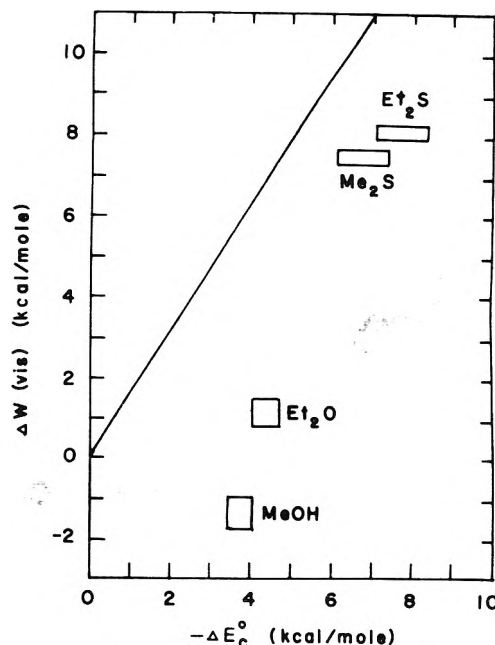


Figure 6. Comparison of data for the blue-shifted iodine band in the vapor phase with that in solution. Line gives correlation of solution data from ref 16c; rectangles give vapor-phase data including error limits.

value can be estimated by assuming a reasonable value for ϵ . For the diethyl ether-iodine complex studied in this work, the absorbance at 59.9 °C at the CT band maximum is 0.569 and that at the extrapolated BS band maximum is 0.169. Thus, $K_c\epsilon^{\text{CT}}$ is $7300 \text{ M}^{-2} \text{ cm}^{-1}$, which is somewhat bigger than the value previously determined by the conventional Benesi-Hildebrand method in this laboratory, and $K_c\epsilon^{\text{BS}}$ is $2170 \text{ M}^{-2} \text{ cm}^{-1}$. For iodine complexes in solution, ϵ^{BS} is of the order of $900 \text{ M}^{-1} \text{ cm}^{-1}$, to within a factor of ~ 2 (except for strong donors where ϵ^{BS} is higher⁴). For iodine complexes with dimethyl and diethyl sulfides, ϵ^{BS} in the vapor phase was determined to be ~ 725 and $\sim 1100 \text{ M}^{-1} \text{ cm}^{-1}$, respectively.³ Neglecting the variation in ϵ over the temperature range and adopting the value of $900 \text{ M}^{-1} \text{ cm}^{-1}$ for ϵ^{BS} in the vapor phase, K_c at 59.9 °C is calculated to be 2.4 M^{-1} for diethyl ether-iodine. Using the ΔE_c° determined in this work, K_c at 35 °C is 4.1 M^{-1} , which compares favorably with the value of $4.3 \pm 0.3 \text{ M}^{-1}$ reported from an isopiestic study.¹⁹ For this same complex in *n*-heptane solution,²⁰ K_c at 25 °C has the smaller value of 1.44 M^{-1} . Applying the same procedure to the methanol-iodine system studied with TMAI₉/TMAI₅ as the constant activity source, $K_c\epsilon^{\text{BS}}$ at 60.2 °C is $2130 \text{ M}^{-2} \text{ cm}^{-1}$. Thus, K_c is 2.4 M^{-1} assuming ϵ^{BS} is $900 \text{ M}^{-1} \text{ cm}^{-1}$. Using ΔE_c° as -3.8 kcal/mol , K_c at 25 °C is 4.7 M^{-1} in the vapor phase, which can be compared with the value of $1.29 \pm 0.09 \text{ M}^{-1}$ in *n*-heptane solution. Even allowing for an error in ϵ^{BS} by a factor of 2, the data are consistent in showing that the equilibrium constants for these weak complexes are larger in the vapor phase.

Acknowledgment. One of the authors (H.C.T.) thanks the Horace H. Rackham School of Graduate Studies at The University of Michigan for a predoctoral fellowship. This research was supported in part by the National Science Foundation through Grant No. GP-38403X.

References and Notes

- (1) H. C. Tse and M. Tamres, *J. Phys. Chem.*, **81**, 1367 (1977).
- (2) H. C. Tse and M. Tamres, *J. Phys. Chem.*, **81**, 1376 (1977).
- (3) M. Tamres and S. N. Bhat, *J. Am. Chem. Soc.*, **95**, 2516 (1973).
- (4) M. Tamres and J. Yarwood in "Spectroscopy and Structure of Molecular Complexes", J. Yarwood, Ed., Plenum Press, New York, N.Y., 1973, Chapter 3.

- (5) M. Tamres in "Molecular Complexes", Vol. I, R. Foster, Ed., Crane, Russak and Co., Inc., New York, N.Y., 1973, Chapter 2.
- (6) J. Grundnes, M. Tamres, and S. N. Bhat, *J. Phys. Chem.*, **75**, 3682 (1971).
- (7) C. N. R. Rao, G. C. Chaturvedi, and S. N. Bhat, *J. Mol. Spectrosc.*, **33**, 554 (1970).
- (8) (a) L. M. Julien, Ph.D. Dissertation, The University of Iowa, 1966; (b) L. M. Julien, W. E. Bennett, and W. B. Person, *J. Am. Chem. Soc.*, **91**, 6915 (1969).
- (9) W. Duerksen and M. Tamres, *J. Am. Chem. Soc.*, **90**, 1379 (1968).
- (10) M. Kroll, *J. Am. Chem. Soc.*, **90**, 1097 (1968).
- (11) *Inorg. Syn.*, **5**, 172 (1957).
- (12) M. Brandon, M. Tamres, and S. Searles, *J. Am. Chem. Soc.*, **82**, 2129 (1960).
- (13) G. Herzberg, "Molecular Spectra and Molecular Structure. I. Spectra of Diatomic Molecules", 2nd ed, Van Nostrand-Reinhold, New York, N.Y., 1950.
- (14) K. Kimura and S. Nagakura, *Spectrochim. Acta*, **17**, 166 (1961).
- (15) F. T. Lang and R. L. Strong, *J. Am. Chem. Soc.*, **87**, 2345 (1965).
- (16) R. S. Mulliken and W. B. Person, "Molecular Complexes: A Lecture and Reprint Volume", Wiley, New York, N.Y., 1969: (a) p 118, (b) p 95, (c) p 159.
- (17) K. Watanabe, T. Nakayama, and J. Mottl, *J. Quant. Spectrosc. Radiat. Transfer*, **2**, 369 (1962).
- (18) (a) R. Paetzold and K. Niendorf, *Z. Phys. Chem. (Leipzig)*, **256**, 361 (1975); (b) R. Paetzold, *Z. Chem.*, **15**, 377 (1975).
- (19) J. Grundnes, S. D. Christian, and V. Cheam, *Acta Chem. Scand.*, **24**, 1836 (1970).
- (20) (a) J. D. Childs, Ph.D. Dissertation, The University of Oklahoma, 1971; (b) S. D. Christian, J. D. Childs, and E. H. Lane, *J. Am. Chem. Soc.*, **94**, 6861 (1972).
- (21) M. Tamres and S. Searles, Jr., *J. Phys. Chem.*, **66**, 1099 (1962).
- (22) J. D. McCullough and I. C. Zimmerman, *J. Phys. Chem.*, **64**, 1084 (1960).

Pressure Dependence of the Rate Constant of the Reaction $\text{H} + \text{CH}_3 \rightarrow \text{CH}_4$

Jung-Tsang Cheng and Chuln-Ilh Yeh*

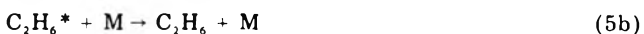
Institute of Chemistry, National Tsing Hua University, Hsinchu, Taiwan 300, Republic of China (Received March 4, 1977)

Ethane gas of 30–2300 Torr has been decomposed by the mercury photosensitization technique at 35 °C to investigate the variation of the rate constant (k_6^{ex}) of the reaction $\text{H} + \text{CH}_3 \rightarrow \text{CH}_4$ upon system pressure. A correlation of the obtained and the published k_6^{ex} has been made. This rate constant is seen increasing with system pressure, following third-order kinetics at a pressure of 50 Torr or less, and falling off around 150 Torr. Through an extrapolation of the data in the falloff region, the second-order k_6^{ex} at the high pressure limit is assessed to be $(2.0 \pm 0.9) \times 10^{14} \text{ cm}^3 \text{ mol}^{-1} \text{ s}^{-1}$.

Introduction

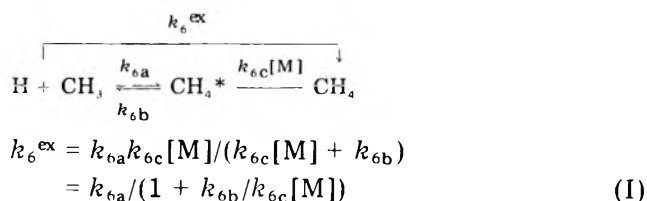
The reactions of hydrogen atoms with hydrocarbon molecules in the gas phase have been of continuous interest.^{1–3} Rate constants for these reactions have been extensively studied under different system conditions. However the reactions between hydrogen atoms and alkyl radicals have not attracted much attention. Although some low pressure rate constants have already been reported for these important radical-atom termination reactions,^{4–8} data in the high pressure region are yet to be measured.

Recently we have studied ethane decomposition at a pressure of 300 Torr.⁹ In that study, the mercury photosensitization technique is used. The significant primary processes of this decomposition reaction at high light intensities have been confirmed as follows:



The rate constant for the termination reaction $\text{H} + \text{CH}_3 \rightarrow \text{CH}_4$ was calculated, based on the above reaction mechanism and the obtained experimental data, to be 1.5

$\times 10^{14} \text{ cm}^3 \text{ mol}^{-1} \text{ s}^{-1}$. This rate constant at 300 Torr is considerably larger than those measured constants (around $3 \times 10^{12} \text{ cm}^3 \text{ mol}^{-1} \text{ s}^{-1}$) reported for this same reaction over the system pressure of a few Torr.^{4–8} This discrepancy is expected from the following unimolecular decomposition mechanism:



According to eq I, the value of k_6^{ex} , the experimental measured rate constant, should be proportional to the system pressure as long as $k_{6c}[\text{M}] \ll k_{6b}$ but level off as $k_{6c}[\text{M}] \doteq k_{6b}$. The purpose of this study is to investigate experimentally the pressure profile of k_6^{ex} and to determine k_{6a} through experiments of the mercury photosensitized decomposition of the ethane molecule.

Experimental Section

The mercury photosensitization technique was used in this investigation to decompose ethane molecules at constant light intensity and 35 °C. Ethane gas of various pressure was allowed to fill a quartz tube as the reactant. The distribution of the photolysis product was analyzed by the gas chromatographic technique. Details of the experimental procedure may be found in the previous report.⁹

Results and Discussion

The variation of the composition of the photolysis product at different photolysis time has been studied for ethane pressures of 30, 100, 300, 800, and 2300 Torr. The measured data are listed in Table I. In this table the yield

TABLE I: Effect of Photolysis Time on the Nature of Products at Various Pressures

Photolysis time, s	Relative yields of products (Y_{RH})					Photolysis time, s	Relative yields of products (Y_{RH})				
	H ₂	CH ₄	C ₂ H ₆	C ₃ H ₈	n-C ₄ H ₁₀		H ₂	CH ₄	C ₂ H ₆	C ₃ H ₈	n-C ₄ H ₁₀
Pressure = 30 Torr						Pressure = 100 Torr					
60		1.17	1000	2.08	0.78	60	0.54	0.40	1000	0.52	0.52
90		1.95	1000	2.82	1.16	120	1.11	0.92	1000	0.98	0.89
120		3.19	1000	3.33	1.30	150	1.37	1.37	1000	1.42	1.17
150		4.29	1000	4.38	1.70	240	2.30	2.77	1000	1.99	1.46
240		7.93	1000	5.90	1.98	300	4.11	3.90	1000	2.60	
300	2.93		1000	7.93		300	2.77	3.70	1000	2.47	1.83
600	5.79		1000	7.80		Pressure = 800 Torr					
Pressure = 300 Torr						90			1000	0.07	0.85
120	1.01	0.25	1000	0.40	0.72	180	1.46	0.05	1000	0.14	1.59
120	0.99	0.43	1000	0.43	0.74	270	2.25		1000	0.20	2.31
180	1.22	0.46	1000	0.68	1.44	360		0.12	1000	0.26	2.84
240	2.03	0.69	1000	0.82	1.51	540	4.51	0.18	1000	0.39	4.20
300	2.59	0.95	1000	1.00	1.83	Pressure = 2300 Torr					
420	3.64	1.69	1000	1.27	2.39	1290	13.0	0.11	1000	0.45	8.49
600	4.98	2.13	1000	1.83	3.08	1500	13.6	0.13	1000	0.56	14.4

TABLE II: Calculated Rates of Product Generation and Steady State Radical Concentrations at the Initial Photolysis Stage

Pressure, Torr	Generation rate $\times 10^{11}$ (mol cm ⁻³ s ⁻¹)				Radical concentration $\times 10^{13}$ (mol cm ⁻³)	
	R_{CH_4}	$R_{C_3H_8}$	$R_{n-C_4H_{10}}$	R_{H_2}	[H] ^a	[CH ₃] ^b
30	2.37	5.59	2.05	1.56	4.81	14.1
100	3.34	4.41	5.41	5.01	4.63	6.20
300	4.40	6.29	10.1	14.1	4.35	6.39
800	1.41	3.51	38.5	35.1	4.04	1.82
2300	0.46	2.00	49.9	49.7	2.29	0.91

$$^a [H] = R_{H_2}/2 \times 10^7 [C_2H_6], \quad ^b [CH_3] = R_{C_3H_8}/2k_7^{1/2} R_{n-C_4H_{10}}^{1/2}$$

 TABLE III: Summary of the Determined Second-Order Rate Constant Values of the Reaction $H + CH_3 \rightarrow CH_4$

Pressure	k_6^{ex} (cm ³ mol ⁻¹ s ⁻¹)	Ref
1.2 Torr of H ₂	1×10^{12}	4
1.3 Torr of Ar	3×10^{12}	5
1.6 Torr of H ₂	1.2×10^{12}	8
2.5 Torr of H ₂	3.3×10^{12}	8
3.4 Torr of H ₂	4.8×10^{12}	8
4.9 Torr of H ₂	3.3×10^{12}	8
6.7 Torr of Ar	1×10^{13}	6
8.0 Torr of Ar	2.3×10^{12}	7
30 Torr of C ₂ H ₆	3.2×10^{13}	This work
100 Torr of C ₂ H ₆	1.1×10^{14}	This work
300 Torr of C ₂ H ₆	1.5×10^{14}	This work
800 Torr of C ₂ H ₆	1.7×10^{14}	This work
2300 Torr of C ₂ H ₆	1.8×10^{14}	This work
Infinite pressure (theoretical prediction)	2.3×10^{14}	10

of each product is expressed as the mole ratio relative to the concentration of the ethane molecule. At constant pressure, these yields increase with photolysis time. Figure 1 shows the variation of yield of major products as a function of the photolysis time for a system of 30 Torr of ethane. The slope of each curve, in this figure, at zero photolysis time may be used to calculate R_{RH} (the rate of the formation of RH at zero conversion), steady state radical concentrations at the initial stage (see Table II), and k_6^{ex} according to eq II-XI of ref 9.

Table III lists second-order k_6^{ex} values calculated in the present study and published in the literature. This rate constant is seen increasing with pressure. Reaction 6 is shown in Figure 2 to follow third-order kinetics at a pressure of 50 Torr or less. This third-order reaction may be described as

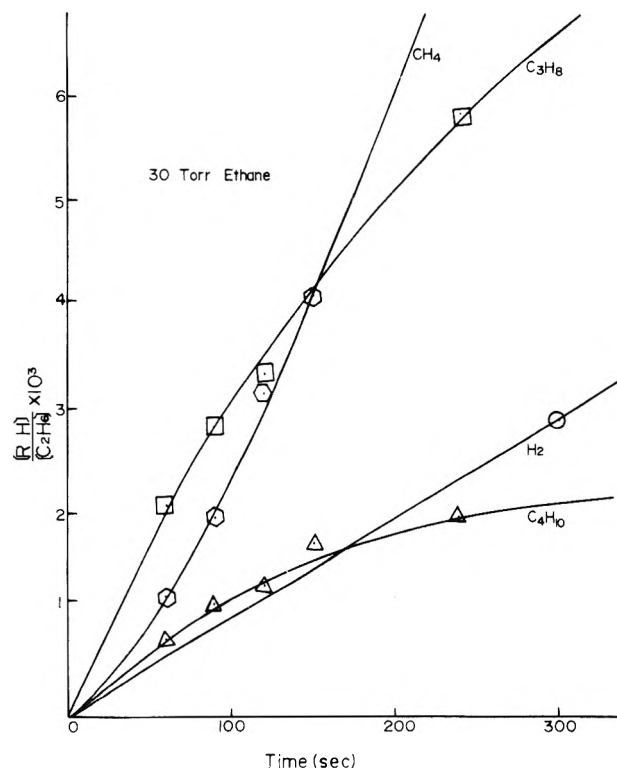
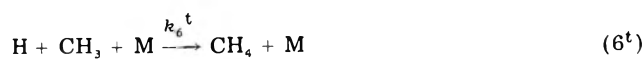


Figure 1. Effect of photolysis time on the nature of products at a pressure of 30 Torr.

The optimized k_6^t in this third-order region is estimated to be 2×10^{19} cm⁶ mol⁻² s⁻¹.

It is of interest to note that this estimated k_6^t is larger than 4×10^{15} cm⁶ mol⁻² s⁻¹, the rate constant reported for the termolecular recombination of hydrogen atoms³ ($H + H + M \rightarrow H_2 + M$), by a factor of 5000. This discrepancy

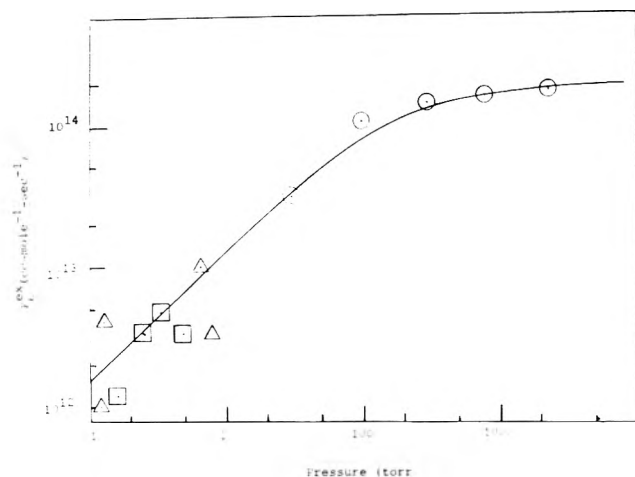


Figure 2. Falloff curve for the rate constant of the reaction $\text{H} + \text{CH}_3 \rightarrow \text{CH}_4$: O, present study; □, Michael, Osborne, and Suess; Δ, ref 4–7. Solid curve in this figure fits the equation $k_6^{\text{ex}} = 2 \times 10^{14} / (1 + 1/6.7 \times 10^{-3}(\text{M}) \text{ (in Torr)}) \text{ cm}^3 \text{ mol}^{-1} \text{ s}^{-1}$.

comes mainly from the difference between the lifetime of the temporarily formed intermediates, H_2^* and CH_4^* . Both of these exciting species are very unstable and tend to redissociate. H_2^* has only one vibrational mode and dissociates therefore at the end of its first vibration. On the other hand, CH_4^* has nine degrees of vibrational freedom. It takes thousands of vibration before the excited energy of CH_4^* flows into one particular C–H bond that breaks. Consequently, CH_4^* rather than H_2^* is more probable to be deactivated to form stable molecule through third body collision. The ascending rate of k_6^{ex} , the measured second-order rate constant, slows down in the pressure range of 100–2300 Torr. Such falloff behavior suggests that k_6^{ex} is attaining its limiting high pressure value, k_{6a} . From high pressure k_6^{ex} values (100, 300, 800, and 2300 Torr), k_{6a} can be roughly estimated from the eq I as $(2.0 \pm 0.9) \times 10^{14} \text{ cm}^3 \text{ mol}^{-1} \text{ s}^{-1}$. This estimated value agrees quite satisfactorily with $2.3 \times 10^{14} \text{ cm}^3 \text{ mol}^{-1} \text{ s}^{-1}$, a theoretically predicted rate constant for reaction 6 at infinite pressure.¹⁰

A correlation work has been performed for k_6^{ex} values in the Table III and eq I. With k_{6a} fixed at $2.0 \times 10^{14} \text{ cm}^3 \text{ mol}^{-1} \text{ s}^{-1}$, the k_{6c}/k_{6b} ratio was varied to meet the experimental data. A solid line, which represents the obtained experimental k_6^{ex} as a function of pressure, is shown in Figure 2 with the following relationship:

$$k_6^{\text{ex}} = 2 \times 10^{14} / (1 + 1/6.7 \times 10^{-3} [\text{M}] \text{ (in Torr)}) \text{ cm}^3 \text{ mol}^{-1} \text{ s}^{-1} \quad (\text{II})$$

Comparing eq I and II, we found $k_{6b}/k_{6c} = 150 \text{ Torr}$. In other words, rates of processes 6b and 6c are equal at the pressure (generally called $P_{D/S=1}$) of 150 Torr. At this ethane pressure, the collision frequency of CH_4^* may be estimated from the collision diameter of methane and

ethane (3.8 and 5.0 Å, respectively)¹¹ through the collision theory equation¹² as $2.2 \times 10^9 \text{ collisions s}^{-1}$. If we assume that CH_4^* will be deactivated upon its first collision, the rate constant k_{6b} at 35 °C may be assessed to be $2.2 \times 10^9 \text{ s}^{-1}$. This assessed decomposition rate constant is smaller than the theoretical calculated value of Rabinovitch et al.¹¹ by a factor of 5, but is very close to $1.5 \times 10^9 \text{ s}^{-1}$, a value obtained by them from old data on the reaction $\text{D} + \text{CH}_3 \rightarrow \text{CH}_3\text{D}$.¹¹

Chen et al. recently studied the pyrolysis of methane¹³ and have determined the rate constant of the following pressure dependent reaction as $\log k_6 = 16.45 - 2.34 \times 10^3/T$



Using this obtained k_{6c} and the RRKM theory, they have calculated the variation of k_6^{ex} with system pressure for temperatures of 1038, 700, and 500 K. To our satisfaction, data for the present investigation (at 35 °C) are only around a factor of 2 higher than their expectation.

The following hydrogen-atom-abstraction reaction is excluded as the cause of this difference:



Since $\log k_{11} = 11.5 - 2.6 \times 10^3/T$ (ref 14–18), k_{11} has a value of $1 \times 10^3 \text{ cm}^3 \text{ mol}^{-1} \text{ s}^{-1}$ at 35 °C. Calculations demonstrated that process 11 contributes less than 1% of the total methane formation in all experiments performed in this study.

Acknowledgment. We gratefully acknowledge the support of the National Science Council of Republic of China under Contract No. NSC-65M-0204-03(02).

References and Notes

- (1) B. A. Thrush, *Prog. React. Kinet.*, **3**, 63 (1965).
- (2) I. M. Campbell and D. L. Baulch, *MTP Int. Rev. Sci.*, **9**, 45 (1972).
- (3) W. E. Jones, S. D. MacKnight, and L. Teng, *Chem. Rev.*, **73**, 407 (1973).
- (4) L. Teng and W. E. Jones, *J. Chem. Soc., Faraday Trans. 1*, **68**, 1267 (1972).
- (5) J. M. Brown, P. B. Coates, and B. A. Thrush, *Chem. Commun.*, 843 (1966).
- (6) A. F. Dodonov, G. K. Lavroskaya, and V. L. Tal'roze, *Kinet. Katal.*, **10**, 477 (1969).
- (7) M. P. Halstead, D. A. Leathard, R. M. Marshall, and J. H. Purnell, *Proc. R. Soc. London, Ser. A*, **316**, 575 (1970).
- (8) J. V. Michael, D. T. Osborne, and G. N. Suess, *J. Chem. Phys.*, **58**, 2800 (1973).
- (9) J. T. Cheng, Y. S. Lee, and C. T. Yeh, *J. Phys. Chem.*, **81**, 687 (1977).
- (10) S. W. Benson and H. E. O'Neil, *Natl. Stand. Ref. Data Ser., Natl. Bur. Stand.*, **No. 21** (1970).
- (11) B. S. Rabinovitch and D. W. Setser, *Adv. Photochem.*, **3**, 1 (1964).
- (12) K. J. Laidler, "Chemical Kinetics", McGraw-Hill, New York, N.Y., 1965.
- (13) C.-J. Chen, M. H. Back, and R. A. Back, *Can. J. Chem.*, **53**, 3580 (1975).
- (14) G. B. Skinner and W. E. Ball, *J. Phys. Chem.*, **64**, 1025 (1960).
- (15) R. H. Snow, *J. Phys. Chem.*, **70**, 2780 (1966).
- (16) R. H. Snow, R. E. Peck, and C. G. Fredersdoff, *AIChE J.*, **5**, 304 (1959).
- (17) J. R. McNesby and A. S. Gordon, *J. Am. Chem. Soc.*, **77**, 4719 (1955).
- (18) J. R. McNesby, *J. Phys. Chem.*, **64**, 1671 (1960).

Redox Mechanisms in an Ionic Matrix. 5. A Kinetic Study on the Direct and Autocatalytic Process $\text{H}_2 + \text{NO}_3^- = \text{H}_2\text{O} + \text{NO}_2^-$ in Molten Alkali Nitrates

E. Desimoni, F. Paniccia,* and P. G. Zambonin

Istituti di Chimica Analitica e Generale, Università degli Studi, 70126 Bari, Italy (Received September 22, 1977; Revised Manuscript Received May 23, 1977)

The kinetics of the oxidation of hydrogen by nitrate ions $\text{NO}_3^- + \text{H}_2 = \text{NO}_2^- + \text{H}_2\text{O}$ (a) in the molten (sodium-potassium) nitrate equimolar mixture was studied in the temperature range 630–710 K by following the hydrogen pressure variations over the reacting system. The experimental findings are explained on the basis of two parallel homogeneous-phase mechanisms: the first one involving the direct reaction between hydrogen and nitrate ions and the second one characterized by an autocatalytic path involving the reaction between hydrogen and nitrite ions. The overall process is in both cases eq a.

In view of a possible utilization of fused nitrates as a solvent for hydrogen-air fuel cells, a systematic study¹⁻⁴ on the chemical and electrochemical behavior of oxygen-hydrogen systems in nitrate melts was initiated by this research group.

In the course of solubility measurements¹ of hydrogen in a molten (sodium-potassium) nitrate equimolar mixture, the presence of a reaction between hydrogen and the melt anions was observed and ascribed to the redox process $\text{H}_2 + \text{NO}_3^- = \text{H}_2\text{O} + \text{NO}_2^-$ (1)

Mechanistic information on this homogeneous system was expected to contribute to a better understanding of the chemical behavior of hydrogen in the given solvent. More interest in the study was represented by the possibility of autocatalytic contributions to reaction 1 due to the different nature of the N-O bonds in the nitrate and nitrite ions.

The kinetic results and the proposed reaction mechanisms are presented and discussed in the present paper.

Experimental Section

Chemicals. The solvent was an equimolar mixture of reagent-grade (sodium-potassium) nitrate. In some experiments, sodium nitrite was added to the basic solvent at initial concentrations ranging between 0.17 and 1.19 *m*. Cylinder hydrogen of high purity was used without further purification.

Apparatus. The reaction cell was similar to the one previously described⁴ for solubility measurements, the main change being a thermostatted cold trap interposed between the reaction vessel and the manometer, in order to keep the water pressure constant in the course of an experiment.

Calibration. The details for the volume calibration procedure can be found in ref 4. In short, it consisted in the expansion of a known number of moles of an inert gas (He in this case) contained in a thermostatted bulb of known volume in an evacuated reaction cell. On measuring the pressure values before and after the expansion, a correlation between the pressure read on the manometer and the moles of gas contained in the reaction cell

$$n_g = A(T)P_g \quad (2)$$

was obtained in the absence of water before each experiment. This calibration method is to be preferred to any other based on direct geometrical calculation of the cell volume since, when working under judiciously controlled conditions, it is independent of the temperature gradients

present in the reaction cell. Since, in the course of each experiment, a given water vapor pressure (between 5 and 25 Torr) was maintained in the cell, expression 2 was modified as follows:

$$n = A(T)(P_t - P_{\text{H}_2\text{O}}) = A(T)P \quad (3)$$

where *n* is the number of hydrogen moles present in the gas phase over the melt, *P_t* the total pressure read on the manometer, *P_{H₂O}* the partial pressure of water, and *P* the actual hydrogen pressure in the reaction cell.

Procedure. Before each experiment, a weighted amount (100–150 g) of nitrate mixture was introduced in the cell at the working temperature. Thereafter a small volume of water was introduced into the cold trap reservoir via a glass capillary crossing the thermostatted mantle, and the capillary was flame sealed at the end of this operation. After a rapid vacuum deaeration (avoiding any significant evaporation of the water introduced into the cold trap) the hydrogen was allowed to flow into the cell up to the desired pressure and a magnetic stirrer immersed in the melt was switched on. The kinetics of hydrogen disappearance was followed up by recording its pressure variation as a function of time.

At the end of each experiment, the total concentration of the nitrite formed was tested by dissolving a weighted amount of the quenched melt in water and by titrating with potassium permanganate.

In some experiments, a spectrophotometric analysis was made of the water present in the cold trap.

Result and Discussion

Typical examples of pressure vs. time curves are reported in Figure 1A, while Figure 1B shows the relevant semilogarithmic plots. Since the final nitrite titrations confirmed the stoichiometry expressed by reaction 1 within the limits of 1–2%, it was possible to evaluate the nitrite concentration at any time just by reading the hydrogen pressure over the reacting system. In fact, by taking into account expression 3 we can write the equation

$$[\text{NO}_2^-] = \frac{A(T)(P_0 - P)}{W} - K_{\text{H}}P \quad (4)$$

where *P₀* and *P* are the initial and actual hydrogen pressure values, *W* is the weight of the solvent in kilograms, and *K_H* is Henry's coefficient for the given hydrogen melt system expressed in mol kg⁻¹ atm⁻¹.

This last datum can be derived from the results reported in ref 1 when the melt density⁵ at the operating temperature is known.

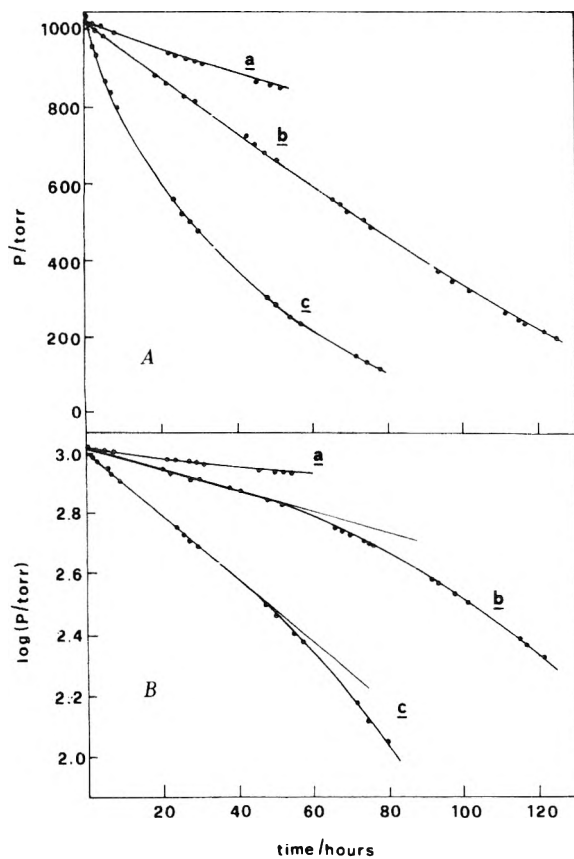


Figure 1. Typical hydrogen pressure vs. time curves (A) with the relevant semilogarithmic plots (B) at different temperatures: (a) $T = 653$ K; (b) $T = 663$ K; (c) $T = 686$ K.

The term $K_H P$ takes into account that at any time a small fraction of the pressure drop was due to the presence of a quasi-equilibrium hydrogen concentration in the melt (under proper stirring conditions).

By assuming reaction 1 as a first-order kinetic process both with respect to hydrogen and nitrate, its rate can be expressed by

$$r = d[\text{NO}_2^-]/dt = k_1[\text{H}_2][\text{NO}_3^-] \quad (5)$$

or by the pseudo-first-order equation

$$r = d[\text{NO}_2^-]/dt = k_1' K_H P \quad (6)$$

since $[\text{H}_2]$ can be written as a function of its pressure and $[\text{NO}_3^-]$ can be considered constant in a molten nitrate solvent. Since $A(T)P_0/W$ is a constant at constant temperature, by differentiating relationship 4 and by taking into account expression 6, we obtain

$$\frac{d[\text{NO}_2^-]}{dt} = - \left[\frac{A(T)}{W} + K_H \right] \frac{dP}{dt} = k_1' K_H P \quad (7)$$

whose integration leads to the expression

$$\log(P/P_0) = -Bt \quad (8)$$

where

$$B = \frac{k_1' K_H}{2.3 \left(K_H + \frac{A(T)}{W} \right)} \quad (9)$$

It was then possible to derive the values of k_1' (and k_1) from the slope B of the experimental curves $\log P$ vs. t (see Figure 1B). The k_1' and k_1 values obtained are listed in columns 3 and 4 of Table I. The confidence limits are $\pm 3\%$. The observed reaction rates were independent from the water pressure. From the linear plot $\log k_1$ vs. T^{-1} the

TABLE I: Kinetic Constants for the Direct Processes $\text{NO}_3^- + \text{H}_2 = \text{NO}_2^- + \text{H}_2\text{O}$ at Different Temperatures

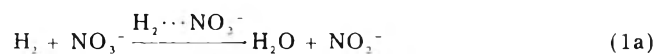
Expt no.	T , K	$(k_1' = k_1[\text{NO}_3^-]) \times 10^3 \text{ s}^{-1}$	$k_1 \times 10^4 / \text{mol}^{-1} \text{ kg s}^{-1}$
1	633	0.21	0.19
2	653	0.80	0.74
3	653	0.59	0.55
4	653	0.62	0.58
5	663	1.2	1.1
6	673	1.3	1.2
7	673	1.6	1.5
8	673	1.9	1.8
9	673	1.9	1.7
10	673	1.7	1.6
11	686	1.7	1.6
12	693	3.8	3.6
13	693	3.7	3.5
14	703	3.9	3.6
15	713	7.9	7.4
16	713	9.0	8.4

activation energy and the preexponential factor of reaction 1 were calculated.

$$E_1 = 38 \pm 1 \text{ kcal mol}^{-1}$$

$$k_1^0 = 5 \times 10^8 \text{ mol}^{-1} \text{ kg s}^{-1} \quad (10)$$

The value of E is lower than the dissociation energies of both processes $\text{H}_2 = 2\text{H}$ ($E_d' = 104.2 \text{ kcal mol}^{-1}$)⁶ and $\text{NO}_3^- = \text{NO}_2^- + \text{O}$ ($E_d'' = 94.2 \text{ kcal mol}^{-1}$)⁷. This experimental information seems to confirm a posteriori the assumption that reaction 1 is a second-order kinetic process, which can be expressed in its simplest form as



As is apparent from Figure 1B, a certain time after the reaction has started, the rate of hydrogen consumption becomes higher than expected on the basis of the assumed second-order process. The analysis of the curves $\log P$ vs. time showed that the interval of validity of kinetic eq 5 is temperature dependent.

Since the water pressure, and hence the water concentration, were kept constant, as previously mentioned, during each experiment, the only variable parameters in the course of the reaction were the concentrations of hydrogen and nitrite. It could then be reasonably assumed that the observed rate of acceleration was due to an interaction between hydrogen and nitrite. However, since the stoichiometric correspondence between hydrogen disappearance and nitrite formation was always found to be valid (vide ante) the hypothesis of an accelerating autocatalytic process (paralleling direct mechanism 1a) appeared to be the most likely



In the given mechanism, X⁻ represent a short-lived intermediate while reaction 12 summarizes all the fast steps following rate-determining step 11. The overall process is still reaction 1.

In order to confirm such an hypothesis, experiments were performed using a nitrate solvent containing a large initial concentration of nitrite (0.17–1.19 *m*). In effect as is apparent from the example reported in Figure 2, the reaction rate increased proportionally to the nitrite concentration.

The analysis of a typical kinetic curve presenting an autocatalytic component was made as in the example reported in Figure 3. Curve a represents the experimental

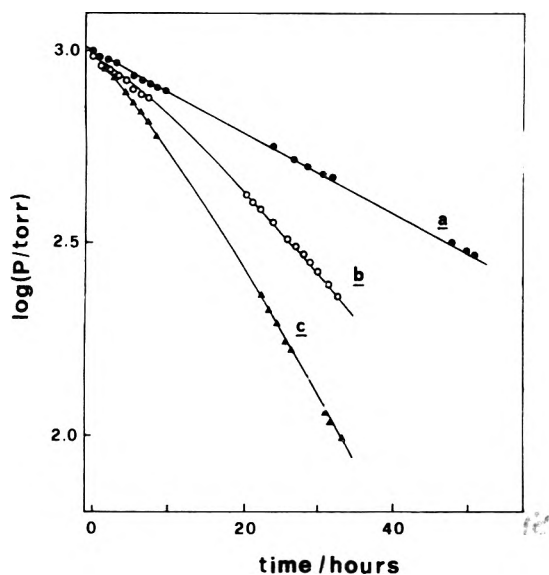


Figure 2. Semilogarithmic plots for kinetic experiments carried out at constant temperature (673 K) in the presence of different initial nitrite concentration: (a) $[\text{NO}_2^-]_i = 0$; (b) $[\text{NO}_2^-]_i = 0.17 \text{ m}$; (c) $[\text{NO}_2^-]_i = 0.42 \text{ m}$.

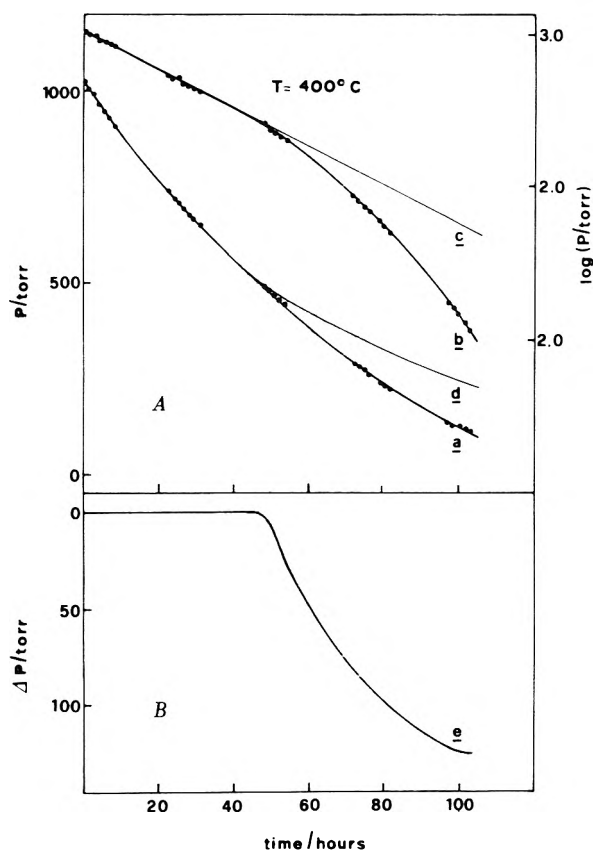


Figure 3. Example of graphical analysis of a kinetic curve presenting a large autocatalytic component ($T = 673 \text{ K}$): (curve a) experimental pressure vs. time variation; (curve b) logarithm of curve a; (curve c) extrapolation from the straight line of curve b; (curve d) antilogarithm of curve c; (curve e) difference between curves a and d.

pressure vs. time variation while curve b gives the logarithm of curve a. By calculating the antilogarithm of curve c, extrapolated from the straight line of curve b, one can obtain the "theoretical" pressure-time curve d uniquely due to the contribution of direct mechanism 1a described by kinetic eq 5. The pressure difference obtained by subtracting curve a from curve d is plotted in Figure 1AB. Its S shape is typical of an autocatalytic process. The zero slope of the initial line of curve e is due to a geometrical

TABLE II: Kinetic Constants for the Autocatalytic Process $\text{NO}_3^- + \text{H}_2 = \text{NO}_2^- + \text{H}_2\text{O}$ at Different Temperatures^a

Expt no.	T, K	$k_{11} \times 10^2 / \text{mol}^{-1} \text{ kg s}^{-1}$	$[\text{NO}_2^-]_i / \text{mol kg}^{-1}$
4	653	0.55	
5	663	0.96	
10	673	1.1 _s	
13	693	4.4	
16	713	13	
17	713	10	
18	623	0.14	1.19
19	645	0.26	1.19
20	656	0.61	0.43
21	673	1.1	0.17
22	673	0.95	0.42

^a $[\text{NO}_2^-]_i$ = initial nitrite concentration.

approximation (i.e., the extrapolation of curve c) used for treating the experimental data.

The kinetic constants for process 11 can be calculated by the following overall reaction rate:

$$d[\text{NO}_2^-]/dt = k_1[\text{NO}_3^-][\text{H}_2] + k_{11}[\text{NO}_2^-][\text{H}_2] \quad (13)$$

By considering expressions 3 and 6, and by introducing a few simple approximations, eq 13 can be written

$$\frac{1}{K_{\text{H}}P} \frac{\Delta[\text{NO}_2^-]}{\Delta t} = k_1' + k_{11}[\text{NO}_2^-] \quad (14)$$

where $\Delta[\text{NO}_2^-]$ represents the nitrite concentration variation during the time interval Δt and can be calculated (as well as $[\text{NO}_2^-]$) on the basis of eq 4. The meaning of the other symbols been previously specified. By introducing the average k_1' values ($k_1' = k_1[\text{NO}_3^-]$) derived from Table I data in eq 14, k_{11} values were calculated.

The average k_{11} values obtained in this way at various temperatures are listed in column three, Table II. The confidence limits are $\pm 10\%$. From the relevant Arrhenius plot, the kinetic parameters were calculated:

$$E_{11} = 46 \pm 3 \text{ kcal mol}^{-1} \\ k_{11}^0 = 1 \times 10^{13} \text{ mol}^{-1} \text{ kg s}^{-1} \quad (15)$$

Note that autocatalytic process 11, in the investigated temperature interval, is characterized by a kinetic constant larger than the one of direct process 1 by about two orders of magnitude. The data obtained up to now do not allow any thorough explanation of this fact, even if, by analogy with similar previously studied^{8,9} systems, the phenomenon might be ascribed to a different bond energy: in the present case, the energy of the O-N bonds in the two species nitrate and nitrite.

At the higher temperatures investigated, a slight decomposition of the solvent can occur¹⁰ with nitrogen dioxide being developed in the gas phase. This will then contribute when performing pressure measurements. The evaluation of the amount of nitrogen dioxide produced was made by adding sodium hydroxide to the water present in the cold trap to capture any acidic gaseous species. An UV spectrophotometric analysis of the final solution showed absorption bands at 302 and 355 μm due¹¹ to the presence of NO_2^- and NO_3^- ions, i.e., the products of NO_2 disproportionation. The height of the bands, however, indicated that, even at 440 °C, the solvent decomposition was very mild and that the NO_2 pressure was not significant with respect to the total pressure present in the reaction cell during the first reaction period. A certain relative increase of the NO_2 pressure undoubtedly occurs in the course of the reaction, when the hydrogen pressure

progressively decreases. This fact is perhaps at the origin of the rather sudden bending of curve $\Delta P-t$ in Figure 1AB when, however, about 90% of reaction is over. The total quantity of NO_2 developed can be evaluated as, in the last favorable conditions, around 0.1–0.5% of the total hydrogen used in the reaction.

Acknowledgment. This work was carried out with the financial assistance of the Italian National Research Council (C.N.R., Roma) and of the NATO Scientific Affairs Division (Bruxelles).

References and Notes

(1) E. Desimoni, F. Paniccia, and P. G. Zambonin, *J. Chem. Soc., Faraday Trans. 1*, **69**, 2014 (1973).

- (2) E. Desimoni, F. Paniccia, L. Sabbatini, and P. G. Zambonin, *J. Appl. Electrochem.*, **6**, 445 (1976).
 (3) E. Desimoni, F. Paniccia, L. Sabbatini, and P. G. Zambonin, Proceedings of the 149th Meeting of the Electrochemical Society, Washington, D.C., 1976.
 (4) E. Desimoni, F. Paniccia, and P. G. Zambonin, *J. Electroanal. Chem.*, **38**, 373 (1972).
 (5) G. J. Janz, "Molten Salt Handbook", Academic Press, New York, N.Y., 1967, p 48.
 (6) L. Pauling, "The Nature of the Chemical Bond", Cornell University Press, Ithaca, N.Y., 1960, p 81.
 (7) E. S. Freeman, *J. Phys. Chem.*, **60**, 1487 (1956).
 (8) P. G. Zambonin and A. Cavaggioni, *J. Am. Chem. Soc.*, **93**, 2854 (1971).
 (9) F. Paniccia and P. G. Zambonin, *J. Phys. Chem.*, **78**, 1693 (1974).
 (10) B. D. Bond and P. W. M. Jacobs, *J. Chem. Soc.*, 1256 (1966).
 (11) J. H. Wetters and K. L. Uglum, *Anal. Chem.*, **42**, 335 (1970).

Model Calculations Describing Bistability for the Stirred Flow Oxidation of Cerous Ion by Bromate

K. Bar-Eli and Richard M. Noyes*

Department of Chemistry, University of Oregon, Eugene, Oregon 97403 and Department of Chemistry, University of Tel-Aviv, Tel-Aviv, Israel (Received June 20, 1977)

Publication costs assisted by the National Science Foundation

Geiseler and Föllner have recently reported that two different steady states may exist for identical flow conditions when cerium(III) is oxidized by acidic bromate in a continuously stirred tank reactor. We have made detailed model calculations for their system and find the experimental results are consistent with the mechanism and rate constants previously proposed to explain this reaction.

Introduction

The oxidation of cerium(III) by acidic bromate exhibits peculiar kinetic features that were first observed by Kasperek and Bruice.¹ When bromate is in excess, virtually no cerium(IV) is formed during an induction period which is followed by an almost discontinuous transition to rapid reaction. The rate then decreases by a factor of much more than 10 by the time the system is half way to its final equilibrium position of almost complete oxidation of cerium. Thompson² studied the somewhat simpler kinetic behavior in excess Ce(III), and Noyes, Field, and Thompson,³ NFT, proposed a detailed chemical mechanism.

The kinetics have been studied further by Vavilin and Zhabotinsky,⁴ by Barkin et al.,⁵ and by Herbo et al.⁶ All investigators are in essential agreement about the experimental facts, but Barkin et al.⁵ interpret their data in terms of the NFT mechanism while Herbo et al.⁶ make an alternative proposal. Noyes and Bar-Eli⁷ have presented arguments favoring the NFT mechanism.

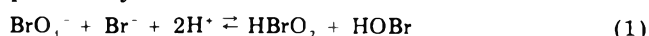
All of the above studies were conducted in batch systems. Geiseler and Föllner⁸ have recently reported some very interesting observations in a continuously stirred tank reactor (CSTR). They simultaneously followed bromide ion potentiometrically and ceric ion spectrophotometrically and noted that two different steady states could be attained with the same rates of flow of reactants. These steady states could be perturbed by temporarily changing the rate of input of a reactant and then restoring the original rate. The system would return to the original

steady state after a short perturbation but could be moved to the other one by a sufficiently long perturbation in the proper direction.

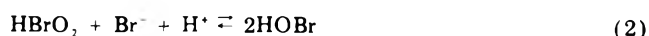
Geiseler and Föllner⁸ simplified the NFT model so that the state of the system could be described by only two parameters and showed that for certain combinations of rate constants the mechanism should yield two stable steady states with an unstable one between. We now report computations with the full NFT model and find an excellent correlation with the experimental observations.

Computations

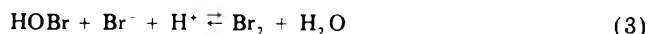
The NFT mechanism consists of the following seven potentially reversible reactions:



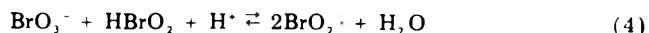
$$k_1 = 2.1 \text{ M}^{-3} \text{ s}^{-1} \quad k_{-1} = 1 \times 10^4 \text{ M}^{-1} \text{ s}^{-1}$$



$$k_2 = 2 \times 10^9 \text{ M}^{-2} \text{ s}^{-1} \quad k_{-2} = 5 \times 10^{-5} \text{ M}^{-1} \text{ s}^{-1}$$



$$k_3 = 8 \times 10^9 \text{ M}^{-2} \text{ s}^{-1} \quad k_{-3} = 110 \text{ s}^{-1}$$



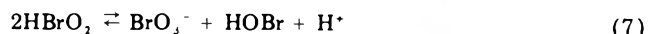
$$k_4 = 1 \times 10^4 \text{ M}^{-2} \text{ s}^{-1} \quad k_{-4} = 2 \times 10^7 \text{ M}^{-1} \text{ s}^{-1}$$



$$k_5 = 6.5 \times 10^5 \text{ M}^{-2} \text{ s}^{-1} \quad k_{-5} = 2.4 \times 10^7 \text{ M}^{-1} \text{ s}^{-1}$$



$$k_6 = 9.6 \text{ M}^{-1} \text{ s}^{-1} \quad k_{-6} = 1.3 \times 10^{-4} \text{ M}^{-3} \text{ s}^{-1}$$



$$k_7 = 4 \times 10^7 \text{ M}^{-1} \text{ s}^{-1} \quad k_{-7} = 2 \times 10^{16} \text{ M}^{-2} \text{ s}^{-1}$$

* Address correspondence to the author at the University of Oregon.

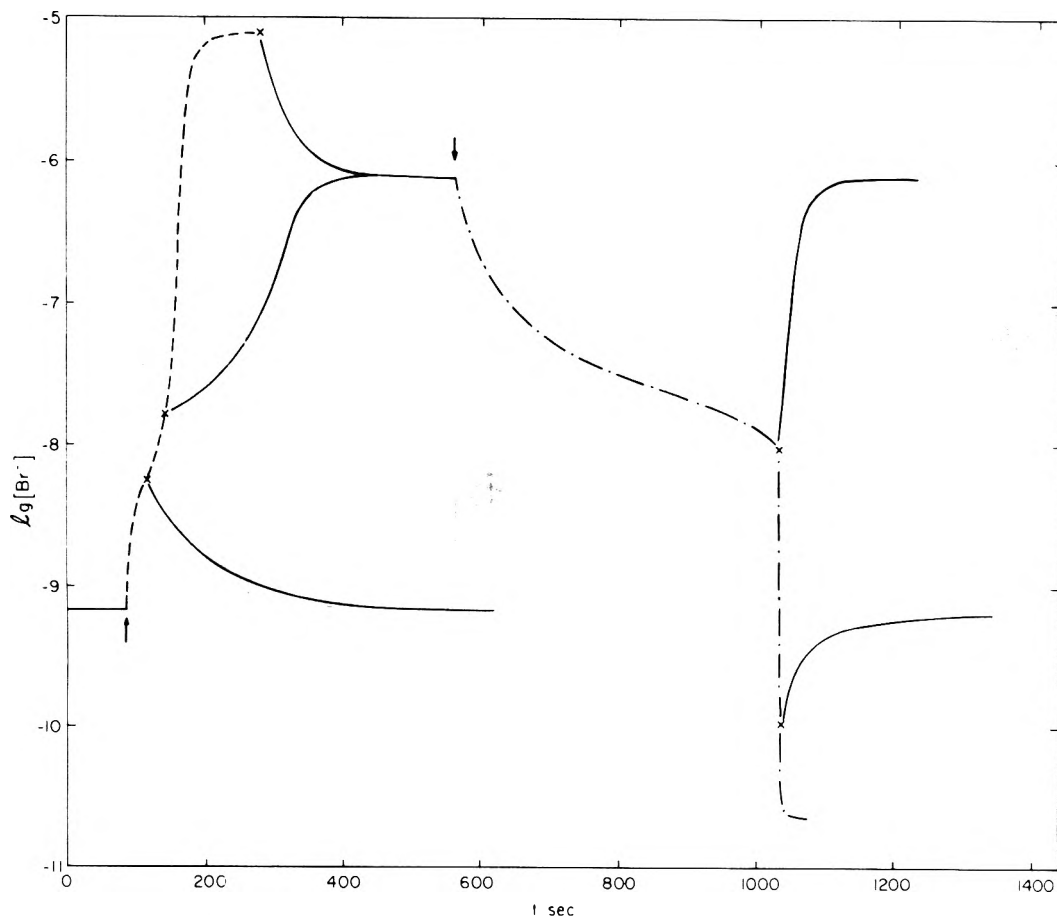


Figure 1. Semilogarithmic plots of $[\text{Br}^-]$ against time. Values of $[\text{Br}^-]_0$ were (—) 10^{-5} M, (---) 10^{-4} M, and (-·-·) 0. Up (down) arrows indicate points at which $[\text{Br}^-]_0$ was increased (decreased) from its original value of 10^{-5} M. Crosses indicate points at which the original flow rate was resumed.

Reasons for selecting these rate constants have been presented elsewhere.⁵ Rate constants are defined so that solvent water does not enter the rate expression but is treated as at unit activity. For each of the other nine chemical species in these equations, the chemical mechanism generates a differential equation for dc_i/dt where c_i is the instantaneous concentration of species i . To each such equation was added a term $-k_0c_i$ where $k_0 = 4 \times 10^{-3} \text{ s}^{-1}$, the ratio of total flow rate to reactor volume in the experiments.⁸ Input of chemicals involved three flows containing BrO_3^- , Br^- , and Ce^{3+} each 1.5 M in H^+ . These inputs were modeled by adding a term $k_0c_j^0$ where c_j^0 is the concentration of species j that would be attained with these flows if no chemical reactions took place. Values of the c_j^0 concentrations were $[\text{BrO}_3^-]_0 = 2 \times 10^{-3}$ M, $[\text{Br}^-]_0 = 1 \times 10^{-5}$ M, $[\text{Ce}^{3+}]_0 = 1.5 \times 10^{-4}$ M, and $[\text{H}^+]_0 = 1.5$ M. These inputs model those used in the experiments by Geiseler and Föllner.⁸

These stiff differential equations were solved numerically by the Gear⁹ method. Perturbations to the system could be introduced by discontinuous changes in $[\text{Br}^-]_0$ without making any other changes.

Results

The computations for these inputs and reactions showed the system could be made to converge to either of two steady state compositions designated SSI and SSII in Table I. Steady state I contains a relatively large concentration of Br^- and very low concentrations of HBrO_2 and BrO_2 ; step 5 is strongly inhibited and very little Ce^{4+} is present. Steady state II contains a much lower concentration of Br^- and much higher concentrations of

TABLE I: Molar Compositions of the Two Steady States Satisfying the Model Equations

Species	SSI	SSII
Br^-	7.755×10^{-7}	6.456×10^{-10}
HOBr	6.522×10^{-8}	2.056×10^{-5}
HBrO_2	3.226×10^{-12}	1.975×10^{-8}
Br_2	5.517×10^{-6}	1.448×10^{-8}
BrO_2	1.971×10^{-12}	1.604×10^{-7}
BrO_3^-	1.998×10^{-3}	1.986×10^{-3}
Ce^{3+}	1.499×10^{-3}	1.130×10^{-4}
Ce^{4+}	9.214×10^{-8}	3.696×10^{-5}
H^+	1.5	1.5

oxybromine intermediates and Ce^{4+} .

Figures 1 and 2 illustrate calculated effects of temporary changes in the rate of input of bromide ion. These figures plot $\log [\text{Br}^-]$ and $[\text{Ce}^{4+}]$ in order to mimic the quantities observed.¹⁰ The agreement with experiment is remarkably good considering the uncertainties in the absolute values of many of the rate constants.

Figure 1 illustrates first the effect on SSII of increasing $[\text{Br}^-]_0$ by a factor of 10. If this flow is continued, the system approaches a new steady state with about 10^4 times as much bromide ion as in SSII. If the rate of input of bromide is returned to its original value, the system will move to SSI or SSII depending upon how long the enhanced flow rate was allowed to persist. It is interesting to note that SSI contains about a tenth as much bromide ion as does the steady state approached when the bromide input is ten times as great.

The right part of Figure 1 shows the behavior if input of Br^- is temporarily stopped ($[\text{Br}^-]_0 = 0$) for a system in SSI. Such a system somewhat resembles a batch reactor

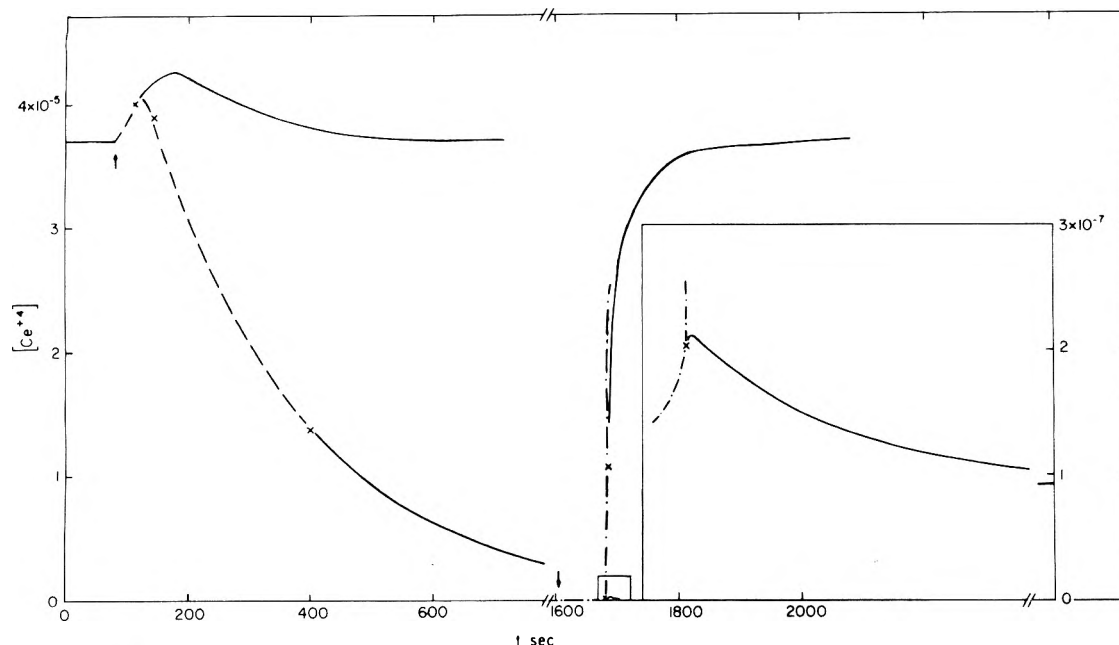


Figure 2. Linear plots of $[Ce^{4+}]$ against time. Symbols are the same as in Figure 1. Inset shows enlargement of concentration scale for the critical region in which rapid reaction commences.

during the induction period. The concentration of bromide drops for a while, and the residual amount is depleted very suddenly when the sequence of steps (4) + $2 \times$ (5) becomes more important than step 2. If input of bromide ion is resumed before that time, the system returns to SSI; if input of bromide is resumed at a later time, it moves to SSII.

The linear plots of $[Ce^{4+}]$ in Figure 2 are similar. The system is initially in SSII, and $[Br]_0$ is suddenly increased by a factor of 10. If the system is returned to the original flow rate after a short enough time, the system returns to SSII. However, if the enhanced bromide input is continued a little longer before it is returned to its previous value, reaction 5 is almost completely inhibited and outflow removes Ce^{4+} with a rate constant $4 \times 10^{-3} s^{-1}$ until SSI is attained.

The right part of Figure 2 shows the result of stopping at 1600 s the bromide input to a system in SSI. The system behaves like a batch reactor in its induction period with little change until about 1800 s when Ce^{4+} suddenly begins to be formed rapidly. The inset in Figure 2 shows that just before this time the system can be returned to SSI by renewing bromide input. At a later time, it will move to SSII even if bromide input is renewed.

A peculiar feature of Figure 2 is that the concentration of Ce^{4+} increases initially when bromide input is increased to a system in SSII even though the ultimate effect of continuing that bromide input is to decrease $[Ce^{4+}]$ by several orders of magnitude! This effect is also observed experimentally.¹⁰ In our previous more simplified efforts to model this kind of system,^{11,12} any addition of Br⁻ would

immediately reduce $[HBrO_2]$ and thereby slow the rate of Ce^{4+} formation. We have not yet determined whether the different effect in the more complete model is "thermodynamic" in the sense that a small increase in bromide input would ultimately generate a different steady state with increased $[Ce^{4+}]$, or whether it is "kinetic" in the sense that a small increase in bromide input would temporarily increase $[Ce^{4+}]$ but would ultimately reduce it if that small increase in flow were maintained.

The calculations reported here reproduce a wealth of experimental detail and do it so successfully they add considerably to our confidence in the validity of the basic mechanism of this reaction.⁷

References and Notes

- (1) G. J. Kasperek and T. C. Bruice, *Inorg. Chem.*, **10**, 283 (1971).
- (2) R. C. Thompson, *J. Am. Chem. Soc.*, **93**, 7315 (1971).
- (3) R. M. Noyes, R. J. Field, and R. C. Thompson, *J. Am. Chem. Soc.*, **93**, 7315 (1971).
- (4) V. A. Vavilin and A. M. Zhabotinsky, *Kinet. Katal.*, **10**, 283 (1971).
- (5) S. Barkin, M. Bixon, R. M. Noyes, and K. Bar-Eli, *Int. J. Chem. Kinet.*, in press.
- (6) C. Herbo, G. Schmitz, and M. van Glabbeke, *Can. J. Chem.*, **54**, 2628 (1976).
- (7) R. M. Noyes and K. Bar-Eli, *Can. J. Chem.*, in press.
- (8) W. Geiseler and H. H. Föllner, *Biophys. Chem.*, **6**, 107 (1977).
- (9) (a) C. W. Gear, "Numerical Initial Value Problems in Ordinary Differential Equations", Prentice-Hall, Englewood Cliffs, N.J., 1971, pp 209-229. (b) A. C. Hindmarsh, "Gear: Ordinary Differential Equation Solver", VCIID-20001 rev. 3, Dec 1974.
- (10) Figure 2 plots $[Ce^{4+}]$ while Figure 3 in ref 8 plots $[Ce^{3+}]$, so observed and calculated effects appear to move in opposite directions.
- (11) R. J. Field and R. M. Noyes, *J. Chem. Phys.*, **60**, 1877 (1974).
- (12) R. J. Field and R. M. Noyes, *Faraday Symp. Chem. Soc.*, **9**, 21 (1974).

The Influence of Solvent upon Linear Enthalpy–Entropy Relationships. Proton Ionization of Substituted Piperidines in Water–Ethanol Mixtures

Guy Berthon,* Marie-Jose Blais, and Octavian Enea

The Laboratory of Thermodynamics and Electrochemistry, University of Poitiers, 86022 Poitiers, France (Received December 14, 1976; Revised Manuscript Received July 12, 1977)

The importance of the role of solute–solvent interactions with respect to substituent effects upon the reactivity of organic substances is discussed using enthalpy–entropy linear relationships which are often characteristic of proton ionization from a series of derivatives from a common parent molecule according to Hepler's approach. Hepler's fundamental distinction between his β_e parameter and Leffler and Grunwald's β_i version was based solely upon solvent γ values. We now demonstrate that an additional factor must be considered so that β_i can be generalized in terms of β_e and β_e in terms of T . Further, conditions for which $\beta_i = \beta_e$ and $\beta_e = T$ are shown to be independent.

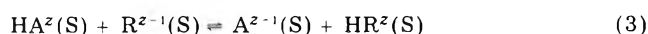
A quantitative study of the extent to which substituent effects determine the reactivity of organic molecules necessitates the use of empirical relationships correlating data from studies of different reactions. Rate or equilibrium constants in particular have been used to forecast the reactivity of new organic substances (these analyses are commonly called "linear free energy relationships").¹

The Hammett relationship is unquestionably the most popular² and its success has given rise to interest in its quantal and thermodynamic⁴ interpretations. In particular Hepler's analyses of substituent effects and solute–solvent interactions for carboxylic acid deprotonation have attracted much attention.^{4,5} The work concludes by establishing a theoretical difference between its β_e parameter⁵ and that of β_i as used by Leffler and Grunwald.⁶

$$\delta \Delta H^\circ = \delta \Delta H^\circ_{\text{int}}(1 + \gamma) + \beta_e \delta \Delta S^\circ \quad (1)$$

$$\delta \Delta H^\circ = \beta_i \delta \Delta S^\circ \quad (2)$$

By way of explanation we might recall that $\delta \Delta H^\circ$ and $\delta \Delta S^\circ$ are the respective enthalpies and entropies of formation for the following reaction



in which a substituted acid HA^z and a reference acid HR^z participate, the symbol (S) denoting that the species are in solution, γ is a solvent parameter, and subscript int refers to internal effects, i.e., to the intrinsic effects of the acid and base under consideration.

Hepler derives the following expression by differentiating β_i and β_e for $\beta_e = T$

$$\beta_i = \beta_e - (1 - \gamma)/(d\gamma/dT) = T - (1 - \gamma)/(d\gamma/dT) \quad (4)$$

and thus β_i ought to vary as the composition of the solvent is varied. However, our previous reports in this area are at variance with this theoretical interpretation.

(a) For proton ionization of a series of piperazines at 25 °C there is a distinct variation in γ as the composition of water–ethanol solvent is varied whereas the β_e parameter remained essentially constant.⁷ β_e was similar to T for the second ionization (265 K) but differed greatly for the first ionization (400 K).

(b) A study of the silver complexation for a series of pyridines in water at 25 °C⁸ had Hepler's theory applied and the $\delta \Delta H^\circ_{\text{int}}(1 + \gamma)$ term approximated to zero so that $\beta_e \approx \beta_i$ as per eq 1. This parameter was equal to 450 K

in the first complexing step but was 300 K = T in the second step.

(c) We have recently investigated the proton ionization of a series of substituted piperidines in water at 25 °C⁹ and found that $\beta_e = \beta_i = T$, the $\delta \Delta H^\circ_{\text{int}}(1 + \gamma)$ term once again being zero; we decided to extend this investigation to a range of water–ethanol mixtures for which the γ parameter varied⁷ to test eq 4.

Experimental Section

Reagents. Piperidine was a Merck product, 2-propylpiperidine was obtained from K and K Laboratories, and the other derivatives from Aldrich.

Sodium perchlorate, potassium hydroxide, and perchloric acid were Prolabo products.

All these substances were of "pro analysi" quality.

The compositions of the water–ethanol mixtures of 52 and 73.4 wt % solvents were verified by appropriate density measurements.

Equipment. A Beckman research pH meter Model 101901 was used. It was equipped with a calomel reference electrode Model 4970 (Beckman) and a glass electrode Model 39004 (Beckman).

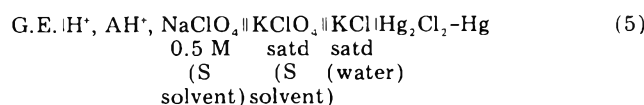
Heat measurements were performed with a CRMT calorimeter (Setaram) and a BCP differential calorimeter (Arion).

All thermal fluxes were recorded using a Servotrace apparatus (Sefram) and automatically integrated by a 2105 M device (LTT).

Techniques. All experiments were performed at 25 °C, with 0.5 M NaClO_4 to ensure a constant ionic strength. Solutions of amines were prepared from solvents which were deaerated before use by bubbling dry nitrogen, and then stored under this atmosphere to avoid carbonation.

They were titrated by pH potentiometry against perchloric acid, which had been previously titrated against $\text{Na}_2\text{B}_4\text{O}_7 \cdot 10\text{H}_2\text{O}$. Secondly, the acid titre was verified against potassium hydroxide previously determined with Kuhlmann potassium hydrogen phthalate.

The electrochemical cells were



where A represents the amine under consideration.

The pH measurements referred to Bates' buffer 5.40 and 6.07 solutions, these being respectively specific to 52 and 73.4% ethanol media.¹⁰

TABLE II: Proton-Ionization Thermodynamic Functions for Piperidine and Its Derivatives in the Solvents Water^a and 52 and 73.4 wt % Water-Ethanol^b

Amine	Water ^a				52 wt % H ₂ O-EtOH				73.4 wt % H ₂ O-EtOH			
	ΔG° kcal mol ⁻¹	$-\Delta H^\circ$ kcal mol ⁻¹	ΔS° cal mol ⁻¹ K ⁻¹	$-\Delta G^\circ$ kcal mol ⁻¹	$-\Delta H^\circ$ kcal mol ⁻¹	ΔS° cal mol ⁻¹ K ⁻¹	$-\Delta G^\circ$ kcal mol ⁻¹	$-\Delta H^\circ$ kcal mol ⁻¹	ΔS° cal mol ⁻¹ K ⁻¹	$-\Delta G^\circ$ kcal mol ⁻¹	$-\Delta H^\circ$ kcal mol ⁻¹	ΔS° cal mol ⁻¹ K ⁻¹
Piperidine	15.41 ± 0.01	13.19 ± 0.07	7.46 ± 0.27	14.39 ± 0.07	13.08 ± 0.07	4.35 ± 0.47	13.85 ± 0.07	12.35 ± 0.05	5.01 ± 0.40	13.85 ± 0.07	12.35 ± 0.05	5.01 ± 0.40
2-Methylpiperidine	15.35 ± 0.01	14.03 ± 0.08	4.42 ± 0.30	14.37 ± 0.04	13.90 ± 0.05	1.54 ± 0.30	13.85 ± 0.05	12.84 ± 0.06	3.36 ± 0.37	13.85 ± 0.05	12.84 ± 0.06	3.36 ± 0.37
3-Methylpiperidine	15.33 ± 0.01	13.75 ± 0.04	5.31 ± 0.17	14.30 ± 0.16	13.87 ± 0.03	1.42 ± 0.64	13.68 ± 0.11	13.87 ± 0.03	-0.68 ± 0.47	13.68 ± 0.11	13.87 ± 0.03	-0.68 ± 0.47
4-Methylpiperidine	15.37 ± 0.01	13.48 ± 0.05	6.35 ± 0.20	14.33 ± 0.11	13.81 ± 0.05	1.72 ± 0.54	13.73 ± 0.12	12.57 ± 0.07	3.87 ± 0.64	13.73 ± 0.12	12.57 ± 0.07	3.87 ± 0.64
2,6-Dimethylpiperidine	15.41 ± 0.01	14.53 ± 0.07	2.97 ± 0.27	14.47 ± 0.08	14.45 ± 0.04	0.03 ± 0.40	13.84 ± 0.03	13.20 ± 0.03	2.11 ± 0.20	13.84 ± 0.03	13.20 ± 0.03	2.11 ± 0.20
2-Ethylpiperidine	15.40 ± 0.01	14.18 ± 0.06	4.09 ± 0.23	14.30 ± 0.07	13.95 ± 0.06	1.17 ± 0.44	13.72 ± 0.08	12.87 ± 0.02	2.80 ± 0.33	13.72 ± 0.08	12.87 ± 0.02	2.80 ± 0.33
2-Propylpiperidine	15.43 ± 0.01	14.44 ± 0.09	3.31 ± 0.33	14.22 ± 0.04	13.99 ± 0.03	0.74 ± 0.23	13.70 ± 0.05	12.95 ± 0.03	2.49 ± 0.27	13.70 ± 0.05	12.95 ± 0.03	2.49 ± 0.27
2,2,6,6-Tetramethylpiperidine	15.48 ± 0.01	14.17 ± 0.14	4.40 ± 0.50	14.62 ± 0.11	15.44 ± 0.07	-2.75 ± 0.60	14.25 ± 0.11	14.21 ± 0.07	0.13 ± 0.60	14.25 ± 0.11	14.21 ± 0.07	0.13 ± 0.60

^a Reference 9. ^b Temperature, 25 °C; ionic strength, 0.5 M KNO₃ in water and 0.5 M NaClO₄ in water-ethanol mixtures.

in the water⁹ and water-ethanol 52 and 73.4 wt %, respectively.

Discussion

First, two preliminary observations: A different straight line is obtained for each solvent because of changes in activity coefficient from one solvent to another. These changes act similarly for the amines under consideration, the point relative to piperidine being roughly situated on the straight line in all three cases.

The straight lines are parallel. The order in which the points specific to each derivative are plotted is sometimes perturbed from one straight line to another, but the slopes remain, to within the limit of the errors, practically equal to the experimental temperature.

The fact that the piperidine point lies on the straight line for each solvent implies that the $\delta\Delta H^\circ_{\text{int}}(1 + \gamma)$ term of eq 1 is nil in the three cases under consideration and β_e is then mathematically equivalent to β_i .

Further, if one applies eq 1 to the whole of the data taken in the form of $\delta\Delta H^\circ$ and $\delta\Delta S^\circ$, points representing $\delta\Delta H^\circ$ and $\delta\Delta S^\circ$ piperidine values now denote common origin for the three solvents (Figure 2). The averaged parameters give the following result: $\delta\Delta H^\circ_{\text{int}}(1 + \gamma) = -0.03 \pm 0.1$ kcal mol⁻¹; $\beta_e = 292 \pm 6$ K.

This latter value is always almost equivalent to T and equivalent to β_i as the origin ordinate may in practice be considered as zero.

Varying solvent composition does not influence β_i and β_e values in this work.

Thus it seems preferable to discuss the distinction of β_i and β_e parameters on the base of relations 1 and 2 rather than on relation 4.

Combination of (1) and (2) results in

$$\delta\Delta H^\circ / \delta\Delta S^\circ = \beta_i = \beta_e + \delta\Delta H^\circ_{\text{int}}(1 + \gamma) / \delta\Delta S^\circ \quad (10)$$

i.e., since

$$\delta\Delta H^\circ_{\text{ext}} = \beta_e \delta\Delta S^\circ + \gamma \delta\Delta H^\circ_{\text{int}} \quad (11)$$

$$\beta_i = \beta_e [1 + \delta\Delta H^\circ_{\text{int}}(1 + \gamma) / (\delta\Delta H^\circ - \delta\Delta H^\circ_{\text{int}}(1 + \gamma))] \quad (12)$$

It is noteworthy from this last equation that the theoretical difference between β_i and β_e depends not only upon the γ solvent parameter, but also on the $\delta\Delta H^\circ_{\text{int}}$ part of $\delta\Delta H^\circ$. This arises independent of whether β_e (or β_i) is or is not equal to T , since eq 12 is set up without any particular condition.

Let us now study the relationship between T and β_e .

From a study of the proton ionization of a series of substituted carboxylic acids at different temperatures around 25 °C, Slade¹³ noticed that, for the species exhibiting ΔG° of the same order, the corresponding segments of the plots of ΔH° vs. ΔS° referring to the narrow temperature range under consideration gave rise to a single straight line of slope equal to 298 K. Therefore he suggested that this phenomenon could well explain reports from other laboratories of linear relationships between ΔH° and ΔS° .

Let us reconsider this remark and imagine a study made, for instance, at five temperatures, one of which is 25 °C.

If the temperatures are chosen sufficiently near to one another so that the slope of each curve drawn from the equation

$$\delta\Delta H^\circ = \delta\Delta G^\circ + T\delta\Delta S^\circ \quad (13)$$

Thus the most important conclusion of this work is that the β_e parameter may equal T because of the peculiar equality

$$\delta \Delta G^\circ = \delta \Delta H^\circ_{\text{int}}(1 + \gamma) \quad (17)$$

while the following expression

$$\delta \Delta H^\circ_{\text{int}}(1 + \gamma) = 0$$

moreover implies that $\beta_i = \beta_e$, these two relationships being independent of each other.

Turning to substituted piperidines proton ionization in particular, on the one hand owing to the "compensation" rule between enthalpy and entropy changes^{4,14} resulting in $\beta_e = T$, on the other hand on account of $\delta \Delta H^\circ_{\text{int}} = 0$ (the term $\delta \Delta H^\circ_{\text{int}}(1 + \gamma)$ does not vary as a function of the solvent whereas γ for the mixtures under consideration does vary⁷), the equality

$$\delta \Delta G^\circ = 0$$

suggests that substituent effects arise solely from solute-solvent interactions. The quantitative assessment of

this hypothesis is currently being studied in our laboratory.

References and Notes

- (1) N. B. Chapman and J. Shorter, "Advances in Linear Free Energy Relationships", Plenum Press, New York, N.Y., 1972.
- (2) L. P. Hammett, "Physical Organic Chemistry", McGraw-Hill: 1st ed, New York, N.Y., 1940; 2nd ed, Tokyo, 1970.
- (3) M. J. S. Dewar, R. Golden, and J. M. Harris, *J. Am. Chem. Soc.*, **93**, 4187 (1971).
- (4) J. W. Larson and L. G. Hepler, "Solute-Solvent Interactions", J. F. Coetzee and C. D. Ritchie, Ed., Marcel Dekker, New York, N.Y., 1969.
- (5) L. G. Hepler, *Can. J. Chem.*, **49**, 2803 (1971).
- (6) J. E. Leffler and E. Grunwald, "Rates and Equilibria of Organic Reactions", Wiley, New York, N.Y., 1963.
- (7) O. Enea, G. Berthon, and K. Houboss, *Bull. Soc. Chim. Fr.*, 1959 (1975).
- (8) G. Berthon, O. Enea, and Y. Fuseau, *Thermochim. Acta*, **16**, 323 (1976).
- (9) M. J. Blais, O. Enea, and G. Berthon, *Thermochim. Acta*, **8**, 433 (1974).
- (10) R. G. Bates, "Determination of pH: Theory and Practice", Wiley, New York, N.Y., 1964.
- (11) S. Kilpi and H. Warsila, *Z. Phys. Chem.*, **A177**, 427 (1936).
- (12) G. L. Bertrand, F. J. Millero, C. Wu, and L. G. Hepler, *J. Phys. Chem.*, **70**, 699 (1966).
- (13) M. D. Slade, Ph.D. Thesis, Brigham Young University, 1971.
- (14) D. H. Everett, "Hydrogen-Bonded Solvent Systems", A. K. Covington and P. Jones, Ed., Taylor and Francis, London, 1968, p 5.

The Ionization of 4-Nitrophenylacetonitrile in Water-Dimethyl Sulfoxide Mixtures¹

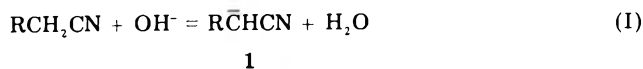
Edward A. Walters²

The Chemical Laboratory, University of Kent at Canterbury, Canterbury, Kent CT2 7NH, England and the Department of Chemistry, University of New Mexico, Albuquerque, New Mexico 87131 (Received January 20, 1977)

Publication costs assisted by the University of New Mexico

The ionization of 4-nitrophenylacetonitrile in water-Me₂SO mixtures was studied by spectrophotometric titration of the acid with solutions of tetramethylammonium hydroxide. Analysis of the spectra supports the conclusion that ionization in hydroxylic solvents produces two forms of the anion, one unspecifically solvated (λ_{max} 535 nm) and the other hydrogen bonded to the nitro group of the anion (λ_{max} 495 nm). In aprotic solvents and in mixed solvents in which the hydroxylic component is strongly associated with the aprotic part only the unspecifically solvated anion is observed. The equilibrium constants for both reactions as a function of $X_{\text{Me}_2\text{SO}}$ over the solvent composition range $X_{\text{Me}_2\text{SO}} = 0.065$ to $X_{\text{Me}_2\text{SO}} = 0.40$ have been measured. $\text{p}K_{\text{a/a}}^{\text{H/A}}$ values for the acid were deduced over the same solvent range. The acidity increases upon addition of Me₂SO, reaches a maximum at $X_{\text{Me}_2\text{SO}} \approx 0.3$, and decreases slightly as the mole fraction of Me₂SO continues to increase. The observed variations are interpreted in terms of improved solvation of the large anion produced on ionization of the acid of the proton in mixed solvents and in terms of marked desolvation of the small hydroxide ion in the presence of Me₂SO.

Attempts have long been made to use the compound 4-nitrophenylacetonitrile [4-NO₂C₆H₄CH₂CN] as an indicator for the establishment of an acidity scale for strongly basic solutions because it appears to be a strong enough acid so the acid dissociation constant can be measured both in completely aqueous and partly aqueous media. It has proved to be an unacceptable indicator because unexplained spectral changes suggest that the ionization is not a simple process.³ We report here a resolution of this problem and a study of the ionization reaction

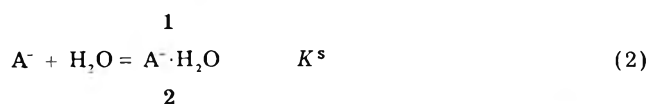
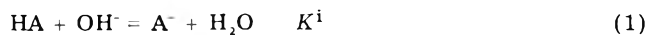


in water-dimethyl sulfoxide (Me₂SO) mixtures over the mole fraction range $X_{\text{Me}_2\text{SO}} = 0.065$ to $X_{\text{Me}_2\text{SO}} = 0.40$.

The intense purple color of 1 was generated many years ago⁴ by reacting the neutral acid with an ethanolic solution

of sodium ethoxide. Schaal⁵ first reported a set of spectra of 1 beginning with an orange-colored aqueous solution which became the more intense purple spectrum upon the addition of ethylenediamine to the water in rather large quantities. These changes were attributed to a pair of successive ionizations to give first 1 and then the dianion 4-NO₂C₆H₄CCN²⁻. More O'Ferrall and Ridd⁶ extended this work and concluded that different equilibrium products are formed in aqueous and methanolic media but that both equilibria have the same stoichiometric dependence upon base concentration. They suggested that the color change reported by Schaal originated in a change in solvent from water to ethylenediamine-water mixtures and that the colors are due to a pair of isomeric species one of which is favored in aqueous solution and the other in different media. More O'Ferrall and Ridd⁶ and shortly afterward Stewart and co-workers⁷ suggested that one color

is due to anion 1 and the other is due to nucleophilic addition of OH^- or OR^- to the aromatic ring. This suggestion was probed by Crampton⁸ and reexamined recently by Minch and co-workers⁹ who studied the ^1H NMR spectra of 1 generated by strong bases in methanolic Me_2SO , aqueous Me_2SO , and diethylamine solutions. Both groups concluded that the purple colored product is formed by proton abstraction from the neutral acid and that no evidence could be found that is attributable to the products of nucleophilic addition to the ring. Minch et al.⁹ also carried out an extensive investigation of the visible spectrum in Me_2SO -water mixtures in which they showed that both the orange and purple species obey Beer's law over a wide concentration range and they are rapidly interconverted exhibiting an isosbestic point at 491 nm. Neither species gave a detectable ESR signal so that radical anions can be eliminated as an explanation. On the basis of identical spectral changes in the presence of bases with different cations it was concluded that ion pairing cannot account for the observations. They suggested that the purple-colored species is anion 1 and that the orange-colored product is 1 in which a water molecule is hydrogen bonded to the oxygen atoms of the nitro group. It is shown in this study that the spectra in H_2O - Me_2SO mixtures can be explained quantitatively by the reaction sequence:



where $\text{HA} = \text{NO}_2\text{C}_6\text{H}_4\text{CH}_2\text{CN}$ and $\text{A}^- = \text{NO}_2\text{C}_6\text{H}_4\text{CHCN}^-$.

Experimental Section

Materials. Dimethyl sulfoxide, 1 L (Fisons, reagent grade), was dried over activated 4A molecular sieves for several days. The dried Me_2SO was transferred under a nitrogen atmosphere to a 2-L distillation flask supplied with a 40-cm Vigreux column, a water cooled condenser, and receiving flasks which were cooled in an ice bath. The system was then evacuated to a pressure of about 0.1 Torr and held there until the Me_2SO stopped bubbling. The apparatus was then slowly backfilled with nitrogen and several grams of powdered sodium amide was added to the Me_2SO . The system was again evacuated and, when the evolution of ammonia had ceased, the Me_2SO was distilled at a temperature of 31–35 °C at a pressure of 0.1–0.2 Torr. A forerun of about 150 mL was collected prior to the main fraction. The temperature of the water bath heating the distillation flask was never allowed to exceed 52 °C.

The receiving flask contained solidified Me_2SO ; it was capped with a three-way stopcock mounted above a standard-taper joint. The flask was evacuated and backfilled with dry nitrogen and stored in the dark. Samples of Me_2SO were removed through the three-way stopcock as needed while maintaining a positive pressure of nitrogen inside the flask.

Water for all solutions was triply distilled; the second distillation was from alkaline potassium permanganate.

Other solvents were all of the high purity grades and were used without additional purification. Tetramethylammonium hydroxide (TMAH) was obtained as a 25% solution in water (Fisons); it was diluted to about 0.15 M to provide a stock solution. This was standardized by titration with 0.100 N HCl. A pH titration showed the presence of a small amount (typically 5–6%) of carbonate so corrections were made for dissolved CO_2 and the stock solution was kept in a Schlenck tube. Aliquots were re-

moved as needed by a calibrated micrometer syringe while a positive pressure of nitrogen was maintained on the tube.

4-Nitrophenylacetonitrile (Eastman) was recrystallized to a constant melting point from ethanol before use: mp 116–117 °C (lit. mp 114–116 °C,¹⁰ 115–116 °C,⁹ 116 °C,¹¹ 116–117 °C¹²).

Spectrophotometric Titrations. Stock solutions of the mixed solvents were prepared by weight and were stored under nitrogen in the dark. Solutions were prepared by adding degassed solvent to a weighed sample of acid in a volumetric flask and shaking until the solid had dissolved. This solution was thermally equilibrated in a constant temperature bath and aliquots of TMAH stock solution were added to produce the anion 1. After each addition the solution was rapidly mixed and a sample was transferred to a 1 × 1 cm spectrophotometer cell and placed in the thermostatted cell compartment of a Perkin-Elmer Model 402 ultraviolet-visible spectrophotometer where it was allowed to equilibrate for 3 min. The remaining solution was stored in the darkened thermostat. Spectra were typically recorded over the region 390–670 nm. On the order of 10–12 spectra were obtained for each titration. Control experiments showed that under these conditions solutions of 1 were stable for the time required to complete a titration; decomposition is apparent at longer time periods. Titrations were customarily carried only to about 15% of completion.

Extinction coefficients of pure 1 were obtained from spectra in the high $X_{\text{Me}_2\text{SO}}$ region where the acid is quantitatively deprotonated. These were invariant in the range $X_{\text{Me}_2\text{SO}} = 0.4$ –0.9. At lower values of $X_{\text{Me}_2\text{SO}}$ differences between the observed spectra and those calculated for 1 (using only one observed point for normalization purposes) gave extinction coefficients for 2. Optical density measurements at 500 and 540 nm and the extinction coefficients for both 1 and 2 at these wavelengths permitted calculation of the concentrations of all the species present in solution. Extinction coefficients employed were $\epsilon_{500}^{\text{A}^-} = 2.47 \times 10^4$, $\epsilon_{540}^{\text{A}^-} = 4.09 \times 10^4$, $\epsilon_{500}^{\text{AS}^-} = 2.75 \times 10^4$, and $\epsilon_{540}^{\text{AS}^-} = 1.82 \times 10^4$ where $\text{A}^- = \text{NO}_2\text{C}_6\text{H}_4\text{CHCN}^-$ (1) and $\text{AS}^- = [\text{NO}_2\text{C}_6\text{H}_4\text{CHCN}] \cdot \text{H}_2\text{O}$ (2).

In order to have thermodynamic equilibrium constants for reactions 1 and 2 which can be compared with each other in different solvents it is necessary to account for the activity of every component:

$$K_{\text{a/a}}^i = [\text{A}^-] \gamma_{\text{H}_2\text{O}} / [\text{HA}] [\text{OH}^-] \quad (3)$$

and

$$K_{\text{a/a}}^s = [\text{AS}^-] / [\text{A}^-] \gamma_{\text{H}_2\text{O}} \quad (4)$$

The activity of pure water is assumed to be unity ($\gamma_{\text{H}_2\text{O}} \rightarrow 1$ as $X_{\text{H}_2\text{O}} \rightarrow 1$). At the concentrations employed (10^{-6} – 10^{-4} M) it is assumed that $\gamma_{\text{A}^-} = \gamma_{\text{OH}^-} = \gamma_{\text{AS}^-}$ and that $\gamma_{\text{HA}} = 1$. Values for $\gamma_{\text{H}_2\text{O}}$ in H_2O - Me_2SO mixtures were recently reported by Fiordiponti, Rallo, and Rodante.¹³ Reproducibility of $\text{p}K_{\text{a/a}}^i$ within a single titration and between separate determinations was less than ± 0.1 pK units and sometimes as low as ± 0.05 units.

Results and Discussion

The Nature of the Ionization Reaction. The relationship between the purple and orange forms of the anion formed on dissociation of 4-nitrophenylacetonitrile has long been an open question. Recently⁹ transformations between these species in alkaline solutions of HA in a variety of solvents suggested that they are in equilibrium with one another. Our studies support this analysis. In dry aprotic solvents such as Me_2SO , DMF, acetonitrile, and propylene

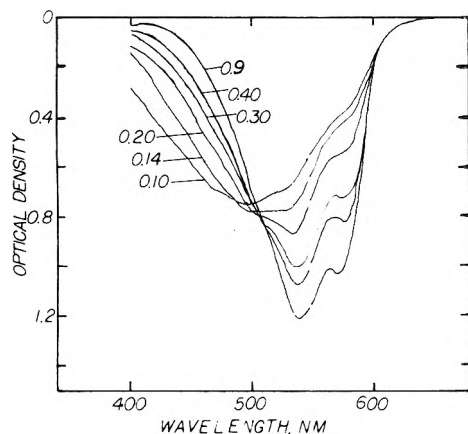


Figure 1. Visible spectra of 4-nitrophenylacetonitrile plus sufficient aqueous tetramethylammonium hydroxide to produce ionization. The spectra were obtained in H₂O/Me₂SO mixtures varying in mole fraction of Me₂SO from 0.10 to 0.90 and were selected so $[A^-] + [AS^-] = 2.9 \times 10^{-5}$ M.

carbonate the solution is purple in color and the spectra are very similar with λ_{\max} at 535 nm and a shoulder at 570 nm. There is no indication of a shoulder at 490 nm. In mixed aqueous solvents a peak appears with λ_{\max} at 490 nm and the solution becomes orange. The composition at which this peak first becomes noticeable depends strongly upon the nature of the cosolvent. In the case of aqueous Me₂SO solutions, there is no discernable change in the spectrum over the region $X_{\text{Me}_2\text{SO}} = 0.4-1.0$. Below $X_{\text{Me}_2\text{SO}} = 0.4$ a shoulder develops at 490 nm and increases in magnitude with decreasing $X_{\text{Me}_2\text{SO}}$ until at a mole fraction of 0.065 the original maximum at 535 nm is barely evident (Figure 1). Addition of the first traces of water to acetonitrile causes the appearance of the 490-nm peak and its importance increases with increasing water content. Behavior is similar in ethylenediamine.⁵ In aqueous DMF a side reaction occurs as indicated by the rapid disappearance of the purple spectrum. Propylene carbonate is not miscible with water so the effect could not be observed.

When alkaline solutions of pure ethanol were used to ionize HA, a shoulder at 490 nm was evident. Upon decreasing X_{EtOH} its importance grew so that by $X_{\text{EtOH}} = 0.4$ it has become the dominant feature.

It appears that the short wavelength (orange) peak is due to interaction between a hydroxylic solvent or solvent component and the anion 1. The feature does not appear in aqueous Me₂SO solvents with $X_{\text{Me}_2\text{SO}} > 0.4$ because the strong Me₂SO-water interaction effectively eliminates the likelihood of water-solute interactions in this region.¹⁴ Several experiments suggest that water is more strongly hydrogen bonded to Me₂SO than to itself.¹⁵ The Me₂SO-H₂O interaction reaches a maximum at about $X_{\text{Me}_2\text{SO}} = 0.33$ (corresponding to a composition of Me₂SO·2H₂O)¹⁶ so that only at lower values of $X_{\text{Me}_2\text{SO}}$ can the water-solute 1 interaction be pronounced enough to alter the visible spectrum.

These considerations suggest that the ionization process of HA consists of the two-step sequence in eq 1 and 2. In high mole fraction Me₂SO solutions and in dry aprotic solvents there is not enough "free" H₂O available to form detectable amounts of the solvated anion 2. In protic solvents and solvent mixtures containing H₂O both reactions 1 and 2 enter.

The spectrum of HA in $X_{\text{Me}_2\text{SO}} \sim 0.95$ with excess base gave a set of extinction coefficients over the wavelength range of 400–580 nm. Their very large values ($\epsilon \sim 10^4$) are indicative of π to π^* electronic transitions¹⁷ for both species.

The visible spectrum of 2 was obtained from the observed spectrum at lower $X_{\text{Me}_2\text{SO}}$ (0.30 and 0.40) by using a single long wavelength absorption to establish $[A^-]$, computing the spectrum for 1 at all other wavelengths, and subtracting this from the observed spectrum. The spectrum of 2 determined in this way has the same general appearance as the spectrum of 1, i.e., there is one rather broad maximum ($\lambda_{\max} \approx 495$ nm) with a shoulder on the long wavelength side. The chief differences are a decrease in extinction coefficient at the maximum by almost a factor of 2 and shift of 40 nm to the blue. Two independent determinations of this spectrum in solvents of different composition ($X_{\text{Me}_2\text{SO}} = 0.30$ and 0.40) gave sets of extinction coefficients which differed from one another by an average of 5%. These two sets of extinction coefficients were then used to compute spectra at various other solvent compositions between $X_{\text{Me}_2\text{SO}} = 0.065$ and $X_{\text{Me}_2\text{SO}} = 0.40$ and at a variety of intensities; these spectra reproduced the observed spectra to $\pm 2\%$ over the wavelength range 460–560 nm.

Additional support for the two-species ionization of HA was obtained from kinetic experiments.¹⁸ A series of temperature-jump experiments were performed on a sample of partially titrated HA in $X_{\text{Me}_2\text{SO}} = 0.20$ in which the magnitude and sign of the optical density change were measured as a function of wavelength. At short wavelengths a decrease in optical density change was observed which diminished in magnitude with increasing wavelengths and disappeared completely at about 505 nm; at still longer wavelengths the optical density change increased in magnitude with increasing wavelength. This is a clear indication of a two-species equilibrium. In addition, a reasonably good isosbestic point can be seen in Figure 1 at about 505 nm; this figure was generated by superimposing spectra selected so $[A^-] + [AS^-] = 2.9 \times 10^{-5}$ M. The isosbestic point is at a slightly longer wavelength than the isosbestic point obtained by Minch⁹ by superimposing spectra. Finally, a kinetic measure of the adequacy of K^i can be obtained from the time-resolved temperature-jump data from the ionization step. In $X_{\text{Me}_2\text{SO}} = 0.30$ the observed first-order rate coefficient for relaxation is given by

$$k_{\text{obsd}} = k_{\text{OH}^-} ([\text{HA}] + [\text{OH}^-]) + k_{\text{H}_2\text{O}} [\text{H}_2\text{O}] \quad (5)$$

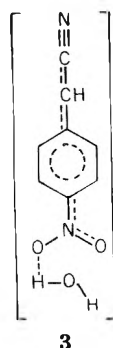
where k_{OH^-} is the catalytic coefficient for proton abstraction by OH⁻ and $k_{\text{H}_2\text{O}}$ applies to the reverse reaction of eq 1. The rate coefficient k_{OH^-} was obtained both from a plot of k_{obsd} vs. $([\text{HA}] + [\text{OH}^-])$, $(k_{\text{OH}^-})_{\text{plot}}$, and by using the relationship

$$k_{\text{H}_2\text{O}} = k_{\text{OH}^-} / K_{\text{a/a}}^i \quad (6)$$

directly in eq 5 and solving for $(k_{\text{OH}^-})_{\text{eq}}$. Here $K_{\text{a/a}}^i = K_{\text{a/a}}^i [\text{H}_2\text{O}] / \gamma_{\text{H}_2\text{O}}$ accounts for the fact that in the rate experiments molar concentration of water must be used. We find close agreement between the independent measures of k_{OH^-} : $(k_{\text{OH}^-})_{\text{plot}} = 1.97 \times 10^5 \text{ M}^{-1} \text{ s}^{-1}$ and $(k_{\text{OH}^-})_{\text{eq}} = 1.95 \times 10^5 \text{ M}^{-1} \text{ s}^{-1}$. These results provide support for the proposed ionization scheme of eq 1 and 2.

The Structure of the Colored Anions. In light of the preceding discussion we identify anion 1 as the source of the purple color. This is the species that is produced upon ionization in dry aprotic solvents.

The orange-colored material is identified with anion 2, the specifically hydrated form of 1. The structure 3 is consistent with the available experimental evidence as was suggested recently by Minch et al.⁹ In 3 the solvent water molecule is hydrogen bonded to one of the oxygens of the nitro group. This is not without precedent. Findlay and



Symons¹⁹ reported that nitrate ions in the protic solvents H₂O and MeOH no longer possess D_{3h} symmetry as indicated by a splitting of the $\bar{\nu}_3$ antisymmetric stretching vibration at about 1384 cm⁻¹. The descent in symmetry is attributed to the formation of a strong hydrogen bond between the protic solvent and one of the nitrate ion oxygens, as in [O₂NO...H-OH]⁻ or [O₂NO...H-OMe]⁻. The reason for hydrogen bond formation is suggested to be the high polarizability of the nitrate ion. As the hydrogen bond forms, negative charge is drawn into this bond very readily thus reducing the possibility of formation of hydrogen bonds at the other two oxygen atoms. The anion 1 should be analogous to nitrate ion; the very long wavelength, low energy, maximum for this absorption (λ_{\max} 535 nm) is evidence that 1 has a high polarizability as does the magnitude of ϵ_{\max} .²⁰ In the specifically solvated anion 3, much of the charge has been localized in the newly formed hydrogen bond resulting in a decrease in polarizability as indicated by a 40-nm shift of λ_{\max} to the blue and a decrease in the extinction coefficient. In addition a weaker, but still apparent hydrogen bond forms between 1 and ethanol in much the same way as methanol and nitrate ion form a hydrogen-bonded complex.¹⁹

It has been reported that the anion of 1-nitroindene and 9-nitrofluorene also exhibit a pronounced blue shift in going from Me₂SO to water.²¹ The shift for 1-nitroindene, 58 nm, is even greater than the one we observe. From their results of ¹H NMR studies of the anion in various protic and aprotic solvents Kerber and Porter conclude that the strong hydrogen bond donors water and trifluoroethanol effectively localize the negative charge of the anions by hydrogen bond formation. In aprotic solvents there is greater charge delocalization resulting, as suggested above, in an increased polarizability of the species which in turn manifest in a shift of the absorption maximum to longer wavelengths. The downfield shifts of the ring proton NMR resonances of 1 upon addition to D₂O to a solvent mixture of Me₂SO-methanol-TMAH⁹ suggest an increase in hydrogen bonding, presumably to the nitro oxygens, with a corresponding drop in the negative charge in the ring.

A large blue shift of the anion spectrum upon going from Me₂SO to water is not consistent with other data. Stewart and O'Donnell²² have examined the spectra of many carbanions in a variety of solvent mixtures, including Me₂SO-H₂O. They have found that the spectrum varies little over the solvent composition needed to ionize the carbon acid. A number of nitro compounds were included in this study. The exceptional behavior of 1 implies a rather specific solute-solvent interaction. In this regard it is significant that the observed spectra can be reproduced by assuming them to be the sum of two separate spectra whose shapes and extinction coefficients do not change with solvent composition.

The Ionization Equilibrium Constant $K_{a/a}^1$. Values for $K_{a/a}^1$ were obtained from eq 3 and the titration spectra over the solvent composition range of $X_{\text{Me}_2\text{SO}} = 0.065$ to $X_{\text{Me}_2\text{SO}}$

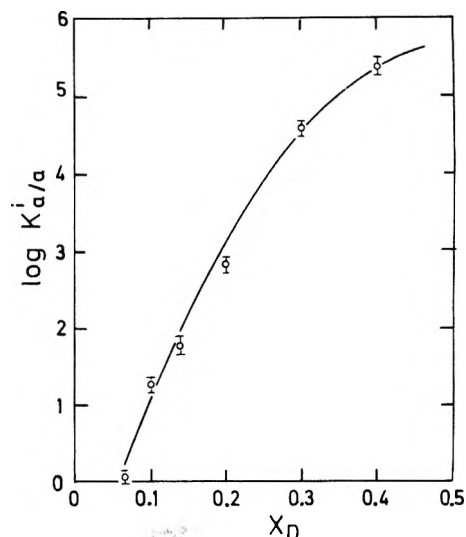


Figure 2. A plot of $\log K_{a/a}^1$ vs. solvent composition of Me₂SO-H₂O mixtures.

TABLE I: Results of the Spectrophotometric Titration of 4-Nitrophenylacetone with Tetramethylammonium Hydroxide in Me₂SO-H₂O Mixtures at 25 °C

$X_{\text{Me}_2\text{SO}}$	$K_{a/a}^1$	$K_{a/a}^s$	$K_{a/a}^{\text{HA}}$	$\text{p}K_{a/a}^{\text{HA}}$
0.065	1.11	20.1	3.54×10^{-15}	14.45
0.10	1.83×10^1	4.36	3.12×10^{-14}	13.51
0.14	5.78×10^1	2.72	4.78×10^{-14}	13.32
0.20	6.63×10^2	1.31	1.77×10^{-13}	12.75
0.30	3.79×10^4	0.649	1.98×10^{-12}	11.70
0.40	2.36×10^5	0.336	2.22×10^{-12}	11.65
1.0				12.3 ^a

^a Personal communication, F. G. Bordwell.

= 0.40. The results are shown in Figure 2 and Table I. $K_{a/a}^1$ rises from a value near unity at the lowest $X_{\text{Me}_2\text{SO}}$ by more than five orders of magnitude in $X_{\text{Me}_2\text{SO}} = 0.40$. Lower mole fractions of Me₂SO could not be used to determine $K_{a/a}^1$ reliably because the peak at 535 nm due to 1 is obscured at lower solvent compositions. The upper bound to solvent composition was $X_{\text{Me}_2\text{SO}} = 0.40$ because at higher mole fractions hydroxide ion is such a strong base that ionization of the acid by added hydroxide is stoichiometric and no equilibrium mixture of acid and conjugate base can be determined from the visible spectra.

Many other investigators have studied equilibria such as eq 1 in water-Me₂SO mixtures and have found similar results. For example, Stewart and co-workers²³ reported very large increases in basicity to amine indicators of 0.011 M tetramethylammonium hydroxide in these mixtures with an increase in the mole fraction of Me₂SO while Bowden and Cockerill^{24,25} reported a similar increase in basicity also of tetramethylammonium hydroxide using a series of substituted fluorenes as the acids. In principal these results can be analyzed in terms of the free energies of transfer of ($\delta\Delta G_{tr}$) reactants and products from a reference solvent to the solvent of interest. A substantial amount of coulometric data has been gathered on the enthalpies of transfer of various species²⁶⁻²⁸ and some information exists on entropies of transfer,^{29,30} but there are not sufficient data to permit a definitive analysis of the effects of the various ions and molecules. There is however general agreement^{23b,31-34} that the observed results are due to an increasingly more positive $\delta\Delta G_t$ for hydroxide ion as $X_{\text{Me}_2\text{SO}}$ increases than it is due to $\delta\Delta G_t$ for other species.

The Anion Solvation Step, $K_{a/a}^s$. The measured titration spectra and $\gamma_{\text{H}_2\text{O}}$ values of Fiordiponti et al.¹³ were

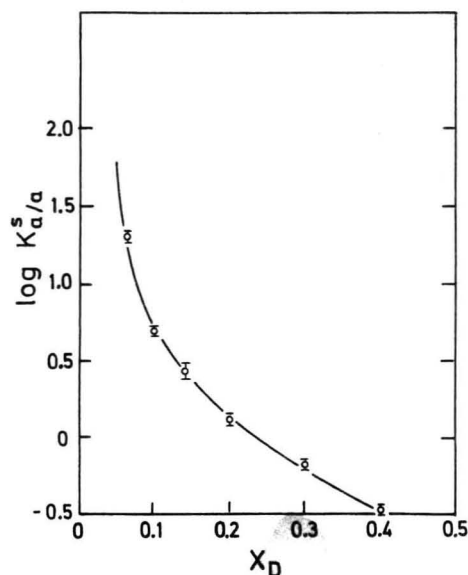
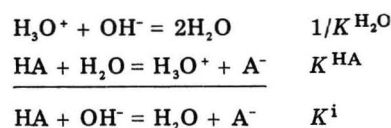


Figure 3. A plot of $\log K_{a/a}^s$ vs. solvent composition of Me₂SO-H₂O mixtures.

used in eq 4 to obtain $K_{a/a}^s$ data over the solvent composition range of $X_{\text{Me}_2\text{SO}} = 0.065$ to $X_{\text{Me}_2\text{SO}} = 0.40$. Results are displayed graphically in Figure 3 and listed in Table I. In contrast to $K_{a/a}^i$, $K_{a/a}^s$ decreases gradually by about two orders of magnitude over the solvent range. On the basis of the known heats of solution of water in H₂O-Me₂SO mixtures it is reasonable to conclude that the chief factor in determining the difference between $\Delta G^s(X)$ and $\Delta G^s(\text{H}_2\text{O})$ is the free energy of transfer of water to the solvent mixture, $\delta\Delta G_t(\text{H}_2\text{O})$. That is, the higher degree of reactant (H₂O)-solvent (H₂O-Me₂SO) interaction produces a shift in the equilibrium of eq 2 in the direction of reactants.

pK of 4-Nitrophenylacetonitrile in Aqueous Me₂SO. The ionization reaction of HA, eq 2, can be recognized as the sum of the ion product of water and the acid dissociation of HA:



so

$$K_{a/a}^{\text{HA}} = K_{a/a}^i K_{a/a}^{\text{H}_2\text{O}} / \gamma_{\text{H}_2\text{O}} \quad (7)$$

$K_{a/a}^{\text{HA}}$ and $\text{p}K_{a/a}^{\text{HA}}$ values are given in Table I and a plot of $\text{p}K_{a/a}^{\text{HA}}$ vs. solvent composition over the range $X_{\text{Me}_2\text{SO}} = 0.065$ to $X_{\text{Me}_2\text{SO}} = 0.40$ is shown in Figure 4. The $\text{p}K_{a/a}^{\text{HA}}$ decreases, acidity of HA increases, steadily by about three units to a minimum in the vicinity of $X_{\text{Me}_2\text{SO}} = 0.35$ after which it appears to increase gradually by about one unit to the final value in pure Me₂SO.

Qualitatively similar curves for the solvent effect on $\text{p}K_a$ of the isoelectric process $\text{BH}^+ + \text{H}_2\text{O} = \text{B} + \text{H}_3\text{O}^+$ where BH^+ is a set of protonated amines have been reported in H₂O/Me₂SO,^{16a,35} in H₂O/MeOH,^{36,37} and in H₂O/*N*-methylpropionamide (NMRP).³⁸ In the Me₂SO/H₂O mixtures a minimum in $\text{p}K_a$ was generally observed in the vicinity of the solvent stoichiometry of Me₂SO:2H₂O ($X_{\text{Me}_2\text{SO}} = 0.33$). At this point solvent-solvent interactions are believed to be at a maximum. Since the solvents used in these experiments vary widely, it is likely that the shapes of the curves in Figure 4 and elsewhere^{16a,35-38} are due to the common component of all the experiments, H₃O⁺.

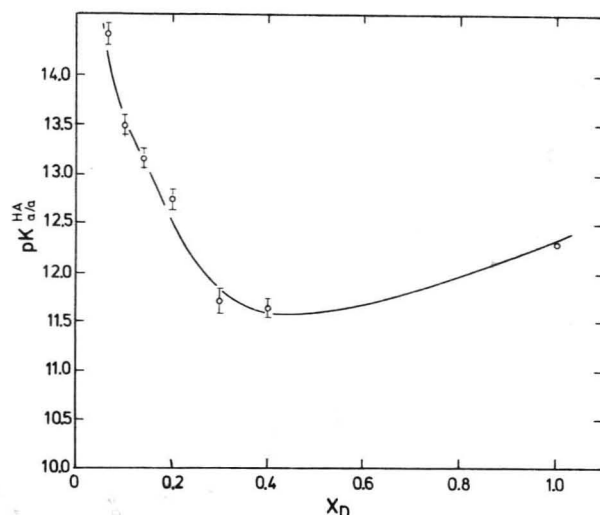


Figure 4. A plot of $\text{p}K_{a/a}^{\text{HA}}$ vs. solvent composition of Me₂SO-H₂O mixtures. The point of $X_{\text{Me}_2\text{SO}} = 1.0$ was determined by F. G. Bordwell.

That is $\Delta G(\text{diss})$ reflects the solvent effects on $\delta\Delta G_t(\text{H}_3\text{O}^+)$, or the shape of the $\text{p}K_a$ curve indicates the solvent effect on the free energy of transfer of the proton. This in turn reflects changes in solvent structure.^{16,23}

Upon addition of Me₂SO to water solvation of the small cation, H₃O⁺, improves^{28a} over the entire solvent composition range making the acidity of the acid HA increase. Initially the increase in H₃O⁺-solvent interaction is rather dramatic and it is maximized at about the same solvent composition at which solvent-solvent interactions are at a maximum due to H₂O to Me₂SO hydrogen bonding ($X_{\text{Me}_2\text{SO}} \approx 0.33$). Further increase in $X_{\text{Me}_2\text{SO}}$ results in a slight decrease in H₃O⁺ solvation. The proton interacts strongly with both water and Me₂SO, but because of the somewhat higher basicity^{16a} of Me₂SO there is a net reduction in $\text{p}K_a$ with increasing $X_{\text{Me}_2\text{SO}}$. The proton seems to be slightly better solvated in the mixed solvent in which solvent structure is most extensive.

Acknowledgment. This research was performed during a sabbatical leave at the University of Kent, Canterbury, Kent, England. The author expresses his gratitude to Professor E. F. Caldin for his generous hospitality during this period and acknowledges valuable discussions with him, B. H. Robinson, O. Rogne, J. Keefe, and R. Fuchs. The author also thanks the Max-Planck-Institut für Strömungsforschung, Göttingen, Germany for preparing the figures.

References and Notes

- (1) Presented in preliminary form at the 172nd National Meeting of the American Chemical Society, San Francisco, Calif., Aug 30, 1976.
- (2) Address correspondence to author at the Department of Chemistry, University of New Mexico, Albuquerque, N. Mex. 87131.
- (3) R. Stewart and J. P. O'Donnell, *J. Am. Chem. Soc.*, **84**, 493 (1962); *Can. J. Chem.*, **42**, 1681 (1964).
- (4) J. T. Hewitt, F. G. Pope, and W. I. Willett, *J. Chem. Soc.*, 1770 (1912).
- (5) R. Schaal, *J. Chim. Phys. Phys.-Chim. Biol.*, **52**, 784, 796 (1955).
- (6) R. A. More O'Ferrall and J. H. Ridd, *J. Chem. Soc.*, 5030 (1963).
- (7) R. Stewart, J. P. O'Donnell, and K. Bowden, *Can. J. Chem.*, **43**, 1225 (1965).
- (8) M. R. Crampton, *J. Chem. Soc. B.*, 85 (1967).
- (9) M. J. Minch, M. Giaccio, and R. Wolff, *J. Am. Chem. Soc.*, **97**, 3766 (1975).
- (10) B. Radziszewski, *Berichte*, **3**, 198 (1870).
- (11) J. R. Knowles and R. O. C. Norman, *J. Chem. Soc.*, 2938 (1961).
- (12) E. F. Caldin, M. Kasparian, and G. Tomalin, *Trans. Faraday Soc.*, **64**, 2802 (1968).
- (13) P. Fiordiponti, F. Rallo, and F. Rodante, *Z. Phys. Chem. (Frankfurt am Main)*, **88**, 149 (1974).
- (14) R. Ruchs, G. E. McCrary, and J. J. Bloomfield, *J. Am. Chem. Soc.*, **83**, 4281 (1961), have reported an enhancement in the rate of the nucleophilic displacement of chloride ions from α -chlorotoluene by thiosulfate in aqueous Me₂SO mixtures which they attribute to de-

- solvation of thiosulfate ions because of the dominant $\text{H}_2\text{O}-\text{Me}_2\text{SO}$ interaction.
- (15) J. M. G. Cowie and P. M. Toporowski, *Can. J. Chem.*, **39**, 2240 (1961); G. J. Safford, P. L. Schaffer, P. S. Leung, G. W. Brady, and E. F. X. Lyden, *J. Chem. Phys.*, **50**, 2140 (1969); F. Franks in "Hydrogen-Bonded Solvent Systems", A. K. Covington and P. Jones, Ed., Taylor and Francis, London, 1968, pp 31-47.
 - (16) (a) Z. Pawlak and R. G. Bates, *J. Solution Chem.*, **4**, 817 (1975); (b) T. Tokuhira, L. Menafra, and H. H. Szmant, *J. Chem. Phys.*, **61**, 2275 (1974).
 - (17) C. N. R. Rao in "The Chemistry of the Nitro and Nitroso Groups", Part I, A. Feuer, Ed., Interscience, New York, N.Y., Chapter 2.
 - (18) E. A. Walters, submitted for publication.
 - (19) T. J. V. Findlay and M. C. R. Symons, *J. Chem. Soc., Faraday Trans. 2*, **73**, 820 (1976).
 - (20) E.g., W. Kauzmann, "Quantum Chemistry", Academic Press, New York, N.Y. 1957, pp 570-583.
 - (21) R. C. Kerber and A. Porter, *J. Am. Chem. Soc.*, **91**, 366 (1969).
 - (22) R. Stewart and J. P. O'Donnell, *Can. J. Chem.*, **42**, 1681 (1964).
 - (23) (a) R. Stewart and J. P. O'Donnell, *J. Am. Chem. Soc.*, **84**, 494 (1962); (b) R. Stewart, J. P. O'Donnell, D. J. Cram, and B. Rickborn, *Tetrahedron*, **18**, 917 (1962).
 - (24) K. Bowden and A. F. Cockerill, *Chem. Commun.*, 989 (1967).
 - (25) K. Bowden and A. F. Cockerill, *J. Chem. Soc. B*, 173 (1970).
 - (26) R. Fuchs and C. P. Hagan, *J. Phys. Chem.*, **77**, 1979 (1973).
 - (27) P. Haberfield, J. Friedman, and M. F. Pinkston, *J. Am. Chem. Soc.*, **94**, 71 (1972).
 - (28) B. G. Cox, G. R. Hedwig, A. J. Parker, and D. W. Watts, *Aust. J. Chem.*, **27**, 477 (1974), and reference cited therein.
 - (29) C. M. Criss, R. P. Held, and E. Luksha, *J. Phys. Chem.*, **72**, 2970 (1968).
 - (30) F. Franks and D. S. Reid, *J. Phys. Chem.*, **73**, 3152 (1969).
 - (31) A. J. Parker, *Chem. Rev.*, **69**, 1 (1969).
 - (32) E. M. Arnett, L. E. Small, R. T. McIver, and J. S. Miller, *J. Am. Chem. Soc.*, **96**, 5638 (1974); E. M. Arnett, D. E. Johnston, and L. E. Small, *ibid.*, **97**, 5598 (1975); E. M. Arnett, D. E. Johnston, L. E. Small, and D. Oancea, *Faraday Symp. Chem. Soc.*, No. 10 (1975).
 - (33) D. J. Cram, "Fundamentals of Carbanion Chemistry", Academic Press, New York, N.Y., 1965, pp 32-45.
 - (34) C. D. Ritchie in "Solute-Solvent Interactions", J. F. Coetzee and C. D. Ritchie, Ed., Marcel Dekker, New York, N.Y., 1969, pp 219-300; C. D. Ritchie and R. E. Uschold, *J. Am. Chem. Soc.*, **89**, 1721 (1967).
 - (35) R. G. Bates, L. Johnson, and R. A. Robinson, *Chem. Anal. (Warsaw)*, **17**, 479 (1972).
 - (36) C. L. deLigny, *Recl. Trav. Chim., Pays-Bas*, **79**, 731 (1960).
 - (37) R. G. Bates, *J. Electroanal. Chem.*, **29**, 1 (1971).
 - (38) R. G. Bates, J. S. Falcone, Jr., and A. Y. W. Ho, *Anal. Chem.*, **46**, 2004 (1974).

Binding of Hydrogen Ions to Anionic Micelles

Clifford A. Bunton,* Klaus Ohmenzetter, and Luis Sepulveda*

Department of Chemistry, University of California, Santa Barbara, California 93106 and the Department of Chemistry, Faculty of Sciences, University of Chile, Santiago, Chile (Received June 9, 1977)

Publication costs assisted by the National Science Foundation

The incorporation of hydrogen ions with anionic micelles of sodium lauryl sulfate, NaLS, has been examined conductimetrically and by using a hydrophilic indicator and the contents of incorporation agree well with those estimated using a glass electrode. A plot of the number of hydrogen ions per micellized sulfate ion against $[\text{H}^+]/([\text{H}^+] + [\text{Na}^+])$ is linear with a slope of 0.82 ($[\text{H}^+]$ and $[\text{Na}^+]$ are total molar concentrations). Conductimetric measurements in mixtures of NaOH and cetyltrimethylammonium bromide, CTABr, suggest that hydroxide ions are not strongly bound to the micelle, but the results could not be interpreted quantitatively.

Micellar catalysis of bimolecular reactions in water depends at least in part upon the ability of the micelle to concentrate reagents into the small volume of the Stern layer.¹ In this model an ionic micelle in water is assumed to be approximately spherical with extensive charge neutralization of the head groups. The rate constants of catalyzed bimolecular reactions generally go through maxima with increasing surfactant concentration, and this behavior can be rationalized in terms of opposing effects in that increasing surfactant concentration "extracts" reagents from water into the micelles, but by increasing the total volume of the Stern layers dilutes these reagents at the micellar surface.²⁻⁸ The incorporation of organic solutes can sometimes be determined by physical studies. For example, Berezin and his co-workers have determined association constants by solubility and have treated the kinetics of several micellar-catalyzed bimolecular reactions assuming that one reactant does not affect incorporation of the other into the micelle.⁶

Many micellar-catalyzed reactions involve hydrophilic ions so that information about their incorporation is useful. For example the acid hydrolysis of acetals is catalyzed by anionic micelles which incorporate both hydrogen ions and

substrate and the variation of rate constants with increasing surfactant concentration can be explained in terms of a progressive dilution of micellar bound reagents with increasing surfactant concentration.^{7b} In principle it is possible to calculate rate constants in the Stern layer from the overall rate constants and reactant concentrations in that layer.

Ion sensitive electrodes are used to calculate the distribution of ions between water and a counter ionic micelle, assuming that the electrode is insensitive to surfactants and micellar bound ions.^{7b,9,10} For example, for aqueous solutions of a strong acid and sodium lauryl sulfate, NaLS, the pH gives the concentration of free hydrogen ions, $[\text{H}^+_{\text{w}}]$, and the relative amount of micellar bound hydrogen ions is given by $([\text{H}^+_{\text{T}}] - [\text{H}^+_{\text{w}}])/[\text{H}^+_{\text{T}}]$, where $[\text{H}^+_{\text{T}}]$ is the stoichiometric concentration of hydrogen ions.^{7b}

There are several problems with this use of ion sensitive electrodes.¹¹ (i) The surfactant may affect the response of the electrode and the magnitude of the liquid junction potential if a salt bridge is used; and (ii) the emf of the electrode is related to mean ion activity rather than concentration. This second problem can in principle be eliminated by using the value of the appropriate activity coefficient, but it is not obvious how this value should be estimated. Because ionic micelles have net charge, the

* Address correspondence to this author at the University of California—Santa Barbara.

TABLE I: Spectrophotometric Determination of ΔpH

$10^3[\text{NaLS}], \text{M}$	$10^2[\text{HCl}], \text{M}$		
	1.0	3.0	10.0
6.0		0.092	0.025
10.0	0.196	0.152	
20.0	0.316	0.204	
30.0	0.370	0.253	0.091
40.0		0.277	
50.0		0.316	
60.0	0.570		0.129

external aqueous solution must carry an equal and opposite charge. Fortunately most experiments are at low surfactant and electrolyte concentrations, so any correction should be small.

It seemed desirable therefore to estimate the extent of micellar incorporation of the hydrogen ion by independent methods involving different assumptions. The hydrogen ion is the obvious candidate because the concentration of free hydrogen ions can also be determined conductimetrically, and by using an indicator which is not bound to the micelle, cf. ref 12.

We have compared these three independent methods, and we have also attempted to use conductivity to estimate the binding of hydroxide ion to cationic micelles of cetyltrimethylammonium bromide, CTABr.

Results and Discussion

Indicator Measurements. In this method the indicator base must be partially protonated in the range of acidities to be studied, but neither the acidic nor the basic forms should be incorporated into the micelle. This approach is similar to that of Mukerjee and Banerjee except that their indicators were incorporated into the micelle.¹²

As an indicator we used maleic acid whose $\text{p}K_a$ has a suitable value.¹³ Maleic acid and its monoanion have very different absorbances, because of conjugation between the double bond and the carboxyl groups and both are very hydrophilic and should not enter the anionic micelle. We showed that the UV absorbances of acid and monoanion are unaffected by NaLS. We also attempted to use formic acid, but the absorbance change on ionization is too small to be useful.

Added electrolytes change acid dissociation constants, and therefore we measured the classical dissociation constants in the various dilute hydrochloric acid solutions in the absence of surfactant. This approach introduces some errors because of the added ions of surfactant and the exchange of cations between water and the micelles, but these errors should be small because most of our experiments were in dilute electrolyte solutions.

Under our acid conditions only the first dissociation of maleic acid is important ($\text{p}K_1 = 1.83$ and $\text{p}K_2 = 6.07$ in water¹³).

In dilute aqueous HCl the relation between absorbance A and pH is given by

$$\text{pH} = \text{p}K_1 - \log \left\{ \frac{(A - A_{A^-})}{(A_{HA} - A)} \right\} \quad (1)$$

(where A_{HA} and A_{A^-} are, respectively, the absorbances of solutions of maleic acid and hydrogen maleate ion of a given concentration).

Therefore when NaLS is added to aqueous HCl the change of pH is given by

$$-\Delta\text{pH} = \log \left\{ \left(\frac{A'_{HA} - A'}{A' - A'_{A^-}} \right) \left(\frac{A - A_{A^-}}{A_{HA} - A} \right) \right\} \quad (2)$$

where the prime denotes absorbances in the presence of the surfactant. The wavelengths were 210, 215, and 220

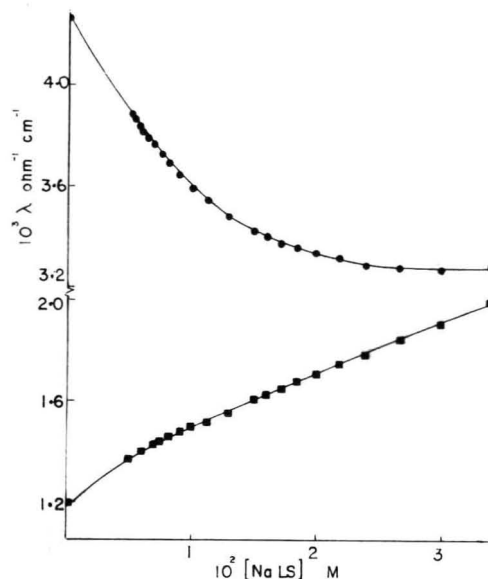


Figure 1. Effect of NaLS on the specific conductivity of 10^{-2} M HCl (●) and NaCl (■).

nm and the different results agreed well.

The change of pH (Table I) gives the relation between free and total hydrogen ions.⁷

$$\Delta\text{pH} = \log \left[\frac{[\text{H}^+]_w}{[\text{H}^+]_T} \right] \quad (3)$$

Conductivity Measurements. Addition of NaLS to dilute HCl decreases the conductivity of the solution because hydrogen ions are incorporated into the micelle but the conductivity increases as expected when NaLS is added to NaCl (Figure 1).

For a mixture of HCl and NaLS the conductivity will depend upon the concentrations and mobilities of the ionic species present and in order to estimate the extent of binding of hydrogen ions to the micelle we have to make the following series of assumptions: (i) the mobilities of the free ions are unaffected by the micelles; (ii) the mobility of the anionic micelle does not change significantly when hydrogen ions enter it and displace sodium ions; and (iii) for every hydrogen ion which enters the micelle one sodium ion is displaced, cf. ref 8.

The first assumption is reasonable because all our experiments were in dilute aqueous solution and the viscosity of the aqueous surfactant is essentially that of water. The second assumption is also reasonable because the micelle is large and approximately 80% of the negative charge of the sulfate head groups is neutralized by cations,^{8,14} so that its ability to carry current is much smaller than that of the hydrogen ion. In addition, the size of the micelle, and therefore its mobility, should only be slightly affected by incorporation of hydrogen ions. The third assumption is the most suspect, but even though it may only be a crude approximation the error so introduced should be small because the difference in the mobilities of the hydrogen and sodium ions is very large.¹⁵ Assumptions (ii) and (iii) might introduce serious errors if applied to systems in which the mobilities of the entering and displaced ions are similar, and we found this problem with mixtures of NaOH and CTABr. Our conclusions regarding conduction by the cations would be little different if we made the extreme and unrealistic assumption that hydrogen ions could enter the micelle without displacing sodium ions.

These assumptions allow us to estimate λ_i , the specific conductance for the hypothetical case in which the micelle does not incorporate hydrogen ions, because it will be the sum of the specific conductances of NaLS and HCl.

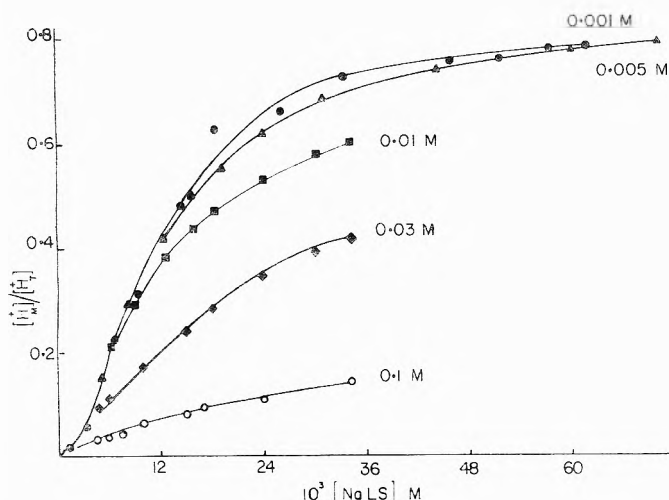


Figure 2. Incorporation of hydrogen ions into micelles of NaLS determined conductimetrically. The total concentrations of HCl are as shown.

However, λ_i can also be regarded as made up of the specific conductance of the hydrogen ion and λ_{res} which is due to all the other ionic species:

$$\lambda_i = \lambda_{NaLS} + \lambda_{HCl} = \lambda_{res} + [H^+]_T \Lambda_{H^+} / 1000 \quad (4)$$

where Λ is the equivalent conductance. In much the same way we can write λ_{mix} , the specific conductance of the actual mixture, as

$$\lambda_{mix} = \lambda_{res} + [Na^+]_E \Lambda_{Na^+} / 1000 + ([H^+]_T - [Na^+]_E) \Lambda_{H^+} / 1000 \quad (5)$$

where $[Na^+]_E$ is the concentration of sodium ions expelled from the micelle.

Equations 4 and 5 give

$$\lambda_{mix} - \lambda_{NaLS} - \lambda_{HCl} = (\Lambda_{Na^+} - \Lambda_{H^+}) [Na^+]_E / 1000 \quad (6)$$

and

$$[Na^+]_E = [H^+]_M$$

where $[H^+]_M$ is the concentration in moles per liter of solution of micelle bound hydrogen ions.

The variation of $[H^+]_M / [H^+]_T$ with NaLS and HCl is shown in Figure 2, and for low acid concentrations the bulk of the hydrogen ions are incorporated in the micelle even at relatively low surfactant concentrations.

Comparison of the Various Experimental Methods. In order to compare the results obtained by the three methods it is useful to define the concentration of hydrogen ions in the Stern layer of the micelle in terms of the number of hydrogen ions per micellized surfactant head group, $m^{s_{H^+}}$:

$$m^{s_{H^+}} = [H^+]_M / ([NaLS] - cmc) = ([H^+]_T - [H^+]_w) / ([NaLS] - cmc) \quad (7)$$

The concentration of hydrogen ions could also be expressed in terms of the volume of the micelle or its Stern layer, but the definition of $m^{s_{H^+}}$ avoids our making assumptions about micellar dimensions or densities.

In this treatment we write the concentration of micellized surfactant as $[NaLS] - cmc$, where the critical micelle concentration, cmc ,¹⁶ is determined in the presence of the acid, although this quantity may change as hydrogen ions enter the micelle and displace sodium ions. However, the uncertainty due to this assumption should not be large, because it decreases with increasing surfactant concentration where $[NaLS] \gg cmc$. The values of the cmc of

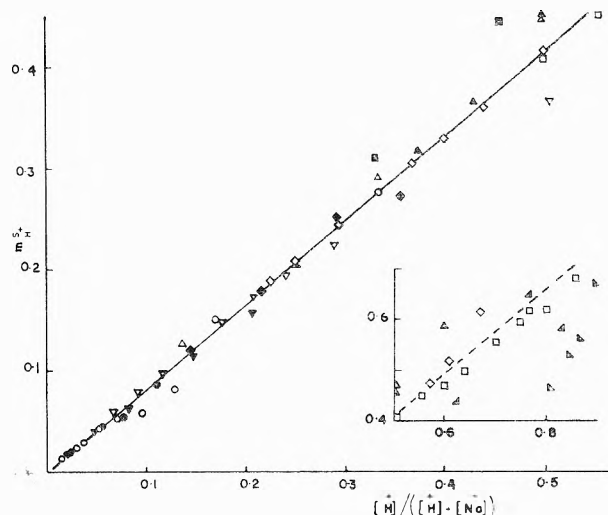


Figure 3. Variation of $m^{s_{H^+}}$ with concentrations of HCl and NaLS. Measurements were made at the following [HCl]: conductivity, (O) 0.001 M, (∇) 0.005 M, (\diamond) 0.01 M, (\circ) 0.03 M, (\times) 0.1 M; indicator, (Δ) 0.01 M, (\blacktriangle) 0.03 M, (+) 0.1 M; pH (\bullet) 0.001 M, (∇) 0.00316 M, (\blacklozenge) 0.01 M, (\blacksquare) 0.03 M.

NaLS in the presence of dilute HCl have been interpolated where necessary from existing data.^{7b,16}

Inspection of the results of the three methods shows that over a wide range of concentrations of HCl and NaLS $m^{s_{H^+}}$ varies linearly with $[H^+] / ([H^+] + [Na^+])$ (these are the total concentrations of the ions, with a slope of 0.82 (Figure 3). For values of $[H^+] / ([H^+] + [Na^+])$ less than 0.45 the three methods agree very well considering the assumptions and experimental errors.

Conductivity is probably the most reliable method, but the three independent methods agree surprisingly well suggesting that our assumptions are reasonable. Although there is considerable scatter in the results in the more acidic solutions most of the data points fall close to the line of slope 0.82 as shown by the broken line in the insert of Figure 3. The deviations are greatest for experiments in 0.1 M HCl where the indicator is almost wholly protonated and where our assumptions about the conductivity experiments are most suspect.

It is suggested that approximately 80% of the charge of the head groups of an ionic micelle is neutralized by counterions in the Stern layer,^{8,14} and our empirical equation (eq 8) (Figure 3), can be rationalization on this

$$m^{s_{H^+}} = 0.82 [H^+] / ([H^+] + [Na^+]) \quad (8)$$

basis, because our results suggest that there is little difference in the binding of hydrogen and sodium ions to the anionic micelle, and approximately 80% of the head groups are neutralized by counterions.^{8,14} However, we have no evidence that this would be true in the general case; indeed there is considerable evidence that the binding of counterions to micelles increases markedly with increasing hydrophobicity of the ion.²⁻⁵ It is important to note that neither our indicator nor pH method depends on assumptions about the displacement of one ion by another at the micellar surface, and the agreement between the methods strengthens earlier interpretations of the kinetic form of micellar-catalyzed acetal hydrolysis.^{7b}

Although our results suggest that the anionic micelle does not discriminate markedly between hydrogen and sodium ions, we do not know how hydrogen ions bind to the lauryl sulfate head groups. Both covalent and hydrogen bonding interactions could be important, and kinetic studies show that the undissociated alkyl sulfuric acids are present in these systems,¹⁷ although their dis-

TABLE II: Conductivities of Mixtures of CTABr and NaOH or NaBr^a

	CTABr	CTABr + NaOH		CTABr + NaBr	
		Obsd	Calcd ^c	Obsd	Calcd ^c
$10^3\lambda$, ^b ohm ⁻¹ cm ⁻¹	0.499	0.686	0.728	0.598	0.632
10^3a , ohm ⁻¹ cm ⁻¹	0.083	0.297	0.319	0.187	0.218
b , ohm ⁻¹ cm ⁻¹ M ⁻¹	0.0208	0.0194	0.0205	0.0205	0.0208

^a At 25 °C, with 10⁻³ M NaOH or NaBr. ^b [CTABr] < 0.02 M. ^c Calculated from conductivities of the pure components.

sociation constants are not known.

Comparison with Other Results. There is extensive evidence of micellar effects upon acid-base equilibria,^{12,18} but it does not give direct information on the micellar binding of the hydrogen ion. The change in protonation of an indicator on addition of an anionic micelle will depend not only upon the availability of hydrogen ions at the micellar surface but also upon the distribution of the indicator base and its conjugate acid between water and the micelles, and on the interactions of the indicator species with the micelle relative to water. It is relatively easy to use hydrophobic indicators which will be incorporated wholly in the micelle, but it is not so easy to deal with the other factors. Our approach of determining the concentration of hydrogen ions left in the water and calculating the concentration in the micelles by difference avoids these problems, although, as we noted earlier, unverifiable assumptions have to be made. It is desirable whenever possible to use more than one method of determining concentrations whenever information is sought on solute binding to micelles.

Interaction of Hydroxide Ion with CTABr. Estimation of the extent of incorporation of hydrogen ions into anionic micelles of NaLS using conductivity depends on approximations which appear to be satisfactory in this system, because the results are confirmed by two other independent methods. The problem is less satisfactory with regard to the binding of hydroxide ions to cationic micelles. There are many kinetic studies of micellar catalysis of reactions in which hydroxide ion acts as a base or nucleophile,²⁻⁵ but attempts to use pH change to determine the extent of incorporation have been unsuccessful,^{7b,10} and it is difficult to envisage a suitable indicator system for use with cationic micelles. We therefore attempted to use conductivity, and compared the effects of NaOH and NaBr on the conductance of CTABr solutions. This test is analogous to that used with mixtures of NaLS with HCl and NaCl (Figure 1), but whereas addition of NaLS to a constant amount of HCl decreased the conductivity, and to NaCl increased it (Figure 1), we saw no such differences in behavior with CTABr.

As is generally found the specific conductivity, λ , of CTABr in water above the cmc increases linearly with concentration,^{9a,19} i.e.

$$\lambda = a + b[\text{CTABr}] \quad (9)$$

This relation is also obeyed for solutions of CTABr with constant NaOH or NaBr and the coefficients a and b are given in Table II. For a given concentration of CTABr the specific conductivity of a mixture of CTABr and 10⁻³ M NaOH is slightly less than that calculated from the specific conductivities of solutions of the pure components, and the slope is decreased, but addition of CTABr to 10⁻³ M NaBr has a rather similar effect, except that the slope changes less (Table II). This addition of CTABr to both NaOH and NaBr decreases the conductivity slightly. We also measured the changes in conductivity of 10⁻² M NaOH on addition of CTABr, but the changes were even smaller than those for 10⁻³ M NaOH.

Our results suggest that hydroxide ion is not strongly incorporated into CTABr micelles, but they do not allow us to estimate the extent of incorporation, and they show that the approximations which appear to be satisfactory with mixtures of HCl and NaLS are not applicable here. There are two obvious differences in the systems. (i) In water the hydrogen ion is very much more mobile than other cations, but the differences in mobilities are smaller for hydroxide ion compared with other anions. Therefore our approximations regarding the exchange of ions between water and micelle are much poorer for the hydroxide than for the hydrogen ion. (ii) The positive charge on a quaternary ammonium ion is shielded by organic groups, whereas the negative charge of a sulfate ion is exposed. As a result hydrophobic and dispersive interactions probably play a much larger role in determining counterionic binding to CTABr than to NaLS.

This accords with Pearson's classification and regards micellized sulfate ions as being harder reagents than micellized quaternary ammonium ions.²⁰

As mentioned earlier, our evidence on the incorporation of hydrogen ions into micelles of NaLS is consistent with the accepted micellar model in which the Stern layer is saturated with counterions and ions are exchanged indiscriminately between water and the Stern layer,^{8,14} but the failure of our treatment of hydroxide ion and CTABr may reflect the experimental limitations of the conductivity method in this system rather than a failure of the model.

Experimental Section

Indicator Measurements. The changes in absorbances of 5×10^{-5} M maleic acid were measured over a range of concentrations of NaLS and HCl at 210, 215, and 220 nm at 25 °C using a Beckman DU-2 spectrophotometer. The absorbances of maleic acid at low pH and of the hydrogen maleate ion are not affected by NaLS.

Conductivity Measurements. Conductivities at 100 Hz and 25 °C were measured using a dipping cell and either a Tinsley 4896 or an Industrial Instruments bridge. Deionized redistilled water was used and the experiments were done under N₂. The values of Δ were from ref 15.

Acknowledgment. Support of this work by the National Science Foundation, Grants CHE75-03660 and Int 76-05770, is gratefully acknowledged, and collaboration was made possible by the University of Chile-University of California Cooperative program. We acknowledge helpful discussions with Dr. L. S. Romsted.

References and Notes

- (1) For discussion of micellar catalysis and inhibition see ref 2-5.
- (2) E. H. Cordes, Ed., "Reaction Kinetics in Micelles", Plenum Press, New York, N.Y., 1973.
- (3) E. H. Cordes and C. Gitler, *Prog. Bioorg. Chem.*, **2**, 1 (1973).
- (4) E. J. Fendler and J. H. Fendler, "Catalysis in Micellar and Macromolecular Systems", Academic Press, New York, N.Y., 1975.
- (5) C. A. Bunton, *Prog. Solid State Chem.*, **8**, 239 (1973); "Micellar Reactions", Chapter 4 in "Application of Biomedical Systems in Chemistry", Part II, J. Byran Jones, Ed., Wiley, New York, N.Y., 1976.
- (6) A. K. Yatsimirski, K. Martinek, and I. V. Berезin, *Tetrahedron*, No. 27, 2855 (1971); K. Martinek, A. K. Yatsimirski, A. P. Osipov, and

- I. V. Berezin, *ibid.*, No. 29, 963 (1973); I. V. Berezin, K. Martinek, and A. K. Yatsimirski, *Russ. Chem. Rev.*, **42**, 787 (1972).
- (7) (a) C. A. Bunton and L. Robinson, *J. Am. Chem. Soc.*, **90**, 5965 (1968); (b) C. A. Bunton and B. Wolfe, *ibid.*, **95**, 3742 (1973).
- (8) L. S. Romsted, presented at the International Symposium on Micellization, Solubilization and Microemulsions, Albany, N.Y., Aug 8–11, 1976.
- (9) (a) E. Keh, C. Garach, and J. Guastalla, *C. R. Acad. Sci. Paris, Ser. C*, **263**, 1488 (1977); (b) W. K. Mathews, J. W. Larsen, and M. J. Pikal, *Tetrahedron Lett.*, 513 (1972).
- (10) J. W. Larsen and L. J. Magid, *J. Am. Chem. Soc.*, **96**, 5664 (1974); **97**, 1988 (1975).
- (11) G. Eisenman, Ed., "Glass Electrodes for Hydrogen and Other Cations", Marcel Dekker, New York, N.Y., 1967; R. G. Bates in "Solute-Solvent Interactions", J. F. Coetzee and C. D. Ritchie, Ed., Marcel Dekker, New York, N.Y., 1969, Chapter 2.
- (12) P. Mukerjee and K. Banerjee, *J. Phys. Chem.*, **68**, 3567 (1964).
- (13) R. M. C. Dawson, D. C. Elliott, W. H. Elliott, and K. M. Jones, "Data for Biochemical Research", Clarendon Press, Oxford, 1959.
- (14) D. Stigter, *J. Phys. Chem.*, **70**, 1323 (1966).
- (15) R. A. Robinson and R. H. Stokes, "Electrolyte Solutions", 2nd ed, Butterworths, London, 1959, Appendix.
- (16) P. Mukerjee and K. J. Mysels, "Critical Micelle Concentrations of Aqueous Surfactant Systems", National Bureau of Standards, Washington, D.C., 1971.
- (17) J. L. Kurz, *J. Phys. Chem.*, **66**, 2239 (1962); V. A. Motsavage and H. B. Kostenbauder, *J. Colloid Sci.*, **18**, 603 (1963).
- (18) C. F. Hisjee and T. A. Downey, *J. Phys. Chem.*, **58**, 835 (1954); L. K. J. Tong and M. C. Glesmann, *J. Am. Chem. Soc.*, **79**, 4305 (1957); M. T. A. Behme and E. H. Cordes, *ibid.*, **87**, 260 (1965); M. T. Behme, J. G. F. Fullington, R. Nole, and E. H. Cordes, *ibid.*, **87**, 266 (1965); C. A. Bunton and L. Robinson, *J. Phys. Chem.*, **73**, 4237 (1969); **74**, 1062 (1970); C. A. Bunton and M. J. Minch, *ibid.*, **78**, 1490 (1974).
- (19) A. B. Scott and H. V. Tartar, *J. Am. Chem. Soc.*, **65**, 692 (1943).
- (20) R. G. Pearson and J. Songstad, *J. Am. Chem. Soc.*, **89**, 1827 (1967).

The Interaction of CO with Very Small Copper Clusters

M. Moskovits* and J. E. Hulse

Lash Miller Laboratories and Erindale College, University of Toronto, Toronto M5S 1A1, Canada (Received July 26, 1976; Revised Manuscript Received August 8, 1977)

Copper clusters ranging in size from monatomic to four-atom particles have been generated by a modified matrix isolation technique which traps these species in solid noble gas at cryogenic temperatures. By doping the matrix with trace amounts of carbon monoxide, species of the form Cu_nCO where $n = 1$ to 4 are formed and identified as well as other hitherto unknown copper-CO species. The CO stretching frequencies of the above molecules approach that of CO chemisorbed on polycrystalline copper very rapidly. The chemisorption bond formed between CO and copper is discussed in light of the reported observations.

Introduction

Recent spectroscopic studies of adsorbed molecules and atoms have been carried out by one of two partly overlapping schools. The first seeks among the surface species intermediates in heterogeneous catalytic reactions, while the second regards the study of surface complexes worthwhile in its own right regardless of the role which they might play in catalysis. The concept of a surface compound is not without controversy. On one hand one can regard chemisorption as being a unique phenomenon which occurs only on crystalline surfaces as a result of interactions with delocalized, "collective orbitals" characteristic of some energy bands in the crystal, while on the other hand one can view chemisorption as an extension of ordinary covalent bond formation similar in nature to that which would occur between the isolated atom or ion and the ad-molecule. The local or nonlocal nature of the chemisorption bond remains a largely unresolved question. Part of the difficulty rests in the fact that here are two problems which go by the same name. The first relates to the difference between the nature of the bond linking a metal atom or a small cluster and a ligand, and that of the ligand, now an ad-molecule, attached to a large metal cluster. The second probes the difference between bonding to a metal atom or a small cluster and that to a single-crystal surface. The distinguishing characteristic between these two cases is surface periodicity.

The role of periodicity in determining surface and bulk electronic properties of materials is a subject of some interest even outside surface chemistry. So, for instance, the band structure of metals is usually formulated in terms of Bloch functions which contain within them the periodicity of the lattice. These theories amply account for properties such as electrical conduction of metals. Liquid metals also conduct, however, despite the absence of

long-range order. More recently, amorphous semiconductors have been developed which exhibit many of the properties of their crystalline analogues in apparent contradiction to the need for periodicity implicit in semiconductor theory. It may be that both a local and a nonlocal description can account for certain bulk and surface phenomena equally well, just as some functions can be equally well described by both a Taylor series and a Fourier series. On the other hand there may be instances in which the two-dimensional periodicity of single-crystal surfaces can give rise to unique properties encountered neither in the coordination chemistry of single metal atoms nor in the surface chemistry of small clusters lacking extensive surface periodicity.

Such nonlocal effects may account for the observed CO stretching frequency shift with coverage (even at low coverages) in CO on (100) Pd.¹ That the addition of a CO molecule at a somewhat remote site from an existing ad-molecule can nevertheless affect its bonding sufficiently to perturb the CO force constant indicates a large "through-metal effect" that cannot be ascribed simply to intermolecular coupling, since the CO stretch-stretch interaction force constant across the metal bond of polynuclear carbonyls is too small to account for the observed shifts.²

The marked crystalline face dependence of the spectra (IR or UPS) of certain adsorbed species also indicates a somewhat nonlocal effect.³

There is, in addition, a conceptual barrier that one must at times resolve with respect to local bonding on crystalline surfaces. A local bond implies to some extent a three-step process:⁴ first the removal of the adsorption site from the crystal, second the formation of the local bond, and finally the placement of the "surface molecule" so formed back into the "matrix" of the surface atoms. A necessary

(though not sufficient) condition for the bond to be local is that the energies of the first and third steps sum approximately to zero. This seems a highly restrictive condition which one might accept as a working approximation for an adsorption site consisting of a single metal atom. When the site involves several metal atoms, however (as in "bridging" CO), the approximation becomes conceptually more taxing.

In addition, the crystal-face index may affect the bonding as a result of the unit mesh geometry which may preclude certain surface structures or through electronic means as suggested by Bond⁵ in which the bonding is local in the sense that chemical links are made to d-orbitals localized on a few surface atoms in the vicinity of the adsorbate. However, only certain "dangling orbitals" which do not take part in the two-dimensional (and hence delocalized) metal-metal bonding can contribute to chemisorption. The directions of the available orbitals and hence the adsorbate geometry vary from one crystalline face to another according to its Miller index.

Choosing the best probe of the locality or nonlocality of the bonding is another problem. In principle, spectroscopies such as ultraviolet-induced-photoelectron spectroscopy and UV-visible spectroscopy, which sample the electronic structure of the surface species directly, should be the most sensitive probes.⁶ In fact, interpretive difficulties make them less than certain indicators.⁷ Comparing adsorbate vibrations as measured by infrared spectroscopy with those of organometallic or carbonyl model compounds and concluding from the similarity in the magnitude of the vibrational frequencies that the bonding is local is also often unjustified. This is especially true when the vibrations are at good "group frequencies" and somewhat remote from the chemisorbed bond as, for instance, in comparing the CH₂ stretching or bending frequencies of chemisorbed ethylene with those in Zeisse's salt or Wilke's compound [Ni(C₂H₄)₃]. Those frequencies are expected to be similar regardless of the mode of bonding. Even for chemisorbed CO in which the CO bond strength is more intimately related to the surface bond, the situation is not without pitfalls. To begin with, the CO stretching force constant is not a unique function of the CO bond strength since its magnitude depends on the two factors, σ donation and π acceptance by the CO moiety in opposite ways (the CO force constant increases with increasing σ donation and decreases with increasing π backbonding).⁸ A given CO force constant, and hence its resulting vibrational frequency, may correspond to a large variety of combinations of these two effects, and therefore to a large variety of metal-CO bond energies. A case in point is, in fact, copper carbonyl⁹ which possesses CO stretching frequencies not dissimilar from Ni(CO)₄ despite the latter's marked greater stability.

One is on safer ground when viewing the trend in the CO stretching force constant (rather than its absolute value) for a series of cluster carbonyls all involving the same metal and differing only in the cluster size. In such a series, the CO stretching frequency may reflect the metal-carbon bond strength to a first approximation, and such a study may indicate how local (in the "metal cluster" rather than the "single crystal" sense) the bonding is by noting how rapidly the CO stretching frequency of a carbonyl bonded to progressively larger clusters approaches that observed in bulklike aggregates or polycrystalline films.

In this paper we report the formation and characterization of copper cluster carbonyls containing up to four coppers (although larger clusters are present as well). The

clusters were generated by matrix isolation in the same manner that we have recently reported for Ni clusters.¹⁰

Experimental Section

Metal cluster compounds were formed by cocondensing monatomic Cu vapor with Ar/CO mixtures onto a cooled CsI plate. The metal vapor was generated by directly (ac) heating a copper-bearing tantalum filament suspended from water-cooled copper electrodes enclosed in a water-cooled cylindrical copper enclosure. Approximately 150 A were passed through the filament. The rate of metal deposition was gauged with a quartz balance mounted in the furnace so as to receive the back-going flux of metal. The quartz balance had a resolution of approximately 20 ng. The ratio between forward-going and backward-going atoms was obtained by calibrating the system with another quartz sensor mounted in place of the CsI plate.

The matrix gas mixture was prepared in a bulb using standard vacuum line techniques. Gas flows were calculated by measuring the pressure drop in a bulb of known volume. Because the pressure decrease in any one run was small, a Validyne pressure transducer was used which enabled the relatively large pressure in the bulb to be electronically zero-suppressed. The fraction of the gas entering the system which actually adhered to the CsI plate was measured by depositing a mixture of CO₂/Ar and noting the absorbance of the 2342-cm⁻¹ vibration of CO₂ (ν_3) for which the extinction coefficient is accurately known.

The CsI plate was mounted with indium gaskets in a copper block which, in turn, was fixed into the tip of either an Air Products displax refrigerator or an Air Products Model LT-3-110 liquid helium continuous flow cryostat, thereby obtaining bottom temperatures of 10 and 4.2 K, respectively. Temperatures were measured with a chromel vs. gold/0.07 at. % iron thermocouple.

The matrices could be warmed to temperatures above their bottom temperatures using a resistance heater attached to the block.

Metal deposition rates were in the range 40–4000 ng/min, while gas from the storage bulb was spent at rates between 0.1 and 2.5 mmol/h, corresponding to approximately 20 to 500 monolayers/min.

IR spectra were recorded on either a Perkin-Elmer 180 or 621 grating spectrometer.

Results

Portions of the spectra obtained when copper atoms were cocondensed with a 1/300 CO-in-argon mixture onto a CsI plate cooled to 11 K are shown in Figure 1. The various scans in that figure were obtained from matrices ranging in copper mole fraction from approximately 0.001 to 0.02. Noteworthy in the spectra of Figure 1 are the features at 2128, 2116, 2107, 2012, 1942, 1934, 1929, 1922, 1892, 1885, 1877, 1871, and 1853 cm⁻¹ which are clearly assignable to CO stretching modes. The band at 2012 cm⁻¹ and the doublet at 1892 and 1877 cm⁻¹ have been previously observed and reported.⁹ They have been assigned to the species CuCO and Cu(CO)₂, respectively, with the doublet splitting in the case of the latter arising from "matrix effects". The species Cu(CO)₃ which absorbs at 1976 and 1985 cm⁻¹ is almost absent, as one would expect in a matrix so dilute in CO. The other bands observed in the spectra shown in Figure 1 are due to copper cluster carbonyls which will be identified in the next section.

In addition to these bands, only bands attributable to water impurity were seen in an infrared scan covering 4000–300 cm⁻¹. In particular, no oxygen was detected in the matrix either as O–O stretching vibrations of coor-

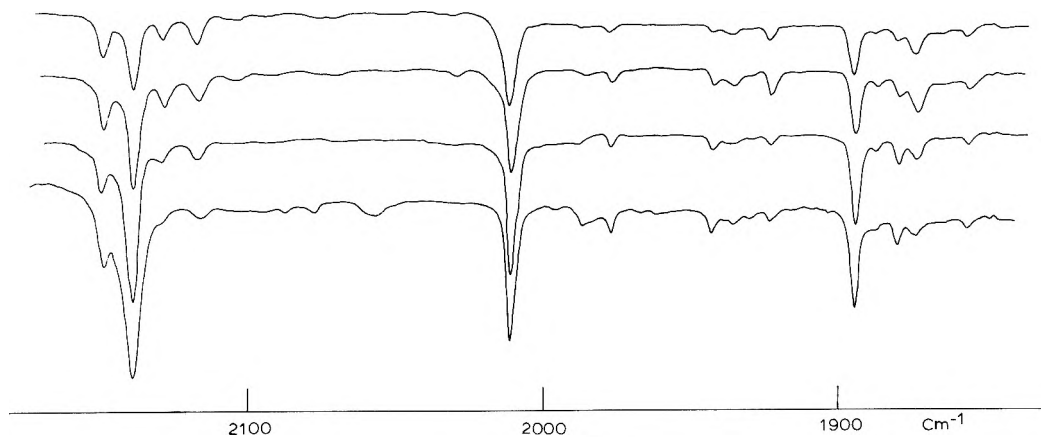


Figure 1. Spectra obtained from matrices formed when Cu atoms were cocondensed with 1/300 CO/Ar mixtures. The four spectra were obtained from matrices progressively more concentrated in metal with the bottom spectrum corresponding to the most dilute matrix. Ordinate is transmittance.

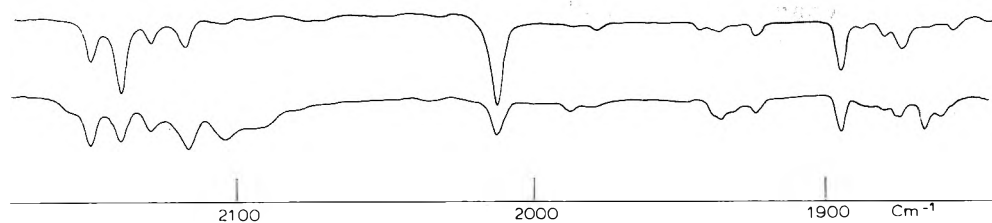


Figure 2. Effect of warm up: top spectrum before, bottom spectrum after warm-up.

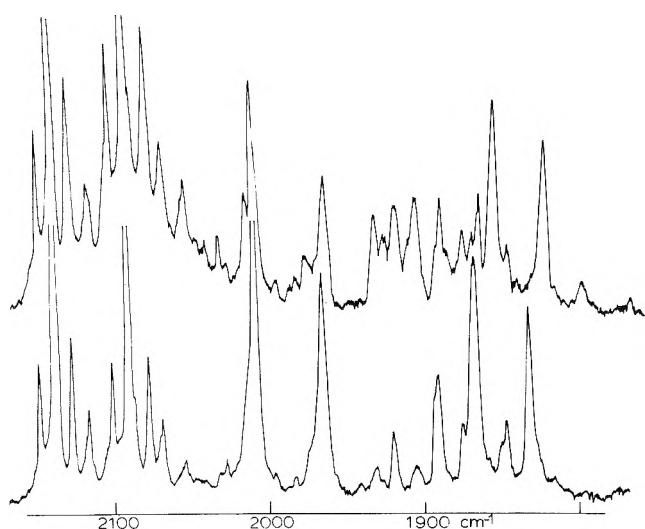


Figure 3. Spectra obtained after cocondensing Cu with $^{13}\text{Co}/^{12}\text{Co}/\text{Ar}$ in the ratio 1/1/300: (bottom) as deposited; (top) after 5 min warm-up. The ordinate is the absorbance.

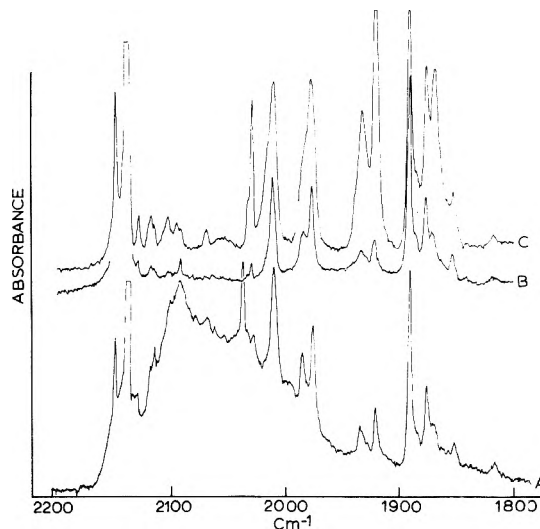


Figure 4. Spectra obtained after cocondensing Cu with CO/Ar in the ratio 1/50. The metal mole fraction in the matrices from which spectra A, B, and C were taken are, respectively 0.015, 0.0016, and 0.0085.

minated dioxygen or as oxide vibrations. The absence of CO_2 also indicated a paucity of oxygen since that species always forms by catalytic oxidation of CO on the hot tantalum filament. The presence of water gave rise to species containing bonded water along with CO and products of reaction with water and CO. These are currently being investigated and will be reported on later.

After warming the matrix whose spectrum is shown in Figure 1 to 32 K for 5 min, the spectrum shown in Figure 2 was obtained. The following points are noteworthy in this spectrum. (a) Of the two "free" CO lines, the one at 2138 cm^{-1} decreases, while the absorption at 2148 cm^{-1} hardly changes. The latter was assigned by Dubost¹¹ and others¹² to a CO-H₂O aggregate which presumably diffuses much less rapidly on warmup than does the unhydrated CO. (b) The absorptions at 2112 cm^{-1} (CuCO) decrease markedly, those at 1892 and 1877 cm^{-1} ($\text{Cu}(\text{CO})_2$) decrease slightly, while the features at 2116 and 2102 cm^{-1} increase.

A feature at 2094 cm^{-1} also grows in as does a shoulder on the high-frequency side of the 2148 cm^{-1} band of hydrated CO. Lines belonging to $\text{Cu}(\text{CO})_3$ increase in size only slightly, implying that Cu diffusion rather than CO diffusion brings about most of the observed changes.

The bands at 2128 and 1871 cm^{-1} show little change, while a new band at 1859 cm^{-1} shows considerable increase.

In addition to the above, a small feature at 2255 cm^{-1} , at a frequency above the CO absorptions, grows in on warmup. Portions of spectra showing the results of cocondensing an equimolar mixture of $^{13}\text{CO}/^{12}\text{CO}$ in argon in a ratio of 1/1/300 is shown in Figure 3.

The dependence of the concentrations of the species formed on the CO concentration was investigated in a series of runs in which the CO/Ar ratio was 1 in 50. A representative selection of these spectra is shown in Figure 4. Note particularly the spectrum resulting when a great deal of metal is present in the matrix.

Discussion

No discussion is possible until the cluster compounds formed in the matrix have been characterized. To do this the number of copper atoms and CO molecules making up the cluster which gives rise to a particular absorption must be determined. Ideally, the geometry of the cluster complex should also be determined since various isomeric forms of a cluster carbonyl may be present in the matrix. Except in special simple cases, however, cluster geometries are not easily obtained from our experiments.

Cluster Size. A careful look at the spectra shown in Figure 1 indicates that, as the total metal concentration within the matrix increases, some bands increase more rapidly than others. This fact can be used to determine the number of metals in the cluster associated with an absorption by making use of a model for matrix cluster formation which we have recently published,¹³ in which we assume that aggregates form via reactions taking place at the matrix-vacuum interface, where the condensate may remain fluid for some time before condensing. This process was simulated numerically by considering many of the possible atom-atom and atom-molecule encounters, setting up the set of simultaneous linear differential equations describing these reactions, and solving them.

The solution yielded a relatively simple and useful result, namely, that in the metal and CO concentration ranges we are using

$$[M_x CO_y]/[MCO] \propto [M]^{x-1} \quad (1)$$

That is, the absorbance of a species containing x metal atoms is approximately proportional to the metal concentration raised to the power $x - 1$ when the absorbance of the former is normalized with that of MCO (or another species containing just one metal atom).

Applying this technique (or rather a variant of it in which the quantity A_x/A_{CO} , the absorbance of an unknown species divided by that of the 2138-cm⁻¹ CO line, was plotted vs. metal concentration), we conclude that the lines at 2128, 2116, and 1871 cm⁻¹ all belong to dicopper species, while that at 2102 cm⁻¹ belongs to a tricopper species (see Figure 5). The species absorbing between 1920 and 1945 cm⁻¹ behaved approximately as mononuclear species. Their behavior was erratic, however, apparently depending on the concentration of water impurity. Indeed in the rare instance when water was excluded almost entirely, these lines were absent. We therefore attribute them to species containing both CO and water or products of reaction with water, and will consider them no further. Likewise, the absorptions at 2255 cm⁻¹ and the shoulder on the high-frequency side of the 2148-cm⁻¹ line also appear to be somehow connected with the water content of the matrix.

CO Stoichiometry. A mixed isotopic (¹³CO/¹²CO) matrix may be used to determine CO stoichiometry as a result of the fact that the symmetry of a molecule possessing more than one equivalent CO will be reduced upon substitution of some ¹³CO's for ¹²CO's. This gives rise to new absorptions. For example, a complex containing only one CO will show two almost equal CO stretching frequencies in an equimolar ¹³CO/¹²CO matrix: one arising from the ¹³CO complex, the other arising from the ¹²CO complex. Should the complex contain two equivalent CO's, one would expect altogether a total of six CO absorptions, two each from the following three complexes: $M_x(^{12}CO)_2$, $M_x(^{13}CO)_2$, $M_x(^{12}CO)(^{13}CO)$. In particular, if the two carbonyls are collinear, the first two complexes will have only one infrared active CO stretching mode each, while the third will have two, one of which correlates with the symmetric stretch of the pure isotopic species and is weak.

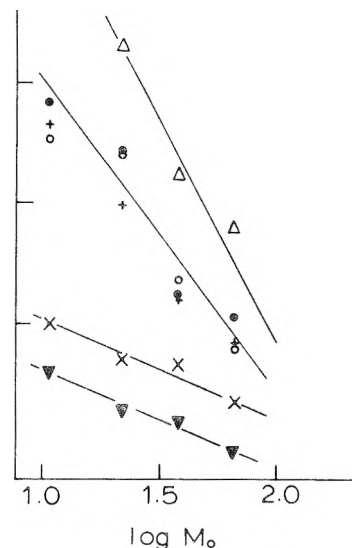


Figure 5. $\log A_x/A_{CO}$ vs. M_0 : A_x represent the absorbance of the 2128 (full dot), 2116 (open dot), 2102 (open triangle), 2012 (full triangle), 1892 (X) and 1871 (crosses) cm⁻¹ lines, A_{CO} is the absorbance of the 2138-cm⁻¹ CO line. The slope of the bottom two lines is 0.42, that of the middle line 1.3, and the top line 2.0. The difference in slope between the lines representing dinuclear and that of mononuclear species is 0.9, while the analogous difference for the trinuclear species is 1.6.

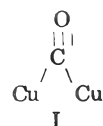
Consequently, the spectrum resulting from a species of the form $M_x(CO)_2$ (having collinear CO's), when formed in an equimolar ¹³CO/¹²CO matrix, will be a triplet in which the center absorption belongs to the mixed isotopic molecule and is roughly twice as intense as either of the two other absorptions, as a result of the increased probability of formation of that species. A word of caution must be said regarding this method of stoichiometry determination. Should the two CO's in a cluster dicarbonyl be terminally bonded to two *different* metal atoms, the interaction force constant connecting the two carbonyls may be small and the isotope pattern will be essentially that of a monocarbonyl. This is a familiar fact in the spectrum of CO chemisorbed on metals in which the CO's are generally bonded one to each surface metal atom.¹⁴ Applying this rationale, we conclude that the absorptions at 2116 and 1871 cm⁻¹ belong to species of stoichiometry Cu_2CO and that at 2102 cm⁻¹ to Cu_3CO . The line which grows in at 1859 cm⁻¹ is suspected to belong to a rotamer of the molecule which absorbs at 1871 cm⁻¹, since in some warmups the former appears with the simultaneous disappearance of the latter before a great deal of growth and decay of any other lines takes place.

This still leaves us with two dicopper monocarbonyl species to explain.

Conventional thinking suggests that the species at 2116 cm⁻¹ arises from a CO terminally bonded to a copper dimer. Thus



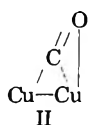
while the low-frequency species belongs to a bridge-bonded CO as follows



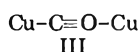
The presence of a species of the latter type presents certain problems. To begin with, a bridge-bonded CO of the type shown is most viable when there is no formal Cu-Cu bond. (The lone 4s electron in each of the coppers is used by each leg of the CO bridge to form a bond).

Carbonyl bridges between nonmetal-metal bonded metals are very rare¹⁵ and even these rare reports have been disputed.¹⁶ Thus the metal-carbon bond in I is expected to be weak, hence its CO stretching frequency higher than what one normally encounters in bridge-bonded carbonyls. Secondly, Pritchard^{3a} reports the CO stretching frequencies of the (100), (110), and (111) single crystal faces of copper to lie in the 2070–2090-cm⁻¹ region, far above the 1871 cm⁻¹ observed by us for Cu₂CO. Both LEED studies¹⁷ and theoretical calculations by Anderson¹⁸ and Ertl¹⁹ place the CO at fourfold copper sites. The spectrum of CO adsorbed on polycrystalline copper also contains only high-frequency modes. So, for instance, the spectra obtained by Eischens²⁰ by exposing a copper-particle-in-silica dispersion to CO, by Pritchard and Sims²¹ by multiple external reflection-specular reflectance spectroscopy of CO-covered, deposited copper films, by ourselves,²² and others all show a relatively narrow band centered at around 2107 cm⁻¹ with a less intense shoulder on the low-frequency side with no other bands present. (One should add parenthetically that Smith and Quets did report other low-frequency bands in the spectrum of CO on silica-supported copper.²³ In view of the absence of these features in any of the other studies, one must conclude that observation is spurious).

These observations may be reconciled either by saying that the bonding is as in I and a multiple bonding situation at a surface is unique or by suggesting that the species giving rise to the 1859-cm⁻¹ absorption is one without a surface analogue, for instance, structures II or III. This is likely the correct explanation since the 1859-cm⁻¹ band shows an uncommonly small ¹³C isotope shift observed as compared to those normally measured for metal carbonyls in this region. For example, the ¹²CO line of Cu(CO)₂ comes at 1892 cm⁻¹ and its ¹³CO counterpart at 1849 cm⁻¹, i.e., 43 cm⁻¹ lower. The ¹³CO counterpart of the 1859-cm⁻¹ line, on the other hand, comes at 1827 cm⁻¹, only 32 cm⁻¹ down. An isotope shift so greatly different from that predicted by taking the square root of the ratio of reduced masses implies that the mode at 1859 cm⁻¹ has a somewhat larger contribution from other bond stretches or bends than is usually encountered in metal carbonyls. This may arise from a departure from geometry I in such a way that one of the copper atoms interacts with the oxygen of the carbonyl as follows:



or perhaps from the following geometry



This speculation is strengthened, although not proved, by a simple valence force field normal coordinate calculation which we performed in which only stretches were considered. The results consistently showed a smaller ¹³C isotopic shift for geometries II and III than for I, using reasonable values for CO, CuC, and CuO force constants.

An extended Hückel molecular orbital calculation also predicted form III to be more stable by about 4 kcal than I. Again this is not conclusive proof, since extended Hückel calculations do not give trustworthy values for molecular energies. What both of these calculations do show, however, is that geometries such as II and III are plausible sources of the line at 1859 cm⁻¹. A geometry similar to II was recently reported²⁴ for a manganese carbonyl.

If the low-frequency absorptions are indeed attributable to species such as II or III, one need no longer assign the

absorptions in the 2116–2094-cm⁻¹ range to CO bonded to single copper sites. The 2116-cm⁻¹ and the 2102-cm⁻¹ lines may now belong to two-center and three-center bonded CO (on Cu), while the 2094-cm⁻¹ line which grows in may be due to four-center bonded CO. It is noteworthy that on prolonged warmup, a CO/Ar matrix rich in copper yields a spectrum which has as its only feature a broad band centered at around 2090 cm⁻¹. Since four-center bonding is the highest coordination possible, it appears, then, that adding more copper atoms to a copper tetramer bonded to a single CO molecule does not alter the CO bond markedly.

In this context, the 2128-cm⁻¹ line is a puzzle. It also behaves like a Cu₂CO species as far as metal concentration dependence and CO isotopic pattern are concerned. Its intensity decreases more rapidly with CO concentration than does that of the 2116-cm⁻¹ line and it hardly grows on warmup. A plausible species that would act in this manner is



This species would give rise to a monocarbonyl isotopic pattern, for reasons stated earlier.

Conclusion

In the preceding we have described the formation and identification of several copper cluster carbonyls and in particular a series of the form Cu_nCO where *n* = 1 to 4. As previously reported for Ni, the spectrum of CO attached to a metal trimer already possesses most of the features of CO chemisorbed on the bulk metal, thereby implying that the bonding of CO to the metal is a local effect, and specifically one involving free-metal-like surface states. While it is tempting to jump to the conclusion at this stage that all chemisorption phenomena are likewise caused and in so doing set foot on the road toward a unified theory of chemisorption, one is utterly unjustified in doing so. Our experiments, at best, suggest that localized bonding takes place in the case of CO and perhaps other σ -donor π -acceptor type molecules, such as NO and C₂H₄, attached to clusters. The possibility still exists that in other systems and on single crystal surfaces a different type of bonding occurs. We have preliminary data, for instance, on the interaction of H₂ with Ni clusters²⁵ under conditions where trinickel groups exist. No evidence of H–H bond scission (i.e., no metal hydride stretch) was observed, although it is known that hydrogen dissociatively chemisorbs on nickel surfaces. This nonobservation may be due to the fact that hydrogen bond cleavage is an activated process which is slow at the low temperature of the matrix. On the other hand, this might imply that hydrogen chemisorption is a radically different process from that of CO adsorption. Perhaps hydrogen requires bulklike metal orbitals with which to interact, forming surface “impurity” states and contributing to the electronic structure of the metal crystal as a whole in a manner analogous to impurities in semiconductors. Moreover, Pritchard’s spectra of CO bonded to single-crystal faces of copper indicate that here again the bonding differs somewhat from that on clusters. Nor should one conclude from our observations that for σ -donor π -acceptor ligands a single metal atom accurately describes a surface. Although much can be learned regarding metal adsorbate bonding by considering single-metal-atom-ligand complexes, our experiments show that the CO in monocopper monocarbonyl is quite different from that in the copper cluster carbonyls and hence from that chemisorbed on copper. In other words, although the CO-metal cluster bond is local in the sense that one need not have

bulklike metal particles to simulate bonding to the surface, the presence of more than one metal atom is nevertheless essential for adequate simulation.

Acknowledgment. We thank the National Research Council of Canada, the Research Corporation, the Atkinson Foundation, and the Connaught Foundation for financial support. One of us (J.E.H.) thanks the National Research Council of Canada for a scholarship.

References and Notes

- (1) A. M. Bradshaw, *Surf. Sci.*, in press.
- (2) H. Haas and R. K. Shellne, *J. Chem. Phys.*, **47**, 2996 (1967).
- (3) (a) M. A. Chesters, J. Pritchard, and M. L. Sims, *J. Chem. Soc., Chem. Commun.*, 1454 (1970); J. Pritchard, *J. Vac. Sci. Technol.*, **9**, 395 (1972); K. Horn, M. Hussain, and J. Pritchard, *Surf. Sci.*, **63**, 244 (1977). (b) P. J. Page and P. M. Williams, *Faraday Discuss.*, **58**, 80 (1974), and other papers in that number.
- (4) J. R. Schrieffer and P. Soven, *Phys. Today*; **24** (April, 1975).
- (5) G. C. Bond, *Discuss. Faraday Soc.*, **41**, 200 (1966).
- (6) J. E. Demuth and D. E. Eastman, *Phys. Rev. Lett.*, **32**, 1123 (1974).
- (7) T. E. Madey, J. T. Yates, Jr., and D. R. Sandstrom, *Treatise Solid State Chem.*, **6B**, 1 (1976).
- (8) E. P. Kündig, M. Moskovits, and G. A. Ozin, *Can. J. Chem.*, **51**, 2737 (1973).
- (9) H. Huber, E. P. Kündig, M. Moskovits, and G. A. Ozin, *J. Am. Chem. Soc.*, **97**, 2097 (1975).
- (10) J. E. Hulse and M. Moskovits, *Surf. Sci.*, **57**, 125 (1976).
- (11) H. Dubost, *Chem. Phys.*, **12**, 139 (1976).
- (12) R. N. Perutz and J. J. Turner, *J. Chem. Soc., Faraday Trans. 2*, **69**, 452 (1973).
- (13) M. Moskovits and J. E. Hulse, *J. Chem. Soc., Faraday Trans. 2*, **73**, 471 (1977).
- (14) R. P. Eischens, S. A. Francis, and W. A. Pliskin, *J. Phys. Chem.*, **60**, 194 (1956).
- (15) E. O. Fischer and K. Bittler, *Z. Naturforsch. B*, **16**, 835 (1961).
- (16) F. A. Cotton and P. L. Hunter, *Inorg. Chem.*, **13**, 2044 (1974).
- (17) K. Horn and J. Pritchard, *Surf. Sci.*, **55**, 701 (1976).
- (18) A. D. Anderson, *Surf. Sci.*, in press.
- (19) G. Doyen and G. Ertl, *Surf. Sci.*, **43**, 197 (1974).
- (20) R. P. Eischens, W. A. Pliskin, and S. A. Francis, *J. Chem. Phys.*, **22**, 1786 (1954).
- (21) J. Pritchard and M. L. Sims, *Trans. Faraday Soc.*, **70**, 427 (1969).
- (22) M. Moskovits, C. J. Hope, and B. Jantzi, *Can. J. Chem.*, **53**, 3313 (1975).
- (23) A. W. Smith and J. M. Quets, *J. Catal.*, **4**, 163 (1965).
- (24) R. Colton, C. J. Commons, and B. F. Hoskins, *J. Chem. Soc., Chem. Commun.*, 363 (1975).
- (25) C. Choi and M. Moskovits, unpublished results.

Excimer-Monomer Emission Ratio in Electrochemiluminescence

Csaba P. Keszthelyi*

Department of Chemistry, University of Colorado, Boulder, Colorado 80309 and The Frank J. Seiler Research Laboratory (AFSC), USAF Academy, Colorado 80840 (Received December 28, 1976; Revised Manuscript Received August 4, 1977)

Publication costs assisted by the Air Force Systems Command

Excimer/monomer emission ratios for both energy deficient and sufficient electrogenerated chemiluminescent (ECL) systems are evaluated from a kinetic standpoint. Correction due to the absorption-fluorescence (ARF) cycle is introduced and a rigorous general expression is given for the excimer/monomer emission ratio.

It has been pointed out¹ that while the [dimer emission intensity/monomer emission intensity] ratio² in optical pumping is a rather straightforward luminophor concentration dependent function, it is not so in the case of electrochemiluminescence (ECL).³ In the present paper we examine in some detail evaluation of this important term as a function of kinetically defined parameters. For the general case, the excimer/monomer emission ratio ϕ_D/ϕ_M has been given by Maloy and Bard⁴ as

$$\frac{\phi_D}{\phi_M} = \frac{k_f'}{k_f} \frac{\tau_D}{1 + \alpha\tau_D k_d} \frac{\alpha}{\tau_M} + (1 + \alpha)k_a[A] \quad (1)$$

where k_f' and k_f are the rate constants for the radiative transitions of the excimer and the monomer, respectively; τ_D and τ_M refer to excited state lifetimes; k_d and k_a are the rate constants that determine the steady-state distribution between excimer and monomer; and α is defined by the ratio of the rate of dimer formation (R_D) to the rate of monomer formation (R_M), i.e.

$$\alpha = R_D/R_M$$

In the special case where no independent excited singlet generation is assumed to occur, R_M approaches zero and consequently α approaches infinity.

* Present address: Department of Chemistry, Louisiana State University, Baton Rouge, La. 70803.

Although the treatment given by Parker⁵ and Birks⁶ for delayed fluorescence is correct, it cannot be carried over to T-route ECL without additional considerations.

In eq 1 if we represent $(k_f'/k_f)\tau_D$ by k where k is a constant, then eq 1 may be rewritten as

$$\frac{\phi_D}{\phi_M} = k \left[\frac{\alpha}{\tau_M + \alpha\tau_M\tau_D k_d} + \frac{k_a[A]}{1 + \alpha\tau_D k_d} + \frac{\alpha k_a[A]}{1 + \alpha\tau_D k_d} \right] \quad (2)$$

The first term inside parentheses can be represented as

$$\frac{\alpha}{\tau_M + \alpha\tau_M\tau_D k_d} = \frac{1}{\tau_D\tau_M k_d} \left[\alpha / \left(\frac{1}{k_d\tau_D} + \alpha \right) \right]$$

now

$$\lim_{\alpha \rightarrow \infty} \left(\frac{\alpha}{a + \alpha} \right) = 1$$

so

$$\lim_{\alpha \rightarrow \infty} \frac{1}{\tau_D\tau_M k_d} \left[\alpha / \left(\frac{1}{k_d\tau_D} + \alpha \right) \right] = \frac{1}{\tau_D\tau_M k_d} \cdot 1 = \frac{1}{\tau_D\tau_M k_d} \quad (3)$$

The second term inside parentheses in eq 2 is

$$\frac{k_a[A]}{1 + \alpha\tau_D k_d}$$

and can be written as

$$\frac{k_a[A]/\tau_D k_d}{(1/\tau_D k_d) + \alpha}$$

since

$$\lim_{\alpha \rightarrow \infty} (a + \alpha) = \alpha$$

and consequently

$$\lim_{\alpha \rightarrow \infty} \left(\frac{b}{a + \alpha} \right) = 0$$

thus

$$\lim_{\alpha \rightarrow \infty} \left[\frac{k_a[A]}{1 + \alpha \tau_D k_d} \right] = \lim_{\alpha \rightarrow \infty} \left[\frac{k_a[A]/\tau_D k_d}{(1/\tau_D k_d) + \alpha} \right] = 0 \quad (4)$$

The third term inside parentheses in eq 2 can be expressed as

$$\frac{\alpha k_a[A]}{1 + \alpha \tau_D k_d} = \frac{k_a[A]}{\tau_D k_d} \left[\frac{\alpha}{(1/\tau_D k_d) + \alpha} \right]$$

and again, since

$$\lim_{\alpha \rightarrow \infty} \left(\frac{\alpha}{a + \alpha} \right) = 1$$

$$\lim_{\alpha \rightarrow \infty} \left[\frac{\alpha k_a[A]}{1 + \alpha \tau_D k_d} \right] = \frac{k_a[A]}{\tau_D k_d} \quad 1 = \frac{k_a[A]}{\tau_D k_d} \quad (5)$$

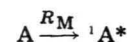
Taking the limit of eq 2 as α approaches infinity, we may apply eq 3, 4, and 5 to obtain

$$\lim_{\alpha \rightarrow \infty} \frac{\phi_D}{\phi_M} = k \left[\frac{1}{\tau_D \tau_M k_d} + 0 + \frac{k_a[A]}{\tau_D k_d} \right] \quad (6)$$

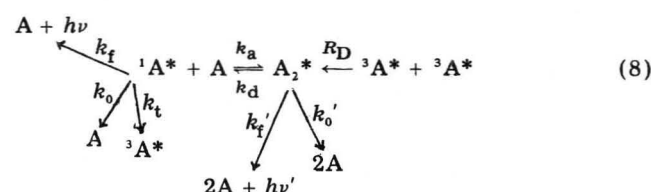
Putting the value of k back, we obtain

$$\lim_{R_M \rightarrow 0} \frac{\phi_D}{\phi_M} = \frac{k_f'}{k_f} \left[\frac{1}{\tau_M k_d} + \frac{k_a[A]}{k_d} \right] = \frac{k_f'}{k_f k_d} \left[\frac{1}{\tau_M} + k_a[A] \right] \quad (7)$$

This equation can also be easily derived directly from the original emission scheme if it is assumed that there is no production of the first excited singlet state from the ground state, i.e., the step



is totally omitted and the scheme becomes



If we define, in the customary way, τ_M and τ_D as

$$1/\tau_M = k_f + k_0 + k_t \quad (9)$$

and

$$1/\tau_D = k_f' + k_o' + k_d \quad (10)$$

the steady state equation for ${}^1A^*$ may be written as

$$k_d[A_2^*] = [(1/\tau_M) + k_a[A]][{}^1A^*] \quad (11)$$

and that for $[A_2^*]$ may be written as

$$R_D + k_a[A][{}^1A^*] = [A_2^*]/\tau_D \quad (12)$$

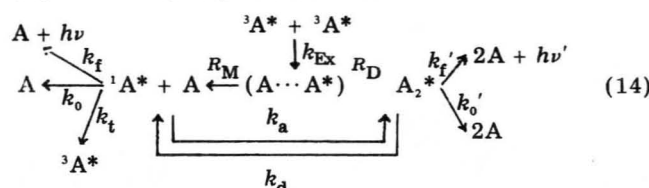
and as ϕ_D/ϕ_M is defined as

$$\frac{\phi_D}{\phi_M} = \frac{k_f'[A_2^*]}{k_f[{}^1A^*]} \quad (13)$$

we may put in the value of $[A_2^*]$ from eq 11 in eq 13 to obtain

$$\frac{\phi_D}{\phi_M} = \frac{k_f'}{k_f k_d} \left(\frac{1}{\tau_M} + k_a[A] \right)$$

which is identical with eq 7 previously derived, the simplest expression for ϕ_D/ϕ_M in a T-route system. At this stage it may be recalled that an ECL encounter complex (a precursor to the excimer) is going to make at best a small contribution to the total luminescence intensity. Although by extending the treatment of Goldschmidt and co-workers,⁷ the two types of encounter complex (ECL vs. TTA) do not coincide in general for the same parent compound, a TTA encounter complex should be regarded as a precursor to the excimer¹ and the following schemes (eq 14 and 22) may be outlined:



Equation 1 is applicable, and in addition the steady state equation for the encounter complex ($A \cdots A^*$) may be expressed as

$$R_M + R_D = k_{Ex} [{}^3A^*]^2 \quad (15)$$

and since

$$\alpha = R_D/R_M$$

$$1 + \alpha = \frac{R_M + R_D}{R_M} = \frac{k_{Ex} [{}^3A^*]^2}{R_M} \quad (16)$$

and

$$\alpha = \frac{k_{Ex} [{}^3A^*]^2}{R_M} - 1 = \frac{k_{Ex} [{}^3A^*]^2 - R_M}{R_M} \quad (17)$$

Using eq 16 and 17 in conjunction with eq 1 we obtain

$$\frac{\phi_D}{\phi_M} = \frac{k_f'}{k_f} \frac{\tau_D R_M}{k_f R_M + \tau_D k_d (k_{Ex} [{}^3A^*]^2 - R_M)} \times \left(\frac{k_{Ex} [{}^3A^*]^2 - R_M}{R_M \tau_M} + \frac{k_a k_{Ex} [A][{}^3A^*]^2}{R_M} \right) = \frac{k_f'}{k_f} \frac{\tau_D}{k_f R_M + \tau_D k_d (k_{Ex} [{}^3A^*]^2 - R_M)} \times \left[{}^3A^* \right]^2 \left(\frac{k_{Ex} + k_a k_d [A]}{\tau_M} - \frac{1}{\tau_M} \right) = \frac{k_f'}{k_f} \frac{\tau_D}{\tau_D} \frac{[{}^3A^*]^2 k_{Ex} (1/\tau_M + k_a[A]) - 1/\tau_M}{R_M + \tau_D k_d (k_{Ex} [{}^3A^*]^2 - R_M)} \quad (18)$$

Getting back to the pure T-route scheme outlined in eq 8, it should be pointed out at this stage that, although we have taken $R_M = 0$, this is really erroneous in practical application because of the relatively high concentration of the fluoroscors used and consequent absorption of the

emitted light and occurrence of the absorption–refluorescence (ARF) cycle,⁸ the extent being dependent on the magnitude of the overlap between the absorption and emission spectra of the compound, and its fluorescence efficiency (ϕ_f). The absorption results in the production of the first excited singlet state $^1A^*$ from the ground state, and in this regard the emission from the dimer A_2^* is unimportant since this is shifted considerably more toward lower wavelengths compared to the absorption spectrum of the ground state [A], and thus no significant overlap and absorption should exist insofar as the dimer emission is concerned.

If the fraction of the overlap of the singlet state emission and the ground state absorption spectra is given by l and the fluorescence efficiency of $^1A^*$ is ϕ_f , then upon the first cycle of emission l amount would be absorbed, and generation of $^1A^*$ would be proportional to l (we, of course, are assuming complete absorption, as is observed). On the next cycle $l \times \phi_f$ amount would be emitted and so $l \times (l\phi_f)$ amount would be absorbed, and the generation of $^1A^*$ would be proportional to $l^2\phi_f$. On the next cycle it would be proportional to $l^3\phi_f^2$ and so on.

The total generation of $^1A^*$ from A due to absorption would thus be proportional to

$$l + l^2\phi_f + l^3\phi_f^2 + l^4\phi_f^3 + \dots = \sum_{n=1}^{\infty} l^n \phi_f^{n-1} = \frac{l}{1 - l\phi_f} \quad (19)$$

For a scheme like the one represented in eq 8 the constant of proportionality can be seen to be

$$\phi_M = k_f [^1A^*] = \frac{k_f k_d [A_2^*]}{[(1/\tau_M) + k_a [A]]} \quad (20)$$

and thus

$$R_M = \phi_M \frac{l}{1 - l\phi_f}$$

and the general eq 1 can be applied with

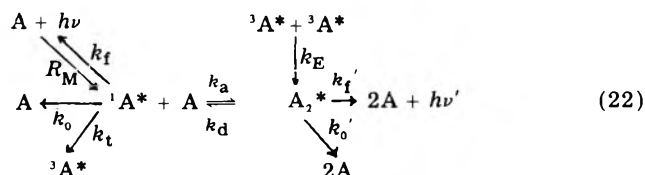
$$\alpha = R_D/R_M$$

and

$$R_M = \frac{l}{1 - l\phi_f} \frac{k_f k_d [A_2^*]}{(1/\tau_M + k_a [A])} \quad (21)$$

Choosing typical values^{9,9} ($l = 0.5$ and $\phi_f = 0.84$ for DPA, $l/(1 - l\phi_f) = 0.86$), this ARF correction has been shown⁸ to introduce significant change in the overall calculations for S-route ECL systems, and, as pointed out below, is also necessary in the general ECL scheme.

For the general scheme



the steady state equation for $[A_2^*]$ becomes

$$k_a [A] [^1A^*] + k_E [^3A^*]^2 = [A_2^*]/\tau_D \quad (23)$$

and that for $[^1A^*]$ is

$$R_M + k_d [A_2^*] = \left(\frac{1}{\tau_M} + k_a [A] \right) [^1A^*] \quad (24)$$

Equating values of $[A_2^*]$ from eq 23 and 24 we obtain

$$\tau_D k_a [A] [^1A^*] + \tau_D k_E [^3A^*]^2 = \frac{1}{\tau_M k_d} + \frac{k_a [^1A^*] - R_M}{k_d}$$

or

$$[^1A^*] k_a [A] (1/\tau_d - \tau_d) + \frac{1}{\tau_M k_d} = \tau_D k_E [^3A^*]^2 + \frac{R_M}{k_d}$$

and

$$[^1A^*] = \frac{\tau_D k_d k_E [^3A^*]^2 + R_M}{[k_a [A] (1 - \tau_D k_d) + (1/\tau_M)]} \quad (25)$$

Since

$$R_M = \frac{l}{1 - l\phi_f} k_f [^1A^*]$$

$$R_M = \frac{l}{1 - l\phi_f} k_f \frac{\tau_D k_d k_E [^3A^*]^2 + R_M}{[k_a [A] (1 - \tau_D k_d) + (1/\tau_M)]}$$

or

$$R_M [(1 - l\phi_f) [k_a [A] (1 - \tau_D k_d) + (1/\tau_M)] - 1] = l k_f \tau_D k_d k_E [^3A^*]^2$$

and, finally

$$R_M = \frac{l k_f \tau_D k_d k_E [^3A^*]^2}{\{(1 - l\phi_f) [k_a [A] (1 - \tau_D k_d) + (1/\tau_M)]\} - 1} \quad (26)$$

Substitution of R_D in place of $k_E [^3A^*]^2$, referring back to a scheme parallel to the one outlined in eq 8 would give us

$$\frac{R_D}{R_M} = \alpha = \frac{(1 - l\phi_f) [k_a [A] (1 - \tau_D k_d) + 1/\tau_M] - 1}{l k_f \tau_D k_d} \quad (27)$$

and use of this value of α in eq 1 gives a rigorously correct and generally applicable equation for all cases.

The continuing interest in electrochemiluminescence in nonaqueous solvents, and the related quest for an electrochemically pumped dye laser¹⁰ favors an in-depth inquiry into ECL dimer formation and related losses. These results pertain to both dc and pulsed electrolysis conditions, though there are special restrictions when dealing with thin-layer ECL cells, and those have been treated separately.¹¹ We should not close without mentioning that the quenching terms k_0 and k_0' in ECL include losses due to the presence of the electrogenerated cations and anions, hence these cannot be readily substituted from conventional fluorescence measurements. At the present level of advancement the common model that treats the ECL annihilation zone as an infinitely thin section of the double layer is no longer satisfactory, and interpenetration of the ECL parent ions¹⁰ needs to be included; this correction is especially needed for emission measured along the plane of the electrode, as would be the case for an electrochemically pumped dye laser.

Acknowledgment. This was presented in part in Paper No. 58 ("Electrochemiluminescence in Non-aqueous Solvents") at the 26th Meeting of the International Society of Electrochemistry, Sept 21–26, 1975, Baden bei Wien, Austria. Valuable comments, contributions, and criticisms by P. K. Dasgupta (Louisiana State University), J. S.

Pekrul (University of Colorado), and Capt. L. P. Davis (FJSRL, USAF Academy) are gratefully acknowledged.

References and Notes

- (1) C. P. Keszthelyi, *Spectrosc. Lett.*, **7**, 409 (1974).
- (2) C. A. Parker and G. D. Short, *Trans. Faraday Soc.*, **63**, 2618 (1967).
- (3) (a) D. M. Hercules, *Acc. Chem. Res.*, **2**, 301 (1969); (b) A. J. Bard, C. P. Keszthelyi, H. Tachikawa, and N. E. Tokel in "Chemiluminescence and Bioluminescence", M. J. Cormier, D. M. Hercules, and J. Lee, Ed., Plenum Press, New York, N.Y., 1973; (c) C. P. Keszthelyi, *J. Am. Chem. Soc.*, **96**, 1243 (1974).
- (4) (a) J. T. Maloy, Ph.D. Thesis, The University of Texas, 1970; (b) J. T. Maloy and A. J. Bard, *J. Am. Chem. Soc.*, **93**, 5968 (1971).
- (5) C. A. Parker and C. G. Hatchard, *Trans. Faraday Soc.*, **59**, 264 (1963).
- (6) J. B. Birks, *J. Phys. Chem.*, **67**, 2199 (1963).
- (7) C. R. Goldschmidt, R. Potashnik, and M. Ottolenghi, *J. Phys. Chem.*, **75**, 1025 (1971).
- (8) C. P. Keszthelyi, N. E. Tokel-Takvoryan, and A. J. Bard, *Anal. Chem.*, **47**, 249 (1975).
- (9) I. B. Berlman, "Handbook of Fluorescence Spectra of Aromatic Molecules", 2nd ed, Academic Press, New York, N.Y., 1971, p 24.
- (10) C. P. Keszthelyi, *Appl. Opt.*, **14**, 1710 (1975).
- (11) C. P. Keszthelyi, *Croat. Chem. Acta*, **48**, 25 (1976).

Calculation of the Energies of Activation for Some Gas-Phase Reactions

Thomas N. Bell

Department of Chemistry, Simon Fraser University, Burnaby, British Columbia, Canada V5A 1S6

and Peter G. Perkins*

Department of Pure and Applied Chemistry, University of Strathclyde, Glasgow G1 1XL, Scotland (Received November 22, 1976; Revised Manuscript Received June 20, 1977)

A method for calculating the energies of activation for gas-phase hydrogen transfer reactions is described. The basis lies in the self-consistent electronic structure of all species lying on the reaction coordinate. ΔE^\ddagger and $\log A$ for the reactions of $\text{CH}_3\cdot$ and $\text{CF}_3\cdot$ with CH_4 , H_2 , and HCl are calculated.

Introduction

In a preliminary communication¹ we outlined a novel method for calculating the energies of activation for hydrogen abstraction reactions in the gas phase. We now give a full account of the method and its application to some gas-phase hydrogen-abstraction reactions.

Method

In previous work a rotationally invariant quantity, the *bond index*, has been defined.^{2,3} This is compounded from the relevant elements of the Coulson bond order density matrix, in turn obtained from a quantum mechanical self-consistent field molecular calculation on the system of interest. The bond index is given by

$$B_{AB} = \sum_{\sigma \in A} \sum_{\lambda \in B} P_{\lambda\sigma}^2$$

where the $P_{\mu\nu}$ are the Coulson density matrix elements. Bond indices for simple molecules such as hydrocarbons follow a pattern which correlates with the chemist's concept of multiplicity of bonds; thus, for ethane, ethylene, and acetylene the C-C bond indices are, respectively, 1.023, 2.032, and 2.998.² Following this trend, we suggest that such bond indices may be used, in conjunction with experimental standard-state heats of atomization, to obtain a set of standard energy terms for a range of bonds. Since the bond index reflects minor variations in the intrinsic bond strength with the environment of the bond in question, the concept should lead to an improvement in the simple calculation of heats of formation for molecules. This is being followed further.⁴

A set of bond indices may be calculated for any system and can thus afford, in principle, the heat of formation for that system in the standard state. Thus, in the case of one or more species undergoing reaction, a grid of points on an energy surface can be set up, the heat of atomization

TABLE I: Bond Energy Parameters

Bond	Energy, kJ mol ⁻¹	Bond	Energy, kJ mol ⁻¹
C-H ^a	420.66	Cl-Cl	-20.49
C-F ^a	504.17	F-F	291.62
C-Cl	336.70	H-F	-140.18
H-Cl ^b	25.87	Cl-F	44.74

^a These values refer to CH in methane and to CF in CF₄ (vide infra). ^b A second value for this parameter is used when there is "bonding" interaction between H and Cl (vide infra).

for the system computed for each, and the reaction followed along a coordinate and over a saddle.

We first calculated the sets of bond indices for the molecules comprising the complete series of fluoro- and chloromethanes. The basic calculations were all performed using a self-consistent molecular-orbital method parameterized as described previously^{5,6} with 3d orbitals included on the chlorine atoms. Bond distances were abstracted from standard compilations.⁷ Bond indices were finally computed from the spinless density matrix. Use of these together with the experimental heats of atomization of the compounds in the standard state at 298 K yielded a set of bond-energy-like parameters relating to each interaction in the molecule.

The latter was effected by taking a weighted sum of the bond indices for each interaction in each molecule and setting this equal to the experimental standard-state heat of atomization⁸ for the systems. Since the approach depends essentially on the assumption that the energies of separate bonds in molecules and radicals are additive, for CH_2Cl_2 (for example) we write

$$2aB_{\text{C-H}} + 2bB_{\text{C-Cl}} + cB_{\text{Cl-Cl}} + 4dB_{\text{Cl-H}} = \Delta H^\circ_{\text{atom}}$$

where $B_{\text{X-Y}}$ is the bond index for the bond X-Y.

TABLE II: Heats of Atomization for Halogenomethanes (kJ mol⁻¹)

	$\Delta H^\circ_{\text{atom}}$ (obsd) ^a	$\Delta H^\circ_{\text{atom}}$ (calcd)
CH ₃ F	1682.8 ± 30	1714.6
CH ₂ ClF	1621.3 ± 21	1626.3
CHClF ₂	1684.9 ± 12	1691.6
CHCl ₂ F	1543.1 ± 21	1535.9
CCl ₂ F ₂	1596.6 ± 8	1598.3
CClF ₃	1767.8 ± 8	1770.3
CF ₄	1953.5 ± 10	1959.8

^a Standard heats of formation taken from ref 4.

An equivalent equation was written for other molecules of the series, so as to generate a set of simultaneous equations. On solution, these yield the weighting coefficients (*a*, *b*, *c*, etc.) and these are the bond-energy parameters. We found that it proved best to leave out all H-H interactions (all of these are of "nonbonding" type), as these terms rendered the equations unstable. Table I lists the parameters obtained. Among these appear several (e.g., H-Cl, H-F) which represent "nonbonding interactions" and the sign of that for H-F shows that these quantities can be negative. Using these, we may compute the heats of atomization of those halogenomethanes not used in the calibration process. The results, given in Table II, are seen to be in good agreement with experiment. The bonding parameters derived here are, of course, tied to our particular scheme of calculation. For another scheme it would be necessary to resolve the above equations. However, the nature of the method does mean that a self-consistent scheme based on the CNDO method is perfectly adequate for the present purpose and no improvement would necessarily be expected by applying a more sophisticated molecular-orbital approach.

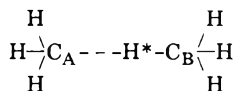
We next transferred the calculational scheme to mutually interacting species. Here again, we obtain the heat of atomization of the system in the standard state and at 298 K at every point on the reaction coordinate. We carry this out by computing the heat of atomization for a set of points on a two-dimensional energy grid. Thus, when the lowest-energy saddle point is obtained, we can compute ΔH° from a knowledge of $\Delta H^\circ_{\text{atom}}$ for the initial state and the transition state. This ΔH° is tied to standard-state conditions and its correction to the relevant reaction temperature must be considered in each case. Because the starting and transition-state enthalpies are affected in the same way by minor variations in bonding parameters, then their difference is not very sensitive to the parameters.

The experimental quantity of interest is the experimental energy of activation, $\Delta E^\ddagger_{\text{expt}}$. From transition-state theory for a bimolecular reaction with *k* expressed in concentration units (L mol⁻¹ s⁻¹), we have $\Delta E^\ddagger_{\text{expt}} = \Delta H^\ddagger_{\text{T}} + 2RT$. Hence, we can compare our computed values directly with those obtainable from experiment by selecting a median temperature in the experimental range for each system.

We applied the approach to calculation of the activation energies for some gas-phase hydrogen-abstraction processes. These included the abstraction of hydrogen from CH₄, H₂, and HCl by CH₃· and CF₃· radicals for which carefully evaluated experimental data are available.⁹ The reaction coordinates were initiated with the CX₃· and substrate molecule 0.5 nm apart and ended with the reactants similarly disposed. A distance of 0.5 nm was chosen, since at that distance there is no interaction between the starting components and between the products. Thus, all bond indices refer to the isolated reactant species. To proceed along the coordinate, it is necessary to reduce the number of degrees of freedom and in practice, for the

systems studied, this can be easily done. In general, the reactions were assumed to take place along the most symmetrical (C_{3v}) path. Details of secondary restrictions for each case are given separately below. It should be noted that we make no assumption of constant bond order in the C--H--X bond while the coordinate is traversed. Moreover, we believe that the method is of more general application and can be adapted for a greater variety of processes than the one dealt with in the present paper.

i. Reaction of CH₃· with CH₄.



As the C_A--H distance was lessened, the H-C_B bond length was concomitantly increased. Furthermore, at the same time the planar C_AH₃· radical was distorted to a pyramid shape while the C_BH₃ moiety was flattened. Both the latter changes were carried out linearly and at points where C_A-H* = C_B-H*, the system is completely symmetrical.

ii. Reaction of CH₃· with H₂, CH₃· with HCl. Here the H-H and H-Cl bonds were lengthened as the C--H* distance was shortened and the C-H bonds bent to the pyramidal angle.

iii. Reaction of CF₃· with CH₄, CF₃· with H₂, CF₃· with HCl. Procedures corresponding to those relevant above were, in general, carried out. However, since the CF₃· radical is pyramidal,¹⁰ its geometry was retained unmodified throughout the whole reaction coordinate, while for simplicity the solid bond angle was maintained equal to 109° 28'.

When considering the C-H and C-F bonding parameters in CH₃·, CF₃·, CF₃H, and CH₄ together with all the transient stages in the reaction, a problem arises. The intrinsic bond energy of, e.g., C-H in CH₃·, is lower than that of C-H in CH₄, and similarly for C-F in CF₃·. Hence, we must have two different C-H bonding parameters to obtain the correct $\Delta H^\circ_{\text{atom}}$ for CH₃· and CH₄. We overcome this difficulty by an appropriate calibration, using the known heats of formation for CH₃· and CF₃·¹¹ and the self-consistent field calculations for the species. This affords a C-H bond factor for CH₃· of 410.79 kJ mol⁻¹. During the course of reaction, however, as CH₃·, for example, is abstracting a hydrogen from a substrate, its C-H bonds "change character" to those in CH₄, which it becomes at the end of the reaction. It is hence necessary that the C-H bonding parameter be some function of the reaction coordinate, thus changing as the latter is traversed.

There is, moreover, a further problem: as the system moves away from the initial point on the coordinate, the planar methyl moiety starts to assume a pyramidal shape while still some distance from the hydrogen which it is to abstract. Now, the isolated pyramidal form of CH₃· is less stable than planar CH₃· by an amount equal to the reorganization energy. Thus, for the isolated, pyramidal CH₃· radical, a third C-H bonding parameter is required. We must therefore take account also of this additional destabilizing contribution in some way (the problem does not arise for CF₃, since this is pyramidal in the initial stage¹⁰).

The reorganization energy from the planar to the pyramidal form of CH₃· is experimentally unknown. We calculated it by performing ab initio extended-basis GTO calculations, using the ATMOL series of programs¹² on the two geometries of the methyl species. By difference between the total energies of the two species, the reorganization energy was found to be 56.41 kJ mol⁻¹. This allows us to calculate the heat of atomization of pyramidal CH₃·

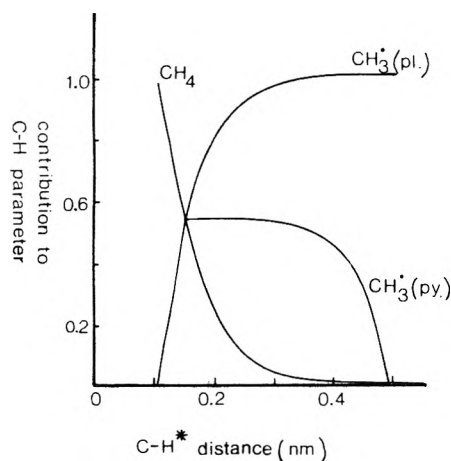


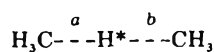
Figure 1. Contributions to the CH bonding parameter along a reaction coordinate.

TABLE III: Variation of CH Bonding Parameters with Central CH* Bond Length

CH* distance, nm	Energy, kJ mol ⁻¹	CH* distance, nm	Energy, kJ mol ⁻¹
0.109	420.66	0.175	409.15
0.120	414.80	0.180	408.94
0.130	412.79	0.185	408.73
0.135	412.12	0.190	408.48
0.140	411.87	0.200	407.98
0.145	411.29	0.250	407.02
0.150	410.79	0.300	406.60
0.155	410.32	0.350	406.68
0.160	409.93	0.400	407.02
0.165	409.61	0.450	407.94
0.170	409.40	0.500	410.79

and, from this and the CH bond index, we obtain a CH bonding parameter of 398.32 kJ mol⁻¹ for the pyramidal species. The next problem is to obtain the function governing the variation of the CH bonding parameter from start to finish of the reaction coordinate. To effect this, we allowed the three species mentioned above to contribute, as shown in Figure 1.

First, the contribution from H₃C-H (i.e., the methane-like CH) was allowed to vary with the C-H* bond length a



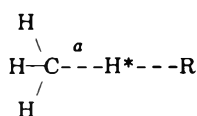
in the same way as does the C-H* index of this bond. In doing this, the second CH* bond length b was maintained at 0.15 nm. The latter figure was chosen since the configuration where $a = b = 0.15$ nm has central C-H bond indices of 0.5. The planar CH₃* contribution is then obtained simply as the inverse of the above. The pyramidal CH₃* species was allowed to contribute in an inverse manner to that of the tail of the "CH₄" curve. The contribution of each species was then read off at a series of C-H* bond lengths and the data normalized to unity. The pyramidal CH₃* species makes its maximum contribution at the crossing point of the two lines of Figure 1 (0.16 nm). Hence, at this bond length, each of the three types of CH bond contributes one-third to the overall multiplying factor. At this point the multiplying factor is, therefore, (410.80 + 420.66 + 398.32)/3 = 409.93 kJ mol⁻¹. A bond-energy factor may now be calculated for each central C-H* bond length, with each species contributing in the ratios derivable from Figure 1. The overall function thus afforded is roughly parabolic. Since for each point on the grid it is necessary to utilize a C-H or C-F bonding parameter, we include here relevant tables (Tables

TABLE IV: Variation of CF Bonding Parameter with Central CH* Bond Length

CH* distance, nm	Energy, kJ mol ⁻¹	CH* distance, nm	Energy, kJ mol ⁻¹
0.109	504.17	0.195	491.12
0.115	498.94	0.200	490.91
0.120	497.27	0.210	490.70
0.125	495.80	0.220	490.53
0.130	494.97	0.230	490.36
0.135	494.55	0.240	490.24
0.140	494.13	0.250	490.07
0.145	493.71	0.260	489.95
0.150	493.42	0.270	489.86
0.155	493.00	0.280	489.78
0.160	492.75	0.290	489.74
0.165	492.37	0.300	489.65
0.170	492.12	0.350	489.44
0.175	491.87	0.400	489.40
0.180	491.70	0.450	489.36
0.185	491.41	0.500	489.36
0.190	491.20		

III and IV) for the purpose.

In reactions of the type



all four C-H bonds are assigned the bond energy factor appropriate to bond length a , since it is this distance which determines the geometry of the CH₃* moiety in the calculation.

In reactions involving CF₃* the radical remains in the pyramidal configuration throughout the coordinate and bond energy parameter variation occurs between the CF bonds in CF₃* and CF₃H, i.e., 489.36 and 504.17 kJ mol⁻¹. Again, the central C-H* bond length determines the appropriate factor to be used.

In the reactions of CH₃* and CF₃* with H₂ and HCl, the "main" H-H and H-Cl bonding parameters were obtained by dividing the experimental standard-state dissociation energies of the molecules by the total H-X bond index. These parameters differ in magnitude from the "nonbonding" type listed in Table I and in the transition-state calculations we must employ both types. For hydrogen and HCl the bonding parameters are 435.97 and 444.76 kJ mol⁻¹, respectively.

As aforesaid, the ΔH^\ddagger values calculated from the reaction coordinate refer to the standard state and 298 K: correction of these to yield ΔH_T^\ddagger at an appropriate temperature T requires a knowledge of C_p° for both reactants and the transition-state complex. It is difficult to calculate C_p° for the latter from first principles, because of the uncertainty in our knowledge of the vibrations arising from the reaction coordinate. Hence, we have preferred to compute ΔC_p° for the change from reactants to transition-state complex by a group contribution method essentially similar to that of Benson.¹¹ Thus, we adopted the data for the free CH₃*, CF₃*, H*, and Cl* moieties and all the molecules, as given in ref 8 for a range of temperature. The variation of C_p° (CH₃ bound) with temperature was abstracted from Benson's compilation¹¹ and similar data for CF₃(bound) were calculated by assuming that

$$C_p^\circ(\text{CF}_3 \text{ bound}) = C_p^\circ(\text{CF}_3\text{H}) - C_p^\circ(1/2\text{H}_2)$$

C_p° for Cl(bound) and H(bound), including that for the central hydrogen, H*, was assumed equal to $C_p^\circ(1/2\text{Cl}_2)$ and $C_p^\circ(1/2\text{H}_2)$, respectively, for any relevant temperature. Using the above data, all the temperature corrections to

TABLE V: Arrhenius Parameters for Hydrogen Abstractions

	T_m , K	ΔE^\ddagger (calcd), ^c kJ mol ⁻¹	ΔE^\ddagger (exptl), kJ mol ⁻¹	$\Delta S_p^{\ddagger 0}$ (calcd), J K ⁻¹ mol ⁻¹	log A (calcd)	log A (exptl)
Forward Reactions						
CH ₃ · + CH ₄	626	59.1	60.7	-73.2	11.86	11.80
CF ₃ · + CH ₄	535	49.6	45.7	-66.5	12.07	11.92
CH ₃ · + H ₂	717	35.8	43.5	-80.7	11.58	11.73
CF ₃ · + H ₂	808	31.7	39.7	-74.9	11.99	11.95
CH ₃ · + HCl	360	18.1	12.9	-77.5	11.46	11.73
CF ₃ · + HCl	386	23.8	21.6	-78.5	11.38	11.27
Back Reactions						
CF ₃ H + CH ₃ ·	498	54.6	41.0-43.5	-72.8	11.67	9.8, 10.0
CH ₄ + H·	1087	41.9	40.2; 51.0 ^a	-66.9	12.66	12.2, 12.6
CF ₃ H + H·	817	37.2	21.0; 46.9 ± 8 ^b	-55.5	13.03	11.86-13.40
CH ₄ + Cl·	389	26.4	16.1	-47.9	12.77	13.42
CF ₃ H + Cl·	400	26.0	35.1	-55.6	12.39	12.23

^a Many values are given; these two have been recommended. ^b Estimated from the reverse reaction. ^c All calculated values are at the median temperature.

the ΔH^\ddagger values are readily made. In no case does the correction exceed ± 4 kJ mol⁻¹.

As a partial check on the correction procedure just described and in order to obtain the preexponential factors for the reactions, we calculated the activation entropy changes, again by the group contribution method. The assumptions and data sources were the same as for the specific heats. The entropy changes calculated refer to the pressure standard state and, for a bimolecular process, must be corrected to the concentration standard state before insertion in the equation

$$A = \frac{e^2 k T}{h} e^{\Delta S_c^{\ddagger 0} / R}$$

Golden¹³ has pointed out how a neglect of this conversion can lead to misconstruction of kinetic results. The appropriate equation is

$$\Delta S_c^{\ddagger 0} = \Delta S_p^{\ddagger 0} - (1 - \gamma) R \ln R' T_m$$

where T_m is the median temperature and $\gamma = 2$ for a bimolecular process.

Results and Discussion

Tables compiled by Trotman-Dickenson and Milne,¹⁴ Ratajczak and Trotman-Dickenson,¹⁵ and Kerr and Ratajczak¹⁶ provide a valuable source of experimental values for the reactions. Furthermore, Arthur and Bell⁹ have reviewed and evaluated data for certain of the reactions studied here and we shall quote data from the latter work exclusively for comparison with the forward reactions and shall have recourse to the former compilations for data for back reactions. Table V lists the activation energies and log A values calculated in the present work, together with the corresponding experimental quantities. A general review of Table V shows that none of the forward reactions have predicted activation energies in error by more than 8 kJ mol⁻¹ (the root mean square error is 5.4 kJ mol⁻¹). We consider this to be a satisfactory result. For the back reactions such a statement is less easy to make, since the experimental data have not been evaluated in so critical a manner. The two back reactions in which the calculated and experimental results are at most variance are those for CH₄ + Cl· and CF₃H + CH₃·. With respect to the log A values, the agreement here is very satisfactory for almost all cases. The root mean square error is 0.15 in log units for the forward reactions, i.e., the calculated A factors differ, on average, by a factor of 1.41. For the back reaction the greatest discrepancies arise for the CF₃H + CH₃· and the CH₄ + Cl· reaction.

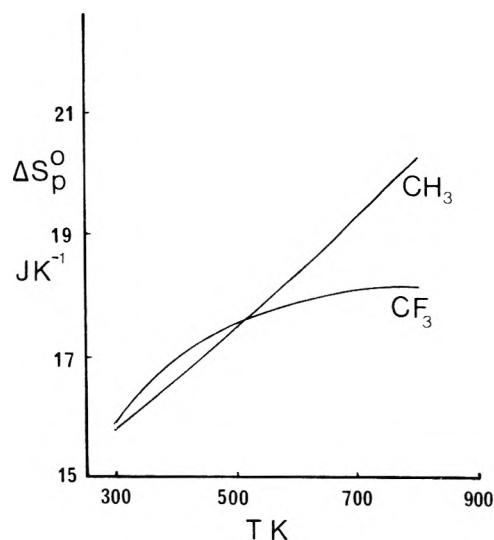


Figure 2. Variation of $\Delta S_p^0(\text{CX}_3(\text{free}) - \text{CX}_3(\text{bound}))$ with temperature.

Since the latter is an important step in the process of chlorination of hydrocarbons and has been studied directly, we consider it in more detail at a later stage.

It is worthy of note that the activation energy for the forward reaction between substrate and the methyl radical is greater than that for the corresponding reaction with CF₃· for all cases but HCl. This parallels experimental observation.^{9,14-16}

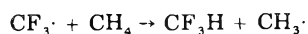
The calculation predicts that only when HCl is the substrate, is the A factor lower for CF₃ than CH₃·: even here the difference is small. The experimental values follow this trend also.

The reason for this is readily seen by reference to Figure 2. Above 500 K the entropy of the CF₃ radical decreases less than that of the CH₃ moiety on going from the free to the bound configuration in the transition state (we assume that the entropy decrease for the substrate is the same for both reactions) whereas below 500 K the reverse is true. This should apply to a wide range of hydrogen abstraction reactions and violation of this finding should indicate that the dimensions of the substrate moiety in the transition state differ greatly from the CH₃· to the CF₃· complex.

i. *The Systems CH₃·, CH₄, and CF₃· with CH₄.* The earlier calculated ΔH^\ddagger values for these reactions have been revised by inclusion of the specific heat correction obtained by the group method. The first reaction has a transition state symmetrical about the central H* atom, resulting in identical activation energies for forward and back reac-

tions. The revised calculated value is in good agreement with experiment. The calculated values for $\log A$ and ΔE^\ddagger for the back reaction $\text{CF}_3\text{H} + \text{CH}_3\cdot$ are both significantly higher than the measured values. It is interesting, however, that at the assumed median temperature of 498 K, the calculated overall k value differs from experiment by a factor of only 3.

Consideration of the experimental ΔE^\ddagger values suggests that the process



is endothermic to the extent of $\sim 4 \text{ kJ mol}^{-1}$. By contrast the calculations predict the process to be exothermic to about the same extent. Unfortunately we cannot resolve the discrepancy easily since the experimental heats of formation of the radicals involved are not known with sufficient accuracy. (This, of course, does not affect the calculated ΔE^\ddagger values, since these are differences.) Evidence may be sought from a comparison of the ΔE^\ddagger values for the reactions of CF_3H with both $\text{CH}_3\cdot$ and $\text{CF}_3\cdot$. Now in nonpolar situations, ΔE^\ddagger for the $\text{CH}_3\cdot$ reaction is greater than that for the $\text{CF}_3\cdot$ reaction⁹ acting on the same substrate. Hence we expect $\Delta E^\ddagger(\text{CH}_3\cdot; \text{CF}_3\text{H})$ to be greater than $\Delta E^\ddagger(\text{CF}_3\cdot; \text{CF}_3\text{H})$. Unfortunately the latter quantity has not been measured but, by comparison with the reaction of $\text{CF}_3\cdot$ with CH_3F or CH_2F_2 , it must be ca. 47 kJ mol^{-1} . This is larger than the quoted experimental value for $\Delta E^\ddagger(\text{CH}_3\cdot; \text{CF}_3\text{H})$ not smaller as would be expected, and hence we believe that our values of both ΔE^\ddagger and $\log A$ for the latter reaction are reasonable ones.

ii. *The Systems $\text{CH}_3\cdot$ with H_2 and $\text{CF}_3\cdot$ with H_2 .* Calculations of a potential energy surface for the $\text{CH}_3\cdot + \text{H}_2$ system have previously been performed and, as well as showing an activation energy for the reaction, these calculations predicted a potential basin at the top of the pass.¹⁷ The low point in this basin was stated to lie at 33.5 kJ below the energy of the reactants $\text{CH}_4 + \text{H}$ (taken as energy zero). This suggests the possible existence of a " CH_5 complex". We did not find any corresponding basin in our reaction coordinate but it must, of course, be remembered that our function is not a potential energy surface but a ΔH surface. Since this is concerned with an ensemble of systems, there is no reason why exactly the same features should be extant upon it.

Direct calculation of A factors has also been previously undertaken for these reactions.¹⁸ The values of ΔS_p^\ddagger obtained were some 70% higher than ours and it is difficult to see how they have been used to obtain A factors in reasonable agreement with experiment.

iii. *The Systems $\text{CH}_3\cdot$ with HCl and CH_4 with $\text{Cl}\cdot$.* The activation energy for the abstraction of H from HCl by $\text{CH}_3\cdot$ is low and it has proved difficult to arrive at con-

sistent experimental results. From their analysis, Arthur and Bell⁹ quote values of 12.9 kJ mol^{-1} and 11.73 for the experimental activation energy and $\log A$ for the first-named reaction. The calculated results for this process differ by 5.2 kJ and 0.27 from these, respectively. For the back reaction here the experimental data are $\Delta E^\ddagger = 16.1 \text{ kJ mol}^{-1}$ and $\log A = 13.42$ (although, more recently, lower values of ΔE^\ddagger have been measured^{21,22}) while we calculate $\Delta E^\ddagger = 26.4 \text{ kJ mol}^{-1}$ and $\log A = 12.77$. The back reaction is the primary process in the free-radical chlorination of methane and experimental data have generally been obtained from competitive chlorination reactions,¹⁹ the absolute quantities being determined by reference to the kinetic parameters for the reaction $\text{H}_2 + \text{Cl} \rightarrow \text{HCl} + \text{H}$.²⁰ The experimental kinetics of such reactions are generally complicated by successive chlorinations and it is perhaps not surprising that we find there the greatest discrepancy between the experimental and calculated quantities.

Acknowledgment. One of us (P.G.P.) wishes to thank Simon Fraser University and, in particular, the Chemistry Department, for generous hospitality.

References and Notes

- (1) T. N. Bell and P. G. Perkins, *Nature (London)*, **256**, 300 (1975).
- (2) D. R. Armstrong, P. G. Perkins, and J. J. P. Stewart, *J. Chem. Soc., Dalton Trans.*, 838 (1973).
- (3) D. R. Armstrong, P. G. Perkins, and J. J. P. Stewart, *J. Chem. Soc., Dalton Trans.*, 2273 (1973).
- (4) A. K. Marwaha and P. G. Perkins, unpublished work.
- (5) D. R. Armstrong, P. G. Perkins, and J. J. P. Stewart, *J. Chem. Soc. A*, 3654 (1971).
- (6) K. A. Levison and P. G. Perkins, *Theor. Chim. Acta*, **14**, 206 (1969).
- (7) "Interatomic Distances in Molecules and Ions", *Chem. Soc., Spec. Publ.*, No. 11 (1958).
- (8) "JANAF Thermochemical Tables", Dow Chemical Co., Midland, Mich., 1965.
- (9) N. L. Arthur and T. N. Bell, *J. Reactive Intermediates* in press.
- (10) J. K. Kochi, "Free Radicals", Vol. 2, Wiley, New York, N.Y., 1973.
- (11) S. W. Benson and H. E. O'Neal, *Natl. Bur. Stand. Circ. No. 21* (1970).
- (12) V. R. Saunders, "The ATMOL Program Series", Atlas Computer Laboratories, Didcot, England.
- (13) D. M. Golden, *J. Chem. Educ.*, **48**, 235 (1971).
- (14) A. F. Trotman-Dickenson and G. S. Milne, *Natl. Bur. Stand. Ref. Data Ser., Natl. Bur. Stand.*, No. 9 (1967).
- (15) E. Ratajczak and A. F. Trotman-Dickenson, "Supplementary Tables of Bimolecular Reactions", UWIST, Cardiff, 1969.
- (16) J. A. Kerr and E. Ratajczak, "2nd Supplementary Tables of Bimolecular Gas Reactions", University of Birmingham, 1972.
- (17) E. Gorin, *Acta Physicochim URSS*, **9**, 691 (1938); E. Gorin, W. Kauzmann, J. Walter, and H. Eyring, *J. Chem. Phys.*, **7**, 633 (1939).
- (18) P. B. Ayscough and J. C. Polanyi, *Trans. Faraday Soc.*, **54**, 960 (1956).
- (19) G. C. Fettis and J. H. Knox, *Prog. React. Kinet.*, **2**, 1 (1964).
- (20) P. G. Ashmore and J. Chanmugan, *Trans. Faraday Soc.*, **49**, 254 (1953); H. Steiner and E. K. Rideal, *Proc. R. Soc. London, Ser. A*, **173**, 503 (1939); W. H. Rodebush and W. K. Klingelhoeffer, *J. Am. Chem. Soc.*, **55**, 130 (1933).
- (21) M. A. A. Clyne and R. F. Walker, *J. Chem. Soc., Faraday Trans. 1*, **69**, 1547 (1973).
- (22) R. Watson, G. Machado, S. Fischer, and D. D. Davis, *J. Chem. Phys.*, **65**, 2126 (1976).

The Generalized Conductance Equation

Mou-Shan Chen* and Lars Onsager

Center for Theoretical Studies, University of Miami, Coral Gables, Florida 33124 (Received March 25, 1977)

For the first time, the conductance equation of strong electrolyte solutions containing any number of ion species of any valence type is computed to the first logarithmic term. The contribution of 1 equiv of j ions to the total conductance of a solution of ionic strength Γ is $\Lambda_j = \Lambda_j^0 - S_j\Gamma^{1/2} + E_j\Gamma \ln \Gamma +$ higher order terms, where Λ_j^0 is the limiting equivalent conductance of j ions, S_j is the Onsager and Fuoss limiting-law slope, and E_j is the coefficient of the first extended term computed in this work. The logarithmic term has contributions from three sources: the relaxation field of a purely electrostatic effect, the relaxation field of hydrodynamic origin, and the electrophoretic effect. These three contributions give a complete logarithmic term in the sense of conformity to Onsager's reciprocal relations of irreversible thermodynamics. The previous computations of the conductance equations for symmetrical electrolyte by Pitts and by Fuoss and Onsager missed the second or the third contribution to the E term and the higher order terms. Therefore their conductance equations are incomplete even to the first logarithmic term.

I. Introduction

The modern theory of strong electrolyte conductance was first developed by Debye and Hückel.¹ Onsager² perfected the kinetic theory to obtain the limiting conductance equation for simple symmetrical electrolytes in 1927, and Onsager and Fuoss³ computed the limiting coefficient of mixed electrolytes in 1932. The generalized equation is

$$\Lambda_j = \Lambda_j^0 - S_j\Gamma^{1/2} + \text{higher order terms}$$

Here Λ is the conductance, S the limiting coefficient, Γ the ionic strength, j is the ionic species, and 0 indicates the limiting value. $S_j = \alpha_j\Lambda_j^0 + \beta_j$, where α and β are two constants depending on dielectric constant D , temperature T , viscosity η of the solvent, valence type of the ions Z_i , ionic mobilities ω_i , and some universal constants. Onsager and Fuoss³ also pointed out that the higher order terms are of the form

$$E_j\Gamma \ln \Gamma + B_j\Gamma + \dots$$

Various schools⁴⁻⁹ made efforts to compute the coefficient E and higher order terms for simple binary electrolytes. However no attempt has yet been made to calculate these coefficients for the case of mixed electrolytes. The purpose of this work is to compute E_j for the general case that the electrolyte solutions contain any number of species of ions of any valence type. The result is a generalized conductance equation to the order of the first logarithmic term, and shows, incidentally, that all those previously computed extended equations for simple binary electrolytes are not even complete to this order. Thus, we have a better and generalized conductance equation. Its application may help to facilitate the analysis of conductance data and its method of computation may enlighten the way for derivation of the other higher order terms.

II. Equation of Continuity

According to the physical model of Debye and Hückel, an ion in solution is surrounded by its ionic atmosphere of opposite charge. When no external field is applied, the ionic atmosphere is spherically symmetric. An external field will perturb this symmetry. The asymmetrical at-

mosphere then exerts an electrostatic force opposite to the external field on the center ion. This is the relaxation effect, which retards the motion of the central ion. Moreover, the ionic atmosphere moves under the external field in a direction opposite to the center ion, carrying with it the nearby fluid particles. Therefore, the center ion is in effect moving in a countercurrent. This is called the electrophoretic effect. When the relaxation field and the electrophoretic effect are computed, the average ionic velocity, and hence, the conductance equation can be obtained easily.

For our computation, we start with the equation of continuity. Define n_{ji} as the time average concentration of i ions in the ionic atmosphere of a j ion located at \vec{r}_1 . Let \vec{r}_2 be the position vector of the volume element whose i ion concentration interests us, and write \vec{r} for $\vec{r}_2 - \vec{r}_1$, we may then write

$$n_{ji} = n_{ij}(\vec{r}_1, \vec{r})$$

Similarly

$$n_{ij} = n_{ij}(\vec{r}_2, -\vec{r})$$

If n_j is the average concentration of j ions in the solution, and if we define $f_{ji}(\vec{r}_1, \vec{r}) = n_j n_{ji}(\vec{r}_1, \vec{r})$, it is obvious that f_{ji} measures the probability of finding an i ion in the volume element at \vec{r}_2 when at the same time a j ion is in a volume element at \vec{r}_1 . Simple consideration establishes the relation that $f_{ij}(\vec{r}_2, -\vec{r}) = f_{ji}(\vec{r}_1, \vec{r})$.

Next, we designate \vec{v}_{ji} to be the time average velocity of an i ion in the ionic atmosphere of a j ion. In the six dimensional space (\vec{r}_1, \vec{r}_2) , the continuity equation reads³

$$-\frac{\partial f_{ji}}{\partial t} = \frac{\partial f_{ij}}{\partial t} = \nabla_1 \cdot (f_{ij} \vec{V}_{ij}) + \nabla_2 \cdot (f_{ji} \vec{V}_{ji})$$

In a steady state

$$\partial f_{ji} / \partial t = 0$$

and

$$\nabla_1 \cdot (f_{ij} \vec{V}_{ij}) + \nabla_2 \cdot (f_{ji} \vec{V}_{ji}) = 0$$

If no external fields are applied, the distribution function is spherically symmetric, hence a function only depends on r , the distance from the reference ion. According to Debye and Hückel¹

* This paper is based on the dissertation submitted by Mou-shan Chen to the Faculty of the Graduate School at Yale University in partial fulfillment of the requirements for the Degree of Doctor of Philosophy.

$$f_{ji}(r_i, r)|_{x=0} = f_{ji}^0(r) = n_i n_j \exp(-e_i \psi_j^0 / kT)$$

where ψ_j^0 , the potential in the neighborhood of a j ion, equals $e_j e^{-\kappa r} / Dr$, and κ , the inverse Debye length, is defined by the equation

$$\kappa^2 = \frac{4\pi}{DkT} \sum_{i=1}^s n_i e_i^2$$

for a solution containing s species of ions of charges e_i , $i = 1, 2, \dots, s$, respectively. When an external field is applied in the direction x and is very weak so that the Wien effect is unobservable, the perturbations to the potential, ψ' , and the distribution function, $f_{ji}^0 \chi_{ji}$, will both be proportional to the field strength X . In the steady state, ψ_j and f_{ji} will be functions of \vec{r} only. Therefore we write

$$\psi_j(\vec{r}) = \psi_j^0(r) + \psi_j'(\vec{r})$$

and

$$f_{ji}(\vec{r}) = f_{ji}^0(r)[1 + \chi_{ji}(\vec{r})]$$

Poisson's equation relates the potential and the ionic distribution such that

$$\nabla^2 \psi_j(\vec{r}) = -4\pi \sum_i e_i f_{ji}(\vec{r}) / Dn_j$$

$$\nabla^2 \psi_j^0(r) = -4\pi \sum_i e_i f_{ji}^0(r) / Dn_j$$

and hence

$$\nabla^2 \psi_j'(\vec{r}) = -4\pi \sum_i e_i f_{ji}^0(r) \chi_{ji}(\vec{r}) / Dn_j$$

Now we express the equation of motion as follows:

$$\vec{\nabla}_{ji} = \vec{\nabla}_{ji}(\vec{r}) = \vec{\nabla}_i^j(\vec{r}) + \omega_i [k_i - e_i \nabla_2 \psi_i(-\vec{r})]_{r=0} - e_i \nabla_2 \psi_j(\vec{r}) - kT \nabla_2 \ln f_{ji}(\vec{r})$$

Here $\vec{\nabla}_i^j(\vec{r})$ is the average fluid velocity at the site of the i ion in the neighborhood of the j ion. Terms in the bracket are contributions of the external field ($k_i = e_i X$ for the conductance problem), the field due to the ionic atmosphere of the i ion, the potential field of the j ion, and the Brownian concentration gradient field.

Putting all these equations together and dropping terms of order k_i^2 and higher, we obtain the continuity equation

$$\nabla \cdot e^\xi \nabla \mu_{ji} = \nabla \cdot e^\xi (\vec{\nabla}_j^i - \vec{\nabla}_i^j) \tag{1}$$

where

$$\xi = \beta_{ij} \frac{e^{-\kappa r}}{r} = - \frac{e_i e_j e^{-\kappa r}}{DkT r}$$

$$\mu_{ji} = (\omega_i k_i - \omega_j k_j)x - (e_i \omega_i \psi_j' - e_j \omega_j \psi_i') - (\omega_i + \omega_j)kT \chi_{ji} \tag{2}$$

$$\nabla = \nabla_2 = -\nabla_1$$

and $\psi_i'(a)$, $\psi_j'(a)$ terms have been dropped for they have no contribution to the conductance equation to the desired order.

To supplement eq 1, we use the following boundary conditions:⁸

(1) The perturbation to the potential vanishes at long distance, i.e.

$$\psi_j'(\vec{r})|_{r \rightarrow \infty} = 0 \tag{3}$$

(2) The potential continues at $r = a$, if we assume the ions have the uniform size a . This leads to

$$\left(r \frac{\partial \psi_i'}{\partial r} - \psi_i' \right)_{r=a} = 0 \tag{4}$$

(3) The total potential field at infinite distance is only that of the external field

$$\nabla \mu_{ji}|_{r \rightarrow \infty} = (\omega_i k_i - \omega_j k_j) i \tag{5}$$

(4) The radial component of the relative velocity of any two ions in contact must vanish.

$$(\vec{\nabla}_{ij} - \vec{\nabla}_{ji}) \cdot \vec{r}|_{r=a} = 0 \tag{6}$$

III. Relaxation Field

To solve the continuity equation for computation of the relaxation field and the electrophoretic effect, we define ψ_j^H , ψ_i^H , and $f_{ji}^0 \chi_{ji}^H$ to be the perturbations of the potentials and the distribution function due to the presence of solvent motion, and define

$$\mu_{ji}^H = (e_i \omega_i \psi_j^H - e_j \omega_j \psi_i^H) - (\omega_i + \omega_j)kT \chi_{ji}^H$$

Then, we can separate the continuity equation into a homogeneous equation and an inhomogeneous equation as follows:

$$\nabla \cdot e^\xi \nabla \mu_{ji}^H = \nabla \cdot e^\xi (\vec{\nabla}_j^i - \vec{\nabla}_i^j) \tag{7}$$

and

$$\nabla \cdot e^\xi \nabla \mu_{ji}' = 0 \tag{8}$$

where

$$\mu_{ji}' = \mu_{ji} - \mu_{ji}^H = (\omega_i k_i - \omega_j k_j)x - [e_i \omega_i (\psi_j' - \psi_j^H) - e_j \omega_j (\psi_i' - \psi_i^H)] - (\omega_i + \omega_j)kT(\chi_{ji} - \chi_{ji}^H)$$

Observe that μ_{ji}^H is the perturbation caused by the motion of the solvent which itself in turn is a perturbation due to the presence of the external field. Hence the μ_{ji}^H is of much higher order than μ_{ji}' . Indeed, it can be shown that while μ_{ji}' contributes to the zeroth order terms of conductance Λ_0 , the first-order correction, i.e., the square root term, and all higher order terms, μ_{ji}^H have contributions only to the relaxation field of order $\Gamma \ln \Gamma$ and up, and to the electrophoretic effect of order Γ and up. For our need of computing conductance to the first logarithmic term, it is not necessary to solve eq 7 explicitly for μ_{ji}^H . To execute the computation we define the relative ionic strength μ_i , the mean mobility $\bar{\omega}$, the limiting transference number t_i , the H matrix element h_{ij} , the coefficient L_{ij} , functions ϕ_{ji} and γ^H by the following equation:

$$\mu_i = n_i e_i^2 / \sum_{i=1}^s n_i e_i^2$$

$$\bar{\omega} = \sum_{i=1}^s \mu_i \omega_i$$

$$t_i = n_i e_i^2 \omega_i / \sum_{i=1}^s n_i e_i^2 \omega_i$$

$$h_{ij} = \frac{t_i \bar{\omega}}{\omega_i + \omega_j} + \delta_{ij} d(\omega_j) \tag{9}$$

$$d(\omega_j) = \sum_{i=1}^s \frac{\omega t_i}{\omega_i + \omega_j}$$

$$L_{ij} = 4\pi t_j \chi_j^p n_i e_i / [DkT(\omega_i + \omega_j) e_j]$$

$$\phi_{ji} = \mu_{ji}^H / \cos \theta, \gamma_p^H = \sum_{i=1}^s t_j \chi_j^p \psi_j^H / e_j \cos \theta$$

where χ_j^P is the j component of the eigenvector of the matrix H corresponding to the eigenvalue q_p , $p = 1, 2, \dots, s$.

Poisson's equation relates χ_{ji}^H and ψ_j^H

$$\nabla^2 \psi_j^H = -\frac{4\pi}{D} \sum_i n_i e_i e^{\xi} \chi_{ji}^H \quad (10)$$

The distribution function χ_{ji}^H can be eliminated from eq 10 by the use of the definition of μ_{ji}^H . The result is

$$\left[\frac{d^2}{dr^2} + \frac{2}{r} \frac{d}{dr} - \left(\frac{2}{r^2} + \kappa^2 g_p \right) \right] y_p^H = \sum_{ij} L_{ij} e^{\xi} \phi_{ji} \quad (11)$$

For dilute solution, $\kappa^2 q_p$ is small compared to $2/r^2$ for small r , and the $\kappa^2 q_p$ term in eq 5 can be dropped without affecting the conductance equation we desire. With this simplification it can be shown that integration of eq 11 gives

$$y_p^H(a) = -\frac{a}{3} \sum_{ij} L_{ij} \int_a^\infty e^{\xi} \phi_{ji} dr \quad (12)$$

when boundary conditions (1) and (2) are used.

The integral in eq 12 is computable from eq 7, which can be expanded as

$$\frac{d^2}{dr^2} \phi_{ji} + \left(\frac{2}{r} - \frac{d\xi}{dr} \right) \frac{d\phi_{ji}}{dr} - \frac{2}{r^2} \phi_{ji} = (V_{j,r}^i - V_{i,r}^j) \frac{d\xi}{dr} \quad (13)$$

where $V_{j,r}^i$ is the radial component of the velocity field \bar{V}_j^i . Multiplying eq 13 by $(r^2/2)e^{\xi}$ on both sides and integrating from a to ∞ gives

$$\frac{1}{2} e^{\xi} r^2 \frac{d\phi_{ji}}{dr} \Big|_a^\infty - \int_a^\infty e^{\xi} \phi_{ji} dr = \frac{1}{2} \int_a^\infty (V_{j,r}^i - V_{i,r}^j) \frac{d\xi}{dr} r^2 e^{\xi} dr$$

The first term on the left is of the order contributing only to the Γ term of the conductance equation and can be dropped, therefore, we have

$$\int_a^\infty e^{\xi} \phi_{ji} dr = -\frac{1}{2} \int_a^\infty (V_{j,r}^i - V_{i,r}^j) \frac{d\xi}{dr} r^2 e^{\xi} dr \quad (14)$$

Using the radial component of the velocity field given by Fuoss and Accascina⁸

$$V_{j,r}^i = \frac{k_i \cos \theta}{2\pi\eta\kappa^2 r^3 (1 + \kappa a)} \left[\left(1 + \kappa a + \frac{\kappa^2 a^2}{2} \right) - (1 + \kappa r) e^{-\kappa r + \kappa a} \right] \quad (15)$$

we obtain from eq 14

$$\int_a^\infty e^{\xi} \phi_{ji} dr = \frac{\beta_{ji} (k_i - k_j)}{4\pi\eta} e^{-\kappa\beta_{ji}} [E_n(2\kappa a) - \frac{1}{2} E_n(\kappa a)] + \text{higher order terms}$$

where $E_n(x)$ is the exponential function defined as

$$E_n(x) = \int_x^\infty \frac{e^{-u}}{u} du$$

Finally, we obtain the relaxation field due to the motion of solvent by observing that

$$\Delta X_j^H = -\frac{\partial \psi_j}{\partial x} \Big|_{r=a} = -\frac{e_j}{a} \sum_p \chi_j^p y_p^H(a)$$

The last equality follows from the boundary condition of the potential functions and the definition of y_p^H . For the low concentrations we are interested

$E_n(x) = -\ln x + \text{higher order terms}$

we can write the relaxation field as

$$\Delta X_j^H = \frac{e_j}{3} \sum_p \chi_j^p \sum_{ij} L_{ij} \frac{\beta_{ji} (k_j - k_i)}{8\pi\eta} \ln \kappa a + O(\kappa^2 a^2)$$

Or

$$\Delta X_j^H = \frac{e_j \kappa^2 \ln \kappa a}{24\pi\eta D k T} \sum_i \frac{\mu_i (k_i - k_j)}{\omega_i + \omega_j} + O(\kappa^2 a^2) \quad (16)$$

when summations over p and j are carried out.

The main contribution to the relaxation field and the electrophoretic effect comes from the potential μ_{ji}' . The second-order differential equation, eq 8, has been analyzed by Fuoss and Onsager,⁷ the approximate solution is

$$\mu_{ji}' = (\omega_i k_i - \omega_j k_j) R \cos \theta \quad (17)$$

with

$$R = \frac{e^{-b} \left(1 + b + \frac{b^2}{2} \right)}{e^{-b} \left(1 + b + \frac{b^2}{2} \right) - 1} \left\{ r - \frac{\beta_{ji}}{\kappa^2 r^2} [1 - e^{-\kappa r} (1 + \kappa r)] \right\} - \frac{e^{-\xi}}{e^{-b} \left(1 + b + \frac{b^2}{2} \right) - 1} \left\{ r - \frac{\beta_{ji}}{\kappa^2 r^2} [1 - e^{-\kappa r} (1 + \kappa r + \kappa r^2)] \right\}$$

where $b = \beta_{ji}/a$.

Poisson's equation can be used to eliminate the distribution functions from eq 17, and simplification by using the various definitions of eq 9 leads to

$$\left[\frac{d^2}{dr^2} + \frac{2}{r} \frac{d}{dr} - \left(\frac{2}{r^2} + \kappa^2 q_p \right) \right] y_p' = \sum_i t_j \chi_j^p \sum_i M_{ij} e^{\xi} (R - r) \quad (18)$$

where

$$M_{ij} = \frac{4\pi n_i e_i (\omega_i k_i - \omega_j k_j)}{D k T (\omega_i + \omega_j) e_j}$$

and

$$y_p' = \sum_\sigma t_\sigma \chi_\sigma^p (\psi_\sigma' - \psi_\sigma^H) / e_\sigma \cos \theta$$

Equation 18 has the same form as eq 13, but since μ_{ji}' is of more important order than μ_{ji}^H , the $\kappa^2 q$ term on the left-hand side cannot be dropped. Nevertheless, $y_p'(a)$ is computable by the application of Green's function method developed by Fuoss and Onsager.⁷ The contribution to the relaxation field is finally obtainable from $y_p'(a)$. The result is

$$\Delta X_j' = -\frac{e_j \kappa}{3 D k T} \sum_\sigma \chi_j^p (t_\sigma \chi_\sigma^p k_\sigma) (1 - q_p^{1/2}) + \frac{e_j^2 \kappa^2 \ln \kappa a}{6 (D k T)^2} \sum_\sigma \frac{\mu_\sigma e_\sigma (\omega_\sigma k_\sigma - k_j \omega_j)}{\omega_\sigma + \omega_j} + O(\kappa^2 a^2) \quad (19)$$

IV. Electrophoretic Velocity

The other ingredient for composing the conductance equation is the electrophoretic velocity, i.e., the retardation

of the ion velocity due to the motion of the surrounding solvent. This is calculable if we know μ_{ji}^i , the total potential of an i ion in the neighborhood of a reference j ion in solution. Assuming the validity of the superposition principle

$$\mu_{ji}^i = -k_i x + e_i \psi_i'(a) + e_i \psi_j(\vec{r}) + kT \ln \left[\frac{f_{ji}(\vec{r})}{n_i n_j} \right] \quad (20)$$

where the first term is the potential due to the external field, the second term is due to the potential of the i ion's own atmosphere, which contributes only to higher order term of conductance, and can be dropped in this computation. The i ion is located at the ionic atmosphere of a reference j ion, which contributes the third term in eq 20. The last term comes from the concentration gradient created by the presence of the reference ion j . From definitions

$$\psi_j = \psi_j^0 + \psi_j^H + (\psi_j' - \psi_j^H)$$

and

$$f_{ji} = f_{ji}^0 [1 + \chi_{ji}^H + (\chi_{ji} - \chi_{ji}^H)]$$

ψ_j^H and χ_{ji}^H are of higher order perturbation terms, and negligible in our computation. Further more, ψ_j^0 and f_{ji}^0 cancel each other from eq 20, and $\ln(1 + \chi_{ji})$ can be approximated by χ_{ji} due to the smallness of the perturbation. The simplified total potential is then

$$\mu_{ji}^i = -k_i x + e_i \psi_j' + kT \chi_{ji} \quad (21)$$

The first approximation of ψ_j' has been computed by Onsager and Kim.¹⁰ The inclusion of this ψ_j' in the total potential modifies only the Γ term in the electrophoretic effect. Therefore, we may drop at this stage the higher order terms from eq 21 and eq 17, and the combination give the total potential for our computation as

$$\mu_{ji}^i = \left[-k_i r + \frac{\omega_i k_i - \omega_j k_j}{\omega_i + \omega_j} (r - R) \right] \cos \theta = -\mu_{ji} \cos \theta \quad (22)$$

If a j ion is at the center of the coordinate system, the total force that acts at an annular volume element $dV = 2\pi r^2 \sin \theta d\theta dr$ located at r, θ is⁷

$$dF_j = -\sum_i n_{ji} \nabla \mu_{ji}^i dV \quad (23)$$

This force will produce a differential velocity $d\vec{V}_j$ at the site of the j ion. By Oseen's equation

$$d\vec{V}_j = [d\vec{F}_j + (\vec{d}\vec{F} \cdot \vec{r}) \vec{r} / r^2] / 8\pi\eta r \quad (24)$$

Only the component of this velocity in the direction of the external field does not average out to zero:

$$dV_{jx} = d\vec{V}_j \cdot \vec{i} \quad (25)$$

Hence, the total electrophoretic velocity produced by all ions around the j ion is from eq 22, 23, 24, and 25:

$$\Delta V_j = \int_a^\infty dV_{jx} = \sum \int_0^\pi \int_a^\infty \frac{f_{ji}}{n_j} \left[\frac{u_{ji}}{r} (1 - \cos^2 \theta) + 2 \cos^2 \theta \frac{du_{ji}}{dr} \right] \frac{2\pi r^2 \sin \theta d\theta dr}{8\pi\eta r} \quad (26)$$

For the weak field problem f_{ji} can be approximated by f_{ji}^0 and the integration gives

$$\Delta V_j = \sum_\sigma \frac{e_j k_\sigma \mu_\sigma \kappa}{6\pi\eta e_\sigma} - \sum_\sigma \frac{\mu_\sigma k_\sigma e_j^2}{12\pi\eta DkT} \kappa^2 \ln \kappa a + \sum_\sigma \frac{\mu_\sigma e_j^2 (\omega_\sigma k_\sigma - \omega_{jj})}{24\pi\eta DkT (\omega_\sigma + \omega_j)} \kappa^2 \ln \kappa a + O(\kappa^2 a^2) \quad (27)$$

where three exponential functions have been expanded, and high order terms dropped.

V. Conductance Equation

At infinite dilution, multiplication of the external force by the mobility gives the ionic velocity, i.e.

$$V_j = k_j \omega_j$$

At finite concentrations, the velocity is modified by the relaxation effect and the electrophoretic effect such that

$$V_j = \omega_j [k_j + e_j (\Delta X_j^H + \Delta X_j')] + \Delta V_j$$

Substituting values of ΔX_j^H , $\Delta X_j'$, and ΔV_j into this equation, we obtain

$$V_j = k_j \omega_j - \sum_\sigma \frac{e_j k_\sigma \mu_\sigma \kappa}{6\pi\eta e_\sigma} - \frac{e_j^2 \omega_j}{3DkT} \sum_p \sum_\sigma \chi_j^p t_\sigma \chi_\sigma^p k_\sigma (1 - q_p) \kappa - \sum_\sigma \frac{\mu_\sigma k_\sigma e_j^2 \kappa^2 \ln \kappa a}{12\pi\eta DkT} + \sum_\sigma \frac{\mu_\sigma e_j^2 (\omega_\sigma k_\sigma - \omega_j k_j) \kappa^2 \ln \kappa a}{24\pi\eta DkT (\omega_\sigma + \omega_j)} + \frac{e_j^3 \omega_j \kappa^2 \ln \kappa a}{6(DkT)^2} \sum_\sigma \frac{\mu_\sigma e_\sigma (k_\sigma \omega_\sigma - k_j \omega_j)}{\omega_\sigma + \omega_j} + \sum_\sigma \frac{e_j^2 \omega_j \mu_\sigma (k_\sigma - k_j) \kappa^2 \ln \kappa a}{24\pi\eta (\omega_\sigma + \omega_j) DkT} + O(\kappa^2 a^2) \quad (28)$$

It is rather easy to compute conductance with the ionic velocity given. By definition, in practical units, $\text{ohm}^{-1} \text{cm}^2 \text{equiv}^{-1}$, the equivalent conductance of j ions is

$$\Lambda_j = \frac{F}{10^{-8} c} \left| \frac{V_j}{X} \right| \quad (29)$$

where F is Faraday's constant, c the velocity of light, and $X = k_j/e_j$ is the external electrical field. Substituting the value of V_j into eq 29, we obtain

$$\Lambda_j = \Lambda_j^0 - \kappa \left\{ \frac{965 |e_j|}{18\pi\eta} + \frac{\Lambda_j^0 e_j}{3DkT} \sum_\sigma t_\sigma \chi_\sigma^p e_\sigma \chi_i^p (1 - q_p^{1/2}) \right\} + \sum_\sigma \left\{ \frac{-965 \mu_\sigma e_\sigma e_j^2}{36\pi\eta DkT} + \frac{965 \mu_\sigma e_j |e_j| (e_\sigma \omega_\sigma + e_j \omega_j)}{72\pi\eta DkT (\omega_\sigma + \omega_j)} + \frac{\Lambda_j^0}{6DkT} \times \left[\frac{\mu_\sigma e_\sigma e_j^2 (e_\sigma \omega_\sigma - e_j \omega_j)}{DkT (\omega_\sigma + \omega_j)} + \frac{e_j \mu_\sigma (e_\sigma - e_j)}{4\pi\eta (\omega_\sigma + \omega_j)} \right] \right\} \kappa^2 \ln \kappa a \quad (30)$$

where Λ_j^0 is the limiting conductance, related to ionic mobility by the equation

$$\Lambda_j^0 = \frac{F}{10^{-8} c} |e_j| \omega_j$$

Converting κ and Γ , the ionic strength, and putting universal constants (electronic charge and Boltzmann constant) into eq 17, we can write the conductance equation in Fuoss and Onsager's³ form:

$$\Lambda_j = \Lambda_j^0 - S_j \Gamma^{1/2} + E_j \Gamma \ln \Gamma + O(\Gamma) \quad (31)$$

Here S_j is the limiting coefficient of Onsager and Fuoss:³

$$S_j = \alpha_j \Lambda_j^0 + \beta_j$$

$$\alpha_j = \frac{2.801 \times 10^6}{(DT)^{3/2}} Z_j \sum_p \sum_\sigma (1 - q_p^{1/2}) \chi_j^p (Z_\sigma t_\sigma \chi_\sigma^p)$$

$$\beta_j = \frac{41.24 |z_j|}{\eta (DT)^{1/2}}$$

$\Gamma = 1/2 \sum_i m_i Z_i^2$, where m_i is the concentration of i ions in moles per liter. E_j is the logarithmic coefficient:

$$E_j = \sum_i (E_{ji}^1 \Lambda_j^0 + E_{ji}^2 + E_{ji}^3)$$

$$E_{ji}^1 = 0.5885 \times 10^{13} \mu_i Z_i Z_j^2 (Z_i |Z_j| \Lambda_i^0 - Z_j |Z_i| \Lambda_j^0) / [(|Z_i| \Lambda_j^0 + |Z_j| \Lambda_i^0) (DT)^3]$$

$$E_{ji}^2 = -0.4332 \times 10^8 \mu_i Z_i Z_j |Z_j| / \eta (DT)^2$$

$$E_{ji}^3 = -0.8665 \times 10^8 \mu_i |Z_i Z_j^3| \Lambda_j^0 / \eta (DT)^2 (|Z_j| \Lambda_i^0 + |Z_i| \Lambda_j^0)$$

VI. Discussion

The generalized conductance equation to the first logarithmic term is given in the last section. The square root term is rather complicated. It involves the eigenvalues and the eigenvectors of a matrix \mathbf{H} . Its method of computation has been discussed in detail by Onsager and Kim.¹⁰ On the other hand, the coefficients of the logarithmic term are much simpler. They are fairly simple rational functions of the individual limiting conductance and charges, and of the relative concentrations. Thus it involves negligible computational effort to exploit the new refinement of the theory in the extrapolation of mobilities to zero concentration. Unfortunately, not many measurements of mixed electrolytes are suitable for analysis of this kind.

Prior to 1969, when we first obtained our result^{11,12} the conductance equations of simple electrolyte of Pitts⁴ and of Fuoss and Onsager and others⁵⁻⁹ were well accepted. Their equations in the expanded form all agreed in the E term, but differ in higher order terms due to different assumptions. The controversy then was which conductance equations had the better higher order terms. Hence, we expected our E coefficient for the simplest case would yield that well accepted value. By eq 31, for 1-1 electrolyte solution, $\Lambda = \Lambda_1 + \Lambda_2$ gives

$$\Lambda = \Lambda_0 - \left[\frac{82.48}{\eta (DT)^{1/2}} + \frac{0.8205 \times 10^6}{(DT)^{3/2}} \Lambda_0 \right] C^{1/2} + \left[\frac{2.943 \times 10^{12}}{(DT)^3} \Lambda_0 - \frac{0.8665 \times 10^8}{\eta (DT)^2} \right] C \ln C + O(C) \quad (32)$$

where C is the concentration of the electrolyte. When this

equation was compared with those of Pitts and Fuoss and Onsager, we were surprised to find that we had a different E coefficient! The second E term in eq 32 is two times the previously reported value.

Our computation of the first logarithmic term shows that it comes from three contributions. The first arises from a more accurate computation of the relaxation field due to the charge asymmetry caused by ion migration. The second is from a further modification of the charge asymmetry by hydrodynamic flow. The third comes from a more accurate computation of the electrophoresis to include the additional hydrodynamic flow due to charge asymmetry. Thus, the last two contributions are reciprocal in the sense of irreversible thermodynamics. Indeed, it is shown¹³ that they complement each other to make the conductance equation conform to Onsager's reciprocal relation.

Previous computations by various schools⁴⁻⁹ missed the second or the third contribution to the logarithmic and the higher order terms. It was recently pointed out by Carman¹⁴ that Pitt's interpretation of the velocity term was questionable, which led to the omission of a $C \ln C$ term, corresponding to our second contribution. Careful analysis of Fuoss and his colleague's works⁵⁻⁸ shows that they did not treat the electrophoretic effect adequately. In their 1959 work,⁸ the contribution of ionic asymmetry and the concentration gradient to the electrophoresis was not considered, while the improved theory of 1962 to 1965⁷ erred in computation of the total potential. Recently, after we had pointed out^{11,12} the errors in previous computations, Murphy and Cohen¹⁵ corrected their earlier results, and obtained a most complete conductance equation for binary system, with a corrected logarithmic term consistent with ours.

Acknowledgment. This research was supported by NIH Grants GM 13190 and GM 20284 to late Professor Lars Onsager, who died when this manuscript was being prepared. The research was also supported by NSF Grant No. CHE75-17533.

References and Notes

- (1) P. Debye and E. Huckel, *Phys. Z.*, **24**, 185, 305 (1923).
- (2) L. Onsager, *Phys. Z.*, **28**, 277 (1927).
- (3) L. Onsager and R. M. Fuoss, *J. Phys. Chem.*, **36**, 2689 (1932).
- (4) E. Pitts, *Proc. R. Soc. London, Ser. A*, **217**, 43 (1953).
- (5) R. M. Fuoss and L. Onsager, *J. Phys. Chem.*, **61**, 668 (1957).
- (6) W. Ebeling, W. D. Kraeft, and D. Kremp, *J. Phys. Chem.*, **70**, 3338 (1966).
- (7) R. M. Fuoss and L. Onsager, *J. Phys. Chem.*, **66**, 1722 (1962); *ibid.*, **67**, 621, 628 (1963); *ibid.*, **68**, 1 (1964); R. M. Fuoss, L. Onsager, and J. F. Skinner, *ibid.*, **69**, 2581 (1965).
- (8) R. M. Fuoss and F. Accascine, "Electrolytic Conductance", Interscience, New York, N.Y., 1959.
- (9) T. J. Murphy, Ph.D. Thesis, Rockefeller University, 1968.
- (10) L. Onsager and S. K. Kim, *J. Phys. Chem.*, **61**, 215 (1957).
- (11) L. Onsager and M. S. Chen, *Proc. Natl. Acad. Sci.*, **63**, 229 (1969).
- (12) M. S. Chen, Ph.D. Thesis, Yale University, 1969.
- (13) M. S. Chen, paper being prepared for publication.
- (14) P. C. Carman, *J. Phys. Chem.*, **74**, 1653 (1970).
- (15) T. J. Murphy and E. G. D. Cohen, *J. Chem. Phys.*, **53**, 2173 (1970).

Compatibility of Conductance Equations with Onsager's Reciprocal Relation

Mou-Shan Chen

Center for Theoretical Studies, University of Miami, Coral Gables, Florida 33124 (Received November 15, 1976; Revised Manuscript Received December 22, 1976)

Onsager's reciprocal relation can be applied to determine the correctness of the computation of a conductance equation. It is found that the $C \ln C$ term of the conductance equation recently evaluated by Chen is, contrary to the result of Fuoss and Onsager, consistent with this law of irreversible thermodynamics.

I. Introduction

It has long been known that the expanded equation of conductance at a low concentration C has the form¹

$$\Lambda = \Lambda_0 - SC^{1/2} + EC \ln C + \text{higher order terms}$$

where Λ_0 is the limiting equivalent conductance, S and E are coefficients depending on the properties of the solvent (dielectric constant D , temperature T , and viscosity η) and the ions (electric charges e_i and mobilities ω_i). The limiting law slope S was first computed by Onsager² for simple electrolytes and by Fuoss and Onsager for mixed electrolytes almost half a century ago. Since then, many efforts have been devoted to the computation of the coefficient E and the higher order terms. The best known results are those of Pitts,³ Fuoss and Onsager,⁴ Fuoss and Accascina,⁵ and Fuoss, Onsager, and Skinner.⁶ These various computations all agree in E , but differ in higher order terms due to different assumptions used. The controversy⁷ then was which equation represented best the higher order terms. Because of the complexity of the theories, this controversy was not resolved. Both the equations of Pitts and Fuoss et al. were well accepted for analysis of conductance data. It had never been suspected that all these equations were incomplete even to the first logarithmic term. Recently, Chen^{8,9} and Onsager and Chen¹⁰ succeeded in the computation of E for a strong electrolyte solution containing any number of species of ions of any valence type. Thus, for the first time, the extended conductance equation was generalized to mixed electrolytes. More significantly, Chen's value of E , for the simplest case, is different from the well-accepted value of Pitts and Fuoss et al. This paper shows the compatibility of Chen's computation with Onsager's reciprocal relation.

II. Theory

For simplicity and clarity in notation and presentation and for easy comparison with Fuoss et al.'s result, which is pertinent only to simple electrolytes, we will discuss the case in which the solution contains only two ion species of concentrations n_1 and n_2 (ions/cm³) and charges $e_1 = z_1e$, $e_2 = -z_2e$, where z_1 and z_2 are the valences, and e the proton charge. Its generalization to mixed electrolytes involves only straightforward efforts.

When a very weak electric field is applied to an electrolyte solution, Ohm's law is obeyed. The current density is proportional to the field strength X . Thus

$$I = n_1 e_1 V_1 + n_2 e_2 V_2 \propto X$$

where V_i is the average velocity of an ion of type i . In the

limit of infinite dilution, there is no ion-ion interaction, and the velocity is given by

$$V_i = \omega_i \kappa_i$$

where $\kappa_i = X e_i$ is the external force applied to an i ion. In terms of the flow density

$$J_i = n_i V_i = n_i \omega_i \kappa_i = \Omega_{ii}^0 \kappa_i$$

At finite concentrations, there is ion-ion interaction which not only modifies Ω_{ii}^0 , but also causes a correction flow density proportional to κ_j , the external force on an ion of the other species. Hence

$$J_i = \Omega_{ii} \kappa_i + \Omega_{ij} \kappa_j \quad i \neq j \quad (1)$$

where Ω_{ij} , the cross term coefficient, measures the interaction of the two ion species. Onsager's reciprocal relation^{1,11} requires that

$$\Omega_{ij} = \Omega_{ji} \quad (2)$$

This means that the modification of the flow of the first ion species caused by a unit force per unit amount of the second species equals the modification to the flow of the second species caused by a unit force per unit amount of the first species. The result of a computation on conductance should conform to this law of irreversible thermodynamics.

According to Chen,^{8,9} the conductance equation for a binary electrolyte is

$$\Lambda = \Lambda_0 - \left[\frac{(z_1 + z_2)e}{6\pi\eta} \left(\frac{F}{300} \right) + \frac{z_1 z_2 e^2 q \Lambda_0}{3DkT(1 + q^{1/2})} \right] \kappa + \left\{ \frac{z_1^2 z_2^2 e^4 q \Lambda_0}{6(DkT)^2} - \left(\frac{F}{300} \right) \frac{z_1 z_2 (z_1 + z_2) e^3}{12\pi\eta DkT} \left[q + \frac{(z_1 - z_2)^2}{z_1 z_2} \right] \right\} \times \kappa^2 \ln \kappa a + O(\kappa^2 a^2) \quad (3)$$

where F is Faraday's constant, κ is the inverse Debye length, a is the ion size parameter, and

$$q = \frac{z_1 \omega_1 + z_2 \omega_2}{(z_1 + z_2)(\omega_1 + \omega_2)}$$

Equation 3 is derived from the average ion velocity computed to be

$$V_i = \omega_i \kappa_i + \left\{ \frac{-z_i^2 z_j \omega_i e^2 (\kappa_i \omega_i - \kappa_j \omega_j) \kappa}{3DkT(1 + q^{1/2})(z_i + z_j)(\omega_i + \omega_j)} - \frac{z_i^3 z_j^2 e^4 \omega_i (\omega_j \kappa_j - \omega_i \kappa_i)}{6(DkT)^2 (z_i + z_j)(\omega_i + \omega_j)} - \kappa^2 \ln \kappa a + \frac{z_i^2 z_j e^2 \omega_i (\kappa_j - \kappa_i)}{24\pi\eta DkT (\omega_i + \omega_j)(z_i + z_j)} \kappa^2 \ln \kappa a \right\} + \left\{ \frac{z_i (\kappa_j - \kappa_i)}{6\pi\eta (z_i + z_j)} \kappa - \frac{z_i^2 e^2 (z_i \kappa_i + z_j \kappa_j)}{12\pi\eta DkT (z_i + z_j)} \kappa^2 \ln \kappa a + \frac{z_i^2 z_j e^2 (\omega_j \kappa_j - \omega_i \kappa_i)}{24\pi\eta DkT (\omega_i + \omega_j)(z_i + z_j)} \kappa^2 \ln \kappa a \right\} + O(\kappa^2 a^2) \quad (4)$$

where $i = 1$ and $j = 2$, or $i = 2$ and $j = 1$.

On the right-side of eq 4, the first term is the limiting velocity, i.e., the velocity of an i ion at infinite dilution, when there is no ion-ion interaction. The terms in the first bracket are due to the relaxation effect, and those in the second bracket are caused by electrophoresis. There are four $\kappa^2 \ln \kappa a$ (equivalent to $C \ln C$) terms, two each from the relaxation and the electrophoretic effect. The derivation of Chen shows that the first relaxation effect of order $C \ln C$ comes from a more accurate computation of the distorted ionic atmosphere, and the second is due to additional ion asymmetry caused by hydrodynamic flow. Analogously, the first electrophoretic effect of order $C \ln C$ is due to the higher order effect of the symmetrical charge distribution, and the second is from an additional electrophoresis due to ion asymmetry. The second $C \ln C$ term of the relaxation and that of the electrophoresis are reciprocal in the sense of irreversible thermodynamics.

The flow density of i ions is

$$J_i = n_i V_i \quad (5)$$

Substituting the value of V_i given by eq 4, and rearranging in the form of eq 1, we obtain from eq 5

$$J_i = \Omega_{ii} \kappa_i + \Omega_{ij} \kappa_j \quad i \neq j$$

with

$$\Omega_{ii} = n_i \omega_i - \left[\frac{z_i^2 z_j e^2 \omega_i^2 n_i}{3DkT(1 + q^{1/2})(z_i + z_j)(\omega_i + \omega_j)} + \frac{n_i z_i}{6\pi\eta (z_i + z_j)} \right] \kappa + \left[\frac{z_i^3 z_j^2 e^4 \omega_i^2 n_i}{6(DkT)^2 (z_i + z_j)(\omega_i + \omega_j)} - \frac{z_i^3 e^2 n_i}{12\pi\eta DkT (z_i + z_j)} - \frac{z_i^2 z_j e^2 \omega_i n_i}{12\pi\eta DkT (z_i + z_j)(\omega_i + \omega_j)} \right] \kappa^2 \ln \kappa a + O(\kappa^2 a^2) \quad (6)$$

and

$$\Omega_{ij} = n_i z_i W_{ij} \quad W_{ij} = \left[\frac{z_i z_j e^2 \omega_i \omega_j}{3DkT(1 + q^{1/2})(z_i + z_j)(\omega_i + \omega_j)} + \frac{1}{6\pi\eta (z_i + z_j)} \right] \kappa - \left[\frac{z_i^2 z_j^2 e^2 \omega_i \omega_j}{6(DkT)^2 (z_i + z_j)(\omega_i + \omega_j)} + \frac{z_i z_j e^2}{24\pi\eta DkT (z_i + z_j)} \right] \kappa^2 \ln \kappa a + O(\kappa^2 a^2) \quad (7)$$

Since $n_i z_i = n_j z_j$ by the requirement of charge neutrality, and since W_{ij} is symmetric in i and j , we have

$$\Omega_{ij} = n_i z_i W_{ij} = n_j z_j W_{ji} = \Omega_{ji}$$

Thus, it is proved that Chen's computation of the conductance equation is consistent with Onsager's reciprocal relation. Observe that in the computation of W_{ij} , the second $C \ln C$ terms of the relaxation and that of the electrophoresis complement each other such that their sum is symmetrical in i and j . In Fuoss et al.'s computation,⁶ the second $C \ln C$ term in electrophoretic effect is missed, and therefore W_{ij} computed from their result is not symmetrical in i and j . Hence, we conclude that Fuoss et al.'s result is not compatible with the fundamental law of irreversible thermodynamics and should be rejected. We did not analyze fully the Pitts equation, but since his value of E is the same as Fuoss et al.'s incomplete value, his equation cannot be correct.

Recently, Murphy and Cohen¹² computed a term Λ_{Chen} , the correction term due to Chen. When this contribution to conductance equation is incorporated to their earliest result,¹³ they obtain an equation to the order C term for binary electrolytes. Their $C \ln C$ term equals that in eq 3, and conforms to the reciprocal relation. The compatibility of their C term with the phenomenological law is still open to question. However for lack of a better one, their equation seems to be the best for analysis of conductance data at the present time.

Acknowledgment. This research as supported by NIH Grant GM 20284-04 and by NSF Grant CHE75-17533. The author thanks the late Professor Lars Onsager for many discussions and also the Center for Theoretical Studies for its hospitality.

References and Notes

- (1) L. Onsager and R. M. Fuoss, *J. Phys. Chem.*, **36**, 2689 (1932).
- (2) L. Onsager, *Phys. Z.*, **27**, 388 (1926); **28**, 277 (1927).
- (3) E. Pitts, *Proc. R. Soc. London, Ser. A*, **217**, 43 (1953).
- (4) R. M. Fuoss and L. Onsager, *J. Phys. Chem.*, **61**, 668 (1957).
- (5) R. M. Fuoss and F. Accascina, "Electrolytic Conductance", Interscience, New York, N.Y., 1959.
- (6) R. M. Fuoss, L. Onsager, and J. F. Skinner, *J. Phys. Chem.*, **69**, 2581 (1965).
- (7) Z. Pitts, B. Z. Tabor, and J. Daly, *Trans. Faraday Soc.*, **65**, 849 (1969).
- (8) M. S. Chen, Ph.D. Thesis, Yale University, 1969.
- (9) M. S. Chen, to be submitted for publication.
- (10) L. Onsager and M. S. Chen, *Proc. Natl. Acad. Sci.*, **63**, 229 (1969).
- (11) L. Onsager, *Phys. Rev.*, **37**, 405 (1931).
- (12) T. J. Murphy and E. G. D. Cohen, *J. Chem. Phys.*, **53**, 2173 (1970).
- (13) T. J. Murphy and E. G. D. Cohen, *Bull. Am. Phys. Soc.*, **13**, 647 (1968).

Electric Transport in Polyelectrolyte Solutions

Marie Kowblansky and Paul Ander*

Seton Hall University, South Orange, New Jersey 07079 (Received September 7, 1976)

Publication costs assisted by Seton Hall University

The interactions of monovalent and divalent cations and monovalent counterions with polyelectrolytes have been investigated at 25 °C by conductance and transference measurements. Conductance data have been obtained in aqueous NaCl and Na₂SO₄ solutions of NaPSS at 25 °C. The simple salt concentration was varied between 0.0010 and 0.010 N, and the polyelectrolyte concentration was varied between 0.00050 and 0.080 N. The agreement between the experimental results and the Manning limiting laws for electrical transport is not good. A phenomenological treatment of the data is proposed whereby the additivity of simple salt and polyelectrolyte conductivities is modified by making use of Manning's theoretical expressions for self-diffusion, which account for Debye-Hückel interactions between the uncondensed simple electrolyte and the polyelectrolyte. The modified additivity equation is shown to hold not only for NaPSS solutions in the presence of NaCl and Na₂SO₄, but for Li⁺ and NH₄⁺ salts of polystyrenesulfonic acid in the presence of Li⁺ and NH₄⁺ chlorides at 25 °C, and for sodium carrageenans in aqueous NaCl solutions at 0 °C as well. Polyion transference numbers, obtained by the Hittorf method, are found to be identical in NaCl and Na₂SO₄ solutions. They are shown to depend primarily on the concentration ratio of polyelectrolyte to simple salt, as do counterion and cation self-diffusion coefficients. Polyion equivalent conductances, which are calculated from specific conductances and transference numbers, are demonstrated to be nearly independent of both the simple salt and polyelectrolyte concentrations.

Introduction

The treatment of the conductance of polyelectrolyte solutions has been problematic since the classical electric transport experiments of Wall et al.^{1,2} For salt-free polyelectrolyte solutions, the conductivity has been interpreted by the empirical equation³

$$\Lambda = f(\lambda_p + \lambda_c^0) \quad (1)$$

where Λ , λ_p , and λ_c^0 are, respectively, the equivalent conductances of the solution, the polyion, and the counterion at infinite dilution in a polyelectrolyte-free salt solution, and f is the fraction of free counterions, with $(1 - f)$ the fraction of condensed counterions. Because of the high potential on the polyion even after counterion condensation, eq 1 must be modified to account for the interaction of counterions with the polyion. Using a line charge model for the polyion and assuming that the condensed counterions have zero mobility, Manning⁴⁻⁹ formulated an expression analogous to eq 1

$$\Lambda = (D_1^p/D_1^0)(\lambda_p + \lambda_c^0) \quad (2)$$

where D_1^p/D_1^0 is the ratio of the self-diffusion coefficients of the counterions in a salt-free polyelectrolyte solution to that in an infinitely dilute polyelectrolyte-free simple salt solution. The diffusion ratio D_1^p/D_1^0 is a measure of the fraction of the free counterions in solution and their Debye-Hückel interaction with the polyion. Caution should be taken in employing the experimental values of D_1^p in eq 2 since the condensed counterions might contribute to D_1^p if the self-diffusion coefficient of the polyion is of the same order of magnitude as that of the counterion.¹⁰

In Manning's conductance theory for salt-free polyelectrolyte solutions f is equated with D_1^p/D_1^0 and, taking into account electrophoretic and relaxation effects, λ_p is calculated to be

$$\lambda_p = \frac{279A |z_c|^{-1} \ln Ka}{1 + 43.2A (|z_c| \lambda_c^0)^{-1} \ln Ka} \quad (3)$$

where $A = \epsilon kT/3\pi\eta e$, ϵ is the dielectric constant of the bulk solvent, k is the Boltzmann constant, T is the absolute

temperature, η is the viscosity of bulk solvent, e is the proton charge, z_c and λ_c^0 are, respectively, the counterion charge and equivalent conductance at infinite dilution, a is the radius of the cylindrical polyelectrolyte, and K the Debye screening constant is given by

$$K^2 = (4\pi e^2/\epsilon kT)\xi^{-1}N_p \quad (4)$$

N_p is the equivalent concentration of polyelectrolyte, and ξ a charge density parameter is given by $e^2/\epsilon kTb$, with b being the structural distance between charges on the polyelectrolyte. It is important to note that λ_p is predicted to depend on the type of counterion species through λ_c^0 and z_c , and on the polyelectrolyte concentration and charge density through K . Thus Λ is also predicted to be dependent on the polyelectrolyte concentration and charge density and on the nature of the counterion species by eq 2.

No conclusive study of the validity of eq 3 has been reported in the literature. Jordan et al.¹¹ found λ_p to be different in HPSS and NaPSS solutions as predicted, yet no concentration dependence for λ_p was observed. Detailed comparisons of the theoretical expression for Λ with measured values for aqueous solutions of alkali metal poly(styrenesulfonates) were made by Kwak and Hayes¹² and by Szymczak, Holyk, and Ander.¹³ These studies verified the predicted decrease in Λ with increasing polyelectrolyte concentration, however, positive deviations from the limiting law were reported, even at the lowest concentrations employed. For divalent salts of poly(styrenesulfonic acid) the equivalent conductivity was shown to be appreciably lower than for the monovalent salts.¹² Although this is in qualitative agreement with Manning's concept of condensation, deviations from the limiting law were significant. Good quantitative agreement between measured and predicted values of Λ was reported by Kwak and Johnston¹⁴ for several monovalent salts of the more rigid polyelectrolyte carboxymethylcellulose. The agreement was good both with respect to the predicted concentration dependence and counterion dependence on the equivalent conductance.

The theory of polyelectrolyte conductance has been extended by Manning⁵ to include polyelectrolyte solutions

containing added simple electrolyte. Using the cylindrical model, the interactions between the polyion and simple ions in an electric field are described by a parameter A_p , which has the units of equivalent conductance

$$A_p = \xi^{-1} [(t_c^{(s)} - 1/\epsilon)\lambda_s + \lambda_p] \quad (5)$$

where $t_c^{(s)}$ is the transference number of the counterion, λ_s is the equivalent conductance of the simple salt, both at the given concentration in the absence of polyelectrolyte, and λ_p the equivalent conductance of the polyion is given by

$$\lambda_p = (F/3000)(\epsilon kT/3\pi\eta e) \ln Ka \quad (6)$$

where F is Faraday's constant and the other symbols have the same meaning as in eq 3, with the exception of K , which is the Debye screening constant for the simple salt in the absence of polyelectrolyte. Thus A_p and λ_p are predicted to depend not only on the counterion but on the coion as well. It is interesting that the theoretical expression for λ_p in salt-free solution has a dependence on ξ , whereas for the salt-containing case it does not.

In this study, values of A_p are determined from conductance data obtained at 25 °C for aqueous NaPSS solutions over the concentration range 5×10^{-4} to 8×10^{-2} N containing 0.00100, 0.00500, and 0.0100 N NaCl or Na_2SO_4 . The experimental A_p values are compared with experimental values obtained for other polyelectrolytes and with those theoretically predicted. A phenomenological interpretation of the equivalent conductance of polyelectrolyte solutions containing simple salts in terms of modified additivity of salt and polyelectrolyte is presented.

Experimental Section

Materials. The NaPSS sample used in this study was the same one described in a previous investigation.¹⁰ Its molecular weight is 70 000 and its degree of sulfonation is 93.1%. Conductance water of better than 1×10^{-6} ohm⁻¹ cm⁻¹ was employed.

All conductivity measurements were made in an oil-filled bath thermostated at 25 ± 0.01 °C. A conductivity cell of a modified Shedlovsky design was employed. The electrodes were lightly platinized with platinum black. Using 0.01 M KCl solution, the value of the cell constant was found to be 1.1273 ± 0.0006 cm⁻¹. A Beckman laboratory conductivity bridge Model RC-18A, which utilized a precision ac Wheatstone bridge, was used for all measurements. Resistance measurements were reproducible to within $\pm 0.05\%$ for all polymer solutions.

Ionic equivalent conductances were calculated from the measured transference numbers and specific conductances by

$$\lambda_p = 1000\kappa T_p/N_p \quad (7)$$

where λ_p and T_p are the equivalent conductance and transference number of the polyion, and κ is the specific conductance of the solution.

Transference numbers for the PSS polyanion were determined in aqueous solutions of NaPSS containing NaCl or Na_2SO_4 by the Hittorf method. A three cell compartment of the type described by Wall et al.¹⁵ was employed with platinum electrodes. The cathode and anode compartments each contained approximately 40 mL of solution and the central compartment contained approximately 70 mL. The cell was thermostated in a constant temperature bath at 25 ± 0.005 °C. The electrical current was supplied by a Keithly Instruments Model 227 dc constant current source. The currents employed ranged from 0.5 to 10 mA ($\pm 0.6\%$), and the electrolysis times

ranged from 0.25 to 2 h. The voltage was not allowed to exceed 100 V.

At the end of each electrolysis the concentration of each of the components in the middle compartment never changed by more than 0.5% from its original value. Transference numbers for the PSS polyion T_p were calculated from

$$T_p = \Delta N_p/N_{el} \quad (8)$$

where N_{el} is the total amount of electricity passed through the solution (in equivalents) and ΔN_p is the concentration decrease (in equivalents) in the cathode compartment.

After electrolysis the solution from the cathode compartment was drained from the transference cell, weighed, and analyzed to determine the polyion concentration. Use was made of ion-exchange resins in the analyses of the solutions. The poly(styrenesulfonate) polyion concentration was determined by passing an aliquot of the solution through Biorad analytical grade cation and anion exchange resins connected in series. The eluted poly(styrenesulfonic acid) was then titrated with standardized sodium hydroxide solution to a methyl red end point. A similar procedure has been employed by Nagasawa et al.¹⁶

It was observed that for each solution, the polyion transference numbers decreased linearly with increasing equivalents of electricity N_{el} passed through the cell. Wall and Hill¹⁷ also report such a finding for salt-free solutions of sodium poly(acrylate). Therefore, for each solution studied, transference numbers were determined at a minimum of four different values of N_{el} , and the resulting transference numbers were extrapolated to $N_{el} = 0$.

Attempts were made to determine the sodium ion transference numbers T_{Na^+} in the solutions. These were found to increase with increasing N_{el} . However, since N_{Na^+} is obtained as a small difference between two large numbers, T_{Na^+} has a relatively large uncertainty, which makes an extrapolation of T_{Na^+} to $N_{el} = 0$ more hazardous than for the case of T_p . Because of this problem the results obtained for T_{Na^+} will not be discussed in the present paper and are being investigated further.

Results and Discussion

The specific conductivity of aqueous NaPSS–NaCl and NaPSS– Na_2SO_4 solutions at 25 °C are given in Table I. Empirically, A_p is evaluated as the slope from the relationship^{5,18}

$$\kappa - \kappa_s = 10^{-3}A_pN_p \quad (9)$$

where κ is the specific conductance of the polyelectrolyte solution with added simple electrolyte and κ_s is the specific conductance of the simple salt solution in the absence of polyelectrolyte. The values of A_p with their experimental uncertainties are listed in Table II. These were obtained from linear regression plots of $(\kappa - \kappa_s)$ vs. N_p for NaPSS solutions containing 0.0100, 0.00500, and 0.00100 N NaCl or Na_2SO_4 . The measured values of κ_s were found to be in excellent agreement with the literature values.²⁰ At each concentration of simple salt the polyelectrolyte concentration was varied so as to keep X in the range 0.5 to 8, where X is defined as the ratio of the equivalent concentrations of polyelectrolyte N_p to simple salt N_s . Included in Table II are the theoretical values of A_p which were calculated from eq 5 and 6 using literature values^{20,21} for $t_c^{(s)}$, λ_s , η , and K , and a value of 2.64 for ξ for NaPSS, the same polyelectrolyte sample used in a previous study.¹⁰

Theoretical values of A_p are predicted to increase with decreasing simple electrolyte concentration and to decrease with increasing coion valence. Yet the experimental results

TABLE I: Specific Conductivity of Aqueous NaPSS-NaCl and NaPSS-Na₂SO₄ Solutions at 25 °C

X ^a	10 ³ κ, ohm ⁻¹ cm ⁻¹					
	NaCl			Na ₂ SO ₄		
	0.0100 N	0.00500 N	0.00100 N	0.0100 N	0.00500 N	0.00100 N
0.000	1.1832	0.5984	0.1242	1.1174	0.5843	0.1248
0.501	1.3357	0.6762	0.1449	1.2766	0.6651	0.1433
1.099	1.5394	0.7780	0.1637	1.4724	0.7594	0.1654
1.900	1.8177		0.1959			
2.895	2.1747	1.0918	0.2279	2.1146	1.0838	0.2337
4.200	2.6484	1.3072	0.2760	2.5919	1.3095	0.2774
5.800	3.2756	1.6178	0.3306	3.2109	1.6075	0.3391
7.900	4.0963	2.0225	0.4153	4.0358	2.0029	0.4141
11.210	5.4543		0.5355			

^a X is the concentration ratio of polyelectrolyte N_p to simple salt N_s, both in equivalents per liter.

TABLE II: A Comparison of Predicted^a and Experimental^b Values of A_p for NaPSS in Aqueous Solutions of NaCl or Na₂SO₄ at 25 °C

N _s	N _p	X	A _p , cm ² ohm ⁻¹ equiv ⁻¹			
			NaCl		Na ₂ SO ₄	
			Expt	Theor	Expt	Theor
0.00100	0.0005-0.008	0.5-8	36.3 ± 0.3	34.9	36.6 ± 0.1	32.7
0.00500	0.0025-0.04	0.5-8	36.5 ± 0.7	26.7	35.9 ± 0.3	24.3
0.0100	0.005-0.08	0.5-8	36.3 ± 0.5	23.1	36.9 ± 0.5	20.3

^a Predicted from eq 5 and 6 using a value of 8 × 10⁻⁸ cm for a, the radius of the PSS polyion.¹⁹ ^b The experimental uncertainty (±) is the standard error of the linear least-squares fit of the data.

presented in Table II demonstrate that A_p is independent of the polyelectrolyte concentration, of the simple salt concentration, and of the coion valence. Holyk, Szymczak, and Ander²² have also obtained values of A_p for NaPSS-NaCl solutions at 25 °C. They found qualitative agreement between the experimental and predicted values of A_p, i.e., an increase in N_s resulted in a decrease in A_p. The apparent discrepancy between the results of the two studies will receive further attention later. However, an observation common to both studies is that theoretical values of A_p consistently underestimate those obtained from experiment.

Since eq 5 predicts A_p to depend on λ_p, the poor agreement between experiment and theory for A_p might be attributable to an inaccurate prediction for λ_p. The experimental values of A_p reported by Ross, Scruggs, and Manning¹⁸ for DNA in LiCl, NaCl, and KCl solutions were also consistently higher than predicted. The largest divergence between experiment and theory was observed in the most concentrated simple salt solutions employed. It was suggested by these authors that the greatest source of uncertainty in the theoretical calculation was in the determination of λ_{DNA}. However, no experimental values for λ_{DNA} were reported. Therefore, to more completely test the Manning theory of electrical transport for salt-containing polyelectrolyte solutions, PSS polyion equivalent conductances were obtained by eq 7 from polyion transference numbers T_p, specific conductances κ, and stoichiometric equivalent concentrations of the polyelectrolyte N_p.

The results of the transference experiments are presented in Figure 1. As in the case of diffusion, X is found to be an extremely useful parameter. When the polyion constituent transference number T_p is studied as a function of X it is found to increase sharply with increasing X, and then to level off to a nearly constant value when X is greater than four. The self-diffusion coefficients¹⁰ of several coions and sodium counterion were also found to be nearly constant at values of X greater than four. In 0.010 and 0.0050 N simple electrolyte T_p is found to be solely dependent on X, the ratio of polyelectrolyte to

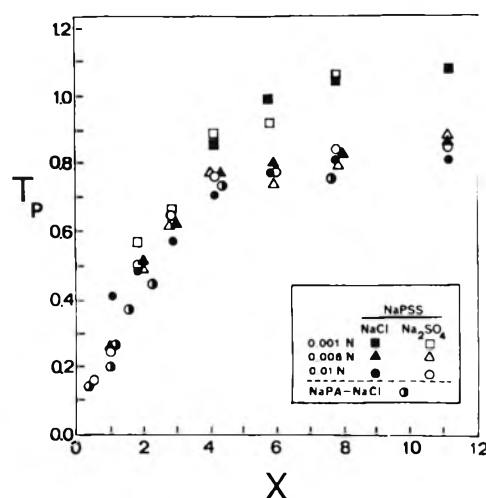


Figure 1. Polyion transference numbers at 25 °C plotted as a function of X for NaPSS solutions containing NaCl or Na₂SO₄. The values of T_p in NaPA-NaCl solutions were obtained from ref 16 and 23.

simple salt, and not on the concentration of either one individually, or on the valence of the coion. In 0.0010 N simple salt the values of T_p are found to be somewhat higher, although the shape of the curve is the same as in the more concentrated simple salt solutions. When the data shown in Figure 1 are compared with the polyion transference data of Nagasawa et al.¹⁶ and Wall and Eitel²³ for NaPA in NaCl solutions, no significant difference is observed between the transport behavior of the two polyions, despite the different nature of the charged groups on the NaPSS and NaPA polymers. This, no doubt, is due to the identical charge densities of the two polyelectrolytes. It should be pointed out that the data of Nagasawa and Wall were obtained in solutions where the polyelectrolyte concentration was held constant and the NaCl concentration was varied between 0.01 and 0.1 N. The decrease in polyion mobility with increasing simple salt concentration was qualitatively interpreted in terms of configurational changes of the polyion with changing ionic strength.

TABLE III: A Comparison of Experimental and Theoretical Values of A_p and λ_p for Aqueous NaCl and Na_2SO_4 Solutions of NaPSS at 25 °C

	NaCl			Na_2SO_4		
	0.00100 N	0.00500 N	0.0100 N	0.00100 N	0.00500 N	0.00100 N
Expt ^a	56.0	45.6	45.2	56.5	44.5	44.7
Theor ^b	64.0	43.2	34.3	58.7	38.0	29.1
			λ_p			
Expt	36.6 ± 0.3	36.5 ± 0.7	36.9 ± 0.5	36.6 ± 0.1	35.9 ± 0.3	36.9 ± 0.5
Theor ^c	34.9	26.7	23.1	32.7	24.3	20.3
Theor ^d	31.9	27.6	27.2	31.9	26.8	26.2
			A_p			

^a The average of all values of λ_p at the given simple salt concentration. ^b Calculated from eq 6. ^c Calculated from eq 5 using values of λ_p calculated from eq 6. ^d Calculated from eq 5 using average experimental values of λ_p .

Manning's treatment assumes a linear model for the polyelectrolyte at infinite dilution and, hence, configurational changes of the polyion with changing polyelectrolyte concentration are not taken into account. The properties of polyelectrolyte solutions are then derived in terms of the interactions of the small ions with the polyelectrolyte, which are determined by the ratio of polyelectrolyte to simple salt X . The validity of this approach even at finite concentrations of polyelectrolyte and simple salt has been demonstrated by diffusion experiments,^{10,24} as well as by various other studies of transport and equilibrium properties of polyelectrolyte solutions.^{25,26} Thus the constancy of T_p at a given value of X , irrespective of the coion charge, the polyelectrolyte or simple salt concentration, or the nature of polyelectrolyte, should be interpreted in terms of the electrostatic interactions of the small ions with the polyion, without resorting to argumentation involving the configuration of the polyion. The values of T_p in 0.0010 N NaCl and Na_2SO_4 are greater than in the higher salt concentrations, probably due to insufficient screening of the charges on the polyion.

The polyion equivalent conductances which were obtained from the transport numbers and specific conductances by eq 7 are presented as a function of X in Figure 2. For each simple salt solution employed, λ_p is seen to be nearly independent of the polymer concentration; only a slightly downward trend is observed with increasing polyelectrolyte concentration or X . This is in agreement with eq 6, which predicts λ_p to be a function of the simple salt concentration and not of the polyelectrolyte. However, quantitatively the agreement between the predicted and measured values of λ_p is not good. Whereas eq 6 predicts a large decrease in λ_p with increasing simple salt concentration, experimentally this is not observed. A comparison of the average experimental and predicted values of λ_p is presented in Table III for each of the simple salt solutions studied. The experimental values of λ_p show no difference between 0.010 and 0.0050 N simple salt solutions, and the difference in λ_p between 0.0010 and 0.0050 N is not nearly as large as is theoretically predicted. Of greater significance is the observed independence of λ_p on the charge of the coion in solution, in contradiction to the predictions derived from eq 6. This is a further substantiation of the conclusions formed on the basis of self-diffusion studies^{10,24} that mono- and multivalent coions interact with the polyion to the same extent.

When the average experimental values of λ_p are used to calculate A_p by eq 5 the agreement between experiment and theory is slightly improved, as is shown in Table III. However, the predicted dependence of A_p on the simple salt concentration is not observed. The lack of fair quantitative agreement between predicted and experimental values of A_p and of λ_p suggests that the Manning theory of electric transport requires modification.

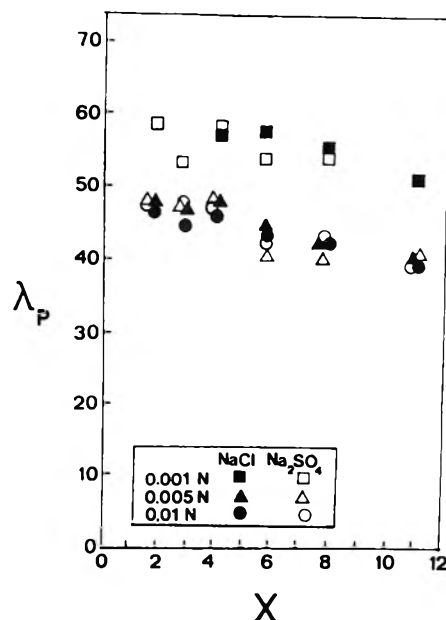


Figure 2. Polyion equivalent conductance at 25 °C in aqueous NaPSS solutions containing NaCl or Na_2SO_4 , plotted as a function of X .

In view of the inadequacy of Manning's theory of electrical transport for salt-containing polyelectrolyte solutions the results of the conductance experiments might better be treated at the present time phenomenologically in terms of an additivity of contributions of the polyelectrolyte and simple salt to the total conductance. Such an approach is usually assumed in describing the behavior of salt-containing polyelectrolyte solutions.^{27,28} Yet experimental evidence indicates that this is not totally justifiable. Experimentally obtained specific conductances for salt containing polyelectrolyte solutions are consistently lower than those predicted by simple additivity. This is demonstrated in Figures 3–5, where the conductance data obtained for lithium, sodium, and ammonium poly(styrenesulfonates) in aqueous solutions of LiCl, NaCl, and NH_4Cl , respectively,^{13,22} are compared with conductivities predicted on the basis of additivity. The conductivities obtained for sodium λ - and κ -carrageenans in aqueous NaCl solutions at 0 °C illustrate the same trends, as is shown in Figures 6 and 7.²⁹ Upon comparing Figures 3–7 it should be noted that the agreement between experimental specific conductances and those obtained from additivity improves with decreasing simple salt concentration when the polyelectrolyte concentration range is constant. At the lowest concentrations of simple salt the concentrations of polyelectrolyte greatly exceed the concentration of simple electrolyte and, as a result, the contribution of the simple salt conductance to the total solution conductance is small and the additivity as-

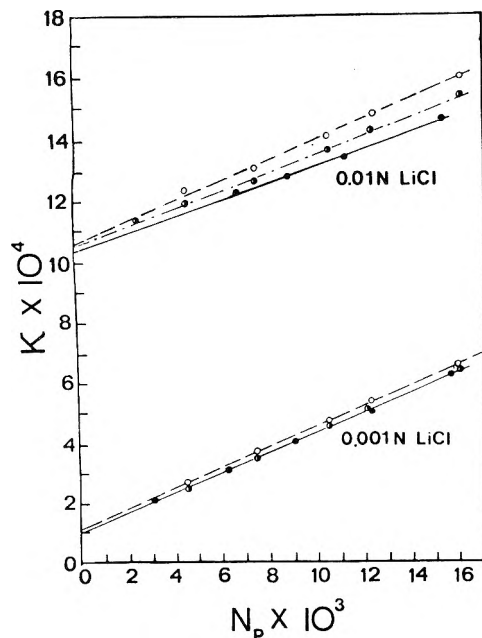


Figure 3. A comparison of the specific conductivities of aqueous LiPSS-LiCl solutions at 25 °C obtained experimentally (●), obtained from additivity (○) as the sum of κ_p and κ_s , and obtained from the modified additivity (◐) given by eq 13. The experimental data were obtained from ref 13 and 22.

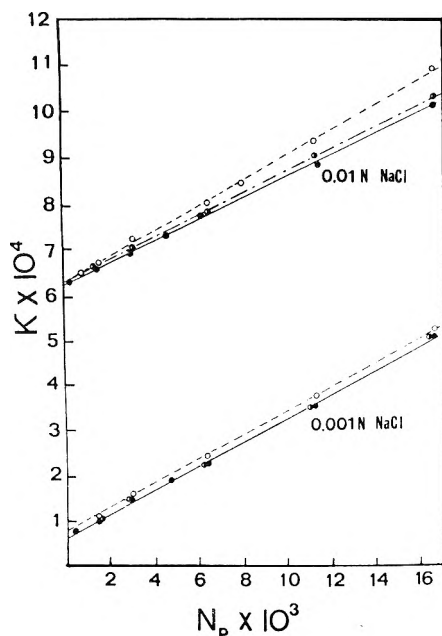


Figure 4. A comparison of the specific conductivities of aqueous NaPSS-NaCl solutions at 25 °C obtained experimentally (●), obtained from additivity (○) as the sum of κ_p and κ_s , and obtained from the modified additivity (◐) given by eq 13. The experimental data were obtained from ref 13 and 22.

sumption appears to be valid. However, at the higher concentrations of simple electrolyte, where the polyelectrolyte and simple salt concentrations are comparable, additivity is not obeyed.

A more sensitive test of additivity makes use of the polyelectrolyte equivalent conductance defined as

$$\Lambda = 10^3 [(\kappa - \kappa_s) / N_p] \quad (10)$$

which in salt-free polyelectrolyte solution reduces to

$$\Lambda = 10^3 (\kappa / N_p) \quad (11)$$

If a true additivity existed, the values of Λ obtained for

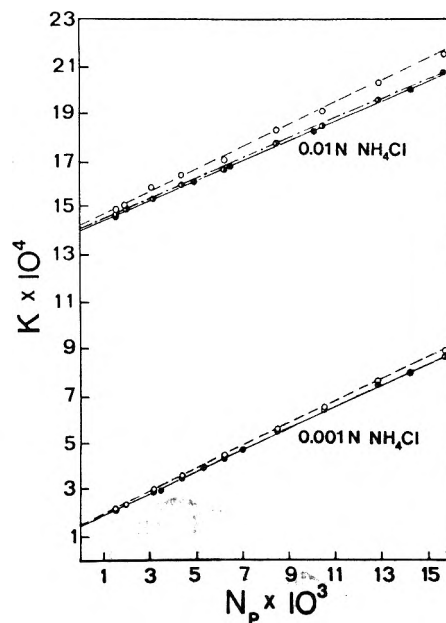


Figure 5. A comparison of the specific conductivities of aqueous $\text{NH}_4\text{PSS-NH}_4\text{Cl}$ solutions at 25 °C obtained experimentally (●), obtained from additivity (○) as the sum of κ_p and κ_s , and obtained from the modified additivity (◐) given by eq 13. The experimental data were obtained from ref 13 and 22.

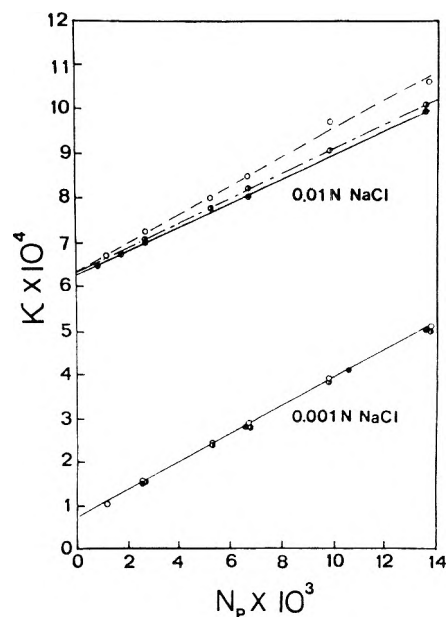


Figure 6. A comparison of the specific conductivities of aqueous sodium κ -carrageenan solutions containing NaCl at 0 °C obtained experimentally (●), obtained from additivity (○) as the sum of κ_p and κ_s , and obtained from the modified additivity (◐) given by eq 13. The experimental data were obtained from ref 29.

a given polyelectrolyte in salt-free and salt-containing solution by eq 11 and 10, respectively, would be identical. However, when Λ is plotted as a function of N_p in salt-free polyelectrolyte solution, it is found to be constant at higher polyelectrolyte concentrations and to rapidly increase with dilution at low polyelectrolyte concentrations; whereas in salt-containing polyelectrolyte solutions, the use of eq 10 results in values of Λ which are fairly constant at high polyelectrolyte concentrations, but sharply decrease with dilution of polyelectrolyte. This is clearly demonstrated for several polyelectrolytes in Figures 8a-12a. Thus the true value of the polyelectrolyte equivalent conductance cannot be calculated from conductance data obtained in salt-containing polyelectrolyte solutions by assuming

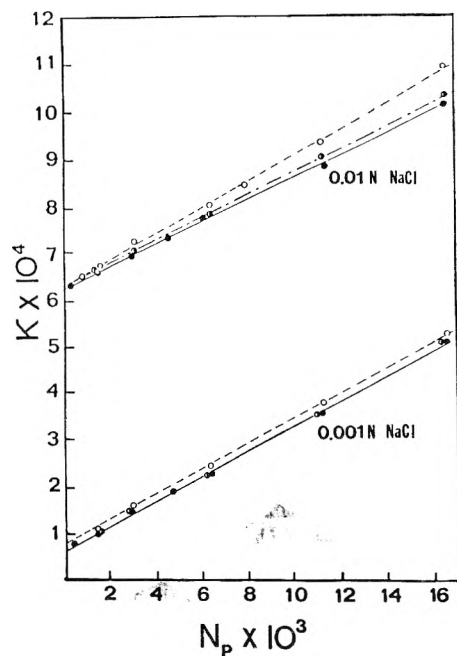


Figure 7. A comparison of the specific conductivities of aqueous sodium κ -carrageenan solutions containing NaCl at 0 °C obtained experimentally (●), obtained from additivity (○) as the sum of κ_p and κ_s , and obtained from the modified additivity (◐) given by eq 13. The experimental data were obtained from ref 29.

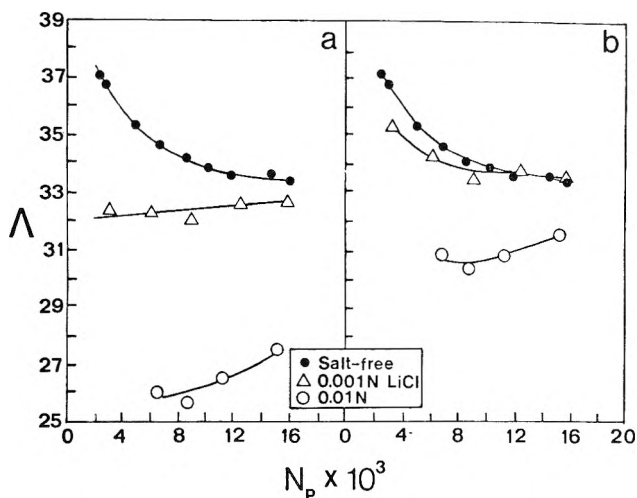


Figure 8. (a) A comparison of Λ values for aqueous solutions of LiPSS in the presence and absence of LiCl at 25 °C. The values of Λ for the LiCl solutions of the polyelectrolyte were calculated from eq 10. (b) The values of Λ for the LiCl solutions of the polyelectrolyte were calculated from eq 14. Experimental data from ref 13 and 22.

additivity of polyelectrolyte and simple salt conductances. The differences between Λ obtained from eq 10 and 11 for the salt-containing and salt-free solutions of the polyelectrolyte must be due to the interactions of the simple salt with the polyelectrolyte. Manning recognized this limitation of the additivity assumption and obtained a parameter A_p , which was interpreted to be a measure of the interaction between the simple electrolyte and polyelectrolyte. From a comparison of eq 9 and 10 it is important to note that, experimentally, A_p is the same quantity as Λ , obtained by assuming additivity in salt solutions of polyelectrolytes. From the data in Table II it appears that Manning's approach is no more satisfactory than the empirical approach of additivity. When a suitable correction is applied to κ_s due to the interaction of the simple salt with the polyelectrolyte, conductance data obtained for polyelectrolytes in the presence of added salt can be satisfactorily treated in terms of additivity. Strauss and

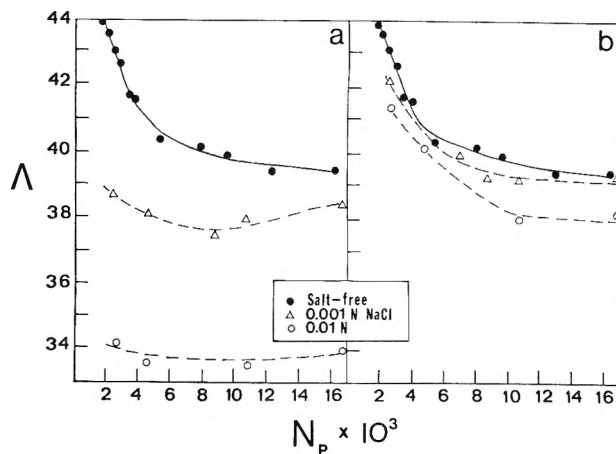


Figure 9. (a) A comparison of Λ values for aqueous solutions of NaPSS in the presence and absence of NaCl at 25 °C. The values of Λ for the NaCl solutions of the polyelectrolyte were calculated from eq 10. (b) The values of Λ for the NaCl solutions of the polyelectrolyte were calculated from eq 14. (Experimental data from ref 13 and 22.)

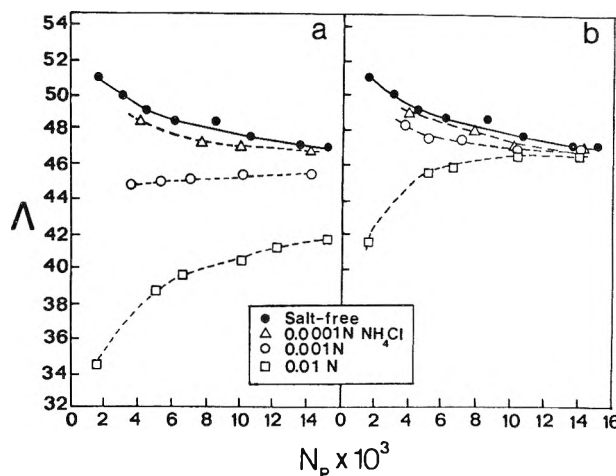


Figure 10. (a) A comparison of Λ values for aqueous solutions of NH_4PSS in the presence and absence of NH_4Cl at 25 °C. The values of Λ for the NH_4Cl solutions of the polyelectrolyte were calculated from eq 10. (b) The values of Λ for the NH_4Cl solutions of the polyelectrolyte were calculated from eq 14. (Experimental data from ref 13 and 22.)

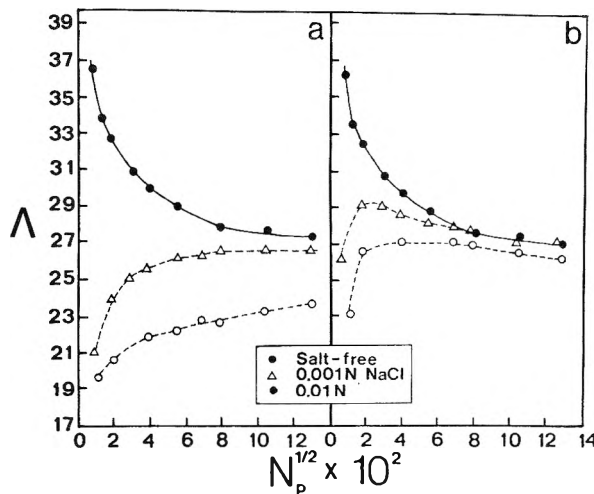


Figure 11. (a) A comparison of Λ values for aqueous solutions of sodium λ -carrageenan in the presence and absence of NaCl at 0 °C. The values of Λ for the NaCl solutions of the polyelectrolyte were calculated from eq 10. (b) The values of Λ for the NaCl solutions of the polyelectrolyte were calculated from eq 14. (Experimental data from ref 29.)

Bluestone noted this and used the model obtained for Donnan membrane equilibrium to correct for the inter-

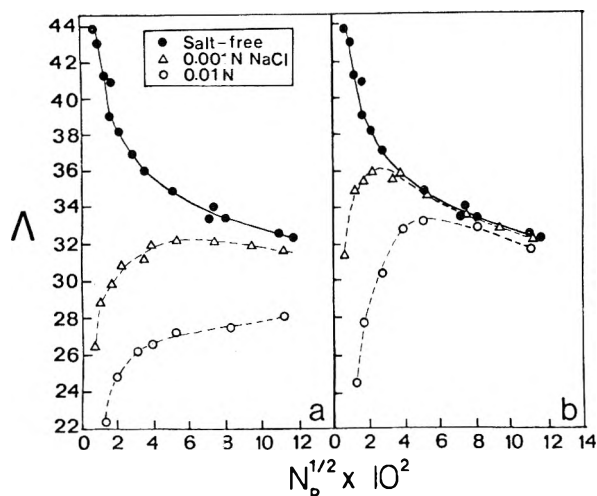


Figure 12. (a) A comparison of Λ values for aqueous solutions of sodium λ -carrageenan in the presence and absence of NaCl at 0 °C. The values of Λ for the NaCl solutions of the polyelectrolyte were calculated from eq 10. (b) The values of Λ for the NaCl solutions of the polyelectrolyte were calculated from eq 14. (Experimental data from ref 29.)

action of simple salt with the polyelectrolyte.^{30,31}

In the absence of simple electrolyte Manning's expression for Λ was derived in terms of the reduction of the specific conductance of the polyion and counterion due to condensation of some of the counterions and Debye-Hückel interactions between the uncondensed counterions and the polyion. This reduction in the conductance was quantitatively expressed in terms of the counterion self-diffusion ratio L_1^p/D_1^0 . An analogous approach can be used to account for the interaction of the added simple electrolyte with the polyelectrolyte. According to the Manning model, neither the counterions nor coions of the added simple salt condense onto the polyion and their Debye-Hückel interactions with the polyion are taken into account in the coion self-diffusion ratio

$$D_2/D_2^0 = 1 - (z_2^2/3)A(\xi; X) \quad (12)$$

where D_2 and D_2^0 are the coion self-diffusion coefficients in a salt-containing polyelectrolyte solution and in an infinitely dilute polyelectrolyte-free salt solution, respectively, z_2 is the valence of the coion, and $A(\xi; X)$ is the small ion-polyion interaction term.^{6-8,10} Utilizing this quantitative formulation for the interaction, the specific conductance due to the simple salt in the presence of polyelectrolyte should be reduced by the same amount, and the effective specific conductance of the simple salt can then be expressed as $\kappa_s(D_2/D_2^0)$. Thus the total specific conductance κ of a polyelectrolyte solution with added simple electrolyte should be equal to the sum of the effective specific conductance of the polyelectrolyte in the absence of simple salt κ_p and the effective specific conductance of the added simple salt $\kappa_s(D_2/D_2^0)$

$$\kappa = \kappa_p + \kappa_s(D_2/D_2^0) \quad (13)$$

The self-diffusion studies previously discussed¹⁰ clearly demonstrated that in the presence of monovalent counterions, both mono- and multivalent coions interact with the polyelectrolyte according to Manning's predictions for monovalent coions. Therefore, the values of D_2/D_2^0 used to correct κ_s in eq 13 should be those predicted for monovalent coions, irrespective of the valence of the coion in solution. When this "modified additivity" proposed by eq 13 is tested for the same polyelectrolyte-simple salt systems previously discussed, it is seen from Figures 3-7

that the modified additivity values of κ are nearly superimposable with the experimental ones.

Rewriting eq 10 in terms of the modified additivity yields

$$\Lambda = 1000 \frac{[\kappa - \kappa_s(D_2/D_2^0)]}{N_p} \quad (14)$$

The validity of this approach is demonstrated in Figures 8b-12b where the experimental values of Λ , calculated by eq 11 and 14 for the salt-free and salt-containing polyelectrolyte solutions, respectively, are compared and found to be nearly identical, except at very low concentrations of polyelectrolyte and at the highest simple salt concentration. The small difference between the salt-free and salt-containing values of Λ in Figures 8b-12b can no doubt be partially attributed to the use of theoretical values of D_2/D_2^0 in eq 14, rather than experimental ones. At a given value of X the values of D_2/D_2^0 were experimentally seen to decrease with increasing ionic strength.¹⁰ Thus the use of experimental diffusion ratios in eq 14 would tend to increase Λ , and even better agreement with the salt-free values would be obtained. In addition, the derivation of the self-diffusion ratio D_2/D_2^0 only takes into account the relaxation effect, thus the discrepancy between the Λ values calculated for salt-free solutions (eq 11) and for salt-containing solutions (eq 14) in Figures 8b-12b may also be due to neglect of the electrophoretic effect. The simple salt interaction correction D_2/D_2^0 is not constant, its value is dependent on X , the ratio of polyelectrolyte to simple salt. Therefore, at a given concentration of simple salt the correction which must be applied to κ_s changes with the polyelectrolyte concentration. The previously mentioned discrepancy in A_p between the data of the present study and that of Holyk, Szymczak, and Ander,²² given in Table IV, can be understood within this framework. In the present study the polyelectrolyte concentration was varied so as to keep X in the same range at each simple salt concentration employed. The study of Holyk et al.²² employed the same range of polyelectrolyte concentrations at each simple salt concentration; therefore, each concentration of simple salt represented a different range of X values and, consequently, different extents of interaction with the polyelectrolyte. A conclusion which may be drawn from Table IV is that when A_p is obtained over an identical range of X values it is independent of the simple salt concentration. When A_p is obtained over a constant range of polyelectrolyte concentrations A_p varies with the simple salt concentration because the range of X values also varies. When κ_s is replaced by $\kappa_s(D_2/D_2^0)$ in eq 9 the values of A_p from the two studies are brought into better agreement, as is shown in Table IV.

Manning's prediction that A_p is solely dependent on the simple salt concentration and valence is not correct. It has been shown above that it is dependent both on the concentration of simple salt and polyelectrolyte, i.e., on X . To get consistency from results obtained over different concentration ranges of polyelectrolyte it was shown that the same correction must be applied to κ_s in eq 9 for A_p as is applied in eq 14 for Λ . For salt-free polyelectrolyte solutions A_p is not defined by the Manning theory, since it is considered to be a measure of the simple salt-polyelectrolyte interaction. However, by using a value of zero for κ_s in eq 9 for salt-free solutions of NaPSS, the slope ($\times 1000$) of the linear regression line of $(\kappa - \kappa_s)$ vs. N_p will be called A_p . This value of A_p for salt-free NaPSS solutions is compared in Table IV with the values of A_p obtained for NaCl and Na₂SO₄ solutions of NaPSS. The salt-free

TABLE IV: A Comparison of the A_p Values for NaCl and Na_2SO_4 Solutions of NaPSS Determined from Experimental Results, Experimental Results Corrected for Salt-Polyelectrolyte Interaction, and Theoretically Predicted Values

Salt	N_s	X	$A_p, \text{cm}^2 \text{ohm}^{-1} \text{equiv}^{-1}$		
			Expt ^a	Corr expt ^b	Theor ^c
NaCl	0.0100	0.5-8	36.9 ± 0.5	38.4 ± 0.2	23.1
	0.00500	0.5-8	36.5 ± 0.7	37.4 ± 0.3	26.7
	0.00100	0.5-8	36.6 ± 0.3	37.9 ± 0.4	34.9
	0.0100 ^d	0.3-1.8	33.5 ± 0.5	37.2 ± 0.5	23.1
	0.00100 ^d	2.5-15	38.2 ± 0.5	38.7 ± 0.4	34.9
	0.000100 ^d	30-150	38.4 ± 0.4	38.4 ± 0.4	43.0
Na_2SO_4	0.0100	0.5-8	36.9 ± 0.5	38.3 ± 0.3	20.3
	0.00500	0.5-8	35.9 ± 0.3	37.4 ± 0.5	24.3
	0.00100	0.5-8	36.3 ± 0.1	38.3 ± 0.4	32.7
Salt-free	0.000 ^d		38.7 ± 0.6^e	38.7 ± 0.6^e	

^a Slope from eq 9. ^b Slope from eq 9, substituting $\kappa_s(D_2/D_2^0)$ for κ_s . ^c From eq 5. ^d Data from ref 22. ^e This value was obtained from the slope of the linear regression line of κ on N_p , although A_p for salt-free polyelectrolyte solutions is not defined by the Manning theory.

value of A_p is higher than any of the A_p values listed in Table IV for solutions containing simple salt, which were calculated by eq 9. However, the values of A_p obtained by substituting $\kappa_s(D_2/D_2^0)$ for κ_s in eq 9 very closely approximate the salt-free value of 38.7. This suggests that A_p may simply be the equivalent conductance of the polyelectrolyte. Furthermore, it has been demonstrated that when a correction, based on the Manning theory, is applied to κ_s , an additivity of simple salt and polyelectrolyte conductances is obtained, and the values of Λ obtained from salt-free and salt-containing polyelectrolyte solutions are nearly equal.

Degree of Counterion Binding

For salt-free polyelectrolyte solutions, the apparent degree of counterion binding can be calculated from eq 1 when the polyion equivalent conductance λ_p and the equivalent conductance of the electroneutral polyelectrolyte Λ are known. It already has been demonstrated that eq 14 can be used to calculate the salt-free value of Λ from data obtained in salt-containing solutions of polyelectrolytes. Therefore f , the effective degree of dissociation of the polyelectrolyte, can be calculated from the conductance data obtained for NaPSS in NaCl and Na_2SO_4 solutions by combining eq 1 and 14.

$$f = \frac{\kappa - \kappa_s(D_2/D_2^0)}{N_p(\lambda_p + \lambda_c^0)} \quad (15)$$

The values of f so calculated are presented in Figure 13. Since Λ calculated by eq 14 is the equivalent conductance of the polyelectrolyte in the absence of simple salt, the calculated values of f are presented as a function of N_p rather than X . From Figure 13 it is seen that f is independent of the charge of the coion. In addition, above 0.010 N NaPSS f is nearly independent of the polyelectrolyte concentration. Between 0.010 and 0.10 N NaPSS the average value of f is 0.39, which compares reasonably well with the constant value of 0.33 predicted from the Manning theory for salt-free NaPSS at infinite dilution. Below 0.010 N NaPSS the value of f decreases with dilution of polyelectrolyte and appears to approach the Manning limiting value.

From conductance and transference measurements, Jordan et al.¹¹ also found f to be only slightly dependent on the polyelectrolyte concentration for salt-free solutions of both isotactic and atactic forms of NaPSS. The average value of f reported by these authors was 0.33, over a polyelectrolyte concentration range of 0.0004 to 0.0015 N. However, a direct comparison with these results is not possible since the polymer used by Jordan et al. had a

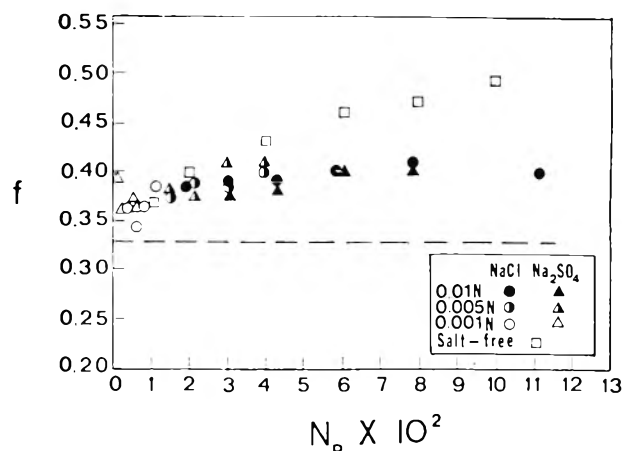


Figure 13. The apparent degree of dissociation f of NaPSS at 25 °C in aqueous solutions of NaCl and Na_2SO_4 as a function of the polyelectrolyte concentration N_p . The broken line is predicted from Manning's theory. The values of f for salt-free solutions of NaPSS are from ref 32.

higher degree of sulfonation, and the investigation was carried out over a lower concentration range of polyelectrolyte.

Dolar et al.³² have also used electric transport measurements to obtain f for salt-free solutions of NaPSS of varying molecular weights. Between 0.01 and 0.0 N polyelectrolyte f was shown to increase from 0.37 to 0.49, which at the lower concentrations of polyelectrolyte shows good agreement with the results obtained in this study, but at the higher NaPSS concentrations the results of the two studies differ by as much as 20%. This discrepancy is at least partially due to the fact that eq 15 makes use of the equivalent conductance of the sodium ion at infinite dilution $\lambda_{\text{Na}^+}^0$ whereas Dolar et al. used the equivalent conductance of the counterion in a solution of 1-1 electrolyte at a concentration corresponding to that of the free counterions in the polyelectrolyte solution λ_{Na^+} . In calculating f at finite concentrations of polyelectrolyte, neither approach is strictly valid. The use of $\lambda_{\text{Na}^+}^0$ neglects the mutual interactions of the simple ions; use of λ_{Na^+} assumes that the interactions between small ions are identical with those in polyelectrolyte-free solutions.

Acknowledgment. The authors are grateful to the American Can Company Foundation for partial support of this work.

References and Notes

- J. R. Huizenga, P. F. Grieger, and F. T. Wall, *J. Am. Chem. Soc.*, **72**, 4228 (1950).

- (2) F. T. Wall, H. Tereyama, and S. Techumpuck, *J. Polym. Sci.*, **20**, 477 (1956).
- (3) T. Kurucsev and B. J. Steel, *Rev. Pure Appl. Chem.*, **17**, 149 (1967).
- (4) G. S. Manning, *J. Phys. Chem.*, **79**, 262 (1975).
- (5) D. I. Devore and G. S. Manning, *J. Phys. Chem.*, **78**, 1242 (1974).
- (6) G. S. Manning, *J. Chem. Phys.*, **51**, 924 (1969).
- (7) G. S. Manning, *J. Chem. Phys.*, **51**, 934 (1969).
- (8) G. S. Manning, *J. Chem. Phys.*, **51**, 3249 (1969).
- (9) G. S. Manning, *Biopolymers*, **9**, 1543 (1970).
- (10) M. Kowblansky and P. Ander, *J. Phys. Chem.*, **80**, 297 (1976).
- (11) D. D. Jordan, T. Kurucsev, and M. L. Martin, *Trans. Faraday Soc.*, **65**, 606 (1969).
- (12) J. C. T. Kwak and R. C. Hayes, *J. Phys. Chem.*, **79**, 265 (1975).
- (13) J. Szymczak, P. Holyk, and P. Ander, *J. Phys. Chem.*, **79**, 269 (1975).
- (14) J. C. T. Kwak and A. J. Johnston, *Can. J. Chem.*, **53**, 792 (1975).
- (15) F. T. Wall, G. S. Stent, and J. J. Ondrejcin, *J. Phys. Colloid Chem.*, **54**, 979 (1950).
- (16) M. Nagasawa, I. Noda, T. Takahashi, and N. Shimamoto, *J. Phys. Chem.*, **76**, 2286 (1972).
- (17) F. T. Wall and W. B. Hill, *J. Am. Chem. Soc.*, **82**, 5599 (1960).
- (18) P. D. Ross, R. L. Scruggs, and G. S. Manning, *Biopolymers*, **14**, 1991 (1975).
- (19) S. Oman and D. Dolar, *Z. Phys. Chem. (Frankfurt am Main)*, **56**, 1 (1967).
- (20) R. A. Robinson and R. H. Stokes, "Electrolyte Solutions", Butterworths, London, 1959.
- (21) B. E. Conway, "Electrochemical Data", Elsevier, New York, N.Y., 1952.
- (22) P. R. Holyk, J. Szymczak, and P. Ander, *Macromolecules*, **80**, 1626 (1976).
- (23) F. T. Wall and M. J. Eitel, *J. Am. Chem. Soc.*, **79**, 1556 (1957).
- (24) A. Kowblansky, R. Sasso, V. Spagnuola, and P. Ander, submitted for publication.
- (25) G. S. Manning, *Annu. Rev. Phys. Chem.*, **23**, 117 (1972).
- (26) G. S. Manning in "Polyelectrolytes", E. Selegny, Ed., Reidel Publishing Co., Dordrecht, Holland, 1974, pp 9-39.
- (27) M. Nagasawa, *J. Polymer Sci., Symposium No. 49*, 1 (1975).
- (28) M. Nagasawa in "Polyelectrolytes", E. Selegny, Ed., Reidel Publishing Co., Dordrecht, Holland, 1974, pp 57-79.
- (29) R. Nelson, Ph.D. Thesis, Seton Hall University, 1969.
- (30) U. P. Strauss and S. Bluestone, *J. Am. Chem. Soc.*, **81**, 5292 (1959).
- (31) S. Bluestone, Ph.D. Thesis, Rutgers, The State University, 1960.
- (32) D. Dolar, J. Span, and S. Isakovic, *Biophys. Chem.*, **1**, 312 (1974).

Activation Parameters for the Diffusion and Viscosity of Ca^{2+} and Ce^{3+} and Their Chelates with EDTA and DCTA in Aqueous Solution

P. L. Mateo,* G. G. Hurtado, and J. B. Vidal-Abarca

Departamento de Química Física, Universidad de Murcia, Murcia, Spain (Received January 21, 1977)

The activation energy, enthalpy, entropy, and free energy for the diffusion of Ca^{2+} and Ce^{3+} ions and their respective chelates with ethylenediaminetetraacetic acid (EDTA) and *trans*-1,2-diaminocyclohexanetetraacetic acid (DCTA) in aqueous solution, and the activation energies for the viscous flow of these solutions have been obtained in the temperature range 10–35 °C. Some speculation is made regarding the comparison of these activation parameters with the ionic radii of the systems in terms of the structure and solvent interaction of these species. The hydrophobic contribution of the cyclohexane ring of DCTA complexes based on their activation entropy values is discussed.

Introduction

The molecular description of liquid ionic solutions lacks appropriate models to account for all the experimental evidence. The study of hydration in terms of solute-solvent interaction, and the transport phenomena of the resulting effective ionic entities in solution can provide valuable information concerning such models.¹

This work, intended as a contribution to the understanding of ionic solutions, presents experimental data for viscosity and diffusion of several ions in aqueous solution. In an attempt to determine the possible influence of complex agents in the transport processes investigated, the chosen system included simple ions, Ca^{2+} and Ce^{3+} , and their complexes with chelating agents, EDTA and DCTA. Experiments were carried out at six different temperatures between 10 and 35 °C to provide information about the activation parameters of these processes.

The experimental technique used to obtain the diffusion coefficients, the capillary cell method, has been shown to provide results which compare well with those obtained by other techniques.²

As expected from the low concentration of the solutions, the viscosity values and corresponding activation energies practically coincide with the respective values for pure

water within the experimental error. However, the diffusion and its activation parameters show a specific trend with distinctive values for each ion. Hydration, hydrogen bonding and hydrophobic interaction, and differences in the structure of chelate ions are discussed as possible sources for the diffusion-related values. The ionic radii of the species present in solution have also been used in the interpretation of the results.

Experimental Section and Results

Viscosity and Diffusion. Viscosity values, η , for the aqueous solutions of Ca^{2+} , Ce^{3+} , $(\text{CaEDTA})^{2-}$, $(\text{CaDCTA})^{2-}$, $(\text{CeEDTA})^{-}$, and $(\text{CeDCTA})^{-}$ ions in 10^{-3} M concentration were obtained using the Ostwald method.

Diffusion coefficients, D , of the above ions in the same solutions were experimentally determined using the capillary cell method of Anderson and Saddington³ as modified by Sancho et al.⁴ The tracer ions used, Ce-144 and Ca-45, were purchased from The Radiochemical Centre, Amersham (U.K.).

Values of η and D were obtained at six temperatures: 10, 15, 20, 25, 30, and 35 °C, and the precision of the temperature control was ± 0.1 °C. The pH of the solutions was adjusted to preclude hydrolysis in the case of the simple ions and, in the case of the chelate solutions, to keep all the metallic cation in its complex form. All chemicals employed were Merck of analytical grade and distilled and deionized water was used throughout.

* To whom correspondence should be addressed. Present address: Departamento de Química Física, Facultad de Ciencias, Universidad de Granada, Granada, Spain.

TABLE I: Viscosity Values, η (cP), for the Solutions Corresponding to the Six Listed Ions in 10⁻³ M Concentration^a

Temp, °C	Ca ²⁺	(CaEDTA) ²⁻	(CaDCTA) ²⁻
10	1.308	1.310	1.313
15	1.140	1.143	1.146
20	1.006	1.008	1.008
25	0.891	0.891	0.894
30	0.798	0.798	0.799
35	0.720	0.721	0.722
Temp, °C	Ce ³⁺	(CeEDTA) ⁻	(CeDCTA) ⁻
10	1.308	1.311	1.310
15	1.142	1.147	1.148
20	1.007	1.014	1.014
25	0.892	0.893	0.893
30	0.798	0.799	0.800
35	0.721	0.722	0.723

^a The mean estimated uncertainty (standard error of the mean of three experimental measurements) is ± 0.005 cP.

TABLE II: Diffusion Coefficients, $D \times 10^5$ cm² s⁻¹, for the Six Listed Ions in 10⁻³ M Concentration^a

Temp, °C	Ca ²⁺	(CaEDTA) ²⁻	(CaDCTA) ²⁻
10	0.448 \pm 0.003	0.324 \pm 0.002	0.271 \pm 0.007
15	0.543 \pm 0.01	0.373 \pm 0.002	0.350 \pm 0.002
20	0.644 \pm 0.005	0.444 \pm 0.005	0.413 \pm 0.008
25	0.693 \pm 0.02	0.504 \pm 0.02	0.454 \pm 0.004
30	0.821 \pm 0.01	0.586 \pm 0.02	0.541 \pm 0.01
35	0.913 \pm 0.008	0.635 \pm 0.02	0.615 \pm 0.009
Temp, °C	Ce ³⁺	(CeEDTA) ⁻	(CeDCTA) ⁻
10	0.291 \pm 0.006	0.266 \pm 0.003	0.215 \pm 0.01
15	0.366 \pm 0.01	0.300 \pm 0.01	0.254 \pm 0.006
20	0.408 \pm 0.02	0.345 \pm 0.009	0.330 \pm 0.006
25	0.460 \pm 0.01	0.408 \pm 0.009	0.355 \pm 0.006
30	0.540 \pm 0.02	0.483 \pm 0.02	0.422 \pm 0.01
35	0.620 \pm 0.004	0.547 \pm 0.01	0.501 \pm 0.01

^a The uncertainties are the standard error of the mean of four different experimental measurements.

Values of the absolute viscosity of the six solutions in centipoises (cP), and the diffusion coefficients for the respective ions in 10⁵ cm² s⁻¹, at each temperature, are shown in Tables I and II, respectively.

Activation Parameters. The parameters A_η , A_D , ΔE_η^\ddagger , and ΔE_D^\ddagger which appear in the equations

$$\eta = A_\eta e^{\Delta E_\eta^\ddagger / RT}$$

and

$$D = A_D e^{-\Delta E_D^\ddagger / RT}$$

are accepted to be functions of temperature, and several linear and potential relations have been proposed for the activation energy of diffusion, ΔE_D^\ddagger , as a function of T .⁵⁻⁷

Given the short range of temperature used in this work (25 °C), we have assumed those parameters to be constant as a first approximation, an assumption that also appears

accepted in the literature for similar cases.⁸⁻¹⁰ Hence, the values of activation energy of viscosity and diffusion were calculated from the least-squares fit of $\ln \eta$ and $\ln D$ respectively vs. $1/T$.

Now using the expression

$$D = \chi^2 (kT/h) e^{\Delta S^\ddagger / R} e^{-\Delta H^\ddagger / RT}$$

proposed by Eyring in the absolute rate theory,¹¹ the diffusion activation enthalpy, ΔH^\ddagger , and entropy, ΔS^\ddagger , were also obtained by the least-squares method of $\ln(D/T)$ vs. $1/T$. For this calculation we have considered those activation parameters to be constant in our range of temperature, and have used a value of 4.6×10^{-8} cm for χ , the mean distance between two equilibrium positions in the direction of the diffusion motion.¹²

Values for the free energy of activation, ΔG^\ddagger , were calculated from the equation $\Delta G = \Delta H - T\Delta S$ using the mean value of T (295.65 K) in the experimental temperature range. Values of ΔE_η^\ddagger , ΔE_D^\ddagger , ΔH^\ddagger , ΔG^\ddagger in kcal mol⁻¹, and ΔS^\ddagger in cal K⁻¹ mol⁻¹ are given in Table III.

Ionic Radii. We will use the Stokes-Einstein,¹³⁻¹⁴ R_{SE} , and Ottar,¹⁵ R_O , mean values in the temperature range for the ionic radii in the following discussion. These values were calculated from the expressions

$$R_{SE} = kT/6\pi D\eta$$

and

$$R_O = kT/8\sqrt{2\pi} D\eta$$

and are shown in Å in Table III. For a more extensive study of these and other values of ionic radii in solution see Mateo et al.¹⁶

Discussion

It is not possible to make a clear distinction between R_{SE} and R_O given their similar values in our results (Table III). Nevertheless, both series of values are initially very acceptable (in spite of the fact that the application of these radii is meant for somewhat larger entities in solution than ours) when compared with the bond lengths proposed by Hoard et al.¹⁷ and Lind et al.¹⁸ for complex species similar to the ones used in our experiments. From the data of these authors a minimum value of 4 Å could be estimated for the radius of (CeEDTA)⁻. The ionic size in solution could also depend on the possible presence of a second coordination sphere¹⁹ although our values do not seem to support this idea.

The ΔE_η^\ddagger values are practically constant for the six solutions (Table III) as could be anticipated from their very similar viscosity values (overlapping within experimental error) at each temperature (Table I). This similarity was nevertheless expected because of the low concentration of the ionic solutions, which is also responsible for the lack of evidence of any decrease in the viscosity in the case of large monovalent ions (i.e., (CeEDTA)⁻ and (CeDCTA)⁻

TABLE III: Activation Parameters and Ionic Radii Values^a

System	ΔE_η^\ddagger , kcal mol ⁻¹	ΔE_D^\ddagger , kcal mol ⁻¹	ΔH^\ddagger , kcal mol ⁻¹	ΔG^\ddagger , kcal mol ⁻¹	ΔS^\ddagger , cal K ⁻¹ mol ⁻¹	R_{SE} , Å	R_O , Å
Ca ²⁺	4.15	4.85	4.25	4.49	-0.8	3.44	3.23
(CaEDTA) ²⁻	4.17	4.82	4.22	4.69	-1.6	4.87	4.57
(CaDCTA) ²⁻	4.17	5.47	4.88	4.73	0.6	5.31	4.99
Ce ³⁺	4.15	5.04	4.44	4.71	-0.9	5.22	4.90
(CeEDTA) ⁻	4.17	5.15	4.55	4.78	-0.8	5.94	5.59
(CeDCTA) ⁻	4.16	5.79	5.18	4.88	1.0	6.79	6.38

^a See text for meaning of symbols. Estimated uncertainties: ΔE_η^\ddagger , ± 0.06 ; ΔE_D^\ddagger , ± 0.2 ; ΔH^\ddagger , ± 0.2 ; ΔG^\ddagger , ± 0.2 ; ΔS^\ddagger , ± 0.1 ; R_{SE} and R_O , ± 0.2 .

as proposed in the literature.¹⁹ Therefore, the viscosity data and their activation energies reported here can be mainly ascribed to the contribution of pure water.

In general, the absolute values of the diffusion activation parameters calculated (Table III) compare well with others obtained by several authors for comparable systems.^{8-10,20,21} Although the ionic solutions are very diluted, the ΔE_D^\ddagger values vary more than the ΔE_n^\ddagger values. An overall view and discussion of the diffusion activation parameters, together with the ionic radii, could then be attempted in terms of the interaction of the ionic species with the solvent. This would include the hydration of calcium and cerium ions in simple or complex form and the resulting hydrogen bonding of the hydrating water molecules with the free water, and the different interaction of the chelating agents EDTA and DCTA with the medium.

Thus, the comparison of Ca^{2+} and Ce^{3+} energetic activation parameters and radii values can be understood as the consequence of the higher hydration of the latter. This is in agreement with Hurtado et al.²² who already obtained 6 and 11 as minimum hydration values for Ca^{2+} and Ce^{3+} , respectively. It is interesting to note that Ce^{3+} shows higher values in radius, ΔE_D^\ddagger , ΔH^\ddagger , and ΔG^\ddagger than $(\text{CaEDTA})^{2-}$ possibly due to the high hydration of Ce^{3+} and the stronger interaction (more enthalpic) of these water molecules with the medium (hydrogen bonding) than the EDTA-water interaction.

The metallic ion produces a clear difference in ΔE_D^\ddagger , ΔH^\ddagger , ΔG^\ddagger , and radii values in the four complex species. Thus, chelated cerium gives rise to higher values in those parameters than does chelated calcium. A speculative explanation to account for this difference might be based on the fact that metal-coordinated water molecules seem to exist in lanthanides complexes in solution,^{17,18} and that there are no such molecules in the case of the Ca complexes,²³ due to a quite different configuration of the complex agents around each cation.

The entropy values (Table III), not yet discussed, deserve special attention. The positive values for the DCTA chelates, in contrast to the other ions, should be interpreted as a result of the hydrophobicity of the cyclohexane ring and the consequent increase in rigidity and order in the surrounding water molecules.²⁴ Thus, the energy barrier for the diffusion given by ΔE_D^\ddagger and ΔH^\ddagger is especially high for both DCTA complex and the comparatively lower values of the ΔG^\ddagger barrier for those ions comes as a result of the entropic contribution to the free energy of activation. These positive entropy values would then be the outcome of the breaking of the mentioned hydrophobic interaction in the activated state during the "diffusion jump" resulting in a momentary "loosening" in the neighboring water molecules. This entropic contribution would hence explain some additional comparisons. For example, the system $(\text{CaDCTA})^{2-}$ shows higher ΔE_D^\ddagger and ΔH^\ddagger and lower ΔG^\ddagger values than those of $(\text{CeEDTA})^-$ while the ΔS^\ddagger value is positive for the former and negative for the latter; similar reasoning would also be valid for the

comparison between Ce^{3+} and $(\text{CaDCTA})^{2-}$.

Our results are consistent with the Eyring relation, $\Delta E_D^\ddagger - \Delta H^\ddagger = RT$, within the limitations of our experimental error. This limitation in the measurements prevented our comparing this expression with the similar one

$$\Delta E_D^\ddagger - \Delta H^\ddagger = RT(C - \ln T)$$

where

$$C = \ln A_D - \ln (\chi^2 k/h) e^{\Delta S^\ddagger / R}$$

which was already proposed and compared with the Eyring relation using diffusion coefficients of 28 different ions at infinite dilution.²⁵

Finally, it should be emphasized that the experimental error in some of the results discussed above makes for a more speculative approach than desirable. We nevertheless believe that the trend in the reported values is consistent with the preceding discussion based primarily on hydration and the hydrophobic character of the DCTA chelates.

Acknowledgment. The authors gladly thank Dr P. A. Lyons for helpful suggestions and Ms. Gonul Velicelebi for stimulating discussion.

References and Notes

- (1) J. P. Hunt, "Metal Ions in Aqueous Solution", W. A. Benjamin, New York, N.Y., 1963, pp 19-45.
- (2) P. L. Mateo, Doctoral Thesis, University of Murcia, Murcia, Spain 1972.
- (3) J. S. Anderson and K. Saddington, *J. Chem. Soc.*, S-381 (1949).
- (4) J. Sancho, J. B. Vidal-Abarca, and G. G. Hurtado, *Anal. Quim.*, **63B**, 611 (1967).
- (5) G. J. Dienes, *Acta Metall.*, **13**, 433 (1965).
- (6) G. B. Gibbs, *Acta Metall.*, **13**, 926 (1965).
- (7) J. Lielmesz and A. P. Watkinson, *J. Chem. Phys.*, **45**, 2809 (1966).
- (8) J. W. Mullin and T. P. Cook, *J. Appl. Chem.*, **13**, 423 (1963).
- (9) E. Fishman and T. Vassiliades, *J. Phys. Chem.*, **63**, 1217 (1959).
- (10) J. W. Mullin and A. W. Nienow, *J. Chem. Eng.*, **9**, 526 (1964).
- (11) S. Glasstone, K. I. Laidler, and H. Eyring, "The Theory of Rate Processes", McGraw-Hill, New York, N.Y., 1941, pp 477-516.
- (12) S. Nir and W. D. Stein, *J. Chem. Phys.*, **55**, 1598 (1971).
- (13) G. Stokes, *Cambridge Phil. Soc. Trans.*, **9**, 5 (1856).
- (14) A. Einstein, *Ann. Phys.*, **17**, 549 (1905); **19**, 371 (1906).
- (15) B. Ottar, "Self-Diffusion and Fluidity in Liquids", Oslo University Press, Oslo, 1958.
- (16) P. L. Mateo, G. G. Hurtado, and J. B. Vidal-Abarca, *Anal. Quim.*, **69**, 717 (1973).
- (17) J. L. Hoard, L. Byungkook, and M. D. Lind, *J. Am. Chem. Soc.*, **87**, 1613 (1965).
- (18) M. D. Lind, L. Byungkook, and J. L. Hoard, *J. Am. Chem. Soc.*, **87**, 1611 (1965).
- (19) S. N. Vinogradov and R. H. Linnell, "Hydrogen Bonding", Van Nostrand, New York, N.Y., 1971, pp 213-215.
- (20) J. C. Bazan and A. J. Arvia, *Electrochim. Acta*, **10**, 10 (1965).
- (21) T. Uminski, J. Dera, and G. Kupryszewski, *Acta Phys. Pol.*, **28**, 17 (1965).
- (22) G. G. Hurtado, P. L. Mateo, and J. B. Vidal-Abarca, *Anal. Quim.*, **69**, 439 (1973).
- (23) F. Bermejo and A. Prieto, "Aplicaciones Analíticas del AEDT y Similares", Santiago University Press, Santiago de Compostela, Spain, 1960, pp 31-43.
- (24) C. Tanford, "The Hydrophobic Effect", Wiley, New York, N.Y., 1973, Chapter 1.
- (25) G. G. Hurtado, P. L. Mateo, and J. B. Vidal-Abarca, *Anal. Quim.*, **70**, 475 (1974).

External Heavy-Atom Effect on the Room-Temperature Luminescence of Adsorbed Dyes[†]

Wayne White and Paul G. Seybold*

Department of Chemistry, Wright State University, Dayton, Ohio 45431 (Received April 21, 1977)

Publication costs assisted by Wright State University

The effect of added alkali halide salts on the room-temperature fluorescence and phosphorescence of 2-naphthalenesulfonate adsorbed on filter paper has been examined. A normal external heavy atom effect on luminescence is observed, increasing strongly in the order NaF < NaCl < NaBr < NaI. The dependence of fluorescence quenching on perturber concentration can be described by a modified version of the Perrin equation. External heavy atoms increase the radiative triplet decay constant k_p more than the competing nonradiative constant k_{qp} . The results are consistent with an exchange interaction model between perturber and dye molecule, in which S \leftrightarrow T transition intensity is borrowed from electronic transitions of the perturbing halide ion, but charge-transfer involvement cannot be completely ruled out.

It is now a quarter century since Kasha¹ showed that environmental atoms of high atom number ("heavy atoms") can alter the rates of molecular spin-forbidden transitions. This *external heavy-atom effect* is distinguished from the *internal heavy-atom effect*, earlier demonstrated by McClure,^{2,3} wherein heavy atoms are chemically bonded to the affected aromatic compound. A large number of subsequent experimental and theoretical studies have been devoted to this topic,⁴⁻²⁵ confirming the original hypothesis¹ that the effect depends on spin-orbit coupling and describing the spectroscopic alterations brought on by the heavy atoms.

Despite the scrutiny it has received, many important features of the external heavy-atom effect remain obscure or confusing. Regarding the fundamental interaction between the aromatic compound and the heavy-atom perturbing species, some authors claim that charge-transfer complexes^{6-8,11,15a} are present, whereas others favor exchange interactions.^{9,13,14,23} Exciplexes have also sometimes been specifically mentioned.^{15b,26,27} The relative influence of external heavy atoms on the primary intersystem crossing rate constants k_{ISC} (nonradiative S₁ \rightarrow T), k_p (phosphorescence T₁ \rightarrow S₀), and k_{qp} (nonradiative T₁ \rightarrow S₀) is also a subject of some disagreement. Most, but not all,¹² studies show k_{ISC} to be the most strongly enhanced.^{6c,8,23a,27} As for the decay of the lowest triplet state, a majority opinion is that k_p is more enhanced by external heavy atoms than is k_{qp} , but both the opposite,^{6c} and a similar enhancement²⁰ have been reported. A related theoretical question concerns the means by which the radiative triplet decay process acquires intensity, whether by borrowing from allowed electronic transitions of the aromatic compound itself, from localized or delocalized transitions of the perturber, or from charge-transfer transitions of their complex.^{14,28} An interesting argument has been given^{6a,6b,8} that the external heavy-atom effect should be more effective when a strong internal heavy-atom effect is present, but a contrary example has appeared.^{10b,29} The functional forms of the dependence of heavy-atom effects on perturber concentration have not been firmly established for many important systems. Finally, even the presumably well-established heavy-atom mechanism for quenching of fluorescence in solution has recently been challenged.³⁰

A difficulty common to almost all previous studies of external heavy-atom effects on total luminescence and triplet state decay has been the necessity of using low-temperature rigid matrices (usually glasses or snows) because molecular phosphorescence is normally observed only under cryogenic conditions. (An exception is the study of Vander Donckt et al.,^{19a} who observed the fluorescence and phosphorescence of several aromatic compounds in room-temperature solutions of dimethylmercury.) The problems inherent in the use of low-temperature matrices are well documented,^{31,32} and include solubility limitations, optical and handling problems associated with cracking and snowing, nonrigidity, nonuniformities in the microenvironments, and sometimes photochemical complications. In general the necessity of carrying out experiments under cryogenic conditions is an inconvenience.

It has recently been discovered that many substituted polar and ionic aromatic compounds phosphoresce at room temperature in air when adsorbed onto certain surfaces.^{33,34} Surfaces promoting this effect include such common materials as filter paper, silica gel, alumina, polycellulose, and asbestos.^{33,34} In our view this phenomenon provides a unique opportunity for investigation of the external heavy-atom effect on total molecular luminescence at room temperature, and in addition its investigation might shed some light on the phenomenon of room-temperature phosphorescence (RTP), which remains essentially unexplained. We have previously reported that an external heavy-atom effect can be induced in these room-temperature systems, and that this effect can be used as a practical aid in luminescence analysis.³⁵ Here we examine several aspects of this problem in greater detail.

Our primary aims in the present study have been (1) to ascertain the functional dependence of the heavy-atom effects on perturber concentration in these room-temperature matrices, both for practical and theoretical use, (2) to determine whether the radiative or the nonradiative triplet decay process is more susceptible to heavy-atom enhancement, and (3) to gain whatever insights the results might reveal about both the mechanism of the external heavy-atom effect and the RTP phenomenon. We have chosen the dye 2-naphthalenesulfonate for special examination because it is readily available, easily purified, displays strong RTP, and appears fairly representative of a broad class of polar and/or ionic naphthalene derivatives in its behavior. Alkali halide salts have been employed as

[†] Presented at the First Chemical Congress of the North American Continent, Mexico City, Dec 3, 1975.

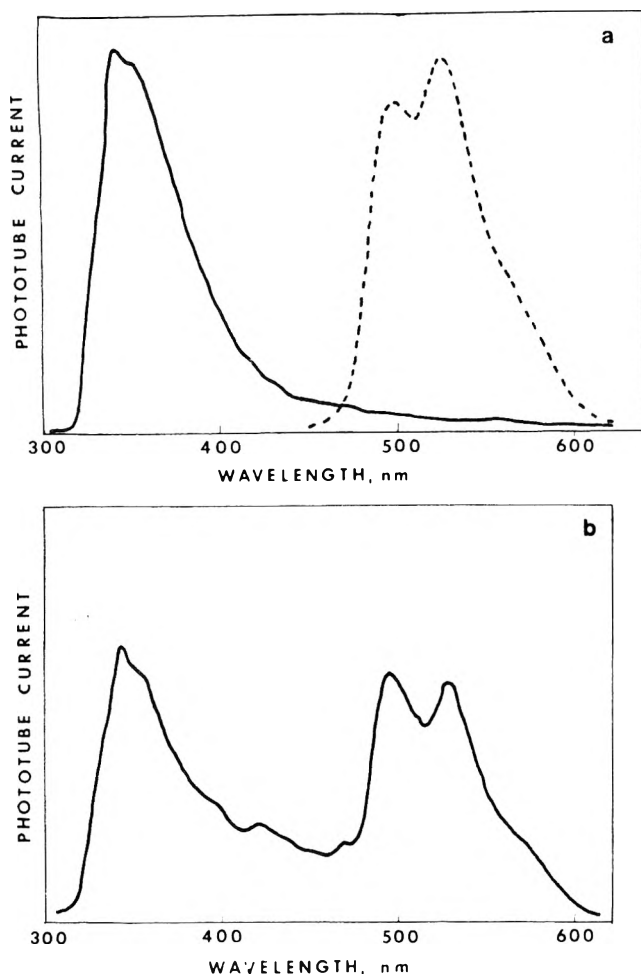


Figure 1. Room-temperature luminescence of 1-naphthol adsorbed on filter paper: (a) (—) total luminescence, (---) phosphorescence; (b) total luminescence when doped with 1.0 M sodium iodide.

heavy-atom perturbors because they are available in high purity and are soluble in high concentrations in aqueous solutions.

Experimental Section

Instrumental. Luminescence spectra were recorded on an Hitachi-Perkin-Elmer MPF-2A fluorescence spectrometer equipped with an R-106 photomultiplier tube (S-19 cathode response). Room-temperature phosphorescence spectra of untreated samples were obtained with a rotating-can phosphorescence accessory, using a specially designed plastic holder and without the usual dewar assembly. Total emission spectra of heavy-atom treated samples were taken using the fluorescence mode of the instrument. Samples on filter paper surfaces were taped to rigid flat-black metal plates, which were then placed securely at a 45° angle in the cuvet compartment. Because humidity strongly quenches the phosphorescence a stream of dry breathing air was directed at the sample during most measurements. Extreme rigidity in the sample position was necessary to assure reproducibility; the cuvet holder was bound with metal wire to prevent any movement, and extreme care was taken in positioning samples.

Chemicals. Alkali halides were reagent grade, carefully desiccated before weighing. Naphthalene derivatives were purified by recrystallization.

Preparation of Heavy-Atom Samples. Dye solutions (10 mM) were prepared with appropriate concentrations of heavy atoms, from 0–1.0 M. These solutions were spotted on Whatman No. 4 filter paper using a 100- μ L pipet and

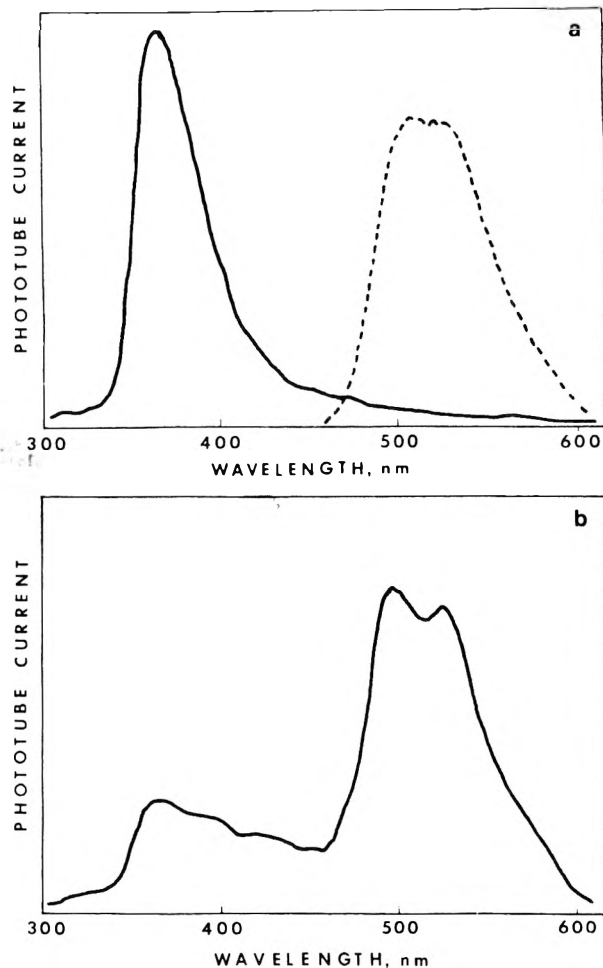


Figure 2. Room-temperature luminescence of 2-naphthol-7-sulfonate adsorbed on filter paper: (a) (—) total luminescence, (---) phosphorescence; (b) total luminescence when doped with 1.0 M sodium iodide.

allowed to dry in air for 20 min. Each sample was then dried with a heat gun for 30 s in a controlled manner. Appropriately sized cuts were taken from the sample spots and taped onto metal plates as described above. Two minutes were allowed for positioning of the sample in the instrument, before initiation of a spectrum. Because the intensity of sample luminescence appeared to be sensitive to ultraviolet light, care was taken to avoid undue exposure.

Results

The effects of heavy-atom treatment on the room-temperature luminescences of 1-naphthol and 2-naphthol-7-sulfonic acid (Na salt) adsorbed on filter paper are shown in Figures 1 and 2. In each case the first spectrum shows the total luminescence of the adsorbed dye as well as its phosphorescence isolated using the phosphorescence accessory; the second spectrum shows the total luminescence of the dye with added 1.0 M sodium iodide. The intensities are arbitrary and not directly comparable, but the common result in these cases is that fluorescence is drastically quenched and phosphorescence enhanced by the added heavy atom. The effect is seen to be somewhat stronger for 2-naphthol-7-sulfonate than for 1-naphthol.

The effect of different concentrations of sodium iodide on the luminescence of adsorbed 2-naphthalenesulfonic acid (Na salt) is demonstrated in Figure 3. This figure illustrates the progressive nature of the influence of the concentration of the heavy-atom perturber. The effects of the salts NaBr and NaI on the room-temperature luminescence of this dye are further illustrated in Figures

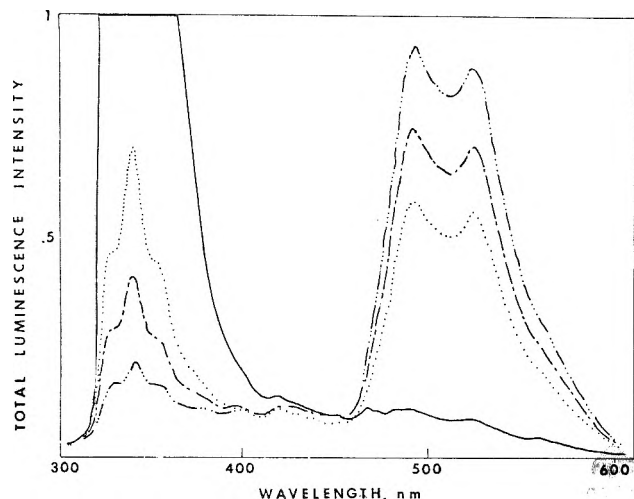


Figure 3. Room-temperature luminescence of 2-naphthalenesulfonate adsorbed on filter paper, with (—) no iodide (peak intensity $\sim 5\times$ that of the 0.30 NaI sample); (···) 0.3 M NaI; (---) 0.42 M NaI; and (-·-·-) 1.0 M NaI.

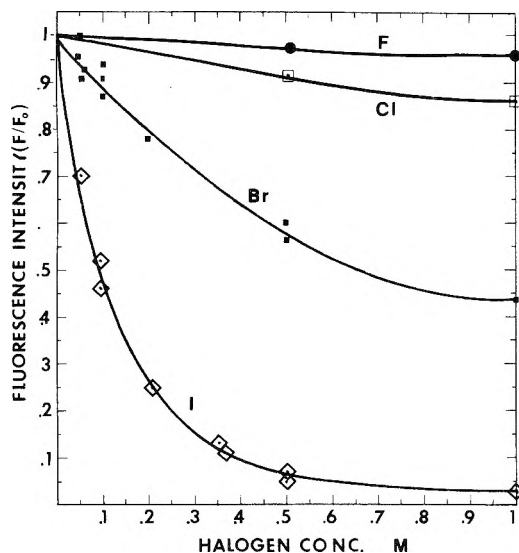


Figure 4. Concentration dependence of fluorescence quenching of adsorbed 2-naphthalenesulfonate by sodium halides.

4 and 5. Each data point in the figures is an average of about four experimental values. Phosphorescence enhancement due to NaF and NaCl, if present, was not measurable, and quenching of fluorescence was relatively small. At 1 M concentrations NaF reduced the fluorescence intensity by about 5% and NaCl by about 14%. The effect of NaBr, although less than that of NaI, is evident both on fluorescence and phosphorescence. Because the phosphorescence intensities of untreated samples were low and difficult to compare with other values, the phosphorescence enhancement data are shown relative to the phosphorescence intensity of a sample treated with 1.0 M sodium iodide.

Discussion

The general results are in qualitative agreement with those found in low-temperature systems,^{5,6} and also with the normal expectation that a spin-orbit coupling effect should increase with the atomic number of the perturbing heavy atom.^{2,7,8,27} The slightly different extents of the effect on the different compounds illustrates the expectation that the effect should vary from compound to compound,^{34,35} possibly depending on such factors as the positions of the energy levels,²² the extent of internal

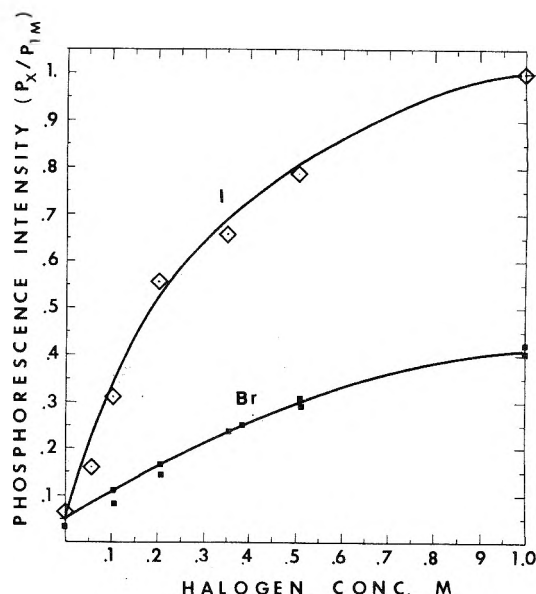


Figure 5. Enhancement of the room-temperature phosphorescence of adsorbed 2-naphthalenesulfonate by added sodium bromide and sodium iodide ($X = \text{halide concentration}$).

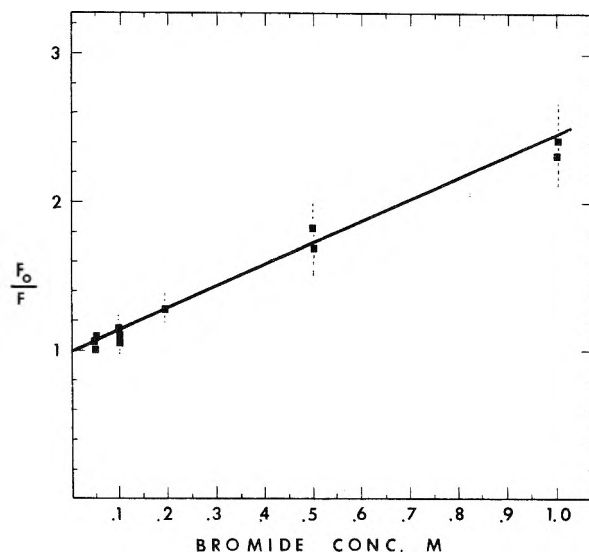


Figure 6. Stern-Volmer plot for quenching of fluorescence of adsorbed 2-naphthalenesulfonate by NaBr.

spin-orbit coupling,^{6a} and the unperturbed phosphorescence yield.²¹

We first examine the quenching of fluorescence by the heavy atoms in the system. Several models have been employed to describe the dependence of fluorescence quenching on the concentration of an external perturber. Because only bromide and iodide ions caused significant quenching, we shall focus attention mainly on these ions. *Dynamic quenching* in solutions is usually described in terms of the classic Stern-Volmer relationship³⁶

$$F_0/F = 1 + k[Q] \quad (1)$$

where F and F_0 are the fluorescence intensities with and without quencher, respectively, $[Q]$ is the quencher concentration, and k is a constant. For the case of *static quenching* in solutions a similar relationship has been proposed^{37,38} in which k is reinterpreted as an equilibrium constant K for the formation of a nonfluorescent complex between fluorophore and quencher. Thus this seemed an appropriate model to examine for the present systems. Attempts to fit our data to this type of dependence are shown in Figures 6 and 7. It is seen that the bromide

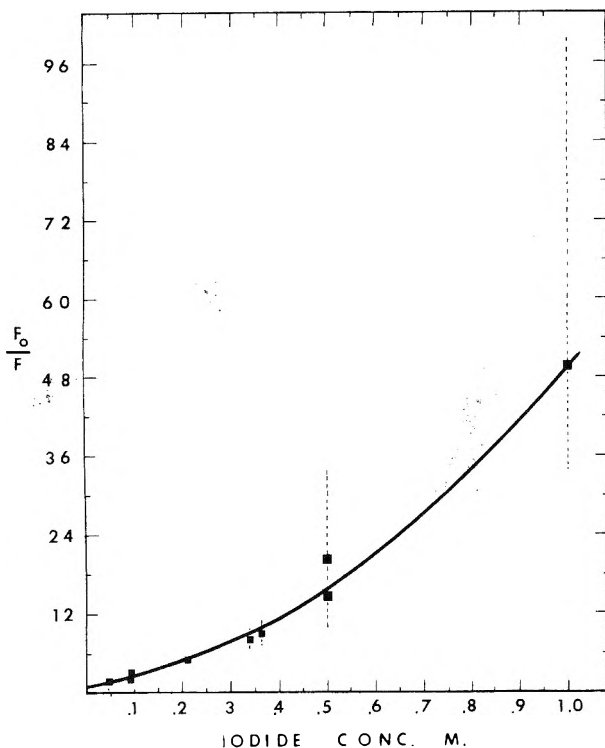


Figure 7. Stern-Volmer plot for quenching of fluorescence of adsorbed 2-naphthalenesulfonate by NaI.

results fit satisfactorily, but that the iodide results cannot be accounted for by this formula.

Another model sometimes used to describe fluorescence quenching is the "quenching sphere" model of Perrin.³⁹ In this model quenching is assumed to be complete for all fluorophore molecules within an "active sphere" of radius R about the quencher, and there is no quenching outside this sphere. This model leads to the dependence

$$F = F_0 e^{-v[Q]} \quad (2)$$

wherein v is the molar "quenching volume". We have compared our data with this model and find, as for the Stern-Volmer model, that the bromine data fit reasonably well, but the iodine data do not. It may be that for bromine and the lighter halogens, for which the data can be fit to either a Stern-Volmer or Perrin variation, quenching is still small enough to fall within some initial linear range of dependence. Only the iodine results, for which quenching is strong, provide a critical test of the dependence on concentration.

The Perrin model itself is unrealistic in several ways. First, it assumes a sharp cutoff in quenching at a distance R , whereas in reality a more gradual distance dependence must exist. This is more a formal than an actual objection, because the statistics of a more gradual variation lead to some "effective radius" at which, say, quenching is 50% effective, and R may be reinterpreted generally in this manner. More serious in the present context, however, is the assumption that at short distances the perturber completely quenches fluorescence. Studies of the internal heavy-atom effect, which is stronger than the external effect studied here, show that fluorine, chlorine, and bromine substituents do not completely quench naphthalene fluorescence.⁴⁰ (In fact the fluorescence yield of 1-fluoronaphthalene is higher than that of naphthalene because a symmetry restriction is removed.) Our data seem to indicate that the fluorescence quenching by each halogen approaches a saturation value; beyond a certain point higher halogen concentrations have little effect on fluorescence intensity.

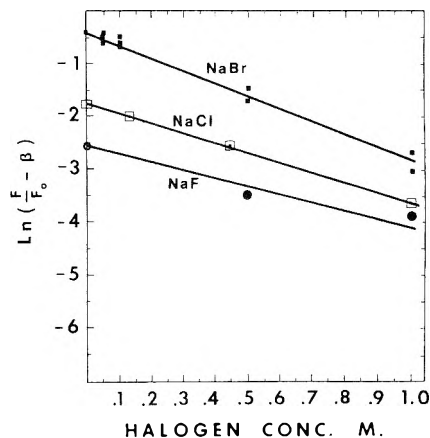


Figure 8. Modified Perrin plots (see text) for quenching of fluorescence of adsorbed 2-naphthalenesulfonate by sodium halides.

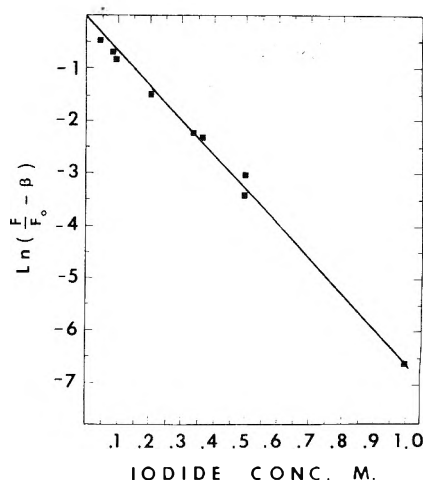


Figure 9. Modified Perrin plot (see text) for quenching of fluorescence of adsorbed 2-naphthalenesulfonate by sodium iodide.

TABLE I

	$v, \text{L mol}^{-1}$	β
Fluorine	1.6	0.93
Chlorine	1.9	0.83
Bromine	2.3	0.36
Iodine	6.5	0.018

Accordingly, we have modified the Perrin equation to account for incomplete quenching by the external perturber. The more general form of Perrin's equation is

$$F/F_0 = (1 - \beta)e^{-v[Q]} + \beta \quad (3)$$

where β is the residual fraction of fluorescence that remains unquenched at high concentrations of perturber. The linear form of eq 3 is

$$\ln\left(\frac{F}{F_0} - \beta\right) = \ln(1 - \beta) - v[Q] \quad (4)$$

If eq 3 and 4 are valid, a plot of $\ln(F/F_0 - \beta)$ vs. $[Q]$ should yield a straight line. Such plots for the four halogens used in the present experiments are shown in Figures 8 and 9. In these, values of β were chosen as reasonable estimates for each halogen, and are close to, but less than, the relative fluorescence intensities at 1 M concentration of halogen. It is seen that good linear plots are obtained in all cases.

Values of v and β from the modified Perrin plots are shown in Table I. We note here that the values calculated for v depend somewhat on the values chosen for β . For

iodine, the radius of the Perrin sphere calculated from v is 14 Å, which can be compared with the ionic radius of the iodide ion of 2.2 Å. This is of the same order of magnitude, or just slightly larger than, values found for heavy-atom quenching in low-temperature systems.^{16,23}

To summarize, a modified Perrin equation gives an excellent fit for all the halogen quenching data, and appears conceptually reasonable for the present case. The Stern–Volmer and normal Perrin models adequately represent the quenching due to the lighter halogens but not iodide results, possibly because quenching by the lighter halogens is slight and falls within some initial linear range of variation. Quenching by iodide could conceivably proceed by a different mechanism from that of the other halogens, but this seems unlikely. Admittedly the modified Perrin equation contains two parameters, and it is not surprising that such an equation yields a better fit for our data than the single parameter Stern–Volmer and Perrin equations. None-the-less the results are sufficiently good that we feel they have some validity.

There is some controversy about whether external heavy atoms increase the radiative triplet decay rate constant k_p or the nonradiative constant k_{qp} more strongly.^{5,6,11,12,14,20,23,27} Most workers have found that the radiative rate is more effectively enhanced,^{5,6,11,12,14,16,23} and in some cases it has been asserted that the nonradiative rate is not enhanced at all.^{11,23} However both a comparable increase in the two rates²⁰ and a stronger enhancement of the nonradiative rate have been reported.^{6c} Our present data on room-temperature luminescence allow a determination of this question for the particular case of 2-naphthalenesulfonate (2-NSA) adsorbed on filter paper.

The phosphorescence yield ϕ_p is equal to

$$\phi_p = \frac{k_p}{k_p + k_{qp}} \phi_T \quad (5)$$

where ϕ_T is the triplet yield. Enhancement of ϕ_p as observed in these experiments can be due either to an increase in ϕ_T or in k_p . If ϕ_p increases more quickly than does ϕ_T the increase occurs because k_p is more enhanced than k_{qp} . It is generally agreed that external heavy atoms strongly enhance the intersystem crossing rate k_{ISC} from the lowest excited singlet state to the triplet. However, if the unperturbed dye has a finite triplet yield there is a limit to how much ϕ_p can be increased by this means since ϕ_T cannot in any case exceed unity.

We do not have a triplet yield value for unperturbed 2-naphthalenesulfonate adsorbed on filter paper, but enough information is available to make a reasonably accurate estimate. Triplet yield studies for naphthalene and a number of other polycyclic aromatic hydrocarbons show convincingly that direct internal conversion $S_1 \rightarrow S_0$ is unimportant in these compounds.^{10c,41,42} Thus $\phi_f + \phi_T \approx 1$. It would be extremely difficult to obtain the fluorescence yield of 2-NSA under the present circumstances, but for a rough and perhaps high estimate we can assume that it approximates the value of simple naphthalene derivatives in low-temperature solution,⁴⁰ i.e., ~ 0.75 . Thus the triplet yield should be of the order of 0.25. Consequently, an increase in k_{ISC} caused by external heavy atoms, no matter how large, cannot increase ϕ_p by more than a factor of about 4. Our experiments indicate that 1 M bromide ion increases the phosphorescence intensity by a factor greater than 8, and 1 M iodide increases this intensity by a factor of about 20. Both of these values are well in excess of any enhancement that could reasonably be expected from increased ϕ_T only. We conclude, therefore, that the radiative rate k_p has been enhanced

more than the nonradiative rate k_{qp} by the external heavy atoms.

What do these results tell us about the mechanism of quenching in this system? In their important early investigation of the external heavy atom effect McGlynn et al.⁶ proposed that the aromatic molecule M and the heavy atom perturber species P form a charge-transfer complex, with M as donor and P as acceptor. They have summarized evidence in support of their model,⁸ and it has been supported in other work.^{11,15a} More recently, some authors^{14,23} have questioned this view and favor a mechanism involving exchange interactions.^{9,13} Unfortunately these two models have proven difficult to distinguish experimentally. Of these two alternatives several lines of circumstantial evidence lead us to favor an exchange mechanism in the present system. First, absorption measurements in solutions²³ have failed to detect complexes between I⁻ ions and either fluorene or triphenylene, although both displayed external heavy-atom effects in low-temperature glasses.²³ Secondly, it is difficult to envision the negative I⁻ ion as an effective electron acceptor in a charge-transfer complex, especially with respect to a neutral aromatic compound such as naphthol. Furthermore, the isoelectronic (to I⁻) species Xe and Cs⁺ are considerably less effective heavy-atom perturbers than is I⁻.^{15a,25,43} although one would expect them to be more effective electron acceptors on the basis of their nuclear charges. This does not, of course, rule out the possible participation of charge-transfer complexes in other systems, e.g. where alkyl halides are used as perturbers.⁶ Nor does it exclude the possibility that charge-transfer transitions in which the I⁻ ion acts as a donor might be involved.³⁰

Both charge-transfer and exchange interactions are relatively short ranged. Taken at face value our iodide quenching radius of 14 Å seems large by either standard, although a radius of 9 Å has been said to be consistent with an exchange mechanism.²³ However, the special nature of the systems under investigation here requires that caution be exercised in interpreting the meaning of the value for R . Presumably the phenomenon of room-temperature phosphorescence arises because dyes become trapped in the interstices of the matrix and there are either protected from oxygen, held very rigid, or subjected to some special kind of interaction.³⁴ Thus the matrix may considerably restrict the spatial freedom of approach and/or contact between fluorophore and quencher, so that the model of a quenching sphere may not really be appropriate.

Of the mixing schemes that have been developed to account for the increased radiative triplet decay, the pronounced increase in k_p is at least consistent with the "second-order multiplicity covariant interaction" picture proposed by Robinson¹³ and supported by Giachino and Kearns¹⁴ and others.²³ In this scheme (exchange) interactions between the partners mix in perturber transitions made allowed by spin-orbit coupling. In the present case this would mean intensity is borrowed from localized transitions of the I⁻ ion. Recent investigations indicate that borrowing from allowed transitions of the aromatic compound itself is not important for the external heavy-atom effect.^{14,15,23c} Still, some type of participation by charge-transfer transitions in the intensity borrowing scheme cannot be completely ruled out. For both exchange and charge-transfer cases intensity borrowing is expected to be proportional to S^4 , where S is the intermolecular MO overlap integral.⁸ We hope that experimental investigations currently underway in our laboratory will help to

shed light on this general question.

Acknowledgment. We thank Dr. Barry Smith for his helpful advice at the beginning of this study.

References and Notes

- (1) M. Kasha, *J. Chem. Phys.*, **20**, 71 (1952).
- (2) D. S. McClure, *J. Chem. Phys.*, **17**, 905 (1949).
- (3) E. H. Gilmore, G. E. Gibson, and D. S. McClure, *J. Chem. Phys.*, **20**, 829 (1952); **23**, 399 (1955).
- (4) E. Clementi and M. Kasha, *J. Chem. Phys.*, **26**, 956 (1957).
- (5) G. W. Robinson, *J. Mol. Spectrosc.*, **6**, 58 (1961).
- (6) (a) S. P. McGlynn, R. Sunseri, and N. Christodouleas, *J. Chem. Phys.*, **37**, 1818 (1962); (b) S. P. McGlynn, M. J. Reynolds, G. W. Daigre, and N. D. Christodouleas, *J. Phys. Chem.*, **66**, 2499 (1962); (c) S. P. McGlynn, J. Daigre, and F. J. Smith, *J. Chem. Phys.*, **39**, 675 (1963); (d) S. P. McGlynn, T. Azumi, and M. Kasha, *ibid.*, **40**, 507 (1964); (e) V. Ramakrishnan, R. Sunseri, and S. P. McGlynn, *ibid.*, **45**, 1365 (1966).
- (7) S. P. McGlynn, F. J. Smith, and G. Cilento, *Photochem. Photobiol.*, **3**, 269 (1964).
- (8) S. P. McGlynn, T. Azumi, and M. Kinoshita, "Molecular Spectroscopy of the Triplet State", Prentice-Hall, Englewood Cliffs, N.J., 1969, Chapter 8.
- (9) (a) G. J. Hoijtink, *Mol. Phys.*, **3**, 67 (1960); (b) C. Dijkgraaf and G. J. Hoijtink, *Tetrahedron Suppl.*, **2**, 179 (1963).
- (10) (a) T. Medinger and F. Wilkinson, *Trans. Faraday Soc.*, **61**, 620 (1965); (b) A. Kearvell and F. Wilkinson, *Mol. Cryst.*, **4**, 69 (1968); (c) A. R. Horrocks and F. Wilkinson, *Proc. R. Soc. London, Ser. A*, **308**, 257 (1968).
- (11) K. B. Eisenthal and M. A. El-Sayed, *J. Chem. Phys.*, **42**, 794 (1965).
- (12) S. Siegel and H. S. Judeikis, *J. Chem. Phys.*, **42**, 3060 (1965).
- (13) G. W. Robinson, *J. Chem. Phys.*, **46**, 572 (1967).
- (14) G. G. Giachino and D. R. Kearns, *J. Chem. Phys.*, **52**, 2964 (1970); **53**, 3886 (1970); **54**, 3248 (1971).
- (15) (a) R. H. Hofeldt, R. Sahai, and S. H. Lin, *J. Chem. Phys.*, **53**, 4512 (1970); (b) R. Sahai, R. H. Hofeldt, and S. H. Lin, *Trans. Faraday Soc.*, **67**, 1690 (1971); (c) K. C. Lin and S. H. Lin, *Mol. Phys.*, **21**, 1105 (1971).
- (16) (a) S. E. Webber, *J. Phys. Chem.*, **75**, 1921 (1971); (b) L. G. Thompson and S. E. Webber, *ibid.*, **76**, 221 (1972).
- (17) (a) P. M. Johnson and L. Ziegler, *J. Chem. Phys.*, **56**, 2169 (1972); (b) Y.-P. Hsu and P. M. Johnson, *ibid.*, **59**, 136 (1973).
- (18) I. B. Berlman, *J. Phys. Chem.*, **77**, 562 (1973).
- (19) (a) E. Vander Donckt, M. Matagne, and M. Sapis, *Chem. Phys. Lett.*, **20**, 81 (1973); (b) E. Vander Donckt and C. Vogels, *Spectrochim. Acta, Part A*, **27**, 2157 (1971).
- (20) Z. R. Grabowska and N. Sadlej in "Proceeding of the International Conference on Luminescence", F. Williams, Ed., Plenum Press, New York, N.Y., 1973, p. 314.
- (21) J. J. Aaron, J. J. Mousa, and J. D. Winefordner, *Talanta*, **20**, 279 (1973).
- (22) (a) M. Zander, *Z. Naturforsch. A*, **28**, 1869 (1973); (b) I. Dreeskamp and M. Zander, *ibid.*, **28**, 1743 (1973); (c) H. Dreeskamp, E. Koch, and M. Zander, *Ber. Bunsenges. Phys. Chem.*, **78**, 1328 (1974); *Chem. Phys. Lett.*, **31**, 251 (1975).
- (23) (a) J. Najbar and W. Barzyk, *J. Lumin.*, **8**, 242 (1974); (b) J. Najbar, *ibid.*, **11**, 207 (1975/76); (c) J. Najbar and A. Chodkowska, *ibid.*, **11**, 215 (1975/76).
- (24) R. P. DeToma and D. O. Cowan, *J. Am. Chem. Soc.*, **97**, 5283, 3291 (1975).
- (25) L. K. Patterson and S. J. Rzed, *Chem. Phys. Lett.*, **31**, 254 (1975).
- (26) B. Stevens, *Adv. Photochem.*, **8**, 161 (1971).
- (27) J. B. Birks, "Photophysics of Aromatic Molecules", Wiley-Interscience, New York, N.Y., 1970.
- (28) N. K. Chaudhuri and M. A. El-Sayed, *J. Chem. Phys.*, **42**, 1947 (1965).
- (29) However see ref 24.
- (30) A. R. Watkins, *J. Phys. Chem.*, **77**, 1207 (1973); **76**, 1885, 2555 (1974).
- (31) E. L. Wehry, *Fluoresc. News*, **8**(3), 21 (1974).
- (32) J. D. Winefordner and P. A. St. John, *Anal. Chem.*, **35**, 2211 (1963).
- (33) E. M. Schulman and C. Walling, *Science*, **178**, 53 (1972); *J. Phys. Chem.*, **77**, 902 (1973).
- (34) P. G. Seybold, R. K. Sorrell, and R. A. Schuffert, Abstracts, presented at the 165th National Meeting of the American Chemical Society, Dallas, Tex., Apr 1973.
- (35) P. G. Seybold and W. White, *Anal. Chem.*, **47**, 1199 (1975).
- (36) O. Stern and M. Volmer, *Phys. Z.*, **20**, 183 (1918).
- (37) H. Boaz and G. K. Rollefson, *J. Am. Chem. Soc.*, **72**, 3435 (1950).
- (38) W. M. Vaughan and G. Weber, *Biochemistry*, **9**, 464 (1970).
- (39) F. Perrin, *Compt. Rend.*, **178**, 1978 (1924).
- (40) V. L. Ermolaev and K. K. Svitashv, *Opt. Spectrosc.*, **7**, 399 (1959).
- (41) C. A. Parker and T. A. Joyce, *Trans. Faraday Soc.*, **62**, 2785 (1966).
- (42) K. Sandros, *Acta Chem. Scand.*, **23**, 2815 (1969).
- (43) A. R. Horrocks, A. Kearvell, K. Tickle, and F. Wilkinson, *Trans. Faraday Soc.*, **62**, 3393 (1966).
- (44) G. Niday and P. G. Seybold, work in progress.

The 123.6-nm Photolysis of 1,2-Fluorochloroethane and 1,1,1-Difluorochloroethane

T. Ichimura, A. W. Kirk, and E. Tschuikow-Roux*

Department of Chemistry, The University of Calgary, Calgary, Alberta, Canada T2N 1N4 (Received June 1, 1977)

1,2-Fluorochloroethane and 1,1,1-difluorochloroethane were photolyzed at 123.6 nm both in the presence and absence of NO. The effects of added CF₄ were also investigated. The results are compared with those obtained for the corresponding 147-nm photolyses. Despite the fairly large increase in the photon energy (37 kcal mol⁻¹), the photochemistry of 1,1,1-difluorochloroethane at 123.6 nm is virtually unchanged from that at 147 nm. While the primary processes occurring in the 123.6-nm photolyses of 1,2-fluorochloroethane are also apparently unchanged, there is an increase in the quantum yield for molecular HCl elimination with a corresponding decrease in carbon-halogen bond fission. This latter finding is qualitatively analogous to previous results obtained for 1,1,1-trifluoro-2-chloroethane. The ability of molecules of this type to absorb very large amounts of energy, and undergo mainly molecular elimination without significant further decomposition of the olefinic elimination products is surprising, yet characteristic. The facile nature of the elimination reactions is thought to be due to the properties of the excited Rydberg states formed at these wavelengths. The reasons for the lack of decomposition of the elimination products are more difficult to understand.

Introduction

We have stated our intention, previously, of investigating the ultraviolet photolyses of haloethanes, particularly chloroethanes, as a function of the wavelength of the incident radiation.¹ Having completed a number of studies on the 147-nm photolyses of ethyl chloride,¹ 1,1-dichloroethane,² 1,1,1-trichloroethane,³ 1,2-fluorochloroethane,⁴ 1,1,1-difluorochloroethane,⁵ and 1,1,1-trifluoro-2-chloroethane,⁶ we have recently begun to investigate the

123.6-nm photolyses of these molecules, beginning with the latter compound.⁶ This paper describes the results obtained for the 123.6-nm photolyses of 1,2-fluorochloroethane (CH₂FCH₂Cl) and 1,1,1-difluorochloroethane (CH₃CF₂Cl). The 123.6-nm photolysis of ethyl chloride has already been carefully investigated by Cremieux and Herman⁷ and to some extent by Tiernan and Hughes.⁸ Molecular elimination of HCl was determined to be the dominant primary process. Cremieux and Herman also

TABLE I: Photolysis of $\text{CH}_3\text{CF}_2\text{Cl}$ at 123.6 nm

Run no.	$P_{\text{CH}_3\text{CF}_2\text{Cl}}$, Torr	P_{additive} , Torr		Quantum yields (Φ)				
				CH_2CF_2	CH_2CHF	CHCF	CH_4	CH_2CFCl
1	6.4			0.83 ₆	0.02 ₅	0.01 ₅	0.01 ₄	
2	6.9			0.80 ₀	0.04 ₈	0.02 ₁	0.02 ₀	0.05 ₄
3	6.9	He	9.4	0.84 ₅	0.02 ₈	0.01 ₈	0.02 ₁	0.04 ₁
4	9.4			0.83 ₁	0.03 ₅	0.01 ₆	0.01 ₈	
5	7.2	NO	0.14	0.81 ₈	0.03 ₂	0.01 ₉	~0.00	0.03 ₆
6	8.1	CF_4	291	0.79 ₂	0.04 ₉	0.00	0.02 ₀	
7	7.5	NO	0.42	0.80 ₅	0.03 ₉	~0.00	~0.00	0.04 ₀
		CF_4	83					
8	8.0	NO	0.41	0.86 ₁	0.03 ₂	0.00	0.00	
		CF_4	237					
9	7.2	H_2S	0.14	0.82 ₀	0.02 ₇	0.01 ₇	0.04 ₁	
10	8.3	HI	0.10	0.80 ₄	0.03 ₃	0.01 ₆	0.04 ₃	

investigated the photolysis of ethyl chloride at 105–107 nm⁷ where again molecular elimination of HCl from electronically excited neutral molecules was prominent. The extent of carbon-halogen bond fission was not large at either wavelength, nor apparently was the extent of the further decomposition of ethylene. It now appears that these observations are characteristic of the vacuum ultraviolet photolyses of chloroethanes. Carbon-halogen bond fission appears to be characteristic of longer wavelength photolyses, that is at the threshold of ultraviolet absorption. Fujimoto and Wijnen⁹ showed this clearly in their study of the photolysis of 1,1-dichloroethane using a medium pressure mercury arc. These early observations coupled with our more recent data have led us to believe that carbon-halogen bond fission is the result of the formation of states corresponding to $n \rightarrow \sigma^*$ transitions and molecular eliminations are the result of the formation of states corresponding to Rydberg transitions such as $n \rightarrow 4s$ and $n \rightarrow 4p$. One might further expect the lifetimes of such states to be commensurate with their degree of vibrational excitation. Sandorfy has independently drawn similar conclusions in his recent reviews.¹⁰

Experimental Section

The photolyses were carried out at room temperature in the same apparatus as described previously.⁴⁻⁶ The titanium filament gettered krypton lamp was similar in design to that used by Gordon et al.,¹¹ the lithium fluoride window having a thickness of 0.5 mm. The lamp was powered by a microwave generator (KIVA Instruments Inc., Model MPG 4M) at a power level that gave an intensity at 123.6 nm of $8.4 \pm 1.2 \times 10^{12}$ photons s⁻¹. Chromatic purity checks using a McPherson (218-0.3 m) vacuum ultraviolet monochromator showed that the contribution to the emission at 165 nm was negligible. The window was opaque to wavelengths shorter than 110 nm. Photolysis times were such that the overall conversions did not exceed 0.1%. Actinometry was based upon the production of acetylene from the photolysis of ethylene ($\Phi = 1.0$ at 123.6 nm).¹²

Product analysis was by flame ionization gas chromatography using the same instrument and conditions that were used to analyze the products of the 147-nm photolyses.^{4,5} The products of the photolysis of $\text{CH}_2\text{FCH}_2\text{Cl}$ (C_2H_4 , $\text{C}_2\text{H}_3\text{F}$, C_2H_2 , *trans*- CHClCHF , *cis*- CHClCHF , $\text{C}_2\text{H}_3\text{Cl}$, $\text{C}_2\text{H}_5\text{F}$, CH_3F , and CH_3Cl) were all identified by the comparison of retention times with those of authentic samples, and sensitivities to the detector subsequently determined.

The one "unidentified" product, eluting just after *cis*- CHClCHF , was again presumed to be 1,4- $\text{C}_4\text{H}_8\text{F}_2$ and assigned a detector sensitivity of twice that of ethylene.⁴ The two other higher molecular weight products previously

detected in small amounts at 147 nm⁴ were not observed. Products of the photolysis of $\text{CH}_3\text{CF}_2\text{Cl}$ included CH_2CF_2 , CH_2CHF , CH_4 , and CH_2CFCl which again were identified by comparisons with authentic samples. The remaining product, CHCF, was identified indirectly by photolysis and subsequent analysis of a sample of 1,1-difluoroethylene and assigned a detector sensitivity equal to that of C_2H_2 , though the latter was not a product of this shorter wavelength photolysis.

The sources and final purities of the $\text{CH}_2\text{FCH}_2\text{Cl}$, $\text{CH}_3\text{CF}_2\text{Cl}$, NO, CF_4 , and H_2S were those described in our previous work.^{4,5} The HI from Matheson was purified by low temperature trap-to-trap distillations. The helium was conventional chromatographic grade of stated purity 99.995%.

Results

There is a general similarity between the data obtained at 123.6 nm and that at 147 nm for both compounds. Table I shows the quantum yields of products obtained in the photolysis of $\text{CH}_3\text{CF}_2\text{Cl}$ and Table II the quantum yields of products for $\text{CH}_2\text{FCH}_2\text{Cl}$. In both cases photolysis times were varied from 30 to 90 min with no apparent effects upon the quantum yields.

$\text{CH}_3\text{CF}_2\text{Cl}$. As in the 147-nm photolysis the dominant product is CH_2CF_2 . There is no discernable increase with increasing pressure in the presence or absence of the radical scavenger NO. The data again⁵ appear to be randomly scattered about a mean value ($\Phi_{\text{CH}_2\text{CF}_2} = 0.82 \pm 0.02$) regardless of any added gas. The yields of CH_2CHF are also similar in magnitude to those observed in the 147-nm photolysis. The variations in yield in the presence of CF_4 and NO fall within the limits of reproducibility and one must conclude that the yield is essentially independent of pressure and the addition of NO. Unlike the 147-nm photolysis, CH_2CFCl was an observed product (runs 2, 3, 5, and 7). These runs suggest that CH_2CFCl is produced in a like manner to CH_2CHF . Acetylene, on the other hand, was not detected at all and the yield of CHCF is very small, approaching zero at high pressures. Methane is the only C_1 product. In the presence of HI and H_2S the quantum yield rises to 0.04. Predictably, the yield is zero in the presence of NO. Methyl chloride was not observed though it is possible that small yields of the order of 0.01 could have escaped detection.

$\text{CH}_2\text{FCH}_2\text{Cl}$. Ethylene and vinyl fluoride are again the major products. The yield of C_2H_4 is unaffected by the addition of NO. If there is a decrease in the yield of C_2H_4 with increasing pressure, it is very slight. Thus the quantum yield varies from 0.26₀ (run 8) at ~500 Torr to 0.29₀ (run 1) at ~4 Torr. The overall decrease in the yield of $\text{C}_2\text{H}_3\text{F}$ with increasing pressure is a little more obvious (cf. runs 1, 2, 5, and 6). There is also a further decrease

TABLE II: Photolysis of $\text{CH}_2\text{FCH}_2\text{Cl}$ at 123.6 nm

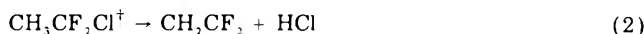
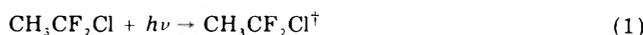
Run no.	$P_{\text{CH}_2\text{FCH}_2\text{Cl}}$, Torr	P_{additive} , Torr	Quantum yields (Φ)									
			C_2H_4	$\text{C}_2\text{H}_3\text{F}$	C_2H_2	<i>trans</i> - CHClCHF	<i>cis</i> - CHClCHF	$\text{C}_2\text{H}_3\text{Cl}$	$\text{C}_2\text{H}_3\text{F}$	CH_3F	CH_3Cl	$1,4\text{-C}_4\text{H}_8\text{F}_2$
1	3.8		0.29 ₀	0.48 ₁	0.14 ₄	0.03 ₂	0.03 ₅	0.03 ₇	0.00	0.01 ₆	0.00	
2	5.8		0.28 ₆	0.47 ₆	0.14 ₀	0.02 ₅	0.02 ₅	0.04 ₀	0.00	0.00	0.00	
3	6.3	NO	0.28 ₅	0.41 ₁	0.13 ₇	0.04 ₄	0.04 ₀	0.00	0.00	0.00	0.00	
4	6.6	H_2S	0.27 ₀	0.40 ₅	0.14 ₁	0.03 ₀	0.03 ₀	0.04 ₃	0.04 ₂	0.04 ₀	0.00	
5	6.6	CF_4	0.28 ₀	0.44 ₇	0.13 ₁	0.04 ₁	0.03 ₁	0.01 ₄	0.04 ₂	0.03 ₂	0.03 ₀	
6	5.1	CF_4	0.27 ₁	0.41 ₀	0.12 ₅	0.04 ₁	0.05 ₁	0.02 ₀	0.04 ₁	0.01 ₁	0.04 ₁	
7	6.8	NO	0.26 ₇	0.40 ₀	0.11 ₀	0.04 ₂	0.04 ₅	0.00	0.00	0.00	0.00	
8	7.1	CF_4	0.26 ₀	0.41 ₈	0.12 ₄	0.04 ₀	0.04 ₅	0.00	0.00	0.00	0.00	

as a result of the addition of NO, particularly at low pressures (cf. runs 2 and 3). The yield of $\text{C}_2\text{H}_3\text{Cl}$, on the other hand, is fairly constant regardless of the total pressure and/or the presence of NO. *cis* and *trans*- CHFCHCl are produced in similar amounts and there is little evidence that these are of radical origin since the addition of NO has no effect. The yield of C_2H_2 is again conspicuous, as it was in the 147-nm photolysis, in that the yield is, to all intents and purposes, independent of total pressure. The ethyl fluoride formed is obviously of radical origin as are the remaining products CH_3F , CH_3Cl , and "1,4- $\text{C}_4\text{H}_8\text{F}_2$ ". All are scavenged by the addition of NO. As the yield of $\text{C}_2\text{H}_3\text{F}$ decreases with increasing pressure, in the absence of NO, there is a corresponding increase in the yield of 1,4- $\text{C}_4\text{H}_8\text{F}_2$. Thus again there appears to be a correlation between the sum of the yields of scavengable $\text{C}_2\text{H}_3\text{F}$ and $\text{C}_2\text{H}_3\text{Cl}$ and the yield of 1,4- $\text{C}_4\text{H}_8\text{F}_2$ as a function of pressure.

Discussion

$\text{CH}_3\text{CF}_2\text{Cl}$. As we have indicated in the Results section, the experimental data obtained for the 123.6-nm photolysis differ very little from those obtained in the 147-nm photolysis. Consequently, our present interpretation of the 123.6-nm data, in terms of primary processes, also differs little from that previously. However, the very similarity of the data for both wavelengths, in spite of a significant increase in the photon energy (37 kcal mol⁻¹) has led us to question our conclusions in the former case with respect to the excitation of the products of the major primary process.

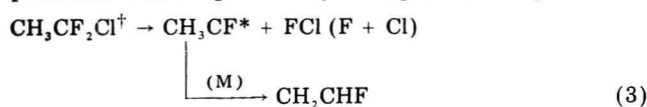
At 123.6 nm the molecule again photodecomposes almost entirely by the molecular elimination of HCl to yield CH_2CF_2 ($\Phi = 0.82$). Since the yield is unaffected by the presence of NO, little or no CH_2CF_2 is formed by radical processes such as disproportionation. There is, in fact, a distinct lack of any radical products. Thus HCl is not only eliminated molecularly, but there is no subsequent dissociation of the HCl into H and Cl atoms. The photoelimination is represented by



At 147 nm the quantum yield of CH_2CF_2 was very similar.⁵ However, it was concluded that there was a small increase with increasing pressure with an apparent corresponding decrease in the quantum yield of CHCF. Thus at 20 Torr, $\Phi(\text{CH}_2\text{CF}_2)$ was ~ 0.74 and at 400 Torr it was ~ 0.80 . This was interpreted as the result of the further decomposition of vibrationally excited ground state CH_2CF_2 at low pressures to give CHCF. This interpretation cannot be extended to the 123.6-nm photolysis, however. At 123.6 nm the photon energy is 231 kcal mol⁻¹. If CH_2CF_2 and HCl were formed in their electronic ground states, the energy available to the products of reaction 2 would be ~ 209 kcal mol⁻¹ since the reaction is 21.9 kcal mol⁻¹ endothermic.^{13,14} The bond strength of HCl is 103 kcal mol⁻¹. For the vibrationally excited ground state HCl not to decompose there would have to be in excess of 100 kcal of vibrational energy in CH_2CF_2 unless a substantial fraction of the excess energy is taken up as energy of overall rotation and relative translation of the products. Since the activation energy for HF elimination from CH_2CF_2 is only ~ 86 kcal mol⁻¹ (ref 15), one might reasonably expect to observe significant if not complete decomposition of CH_2CF_2 to give CHCF particularly at lower pressures. The yield of CHCF at 123.6 nm is, in fact, very small. Therefore, it is unlikely that both of the

products of reaction 2 are in their electronic ground states. Since there is insufficient energy to produce electronically excited singlet states of both CH_2CF_2 and HCl ,^{16,17} and the simultaneous formation of triplet states, while energetically feasible, would result in the immediate dissociation of triplet HCl into atoms, we are inclined to believe that CH_2CF_2 is produced in an excited singlet state which is subsequently efficiently quenched to the vibrationally excited ground state with necessarily less than ~ 86 kcal of excess energy. The yield of CHCF may reflect the slowness of the fraction of CH_2CF_2 which does not meet this condition either because some CH_2CF_2 molecules are not in fact efficiently quenched or because a small fraction of molecules may be formed in the vibrationally excited ground state only to decompose immediately at low pressures to CHCF . Since there is also probably sufficient excess energy (172 kcal) even at 147 nm to produce excited singlet CH_2CF_2 and ground state HCl , it may well be that this is indeed the case and that our previous conclusions could be incorrect.

The quantum yield of CH_2CHF at 123.6 nm is again small ($\Phi = 0.03$), and no acetylene is observed. The production of CH_2CHF may be represented by



The carbene it seems, either does not initially have sufficient energy to decompose to C_2H_2 even after intramolecular rearrangement to give CH_2CHF , or it is efficiently quenched, perhaps from an excited state, to vibrationally excited ground state CH_2CHF with less than ~ 71 kcal mol^{-1} , the activation energy for HF elimination to give C_2H_2 .¹⁸ It is also possible that FCl is formed with sufficient excess energy to decompose to $\text{F} + \text{Cl}$. Such a process is barely distinguishable from $\text{C}-\text{Cl}$ bond fission followed by $\text{C}-\text{F}$ bond fission from CH_3CF_2 . The lack of radical disproportionation/combination products is not necessarily conclusive since individual yields could well be below our detection limits.

Again some carbon-carbon bond cleavage ($\Phi = 0.04$) appears to occur, if the yield of CH_4 obtained in the presence of H_2S and HI is taken to be a measure of the resulting CH_3 radicals. The detection of small amounts of CH_2CFCl indicates that HF elimination from $\text{CH}_3\text{CF}_2\text{Cl}$ also occurs at 123.6 nm ($\Phi = 0.05$), reaction 4. This



product was not observed at 147 nm and thus HF elimination is the only reaction peculiar to the 123.6-nm photolysis.

The far-ultraviolet spectrum of $\text{CH}_3\text{CF}_2\text{Cl}$ has been measured.¹⁹ At 123.6 nm the absorption is confidently ascribed to the formation of a Rydberg state ($4p \leftarrow \bar{\text{Cl}}$). Figure 4 of ref 19 shows that at 147 nm the absorption corresponds to both Rydberg ($4s \leftarrow \bar{\text{Cl}}$) and antibonding states ($\text{C}-\text{Cl} \leftarrow \bar{\text{Cl}}$) with an extinction coefficient of approximately $200 \text{ L mol}^{-1} \text{ cm}^{-1}$. However, we have previously⁵ determined the decadic extinction coefficient at 147 nm to be $\sim 680 \text{ L mol}^{-1} \text{ cm}^{-1}$. If we accept the higher Xe resonance line value, then at 147 nm the majority of excited molecules could also be of the Rydberg type. Notwithstanding, the data at 123.6 nm, at least, show quite clearly that molecular elimination of HCl occurs from a Rydberg state.

$\text{CH}_2\text{FCH}_2\text{Cl}$. The production of nonscavengeable ethylene is again thought to be due to the elimination of FCl from an initially formed excited state. The quantum

yield at ~ 6 Torr is 0.28 (run 3) and 0.26 at ~ 560 Torr (run 8). At 147 nm this process exhibited a larger pressure dependence⁴ which was attributed to the collisional modification of an excited state ($\text{CH}_2\text{FCH}_2\text{Cl}^{(1)}$) to another state decomposing by carbon-halogen bond fission, a process seen to increase with increasing pressure. If we assume at 123.6 nm that $\text{CH}_2\text{FCH}_2\text{Cl}^{(1)}$ is still formed but with a shorter lifetime due to vibrational excitation, then one would expect the yield of ethylene to be less dependent upon pressure and one would also expect a corresponding decrease in the extent of carbon-halogen bond fission. This appears to be the case. It will be seen that, after computing the sum of the quantum yields of all other processes, the quantum yield for carbon-halogen bond fission is now only 0.05. The singular pressure dependence of the yield of C_2H_4 at 147 nm led us to propose that other primary processes such as HCl elimination were the result of the decomposition of a second state, $\text{CH}_2\text{FCH}_2\text{Cl}^{(2)}$. At 123.6 nm, of course, we no longer have the same grounds for such a distinction since the yield of C_2H_4 varies little with pressure. However, since the yield of nonscavengeable $\text{C}_2\text{H}_3\text{F}$ has increased from 0.29 at 147 nm to 0.41 at 123.6 nm while the low pressure yield of C_2H_4 has, if anything, decreased, we are inclined to retain this two-state hypothesis. Thus $\text{CH}_2\text{FCH}_2\text{Cl}^{(1)}$ gives rise to C_2H_4 or is induced by collisions to undergo carbon-halogen bond fission, reactions 5 and 6, while $\text{CH}_2\text{FCH}_2\text{Cl}^{(2)}$ is thought

	$\langle \Phi \rangle$	ΔH_{Rx} , kcal mol^{-1}	
$\text{CH}_2\text{FCH}_2\text{Cl}^{(1)}$			
$\rightarrow \text{C}_2\text{H}_4 + \text{FCl}$	0.27	~ 68	(5)
$\xrightarrow{\text{M}} \text{C}_2\text{H}_4\text{F} + \text{Cl}$	0.05		(6)
$\text{CH}_2\text{FCH}_2\text{Cl}^{(2)}$			
$\rightarrow \text{C}_2\text{H}_3\text{F} + \text{HCl}$	0.41 _s	~ 12	(7)
$\rightarrow \text{cis-CHClCHF} + \text{H}_2$	0.03 _s	~ 31	(8)
$\rightarrow \text{trans-CHClCHF} + \text{H}_2$	0.03 _s	~ 30	(9)
$\rightarrow \text{C}_2\text{H}_3\text{Cl} + \text{HF}$	0.03	~ 11	(10)
	$\Sigma \Phi = 0.83_s$		

to give rise to $\text{C}_2\text{H}_3\text{F}$, *cis-CHClCHF*, *trans-CHClCHF*, and $\text{C}_2\text{H}_3\text{Cl}$ by the corresponding eliminations of HCl , H_2 and HF , reactions 7-10. The ΔH values refer to ground state reactants and products.

The extent of carbon-carbon bond cleavage (0.04) is given by the yields of CH_3Cl and CH_3F obtained in the presence of H_2S . The yield of acetylene varies from 0.14 at ~ 6 Torr to 0.12 at ~ 560 Torr. Taking all these processes including the production of ethylene into account gives a total quantum yield of ~ 1.00 at all pressures. Therefore, the quantum yield for carbon-chlorine bond fission as evidenced by the formation of $1,4\text{-C}_4\text{H}_8\text{F}_2$ cannot exceed ~ 0.05 .

As in the 147-nm photolysis, the source of the acetylene is unclear. The fact that it varies very little with pressure is significant in that it is somewhat uncharacteristic of the decomposition of an olefin formed entirely in the vibrationally excited electronic ground state. At 147 nm it was concluded that C_2H_4 was unlikely to be the source of the acetylene. The preferred sources were $\text{C}_2\text{H}_3\text{Cl}$ and/or $\text{C}_2\text{H}_3\text{F}$. At the shorter wavelength, with an additional 37 kcal of excess energy available to the products of the elimination reactions, the lack of decomposition of the olefins now suggests that they are formed for the most part in electronically excited states. It may be that the acetylene arises from that smaller fraction of an olefin that is simultaneously formed in the vibrationally excited ground

state and subsequently completely decomposes.

Summary

The overall effects of increased photon energy upon the nature of the primary processes and their quantum yields are surprisingly small. Molecular eliminations are still the major modes of photodecomposition at 123.6 nm. We interpret this simply as the result of a deeper penetration into the Rydberg bands of $\text{CH}_3\text{CF}_2\text{Cl}$ and $\text{CH}_2\text{FCH}_2\text{Cl}$ as the wavelength is changed from 147 to 123.6 nm. Thus in the 123.6-nm photolysis of $\text{CH}_3\text{CF}_2\text{Cl}$ the main effect of the shorter wavelength is to allow the molecular elimination of HF, a process not observed at 147 nm. In the 123.6-nm photolysis of $\text{CH}_2\text{FCH}_2\text{Cl}$, the shorter wavelength radiation again appears to produce two excited states but in a different ratio to one another and produces, in one case at least, a species with a shorter lifetime. Less carbon-halogen bond fission is observed as a result of the latter.

The fact that even at the shorter wavelength the olefins still do not decompose to any great extent is noteworthy. The excess energies available to the olefins are generally such that in most cases it is unlikely that they are produced in vibrationally excited ground states.

Acknowledgment. The support of the National Research Council of Canada is gratefully acknowledged. We also thank Dr. D. Salomon for helpful comments.

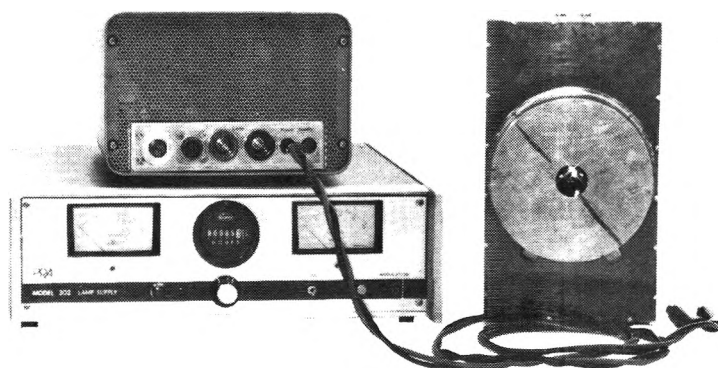
References and Notes

- (1) T. Ichimura, A. W. Kirk, G. Kramer, and E. Tschuikow-Roux, *J. Photochem.*, **6**, 77 (1976).

- (2) D. Salomon, A. W. Kirk, and E. Tschuikow-Roux, *Int. J. Chem. Kinet.*, **9**, 619 (1977).
- (3) D. Salomon, A. W. Kirk, and E. Tschuikow-Roux, *J. Photochem.*, **7**, 342 (1977).
- (4) T. Ichimura, A. W. Kirk, and E. Tschuikow-Roux, *Int. J. Chem. Kinet.*, in press.
- (5) T. Ichimura, A. W. Kirk, and E. Tschuikow-Roux, *Int. J. Chem. Kinet.*, in press.
- (6) T. Ichimura, A. W. Kirk, and E. Tschuikow-Roux, *J. Phys. Chem.*, **81**, 1153 (1977).
- (7) L. Cremieux and J. A. Herman, *Can. J. Chem.*, **52**, 3098 (1974).
- (8) T. O. Tiernan and B. H. Hughes, *Adv. Chem. Ser.*, **No. 82**, 412 (1968).
- (9) T. Fujimoto and M. H. J. Wijnen, *J. Chem. Phys.*, **56**, 4032 (1972).
- (10) (a) C. Sandorfy, *Z. Phys. Chem. (Frankfurt am Main)*, **101**, 307 (1976); (b) "Theory and Practise of MO calculations on Organic Molecules", Elsevier, New York, N.Y., 1977.
- (11) R. Gordon, R. E. Rebbert, and P. Ausloos, *Natl. Bur. Std. Tech. Note*, **No. 494** (1969).
- (12) P. Potzinger, L. C. Glasgow, and G. von Büнау, *Z. Naturforsch. A*, **27**, 628 (1972).
- (13) S. W. Benson, "Thermochemical Kinetics", Wiley, New York, N.Y., 1968.
- (14) E. Tschuikow-Roux and K. R. Maltmar, *Int. J. Chem. Kinet.*, **7**, 363 (1975). Heats of formation (kcal mol⁻¹) estimated by group additivity; $\Delta H_f^\circ(\text{CH}_3\text{CF}_2\text{Cl}) = -116.4$, $\Delta H_f^\circ(\text{CH}_2\text{CF}_2) = -72.4$, and $\Delta H_f^\circ(\text{CH}_2\text{CHF}) = -33.5$.
- (15) J. M. Simmie and E. Tschuikow-Roux, *J. Phys. Chem.*, **74**, 4075 (1970).
- (16) D. A. Armstrong and C. Willis, *Int. J. Radiat. Phys. Chem.*, **8**, 221 (1976). The first excited triplet and singlet states of HCl are approximately 5 and 9 eV above the ground state, respectively.
- (17) It is assumed that the lower excited states of CH_2CF_2 have excitation energies roughly similar to those of ethylene: R. J. Buunker and D. Peyerimhoff, *Chem. Phys.*, **9**, 75 (1976). That is, a first excitation triplet (planar) at ~4 eV and a first excited singlet (planar) at ~7 eV. The twisted forms are ~1 eV lower in energy.
- (18) J. M. Simmie, W. J. Quiring, and E. Tschuikow-Roux, *J. Phys. Chem.*, **74**, 992 (1970).
- (19) J. Doucet, P. Sauvageau, and C. Sandorfy, *J. Chem. Phys.*, **62**, 355 (1975).

NEW ARC LAMP SYSTEMS

- **6-10X more power for given lamps**
- **Allows for use of lower-powered lamps for REDUCED OPERATING COST.**
- **Compact**
- **Excellent stability**
- **Versatile**



The regulated power supplies are:

- **modulatable up to 50KHz**
- **capable of pulsed mode operation**
- **highly regulated**
- **low RF, filtered single pulse starters**

The supplies can power most arc lamps from 75w-1000w

PRA

Photochemical Research Associates Inc.
University of Western Ontario
Department of Chemistry
London, Ont., Canada N6A 3K7
(519) 679-6181 Telex 064-7597

New...for the Physical Chemist

ENERGY AND THE ATMOSPHERE

A Physical-Chemical Approach

Ian M. Campbell

A broad, interdisciplinary view of energy conversion and chemical conversions on the earth and in its atmosphere. Compares the "energy crisis" with the natural fluxes of energy, such as planetary energy balance, photosynthesis, natural and synthetic fuel resources, and the efficiency of power cycles. Develops complementary topics of the generation of pollutants in fossil-energy conversion and the subsequent atmospheric photochemistry.

approx. 400 pp. (1-99482-0) cloth 1977 \$32.50 (tent.)
approx. 400 pp. (1-99481-2) paper 1977 \$13.95 (tent.)

STATISTICAL MECHANICS, 2nd Ed.

Joseph Edward Mayer & the late Maria Goeppert Mayer

An up-to-date new edition of a classic work first published in 1940. Chapters and sections are self-contained, giving definitions of symbols, explanations of notation and statements of the basic starting equations, and references to previous sections and equations. Includes an historical perspective discussing the use of probabilities and probability densities; the logic and formalism of the Gibbs ensemble method with master equations and their interrelations.

491 pp. (1-57985-8) 1977 \$23.50

ADVANCES IN CHEMICAL PHYSICS, Vol. 36

I. Prigogine & Stuart A. Rice

Contents: Semiclassical Theory of Bound States (I. Percival). The Correspondence Principle in Heavy-Energy Surfaces and Elastic and Inelastic Scattering (E. Truhlar and R. Wyatt). Theoretical Aspects of Ionization Potentials and Photoelectron Spectroscopy: A Green's Function Approach (L. Cederbaum and W. Domcke). Application of Diagrammatic Quasideterminate RSPT in Quantum Molecular Physics (V. Kvasnicka). Interactions of Slow Electrons with Benzene and Benzene Derivatives (L. Christophorou, M. Grant, and D.M. Corkle).

541 pp. (1-02274-8) 1977 \$36.50

SELF-ORGANIZATION IN NONEQUILIBRIUM SYSTEMS

From Dissipative Structures to Order through Fluctuations

G. Nicolis & I. Prigogine

Because evolutionary processes lead to vast diversification and increasing complexity, the behavior of a macroscopic system with many interacting subunits can substantially differ from the random superposition of the independent subunits' evolution. This monograph explores the self-organization phenomena arising in such systems while giving a unified treatment of self-organization based on the techniques of irreversible thermodynamics, nonlinear mathematics, and kinetic theory.

491 pp. (1-02401-5) 1977 \$27.50

PHYSICAL CHEMISTRY OF SURFACES, 3rd Ed.

Arthur W. Adamson

"In this third edition of a text which is, by now, considered a classic, Dr. Adamson has updated the references and added the latest techniques... well written and the topics are logically presented. It is, in addition, an excellent source for references in the literature. The field is covered well and all fundamental aspects are touched upon"—J. of Electrochemical Soc.

698 pp. (1-00794-3) 1976 \$26.50

PRINCIPLES OF ULTRAVIOLET PHOTOELECTRON SPECTROSCOPY

J. Wayne Rabalais

A detailed presentation of the principles of UV photoelectron spectroscopy in terms of modern chemical physics, i.e., the phenomenon of photoionization and its resulting consequences by means of modern quantum chemical methods.

454 pp. (1-70285-4) 1977 \$29.95

MOLECULAR SYMMETRY AND GROUP THEORY

A Programmed Introduction to Chemical Application

Alan Vincent

A programmed introduction to the use of symmetry methods that takes the reader through the essentials of group theory to the point at which elegant symmetry methods can be used to solve molecular problems. The book covers, in detail, molecular vibrations, hybrid orbitals, MO correlation diagrams, and other bonding applications.

156 pp. (1-01867-8) cloth 1977 \$13.50

156 pp. (1-01868-6) paper 1977 \$5.95

CLASSICAL KINETIC THEORY OF FLUIDS

P. Résibois & M. De Leener

This self-contained introduction to the methods of nonequilibrium statistical mechanics starts from first principles and advances to the point where comparison with experiment is possible. Brownian motion and the Boltzmann equation are presented in a unique language framework that makes the corresponding modern approaches of correlation function method and generalized kinetic equations appear as a natural generalization.

412 pp. (1-71694-4) 1977 \$29.50

ADVANCES IN PHOTOCHEMISTRY, Vol. 10

J.N. Pitts, Jr., George S. Hammond, & Klaus Gollnick

Contents: Vapor Phase Photochemistry of the Neutral Oxides and Sulfides of Carbon • Photolysis of Saturated Alcohols, Ethers, and Amines • Excitation and Deexcitation of Benzene • Primary Photo-processes of Organo-Transition Metal Compounds • Intramolecular Proton Transfer in Electronically Excited Molecules • Excited State Behavior of Some Bichromophic Systems.

496 pp. (1-02145-8) 1977 \$29.50

VISCOSITY AND DIFFUSIVITY

A Predictive Treatment

Joel H. Hildebrand

This monograph, consisting of thirteen papers written during 1971-1976, presents a coherent, predictive treatment of simple liquids free from assumptions such as cages, cells, clusters, liquid lattices, monomers and dimers, and significant structures. Treatments are based upon consistent, physical concepts.

109 pp. (1-03072-4) 1977 \$9.50

AN INTRODUCTION TO CLAY COLLOID CHEMISTRY, 2nd Ed.

H. van Olphen

This updated and enlarged edition includes: new information on surface characterization and adsorption mechanisms; recent results in the area of clay-organic interaction—the intercalation and intersalation of kaolinite mineral; and increased attention to the possible role of clays in biological evolution.

318 pp. (1-01463-X) 1977 \$21.50

Available at your bookstore or write to Nat Bodian, Dept. 092.

WILEY-INTERSCIENCE

a division of John Wiley & Sons, Inc.

605 Third Avenue
New York, N.Y. 10016

In Canada: 22 Worcester Road, Rexdale, Ontario



Prices subject to change without notice.

092 A 8328-51